Establishment of Experimental Severe Congenital Neutropenia (CN) Models in Zebrafish

Dissertation

der Mathematisch-Naturwissenschaftlichen Fakultät

der Eberhard Karls Universität Tübingen

zur Erlangung des Grades eines

Doktors der Naturwissenschaften

(Dr. rer. nat.)

vorgelegt von

M.Sc. Larissa Doll

aus Karlsruhe

Tübingen

2024

Gedruckt mit Genehmigung der Mathematisch-Naturwissenschaftlichen Fakultät der Eberhard Karls Universität Tübingen.

Tag der mündlichen Qualifikation:	23.06.2025
Dekan:	Prof. Dr. Thilo Stehle
1. Berichterstatter/-in:	Prof. Dr. Rita Triebskorn
2. Berichterstatter/-in:	Prof. Dr. Julia Skokowa
3. Berichterstatter/-in:	PD Dr. Friedrich Kapp

Eidesstattliche Erklärung

Ich, Larissa Doll, versichere hiermit, dass ich die vorliegende Arbeit eigenständig und ausschließlich unter Verwendung der angegebenen Quellen und Hilfsmitteln angefertigt habe. Alle Ausführungen, die anderen Schriften wörtlich oder sinngemäß entnommen wurden, sind kenntlich gemacht worden.

…….. …….

Ort, Datum Unterschrift: Larissa Doll

TABLE OF CONTENTS

ABBREVIATIONS I: GENERAL

Abbreviation	Definition	Abbreviation	Definition
∆T12-G14	Deletion of threonine position 12 to glycine position 14	HS(P)C	Hematopoietic stem (and progenitor) cell
AML	Acute myeloid leukemia	Indel	Insertion or deletion
ATG	Start codon	iPSCs	Induced pluripotent stem cells
Atg-MO	ATG binding morpholino	MDS	Myelodysplastic syndrome
c.347_351del	Deletion of nucleotides 347 to 351	MO	Morpholino
c.351_357del	Deletion of nucleotides 351 to 357	mRNA	Messenger RNA
Cas9	CRISPR-associated protein 9	NETs	Neutrophil extracellular traps
CHT	Caudal hematopoietic tissue	p.Gln141*	Mutation of the glutamine at position 141 to a stop codon
CMP	Common myeloid progenitor	p.Gly132Arg	Mutation of the glycine at position 132 to arginine
CN	Severe congenital neutropenia	pH3	Phospho-histone H3
COPI	Coat protein complex I	p.Met1Ile	Mutation of the first methionine to isoleucine
CRISPR	Clustered regularly interspaced short palindromic repeats	PBI	Posterior blood island
DNA	Desoxyribonucleic acid	PMN	Polymorphonuclear neutrophil
dpf	Days post fertilization	RBI	Rostral blood island
DTT	Dithiothreitol	RNA	Ribonucleic acid
e.g.	For example	RNP	Ribonucleoprotein complex
E1-MO	Exon1 splicing *hax1* morpholino	ROS	Reactive oxygen species
E2-MO	Exon2 splicing *hax1* morpholino	RT-qPCR	Real-time quantitative polymerase chain reaction
EMP	Erythromyeloid progenitors	SB	Sudan black staining
ER	Endoplasmic reticulum	Tg	Transgenic reporter line
F1	First generation	TM	Transmembrane domain
F2	Second generation	TUNEL	Terminal deoxynucleotidyl transferase dUTP nick end labeling
GFP	Green fluorescent protein	UPR	Unfolded protein response
GMP	Granulocyte-macrophage progenitor	VDA	Ventral wall of the dorsal aorta
GOI	Gene of interest	WISH	Whole-mount *in situ* hybridization
hpf	Hour post fertilization	WT	Wild-type

ABBREVIATIONS II: GENES AND PROTEINS

Abbreviation		Definition
Human gene – protein	**Zebrafish** gene – protein	
ATF4 - ATF4	*atf4* – Atf4	Activating transcription factor 4
ATF6 - ATF6	*atf6* – Atf6	Activating transcription factor 6
CDK - CDK	*cdk* – Cdk	Cyclin-dependent kinase
CEBPA – C/EBPα	*cebpa* – C/ebpα	CCAAT/enhancer-binding protein alpha
CEBPB – C/EBPβ	*cebpb* – C/ebpβ	CCAAT/enhancer-binding protein beta
CEBPE – C/EBPε	*cebp1* – Cebp1	CCAAT/enhancer-binding protein epsilon/one
COPZ1 – COPZ1	*copz1* – Copz1	COPI coatomer subunit zeta 1
CSF3 – G-CSF	*g-csfa/b* – G-csfa/b	Granulocyte colony-stimulating factor (a or b)
CSF3R – G-CSFR	*csf3r* – G-csfr	Granulocyte colony-stimulating factor receptor
DDIT3 - CHOP	*ddit3* – Chop	DNA damage-inducible transcript 3 C/EBP homologous protein
-	*drl*	Draculin
EIF2AK3 – PERK	*eif2ak3* - Perk	Eukaryotic translation initiation factor 2-alpha kinase 3 Protein kinase R-like endoplasmic reticulum kinase
ELANE - NE	no ortholog	Neutrophil elastase
ERN1 - IRE1	*ern1* – Ire1	Endoplasmic reticulum to nucleus signaling 1 Inositol-requiring enzyme 1
ERO1 – ERO1	*ero1a/b* – Ero1a/b	Endoplasmic reticulum oxidoreductase 1 (a or b)
G6PC3 – G6PC3	*g6pc3* – G6pc3	Glucose-6-phosphatase catalytic subunit 3
GATA1 – GATA1	*gata1* – Gata1	GATA-binding factor 1
CSF2 – GM-CSF	-	Granulocyte-macrophage colony-stimulating factor
HAX1 – HAX1	*Hax1* – Hax1	HCLS1-associated protein X1
-	*hbae1.1* – Hbae1.1	Hemoglobin, alpha embryonic 1.1
HCLS1 – HCLS1	*hcls1* – Hcls1	Hematopoietic cell-specific Lyn substrate 1
HIF1A – HIFα	-	Hypoxia-inducible factor 1 alpha
HTRA - HTRA	-	High-temperature requirement A serine peptidase
-	*itga2b* – Cd41	Integrin α2b
JAGN1 – JAGN1	*jagn1a/b* – Jagn1a/b	Jagunal homolog 1 (a or b)
JAK - JAK	-	Janus kinases
-	*lcp* – Lcp	L-plastin
LYZ-LYZ	*lyz* – Lyz	Lysozyme C
-	*mpeg1.1* – Mpeg1.1	Macrophage-expressed gene 1
MPO – MPO	*mpo* - Mpo	Myeloperoxidase
PARL – PARL	-	Presenilin-associated rhomboid like
PKD2 – PKD2	-	Polycystin-2
PPP1R15A - GADD34	*ppp1r15a* – Gadd34	Protein phosphatase 1 regulatory subunit 15A Growth arrest and DNA damage-inducible protein 34
SBDS - SBDS	*sbds* - Sbds	Shwachman-Bodian-Diamond syndrome
SPI1 – PU.1	*spi1b* – Pu.1	Spi-1 proto-oncogene (b)
SRP54 – SRP54	*srp54* – Srp54	Signal recognition particle 54
STAT – STAT	-	Signal transducer and activator of transcription
(s)*XBP1* – (s)XBP1	*(s)xbp1* – (s)Xbp1	(Spliced) X-box binding protein 1

SUMMARY

Severe congenital neutropenia (CN) is a genetically heterogeneous condition characterized by an inborn neutrophil deficiency. It is caused by germline mutations in various genes, including autosomal recessive mutations in *HAX1*, *JAGN1*, or *COPZ1*. CN patients suffer from severe infections from birth, and without treatment, these can be life-threatening. Current understanding of CN pathophysiology is mainly based on *in vitro* assays and clinical observations. To date, no faithful mouse models have been described. Mice deficient in HAX1 or JAGN1 are prematurely lethal and don't develop neutropenia, and a COPZ1 model has not yet been established. The evolutionary conservation of most processes underlying hematopoiesis between humans and zebrafish makes it an ideal alternative vertebrate model system to study normal and malignant granulopoiesis.

The aim of this study was to establish *HAX1*-, *JAGN1*-, and *COPZ1*-associated CN zebrafish models to study the underlying pathomechanisms and the discovery of new therapeutic approaches. We have successfully established three CN models by mimicking the human mutations in the zebrafish orthologs *hax1*, *jagn1b*, and *copz1*. Using these models, we studied different processes, such as the induction of unfolded protein response (UPR), apoptosis of myeloid progenitors, and the impairment of the G-CSFR pathway, which were previously described as potential causes of neutropenia development. Despite active UPR upon different Jagn1b alterations and an increase in apoptotic cells after downregulating *hax1* or *jagn1b*, we dismissed these processes as solely neutropenia-causing mechanisms since the chemical induction of UPR or apoptosis did not lead to a reduced number of neutrophils. In the *HAX1*- and *JAGN1*-associated CN models, the analyses of the G-CSFR pathway showed an altered signaling, resulting in a decreased expression of the central regulator of steady-state granulopoiesis, *cebpa*. Similarly, a reduced expression of *CEBPA* was seen in HSPCs carrying truncated COPZ1. Moreover, treating our zebrafish CN models with the HIF1α activator, IOX2, or the pan-CDK inhibitor, flavopiridol, rescued their neutropenia phenotype. The activation of HIF1α is associated with *CEBPA* activation and the inhibition of CDK2/4 mimics C/EBPα function. These mechanisms of action could compensate for the reduced *cebpa* expression and explain the induction of granulopoiesis after IOX2 or flavopiridol treatment. However, the underlying cause of

neutropenia development is a complex process involving several interrelated mechanisms. Our CN zebrafish models, established during this PhD, have allowed us to get closer to understanding these mechanisms and are a potential tool for further studies. In addition, these models enable rapid testing of the *in vivo* effects of candidate therapeutics on granulopoiesis, an essential step toward the clinical translation of our experimental findings.

ZUSAMMENFASSUNG

Schwere kongenitale Neutropenie (CN) ist ein genetisch heterogener Krankheitszustand, der durch einen angeborenen Neutrophilenmangel charakterisiert ist. Diese Krankheit wird durch Keimbahnmutationen in verschiedenen Genen verursacht, darunter autosomal rezessive Mutationen in *HAX1*, *JAGN1* und *COPZ1*. CN-Patienten leiden von Geburt an unter schweren Infektionen, welche ohne Behandlung lebensbedrohlich sein können. Das derzeitige Verständnis der CN-Pathophysiologie basiert hauptsächlich auf In-vitro-Analysen und klinischen Beobachtungen. Bislang wurden noch keine zuverlässigen Mausmodelle beschrieben. Mäuse mit einem Mangel an HAX1 oder JAGN1 sind vorzeitig letal und entwickeln keine Neutropenie, und ein COPZ1-Modell wurde noch nicht entwickelt. Die meisten Prozesse der Hämatopoese sind zwischen Mensch und Zebrafisch evolutionär konserviert. Daher ist der Zebrafisch ein ideales alternatives Wirbeltiermodellsystem zur Untersuchung der normalen und malignen Granulopoese.

Das Ziel dieser Studie war es, *HAX1*-, *JAGN1*- und *COPZ1*-assoziierte CN-Zebrafischmodelle zu etablieren, um die zugrunde liegenden Pathomechanismen zu untersuchen und neue therapeutische Ansätze zu finden. Wir haben erfolgreich drei CN-Modelle etabliert, indem wir die menschlichen Mutationen in den Zebrafischorthologen *hax1*, *jagn1b* und *copz1* nachgebildet haben. Anhand dieser Modelle untersuchten wir verschiedene Prozesse, wie die Aktivierung der Antwort auf ungefaltete Proteine (UPR), die Apoptose myeloischer Vorläuferzellen oder die Beeinträchtigung des G-CSFR-Signalweges, die zuvor als mögliche Ursachen für die Entstehung von Neutropenie beschrieben wurden. Trotz aktiver UPR bei verschiedenen Jagn1b-Mutationen und einer Zunahme apoptotischer Zellen nach der Herunterregulierung von *hax1* oder *jagn1b* schlossen wir diese Prozesse als alleinige Neutropenie-verursachende Mechanismen aus, da die chemische Induktion von UPR oder Apoptose nicht zu einer verringerten Anzahl von Neutrophilen führte. In den *HAX1*- und *JAGN1*-assoziierten CN-Modellen zeigten die Analysen des G-CSFR-Signalwegs eine veränderte Signalübertragung, die zu einer verringerten Expression des zentralen Regulators der Steady-State-Granulopoese, *cebpa*, führte. In ähnlicher Weise wurde eine verringerte *CEBPA*-Expression in HSPZ beobachtet, die mutiertes COPZ1 aufweisen. Darüber hinaus konnte durch die Behandlung unserer Zebrafisch-

CN-Modelle mit dem HIF1α-Aktivator IOX2 und dem pan-CDK-Inhibitor Flavopiridol der Phänotyp der Neutropenie korrigiert werden. Die Aktivierung von HIF1α ist mit der von *CEBPA* verbunden, und die Hemmung von CDK2/4 imitiert die C/EBPα-Funktion. Diese Wirkmechanismen könnten die verminderte *cebpa*-Expression kompensieren und die Induktion der Granulopoese nach IOX2- oder Flavopiridol-Behandlung erklären. Die zugrundeliegende Ursache der Neutropenie ist ein komplexer Prozess, an dem mehrere miteinander verbundene Mechanismen beteiligt sind. Unsere CN-Zebrafischmodelle, die im Rahmen dieser Doktorarbeit entwickelt wurden, haben es uns ermöglicht, dem Verständnis dieser Mechanismen näher zu kommen und sind ein potenzielles Instrument für weitere Studien. Darüber hinaus ermöglichen die CN-Zebrafischmodelle eine schnelle Testung der In-vivo-Effekte von Therapeutika-Kandidaten auf die Granulopoese, was ein wesentlicher Schritt zur klinischen Umsetzung unserer experimentellen Ergebnisse ist.

LIST OF PUBLICATIONS

All relevant publications are listed below. The author's contribution is highlighted in bold.

A. **L. Doll**, N. Aghaallaei, A.M. Dick, K. Welte, J. Skokowa, B. Bajoghli, '*A zebrafish model for HAX1-associated congenital neutropenia*'. *Haematologica* 2021; 106 (5): 1311-1320.

B. **L. Doll**, K. Welte, J. Skokowa, B. Bajoghli, *'A JAGN1-associated severe congenital neutropenia zebrafish model revealed an altered G-CSFR signaling and UPR activation.*' *Blood Adv* 2024; 8 (15): 4050–4065.

C. N. Borbarán Bravo, E. Deordieva*, **L. Doll***, M. ElGamacy*, B. Dannenmann*, J. Azevedo*, S. Bräuning, V. Zakharova, C. Lengerke, M. Sturm, O. Rieß, C. Zeidler, K. Welte, A. Shcherbina, M. Klimiankou, J. Skokowa, *'A New Severe Congenital Neutropenia Syndrome Associated with Autosomal Recessive COPZ1 Mutation' Blood* 2025*;* 145 (20): 2317-2335*.*
(*Contributed equally to the work as second authors)

D. M. Nasri*, B. Dannenmann*, **L. Doll**, B. Findik, F. Bernhard, S. Kandabarau, M. Kliminakou, M. Gawaz, C. Lengerke, C. Zeidler, K. Welte, J. Skokowa, *'Flavopiridol restores granulopoiesis in experimental models of severe congenital neutropenia.' Mol Ther* 2025; 33 (6): 2851-2871.
(*Contributed equally to the work as first authors)

PERSONAL CONTRIBUTION

The following section outlines my personal contributions to the publications listed in the preceding section.

A. First author and main investigator. Involved in designing the work, performing most of the experiments and data analyses as well as manuscript preparation.

B. First author and main investigator. Designed the work and performed the experiments. Leading role in data analyses and interpretation. Prepared all the figures and wrote the manuscript (together with J. Skokowa and B.Bajoghli).

C. Co-second author (with E. Deordieva, M. ElGamacy, B. Dannenmann, and J. Azevedo). Created a *COPZ1*-associated CN zebrafish model: designed the work and performed all the zebrafish-related experiments. Analyzed and interpreted the data. Prepared the figures and figure legends. Wrote the Results, Material and Method, and Discussion sections related to the zebrafish part of the manuscript.

D. Second author. The established *HAX1*- and *JAGN1*-associated CN zebrafish models were used to study the effects of flavopiridol on granulopoiesis, and the downstream mechanism was investigated using *cebpa* knockdown. Designed the work and performed all the zebrafish-related experiments. Analyzed and interpreted the data. Prepared the figures and figure legends. Wrote the Results, Material and Method, and Discussion sections related to the zebrafish part of the manuscript.

PARTICIPATION IN SCIENTIFIC CONFERENCES

A. **L. Doll**, '*Establishment of zebrafish models for severe congenital neutropenia'*. Oral presentation, Mypred Winter School on experimental models for hematopoiesis and leukemogenesis, Feldberg Falkau, Germany, 2024.
B. **L. Doll**, N. Aghaallaei, K. Welte, J. Skokowa, B. Bajoghli, '*A zebrafish model for JAGN1-associated severe congenital neutropenia*'. Poster presentation, Annual Meeting of the European Hematology Association (EHA), Frankfurt, Germany, 2023.
C. **L. Doll**, N. Aghaallaei, K. Welte, J. Skokowa, B. Bajoghli, '*A zebrafish model for severe congenital neutropenia (CN) with JAGN1-deficiency* '. Oral presentation, Annual Meeting of the German Society of Pediatric Oncology and Hematology (GPOH), Frankfurt, Germany, 2022.
D. **L. Doll**, N. Aghaallaei, K. Welte, J. Skokowa, B. Bajoghli, '*A zebrafish model for severe congenital neutropenia with Jagn1b-deficiency* '**.** Poster presentation, Annual meeting of the American Society of Hematology (ASH), Virtual Meeting, 2020. ASH Abstract Achievement Award.
E. **L. Doll**, N. Aghaallaei, K. Welte, J. Skokowa, B. Bajoghli, '*Modeling HAX1- and JAGN1-associated CN in zebrafish'*. Oral Presentation, 1st Early Career Investigators' Workshop (ECI) organized by our COST ACTION EuNet-INNOCHRON, Genova, Italy, 2020.
F. **L. Doll**, N. Aghaallaei, K. Welte, J. Skokowa, B. Bajoghli, '*Hax1 is indispensable for neutrophil development in zebrafish*'**.** Oral presentation, Annual meeting of the American Society of Hematology (ASH), Orlando, USA, 2019. ASH Abstract Achievement Award.
G. **L. Doll**, N. Aghaallaei, K. Welte, J. Skokowa, B. Bajoghli, '*Hax1 is indispensable for neutrophil development in zebrafish*'**.** Oral presentation, SCNIR Advisory Board meeting, Orlando, USA, 2019.
H. **L. Doll**, N. Aghaallaei, K. Welte, J. Skokowa, B. Bajoghli, '*A zebrafish model for severe congenital neutropenia with HAX1 deficiency*'. Annual Meeting of German Society of Hematology and Oncology (DGHO), Berlin, Germany, 2019.

1. INTRODUCTION

1.1. HEMATOPOIESIS OVERVIEW

Hematopoiesis is the process of blood cell development. In adults, a multipotent hematopoietic stem cell (HSC) in the bone marrow is the starting point, which gives rise to the different mature blood cell types. HSCs produce either oligopotent common lymphoid or myeloid progenitors. During lymphoid lineage commitment, hematopoietic stem cells differentiate into common lymphoid progenitors and then into B-, T-, and natural killer cells. During myeloid lineage commitment, HSCs differentiate into common myeloid progenitors (CMP) and then into platelets, macrophages, erythrocytes, and granulocytes[1,2] (FIGURE 1).

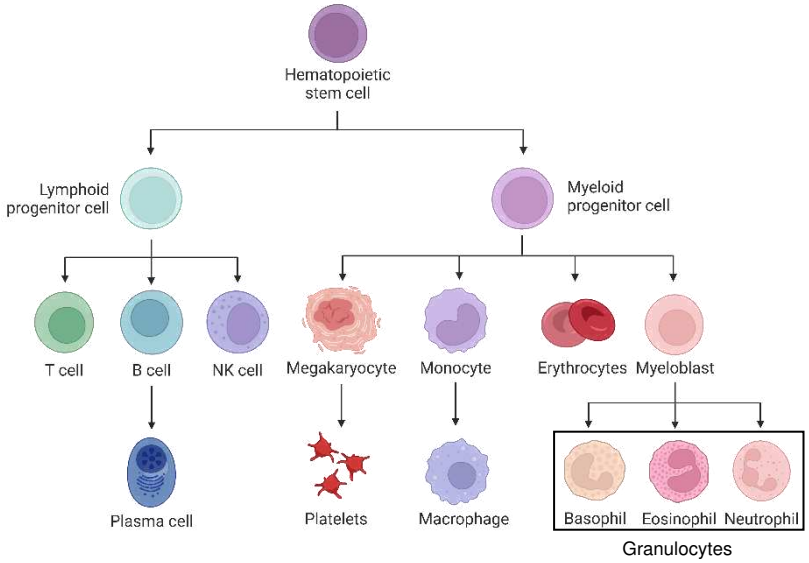

FIGURE 1. DEVELOPMENT OF THE DIFFERENT BLOOD CELL TYPES. ADAPTED AND SIMPLIFIED FROM 'A CLONOGENIC COMMON MYELOID PROGENITOR THAT GIVES RISE TO ALL MYELOID LINEAGES.' *NATURE* 404, 193-197 (2000). CREATED WITH BIORENDER.COM.

1.1.1. GRANULOPOIESIS

The process by which granulocytes are produced is called granulopoiesis. Granulocytes are essential cells from the innate immune system that play an important role in attacking pathogens, allergens, and other irritants that invade the body. Circulating granulocytes are characterized by specific granules in their cytoplasm and are divided into basophils, eosinophils, and neutrophils. In humans, neutrophils are the most frequent type of circulating leukocytes (white blood cells), accounting for between 50 and 70%, whereas in mice, neutrophils account for 10–25% of circulating leukocytes[3]. In contrast, in zebrafish, a relatively low number of neutrophils are found in circulation[4]. Neutrophil granulocytes present a characteristic multilobed nucleus and

cytoplasm filled with granules. Neutrophils are rapidly and constantly produced in the bone marrow. However, once neutrophils enter blood circulation, their half-life is only– 6-8 hours, resulting in a high neutrophil production rate[5]. Granulopoiesis is divided into two stages: granulocyte lineage determination and committed granulopoiesis[6].

1.1.1.1 Granulocyte lineage determination

Granulocyte lineage determination begins with hematopoietic stem cells, giving rise to an oligopotent common myeloid progenitor. This progenitor forms the foundation of the myeloid lineage of hematopoiesis. Subsequently, these progenitor cells transition to granulocyte-monocyte progenitors (GMP), which can give rise to myeloblasts, the first unipotent cell responsible for generating granulocytes[6,7] (**FIGURE 2**). Granulopoiesis is tightly regulated by several transcription factors activated by myeloid-specific growth factors. The transcription factor CCAAT enhancer-binding protein α (C/EBPα) primes the myeloid gene expression program at a very early stage of hematopoiesis and is necessary for the transition from CMP to GMP[8]. C/EBPα is considered the master regulator of granulopoiesis under normal conditions (steady-state granulopoiesis)[9,10]. Furthermore, regulation of the transcription factor PU.1 is essential for the transition from GMP to granulocytes or monocytes. High expression of the PU.1 coding gene SPI1 (Spi-1 proto-oncogene) leads to monocytic differentiation, whereas a low expression level leads to granulocytic differentiation[9]. These transcription factors are activated by the growth factors granulocyte-macrophage colony-stimulating factor (GM-CSF) and granulocyte colony-stimulating factor (G-CSF), which play an essential role in granulocyte lineage commitment[11].

1.1.1.2 Committed granulopoiesis

Committed granulopoiesis starts from the myeloblast and involves differentiation into mature granulocytes. Neutrophils are the most frequent granulocytes and our primary research focus; therefore, neutrophil differentiation is described next. Myeloblasts are characterized by a large oval nucleus and little cytoplasm with no granules. The next developmental stage is the promyelocyte, with an oval nucleus and more cytoplasm than the myeloblast, where the primary granules begin to develop[7]. Primary granules are the first to be synthesized and store the lysosomal protein myeloperoxidase (MPO) together with proteolytic mediators including azurocidin, cathepsin G, defensins, elastase, and proteinase-3[6,12]. During the next developmental step, the myelocyte

stage, the secondary granules are synthesized. The secondary granules, among others, contain collagenase, gelatinase, lactoferrin, lysozyme C (LYZ), and membrane receptors[6,12]. In the subsequent developmental stages, beginning with the myelocyte and progressing through the metamyelocyte and band cell, the nucleus undergoes a gradual size reduction and takes on a curved kidney-shaped appearance. During the metamyelocyte stage, the tertiary granules are produced with common granule content with secondary granules, including acyltransferase and cathepsin. The last step of maturation is the emergence of a segmented nucleus and the appearance of secretory vesicles. Secretory vesicles are essential for the delivery of membrane-associated receptors to the cell surface. After completing maturation, these cells are called polymorphonuclear neutrophils (PMN)[6,12] (**FIGURE 2**).

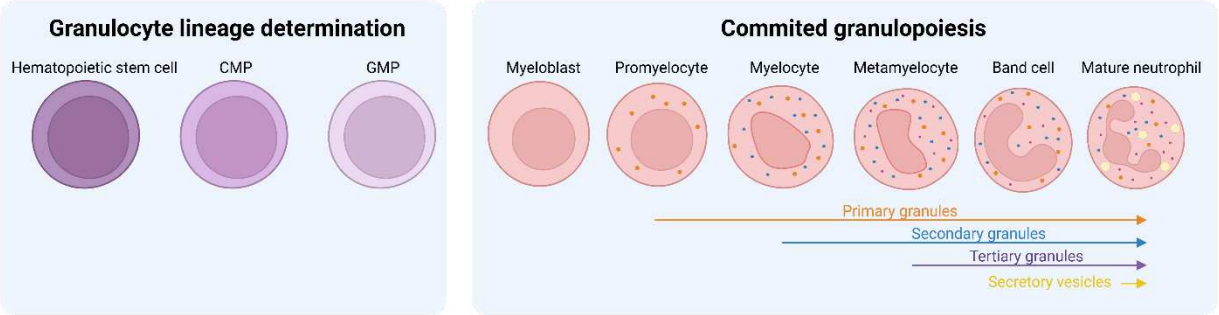

FIGURE 2. NEUTROPHIL DEVELOPMENT AND GRANULE FORMATION. ADAPTED FROM 'GRANULOPOIESIS AND GRANULES OF HUMAN NEUTROPHILS.' *IMMUNOL REV* 273, 11-28 (2016). CREATED WITH BIORENDER.COM.

PMNs are released from the bone marrow into the bloodstream. Neutrophils are the first line of defense against infections, including bacterial and fungal infections, before activation of humoral and cellular immune responses[13]. They also act as instructors of the immune system by recruiting and activating other immune cells[14]. Nevertheless, neutrophils are the first to migrate towards the site of infection from the hematopoietic tissue through the vasculature and exert their anti-pathogenic or proinflammatory roles by phagocytosis, neutrophil extracellular trap (NET) formation, reactive oxygen species (ROS) generation, and degranulation[14]. Upon external stimuli, neutrophil granules are mobilized in the opposite order of their formation, and secretory vesicles are mobilized to the cell surface first. The primary granules mainly release their content into phagolysosomes, which are formed by the fusion of primary granules and phagosomes that contain engulfed microorganisms[12]. These compartments provide confined spaces for toxic oxidative reactions that are designed to kill pathogens. Finally, the neutrophils also play a role in tissue repair and the resolution of inflammation by releasing factors promoting wound healing and removing cellular debris[14,15].

1.1.1.3 Steady-state and emergency granulopoiesis

The regular formation of granulocytes is known as steady-state granulopoiesis. Nevertheless, during infection or inflammation, the production rate of granulocytes is increased and accelerated. This process is referred to as emergency granulopoiesis. Neutrophils exhibit rapid daily homeostatic turnover. Thus, a delicate balance between granulopoiesis, bone marrow retention, release into circulation, and migration into peripheral tissues is essential. Neutrophil development can switch from steady-state to emergency granulopoiesis, and vice versa, depending on the presence of granulopoietic cytokines, such as G-CSF, and the activation of specific transcription factors such as C/EBPα or CCAAT enhancer-binding protein β (C/EBPβ)[10,16]. Under normal conditions in steady-state granulopoiesis, *CEBPA* expression actively limits the proliferation of HSCs by inhibiting the activity of cyclin-dependent kinases (CDK) 2 and 4, which are essential for the cell cycle[10,17]. In response to infection or inflammation, emergency granulopoiesis is activated, which increases the number of circulating neutrophils. The transcription factor C/EBPβ is a key regulator of this type of granulopoiesis. C/EBPα and C/EBPβ share many common targets associated with granulocytic differentiation, excluding C/EBPα targets that affect cell proliferation. The activation of C/EBPβ allows the proliferation of granulocytic progenitors, increasing neutrophils in blood circulation[16]. Under normal conditions, the level of G-CSF in circulation is very low but is rapidly elevated under different circumstances, such as infection, inflammation, or stress, activating emergency granulopoiesis through the JAK-STAT pathway, triggering *CEBPB* expression[12,18].

1.2. NEUTROPENIA

Neutropenia is a condition defined by a reduced number of neutrophils. It can be graded depending on the number of circulating neutrophils as mild (1000-1500 cells/µl), moderate (500-1000 cells/µl), or severe (< 500 cells/µl)[19]. This condition can also be classified according to its origin as acquired or congenital. Depending on etiology and underlying pathology, acquired neutropenia can be divided into nutrition-related, infection-related, drug-induced, chronic idiopathic, and immune-associated neutropenia[20]. The focus of this work lies on severe congenital neutropenia (CN).

1.2.1. SEVERE CONGENITAL NEUTROPENIA

Severe congenital neutropenia is characterized by a profound deficiency of neutrophils that leads to life-threatening infections starting from birth. This disease is a rare genetically heterogeneous condition with an estimated prevalence of 1–8.5 cases per million individuals, depending on geographic region and ethnic background[21-24]. CN is caused by germline mutations in various genes, including *ELANE, HAX1, JAGN1, and COPZ1,* among others (**FIGURE 3**).

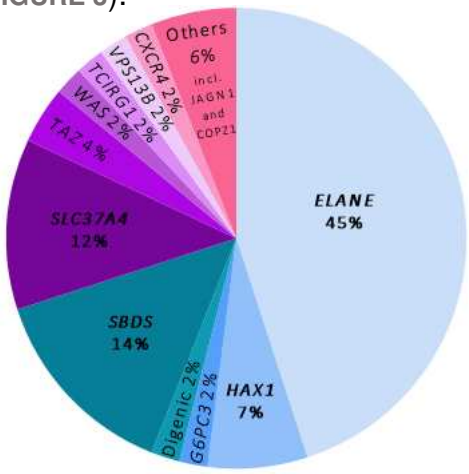

FIGURE 3. SEVERE CONGENITAL NEUTROPENIA-CAUSING MUTATED GENES. ADAPTED FROM 'SEVERE CONGENITAL NEUTROPENIAS.' *NAT REV DIS PRIMERS* 3, 17032 (2017).

The type of inheritance (autosomal dominant or recessive) depends on the mutated gene. Mutations in genes with autosomal dominant inheritance seem more prevalent worldwide, whereas mutations in genes with autosomal recessive inheritance are typically diagnosed in consanguineous populations[24]. Regardless of the neutropenia-causing mutation, most patients show maturation arrest of granulopoiesis at the promyelocytic stage[24]. In addition to neutropenia, individuals with CN may exhibit various hematopoietic or extra-hematopoietic symptoms, and the specific symptoms can differ depending on the mutation involved and the individual patient. Currently, the treatment of choice for neutropenia is the daily administration of recombinant human G-CSF (rhG-CSF), which induces compensatory granulopoiesis by activating c/EBPβ-dependent emergency granulopoiesis[18,25]. Although rhG-CSF treatment has significantly enhanced the quality of life of individuals with CN, some patients do not respond to rhG-CSF doses as high as 50µg/kg/day[26]. This leaves them with no alternative treatment, except for bone marrow transplantation. Furthermore, around 20% of CN patients eventually develop myelodysplasia (MDS) or acute myeloid leukemia (AML)[27,28]. These circumstances emphasize the urgent need for alternative therapeutic approaches.

Some patients develop CN caused by unknown mutations. Our laboratory recently discovered a new gene, *COPZ1*, coding for the COPI coat complex subunit zeta 1, which, upon mutation, can lead to neutropenia. HAX1, JAGN1, and COPZ1 and their role in granulopoiesis and CN upon mutation will be further described below.

1.2.1.1 HCLS1-associated protein X-1 (HAX1)

HAX1 is a ubiquitously expressed protein, localized mainly in the mitochondria, but also in the endoplasmic reticulum (ER) and nucleus. This protein plays a role in various biological functions such as neutrophil development, apoptosis, and regulation of the actin cytoskeleton among many others[29]. It accomplishes this by serving as an adaptor protein in conjunction with HCLS1 (hematopoietic cell-specific lyn substrate 1), downstream of the G-CSFR pathway (FIGURE 4), for neutrophil development[30,31], with HTRA (high-temperature requirement A serine peptidase) and PARL (presenilin-associated rhomboid-like protein) for apoptosis[32], and with PKD2 (polycystin-2) and cortactin for actin cytoskeleton regulation[33].

In the G-CSFR pathway, HAX1 binds to phosphorylated HCLS1. This complex recruits the transcription factor LEF-1 (lymphoid enhancer-binding factor 1) and transports it into the nucleus. In the nucleus, LEF-1 activates the transcription of essential granulopoiesis factors such as *CEBPA* and *HCLS1* and autoregulates itself (FIGURE 4). Autosomal recessive loss-of-function mutations in *HAX1* cause severe congenital neutropenia. HAX1 deficiency is associated with an impaired G-CSF signaling pathway[31]; by losing the functional HAX1, the HCLS1-HAX1-LEF-1 complex cannot be properly formed, LEF-1 cannot be adequately transported to the nucleus, and thus, C/EBPα-triggered granulopoiesis cannot be initiated. Additionally, lack of HAX1 leads to altered mitochondrial membrane potential[34] and elevated apoptosis of myeloid progenitor cells[34,35].

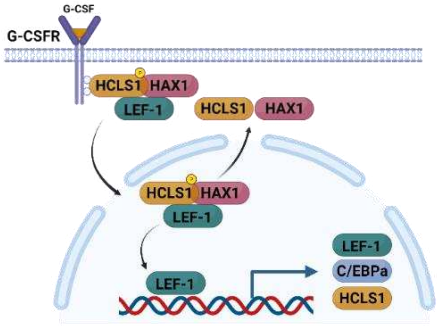

FIGURE 4. THE ROLE OF HAX1 DOWNSTREAM THE G-CSFR SIGNALING. ADAPTED FROM 'INTERACTIONS AMONG HCLS1, HAX1 AND LEF-1 PROTEINS ARE ESSENTIAL FOR G-CSF-TRIGGERED GRANULOPOIESIS'. *NAT MED* 18, 1550-1559 (2012). CREATED WITH BIORENDER.COM.

In addition to severe neutropenia, some CN patients with *HAX1* mutations may experience neurological symptoms such as mental and psychomotor retardation and seizures. The symptoms and severity depend on the location of the mutation in the *HAX1* gene and vary among individuals[36].

1.2.1.2 Jagunal homolog 1 (JAGN1)

JAGN1 is also a ubiquitously expressed protein. It is considered an ER-membrane binding protein with four transmembrane domains, while the N- and C-terminal domains extend into the cytoplasm[37]. This protein is evolutionarily highly conserved, from *Drosophila melanogaster*, where it was originally discovered[38], to humans. Despite this remarkable evolutionary stability, the precise function of the JAGN1 protein remains unknown. In *Drosophila melanogaster*, the *JAGN1* orthologous gene *jagunal* is involved in various cellular processes. These processes include vesicular trafficking during oogenesis[38], and asymmetric ER partitioning and spindle orientation in embryonic neuroblasts[39]. Additionally, it has been proposed that Jagunal plays a role in the signaling and distribution of ER membranes in *D. melanogaster* stem cells as they determine their fate[40].

JAGN1 mutations have been described in rare cases of CN. Several autosomal recessive mutations of this gene can lead to neutropenia[41]. The majority of mutations affect the highly conserved N-terminal coding domain, although some also target the transmembrane and C-terminal domains (FIGURE 5).

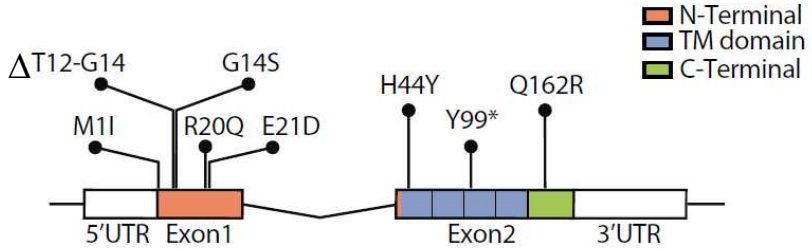

FIGURE 5. CN-CAUSING MUTATIONS IN *JAGN1*. *BASED ON THE DATA FROM* 'JAGN1 DEFICIENCY CAUSES ABERRANT MYELOID CELL HOMEOSTASIS AND CONGENITAL NEUTROPENIA.' *NAT GENET* 46, 1021-1027 (2014).

JAGN1-associated CN patient cells displayed abnormalities in the ER ultrastructure and a decrease in the amount of granules[41]. Furthermore, *JAGN1* deficiency is linked to aberrant G-CSFR signaling pathway and G-CSFR glycosylation[41]. Moreover, mutations in *JAGN1* affect NET formation[42], MPO levels[42], and activation of apoptosis[41]. In addition to severe neutropenia, patients with *JAGN1* mutations may have extra-hematopoietic symptoms such as short stature, scoliosis, pancreatic insufficiency, and bone abnormalities. The presence of symptoms and their severity

depend on the mutation position and vary among individuals[41]. The mechanism underlying the development of neutropenia downstream of *JAGN1* mutations remains poorly understood and requires further elucidation.

1.2.1.3 COPI coat complex subunit zeta 1 (COPZ1)

Severe congenital neutropenia is a genetically heterogeneous disease. Despite the discovery of many implicated genes (**FIGURE 3**), the genetic etiology is still unclear in many cases. We need in-depth genomic analyses to discover new mutations implicated in neutropenia development. One of the mutated genes involved in neutropenia development discovered in our laboratory is *COPI coat complex subunit zeta 1* (*COPZ1)*. COPZ1 is a member of the coatomer protein I (COPI) complex, which plays an essential role in vesicular trafficking within the Golgi complex and from the Golgi back to the ER (retrograde transport)[43]. The COPI complex is composed of seven subunits, namely α, β, β', γ, δ, ε, and ζ (or zeta)[43]. It was previously described that JAGN1 interacts with COPα, COPβ', and COPγ [41], linking JAGN1 directly with the COPI complex. Three CN patients from two independent families carrying a homozygous mutation in *COPZ1* were discovered. *COPZ1* mutations either lead to a truncated protein at amino acid position 141 (p.Gln141*) or a missense mutation at position 132 (p.Gly132Arg). Besides severe neutropenia, these patients suffered from other hematopoietic and extra-hematopoietic symptoms such as lymphopenia or autistic behavior disorder with mental retardation. The symptoms and disease severity varied among these three patients. Nothing is known about the role of COPZ1 in granulopoiesis and neutropenia pathogenesis.

1.3. ZEBRAFISH AS A MODEL SYSTEM FOR NORMAL AND MALIGNANT GRANULOPOIESIS

The zebrafish, *Danio rerio*, has been established as a powerful and widely used model system. Many of the mechanisms involved in granulopoiesis are conserved between this model system and humans. Zebrafish produce neutrophils during primitive and definitive hematopoiesis. The primitive wave occurs within 24 hours post-fertilization (hpf), after which blood circulation starts. The first primitive neutrophils are produced in the rostral blood island (RBI)[44], followed by a transient wave of neutrophils derived from erythromyeloid progenitors (EMP) in the posterior blood island (PBI)[45,46]. At definitive hematopoiesis, neutrophils arise from HSCs that reside in the ventral wall of

the dorsal aorta (VDA), the mammalian equivalent of the aorta-gonad-mesonephros[46,47]. These HSCs subsequently migrate to the caudal hematopoietic tissue (CHT), which corresponds to the fetal liver in mammals and becomes the primary site for neutrophil production during larval development (**FIGURE 6**). The neutrophils generated from CHT are considered to be similar to the neutrophils produced by adult definitive hematopoiesis[48]. At five days post fertilization (dpf), the HSCs arrive at the kidney marrow, the mammalian equivalent of the bone marrow. Once established in the kidney, these self-renewing HSCs maintain the production of myeloid, erythroid, and lymphoid lineages throughout the zebrafish's life, supporting definitive adult hematopoiesis.[44,46].

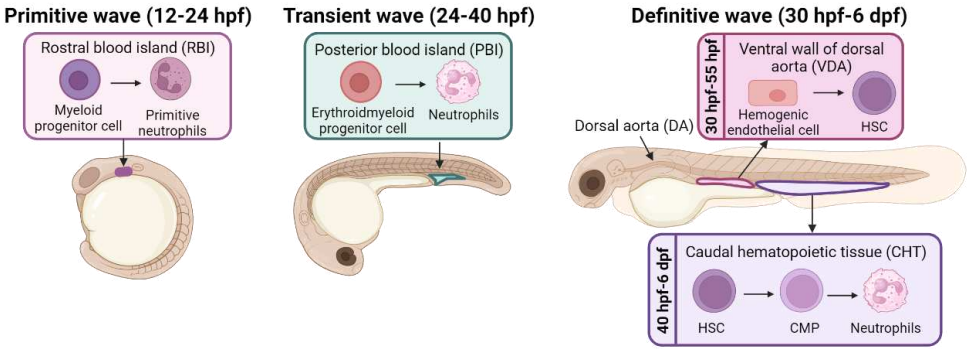

FIGURE 6. ZEBRAFISH EMBRYONIC GRANULOPOIESIS. ADAPTED FROM 'OPPORTUNITIES PRESENTED BY ZEBRAFISH LARVAL MODELS TO STUDY NEUTROPHIL FUNCTION IN TISSUES.' *INT J BIOCHEM CELL BIOL* 148, 106234 (2022). CREATED WITH BIORENDER.COM.

The zebrafish has been established as an essential model organism for studying normal and malignant hematopoiesis[44,49,50]. Its fully sequenced genome shares approximately 70% of the genes with humans[51], making it an effective model for human genetic diseases. Zebrafish can easily be genetically modified using gain- or loss-of-function techniques. Gain-of-function studies can be performed using different approaches. One approach involves the overexpression of a gene of interest (GOI), often through microinjection of messenger RNA (mRNA) coding either the wild-type (wt) or the protein with a specific mutation. With this approach, the GOI is overexpressed in the whole embryo[52]. Transient transgenic approaches are used to overexpress a gene in a tissue- or cell-specific manner. For this purpose, a plasmid coding the GOI (wt or mutated) under the control of a specific promotor is injected into the one-cell stage and is integrated into the genome through, e.g., the Tol2 transposon system[53]. This technique can also be used with an inducible promotor, e.g., by heat[54]. Creating a stable transgenic line is also possible if the integrated construct is transmitted to the next generation. Loss-of-function studies are mainly performed using

either antisense morpholino oligonucleotides (MO) or CRISPR/Cas9-induced knockout. Morpholinos are designed to bind to the mRNA on the start codon, blocking the translation (ATG-morpholino) or at the exon-intron junction, avoiding splicing and leading to intron retention (splicing morpholino). This results in no or most probably truncated and non-functional proteins, respectively[55,56]. The CRISPR/Cas9 technique is a genome engineering tool that uses guide RNAs to direct the Cas9 endonuclease towards a gene-specific loci to create a double-strand break. With the induction of the DNA repair mechanism, small insertions or deletions (Indels) can occur. In the case of CRISPR/Cas9-induced knockouts, the Indels lead to gene disruption. The knockout can be transient and mosaic if CRISPR/Cas9 components are injected into the one-cell stage. However, the knockout is considered stable if the gene disruption is inherited across generations[57].

Another benefit of the zebrafish is its external fertilization and high number of offspring, making it an ideal model system for large-scale genetic studies and drug screening[58]. Combining these features with the use of transgenic (tg) reporter lines, fluorescent reporters under the regulation of cell- or tissue-specific expressing promotors, allows us to study the effects directly on specific cell types or tissues. Several transgenic reporter lines have been developed to study granulopoiesis and visualize neutrophils. These reporter lines include tg(mpo:*gfp*)[59] and tg(lyz:*DsRed*)[60], where the green fluorescent protein (GFP) or red fluorescent protein (DsRed) are expressed under the control of the neutrophil-specific promotors mpo or lyz, respectively. Using these lines, the effect on neutrophil counts and functionality, including migration and phagocytosis, upon genetic manipulation or treatment can be studied *in vivo*.

Other complementary techniques to stain and study neutrophils are Sudan black staining[61], which primarily stains the neutrophil granules, and whole-mount *in situ* hybridization (WISH) for neutrophil-specific genes, e.g., *mpo* and *lyz*. WISH is a widely used technique for studying specific genes' spatial and temporal expression patterns based on a digoxigenin-labeled gene-specific probe[62]. This technique is also used to analyze other hematopoietic cells evaluating the expression pattern of cell-specific genes, including *cmyb* for hematopoietic stem and progenitor cells (HSPCs)[49,63,64], *spi1 proto-oncogene b* (*spi1b)* for early myeloid progenitors[49,65], *GATA-binding protein 1a* (*gata1a*) and *hemoglobin, alpha embryonic 1.1* (*hbae1.1)* for erythrocytes[49,66] and *macrophage-expressed gene 1.1* (*mpeg1.1)* for macrophages[49,67].

In recent years, zebrafish have become a popular alternative model for studying severe congenital neutropenia. Several CN models recapitulating patients' phenotypes have been developed, including zebrafish deficient in *g-csfr*[68,69], *srp54*[70,71], *sbds*[72], *g6pc3*[73], *or taz*[74].

2. AIMS OF THE STUDY

This study's principal aim was to develop three gene-specific severe congenital neutropenia (CN) zebrafish models: *HAX1*-CN, *JAGN1*-CN, and *COPZ1*-CN. These three models were used to analyze the pathomechanisms underlying neutropenia development upon mutation of the studied genes. Different hypotheses have been described, including the activation of unfolded protein response, increased apoptosis of myeloid progenitors, and impaired G-CSFR signaling, and we studied these hypotheses using the generated CN zebrafish models.

No faithful *in vivo* models have been established before for these CN-causing genes. Hax1-deficient and Jagn1-deficient mice are both prematurely lethal and don't display neutropenia. The involvement of the COPZ1 mutation in CN development was described by us very recently, and no mouse model has been established yet. The zebrafish is an ideal vertebrate *in vivo* model for studying normal and malignant granulopoiesis. This model system can bridge the gap between *in vitro* analyses and clinical observations.

This study's secondary aim was to discover alternative therapies for CN using the established zebrafish CN models. The objective was to use candidate drugs selected based on their capacity to reverse the altered signaling pathways found *in vitro*, test their efficiency on the zebrafish CN models, and understand their underlying mechanism of action.

3. RESULTS & DISCUSSION

3.1. DEVELOPMENT OF A *HAX1*-ASSOCIATED CN ZEBRAFISH MODEL

Covered in the published manuscript:

A. L. Doll, N. Aghaallaei, A.M. Dick, K. Welte, J. Skokowa, B. Bajoghli, '*A zebrafish model for HAX1-associated congenital neutropenia*.' *Haematologica* 2021;106(5):1311-1320.

HAX1 is the most common mutated gene in CN patients after *ELANE*. Establishing a *HAX1*-associated CN mouse model was unsuccessful. *Hax1*$^{-/-}$ mice suffer postnatal lethality due to neuronal apoptosis and display normal granulopoiesis[75]. Thus, our current insights are primarily derived from clinical observations and *in vitro* experiments directly from primary patient samples or model systems as *in vitro* neutrophil differentiation of patient-derived induced pluripotent stem cells (iPSCs)[76,77]. However, to completely elucidate the function of HAX1 in granulopoiesis and identify novel treatment strategies, the field desperately needs a suitable *in vivo* model.

In our study, we aimed to develop a zebrafish model for *HAX1*-associated CN. Our phylogenetic and gene synteny analyses proved high conservation of HAX1 during evolution, including its presence in zebrafish. In humans, *HAX1* is ectopically expressed among tissues, and its function depends on the interaction partner present[29]. To study the spatial expression of *hax1* in zebrafish, we performed whole-mount *in situ* hybridization in different developmental stages. We observed an ectopic expression of *hax1* during early embryonic development (5 and 11hpf) and a hematopoietic tissue-specific expression at 20 hpf. We confirmed the expression in the hematopoietic tissue with double fluorescent *in situ* hybridization against *hax1* and the HSPC marker *cmyb.* Furthermore, we saw *hax1* expression in hematopoietic tissue in later stages of development, including 24 and 48hpf. Moreover, two single-cell RNA-sequencing databases of adult zebrafish whole kidney marrow, akin to mammalian bone marrow, confirmed *hax1* expression in different hematopoietic cells, including neutrophils[78,79].

Some *HAX1*-associated CN patients, besides severe neutropenia, display neurological defects. In humans, it is known that HAX1 has different isoforms generated by

alternative splicing, and an isoform-dependent genotype-phenotype association is described. Two variants play a significant role: the full-length variant, including all exons (variant 1), and the alternative variant, with a shortened exon 2 (variant 2). Most CN-causing mutations are localized in exon 2, and the patient's symptoms vary depending on the affected isoforms[36,80]. If the mutation is localized on the part of exon 2 missing in variant 2, the CN patients develop severe neutropenia without neurological defects. When the mutation is localized in the portion of exon 2 present in both isoforms, the patient will develop neurological impairments besides severe neutropenia. This is due to the high expression of variant 2 in the brain[36,80]. In contrast, we only found one *hax1* variant in zebrafish by amplifying and sequencing the Hax1 coding region in cDNA obtained from 2dpf wild-type embryos. However, at 96hpf, we observed *hax1* expression in the liver, intestine, and, more importantly, in the optic tectum of the brain. Interestingly, the optic tectum, akin to the superior colliculus in mammals, is one of the most conserved sections of the vertebrate brain across species, and in zebrafish, it is a region where neurogenesis persists throughout life[81]. The high *hax1* expression in the brain hints at its importance in zebrafish. Hax1 mutation may also affect normal neurological development in zebrafish. Our primary focus was hematopoiesis, but this model could also be used to study its effects on the brain and other organs, such as the liver and intestine.

We proceeded to study the role of Hax1 in hematopoiesis by interfering with its function. We used two approaches: a morpholino-based knockdown strategy and a transient CRISPR/Cas9-induced knockout. Morpholinos are synthetically synthesized antisense oligos that bind to the mRNA. In our approach, we used three different morpholinos: one ATG-morpholino (atg-MO), which binds to the start codon, avoiding the translation of the mRNA into protein, and two splicing morpholinos, which bind to the exon-intron splicing site of exon1-intron1 (e1-MO) and exon2-intron2 (e2-MO). After morpholino microinjection into the blastomere of zebrafish embryos, both splicing morpholinos led to partial or total intron retention. The sequence analyses showed the presence of multiple stop codons in the retained intron sequence, which most probably led to the translation of a truncated Hax1 protein. Moreover, quantitative analyses showed that the expression levels of wild-type *hax1* were reduced by up to 90% in e1-MO injected and up to 70% in e2-MO injected embryos. To analyze whether the interference with Hax1 function affected granulopoiesis, we performed whole-mount *in*

situ hybridization against the neutrophil marker gene *myeloperoxidase* (*mpo*) in 1dpf embryos. Then, we quantified the number of *mpo*$^{+}$ neutrophils in the hematopoietic tissue of uninjected wild-type embryos and compared them with atg-MO, e1-MO, and e2-MO injected embryos (hereafter called morphants). The number of neutrophils was significantly reduced in the morphants compared to their wild-type siblings. Moreover, the morpholinos were also injected in embryos from the tg(mpo:*gfp*) transgenic reporter line, where *gfp* is expressed under the control of the mpo promotor, resulting in GFP^{+} neutrophils. After quantifying mpo:*gfp*$^{+}$ neutrophils of 48hpf wild-type embryos and morphants, previous results were confirmed, and we saw a significant reduction in the neutrophil counts in the morphants compared to the wild-type embryos. To test whether the *hax1*-knockdown-induced neutropenia phenotype was specifically due to the disruption of Hax1 function, we overexpressed full-length wild-type *hax1* in the e1-MO and e2-MO morphants with tg(mpo:*gfp*) background. The presence of wild-type Hax1 restored the neutropenia phenotype. Furthermore, to rule out that the injection had a negative effect on neutrophil development, we injected control morpholino into tg(mpo:*gfp*) embryos. After quantification of mpo:*gfp*$^{+}$ neutrophils in control morpholino-injected embryos and wild-type controls, we saw no significant differences between the neutrophil counts. Therefore, we concluded that the injection process itself does not affect neutrophil development. As proof of principle, we induced a transient *hax1* knockout using CRISPR/Cas9 in tg(mpo:*gfp*) embryos. We saw fewer mpo:*gfp*$^{+}$ neutrophils in the CRISPR/Cas9-injected embryos compared to the uninjected littermates. Altogether, these results show that the reduction of neutrophils is a consequence of Hax1 function interference, highlighting the essential role of Hax1 in neutrophil development.

It is known that HAX1 plays an essential role in migration and chemotaxis in neutrophils[82]. Therefore, we proceeded to analyze the neutrophil functionality upon *hax1* knockdown in zebrafish. For this purpose, we injected fluorescent-labeled bacterial debris, more specifically Alexa594-conjugated *Staphylococcus aureus,* into the notochord of 2dpf tg(mpo:*gfp*) wild-type embryos and e1-MO morphants. Two hours later, we observed the migratory and phagocytic capacity of the neutrophils using confocal microscopy. We analyzed whether the mpo:*gfp*$^{+}$ neutrophils migrate towards the infection site with fluorescent-labeled bacteria debris and phagocyte them. We saw no significant difference in migration behavior or phagocytic activity after comparing

wild-type neutrophils with the remaining neutrophils in *hax1* morphants. We cannot guarantee that the remaining neutrophils have an impaired Hax1 function because by using a morpholino-based knockdown, there is still a remaining portion of wild-type Hax1. However, the e1-MO efficiency was very high, resulting in a 90% reduction of *hax1* expression, indicating a substantial likelihood of impaired Hax1 function. Altogether, the *hax1* knockdown did not affect the functionality of the remaining neutrophils.

Based on single-cell RNA sequencing databases of zebrafish hematopoietic cells, *hax1* is also expressed in other blood cell types[78,79]. Thus, we examined the effect of *hax1* knockdown on other immature and mature blood cells. In pursuit of this aim, we performed WISH against different hematopoietic cell-specific marker genes in *hax1* morphants and wild-type embryos. To study immature cells, we examined HSPCs using *cmyb* and early myeloid progenitors using *spi1b* (Pu.1) in 2dpf embryos. No significant differences were observed in the expression pattern of both early hematopoiesis marker genes after *hax1* knockdown. Next, we studied the effect on other mature myeloid cells. We used *gata1a* and *hbae1.1* as marker genes to examine the impact on erythrocytes. WISH analyses showed no detectable differences in the expression patterns of both erythroid markers in the morphants compared to wild-type embryos at 1 dpf. These results and the presence of circulating red blood cells in the morphants during various developmental stages suggest that Hax1 does not play a critical role in embryonic erythropoiesis. We also evaluated different marker genes to study the effect on macrophages, including *mpeg1.1*, *csf3r*, and *lcp* (*l-plastin*). While *mpeg1.1* is a specific marker for macrophages, *csf3r,* and *lcp* are expressed in macrophages and neutrophils. By comparing the expression patterns of these genes in wild-type embryos and *hax1* morphants, we found no significant differences in the number of *mpeg1.1*$^{+}$ macrophages. Still, the numbers of *csf3r*$^{+}$ and *lcp*$^{+}$ cells were significantly reduced in the morphants. These results suggest that the interference with Hax1 function does not affect monopoiesis, and the reduced numbers of *csf3r*$^{+}$ and *lcp*$^{+}$ cells only confirm the reduction in neutrophils. Moreover, we studied the expression of the neutrophil marker *lyz* (*lysozyme C)* and confirmed once again the reduction of neutrophils upon *hax1* knockdown. In conclusion, these results suggest that loss-of-function of Hax1 leads to neutropenia without affecting other hematopoietic cells, mimicking *HAX1*-associated CN patients' phenotype.

Once this promising *in vivo* model for the research of *HAX1*-associated CN was established, we proceeded to study the underlying pathomechanism of neutropenia. HAX1 is described as an anti-apoptotic protein[29], and the apoptosis of myeloid precursor cells could be the underlying mechanism of the disease[83]. To address whether Hax1 loss-of-function influenced apoptosis, we used three different approaches. First, a terminal deoxynucleotidyl transferase dUTP nick end labeling (TUNEL) assay was performed to detect apoptotic cells in wild-type, control morpholino injected embryos, and *hax1* morphants. Compared to their wild-type counterparts and control-morpholino-injected embryos, *hax1* morphants had an increased number of apoptotic cells at 1dpf. By 2dpf, the number of apoptotic cells was comparable between the uninjected and *hax1* morphants. As a second approach, we used the vital fluorescent dye acridine orange, which labels apoptotic cells. The incubation of wild-type embryos and *hax1* morphants in acridine orange reproduced the result obtained by the TUNEL assay. Independent of the used approach, the apoptotic cells were distributed throughout the embryo and not restricted to the hematopoietic tissue. To examine more closely if the neutrophils or progenitors entered apoptosis upon *hax1* knockdown, we incubated wild-type and *hax1* e1-MO injected tg(lyz:*DsRed*) embryos with a caspase 3/7 reporter. This reporter produces a green fluorogenic signal upon cleavage by activated caspase-3 or caspase-7. Using confocal imaging, we analyzed whether lyz:*DsRed*$^{+}$ neutrophils entered apoptosis and saw that the frequency of apoptotic neutrophils was comparable between wildtype and *hax1* morphants at 2dpf. Altogether, this data showed that the interference with Hax1 function leads to an increase in apoptotic cells, but only in early developmental stages and not in a hematopoietic tissue-specific manner. The anti-apoptotic function of HAX1 was already described[29]. Nevertheless, our data contradicts the assumption that the underlying pathomechanism of neutropenia is the apoptosis of myeloid progenitor cells[83]. We were able to show that the number of apoptotic myeloid progenitors did not increase upon *hax1* knockdown using the caspase 3/7 reporter in tg(lyz:*DsRed*) embryos. The expression of *lyz* starts as soon as the promyelocytic stage. Therefore, the analyzed lyz:*DsRed*$^{+}$ cells include immature and mature neutrophils. Furthermore, mice lacking *Hax1* show neuronal apoptosis without showing effects on granulopoiesis[75]. All these data together suggest that the impaired anti-apoptotic function of HAX1 may play a role in the development of neurological symptoms in some *HAX1*-associated CN

patients but is not the underlying cause of neutropenia development. Furthermore, we analyzed the proliferation by performing immunostaining against the proliferation marker phospho-histone H3 (pH3). The comparison of the overall proliferation in the tail region of 2dpf wild-type embryos and *hax1* morphants showed no significant difference. Therefore, the *hax1* knockdown did not affect the proliferation capacity of the cells.

Another described function of HAX1 is its role as an adapter protein in the G-CSFR pathway[31]. The impaired signal transduction of this pathway is described in *HAX1*-associated CN patients[31]. Therefore, we proceeded to study the G-CSFR pathway in our zebrafish model. The conservation of the G-CSFR pathway and its role in granulopoiesis in zebrafish was previously described[68,84,85]. To study the effect of overexpression of *g-csfa* (zebrafish ortholog of G-CSF) on granulopoiesis in wildtype and *hax1* morphants, we used a bi-directional heat-inducible plasmid[54], coding *g-csfa* and *gfp* sequences. This plasmid was injected into zebrafish blastomere alone or in combination with *hax1* e1-MO. At 21hpf the expression of the *g-csfa* and the marker gene *gfp* was induced by heat shock (1h 39°C). Then, the GFP$^+$ embryos were selected for WISH staining for the neutrophil marker *mpo* at 1dpf. The GFP signal was a marker for successful plasmid integration and gene expression; thus, the GFP$^+$ embryos overexpressed *g-csfa*. The analysis and quantification of *mpo*$^+$ neutrophils confirmed that the overexpression of *g-csfa* induced granulopoiesis in wild type, leading to higher numbers of neutrophils than in uninjected embryos. Additionally, the overexpression of *g-csfa* in *hax1* morphants rescued the neutropenia phenotype, similar to *HAX1*-associated CN patients treated with rhG-CSF. To further study the effects of *hax1* knockdown on G-csfr signaling, we analyzed the effect on the downstream key regulator of steady-state granulopoiesis, *cebpa*. First, we measured the expression level using real-time quantitative polymerase chain reaction (RT-qPCR) and saw a significant reduction in expression upon *hax1* knockdown. Then, we quantified the number of *cebpa*-expressing cells using WISH in wild-type embryos and *hax1* morphants. The quantitative analysis showed a decrease in the number of *cebpa*-expressing cells after *hax1* downregulation. Furthermore, we saw a reduced expression level of the G-csfr downstream target, *hcls1*. These results argue for an impaired steady-state granulopoiesis upon *hax1* knockdown. In agreement with our data, previous studies showed the downregulation of *CEBPA* and *HCLS1* expression

in *HAX1*-associated CN patient cells[31]. It is also known that the key regulator of steady-state granulopoiesis C/EBPα regulates *CSF3R* expression[86]. This positive feedback loop seems evolutionarily conserved between zebrafish and humans[85]. Zebrafish Cebpa mutants display a reduced *csf3r* expression[87]. Moreover, our data suggest an indirect hint of this regulation by fewer *csf3r*$^{+}$ cells and a decreased expression level of *cebpa* upon *hax1* downregulation. Furthermore, we analyzed the expression level and expressing cells of the key regulation of emergency granulopoiesis, *cebpb.* Interestingly, we observed an increase in the expression level and *cebpb*-expressing cell numbers upon interfering with Hax1 function, arguing for an active emergency granulopoiesis. Upon rhG-CSF stimulation, *CEBPB* expression is also upregulated in *HAX1*-associated CN patients[88]. Altogether, this data indicates that the underlying pathomechanism downstream of mutated HAX1 could be an impaired steady-state granulopoiesis due to an inefficient G-CSFR signaling pathway. It is, however, important to consider that we did not assess the effect of *hax1* knockdown directly on *hax1*-deficient neutrophils, and our data can't rule out the possibility that the effects we see are due to an altered cell number rather than changed expression in each cell. Nevertheless, our results strongly suggest an altered G-csfr signaling.

To conclude, we have successfully established a promising *in vivo* CN model that mimics the phenotype of *HAX1*-associated CN patients and can be used to investigate further the pathomechanism, study the effect of HAX1-deficiency on other organs, discover new therapeutic targets for *HAX1*-associated CN patients, and perform drug screening. Furthermore, a stable Hax1-deficient zebrafish line will help to investigate the role of Hax1 alone and in combination with other leukemia-associated gene mutations in MDS development and leukemogenesis.

3.2. DEVELOPMENT OF A *JAGN1*-ASSOCIATED CN ZEBRAFISH MODEL

Covered in the published manuscript:

B. L. Doll, K. Welte, J. Skokowa, B. Bajoghli, '*A JAGN1-associated severe congenital neutropenia zebrafish model revealed an altered G-CSFR signaling and UPR activation.' Blood Adv* 2024; 8 (15): 4050–4065.

Different autosomal recessive mutations in *JAGN1* can cause severe congenital neutropenia. The mechanism underlying neutropenia development downstream of

JAGN1 mutations is still poorly understood. The rarity of the cases and the absence of an *in vivo* model hinders this understanding. *Jagn1*$^{-/-}$ mice are embryonically lethal, while the conditional knockout in mouse hematopoietic cells does not affect neutrophil counts[89]. The development of an alternative *in vivo* model is essential to study the role of JAGN1 in granulopoiesis and the effects of the *JAGN1* mutations on neutrophil development.

Phylogenetic and syntenic analyses revealed a high conservation of JAGN1 during evolution, starting from *Drosophila melanogaster*, where it was initially discovered[38], until humans. However, zebrafish have two *JAGN1* paralogs: *jagn1a* and *jagn1b*. Different RNA single-cell sequencing databases[78,79] of adult kidney marrow, akin to human bone marrow, show differential expression of both paralogs among the hematopoietic cells. *Jagn1b* seems ectopically expressed among the different blood cell types, especially in macrophages and neutrophils. Meanwhile, *jagn1a* expression appears to be limited to macrophage-myeloid progenitors and macrophages. Furthermore, a comparison of the transcriptome dataset of HSPC (marked by *draculin* expression) with niche cells showed that *jagn1a* was not expressed in HSPCs or the niche, while *jagn1b* was expressed in both cell compartments[90]. The expression of the paralogs was then analyzed in sorted neutrophils of 5dpf embryos, where *jagn1a* RNA was not detectable with RT-qPCR. Moreover, we studied the presence of Jagn1 protein in zebrafish neutrophils using whole-mount double immunostaining of tg(mpo:*gfp*) zebrafish embryos with α-GFP, labeling the neutrophils, and the human α-JAGN1 antibody. With this experiment, we demonstrated that Jagn1 is present in zebrafish neutrophils. Unfortunately, the α-JAGN1 antibody binds to the first 40 amino acids, which are remarkably conserved between species and very similar between Jagn1a and Jagn1b. Therefore, we could not distinguish between the presence of the Jagn1 paralogs. Nevertheless, according to the expression levels of *jagn1a* in the sorted neutrophils, we could assume that the α-JAGN1 signal corresponds to the presence of Jagn1b protein.

To study the role of JAGN1 in granulopoiesis and neutropenia development, we interfered separately with the function of both JAGN1 paralogs. For this purpose, we used ATG-binding morpholinos, which specifically blocked the translation of either *jagn1a* or *jagn1b (*hereafter called morphants*)*. The specificity of the morpholinos was

tested by co-injection with *gfp* coding mRNA containing the corresponding morpholino-binding ATG sequences of either *jagn1a* or *jagn1b*. After the co-injection, the morpholinos bind to the ATG, blocking *gfp* translation. In both cases, the embryos injected with morpholino and *gfp* coding mRNA were GFP-negative. Contrarily, overexpression of *gfp* coding mRNA alone led to GFP-positive embryos. Next, we assessed the effect on neutrophil development using WISH against the neutrophil marker *lyz* in 2.25 dpf embryos. After interfering with Jagn1a or Jagn1b function, we saw a significant decrease in the number of neutrophils compared to their wild-type counterparts. We were able to reproduce these results by injecting the morpholinos into the tg(mpo:*gfp*) reporter line. However, the injection of a control morpholino did not affect neutrophil counts. Additionally, we conducted rescue experiments where the morpholinos were co-injected with full-length wild-type *jagn1a* or *jagn1b* mRNA, featuring diverse sequences around the ATG region that are not susceptible to morpholino targeting. Then, the neutrophil counts were assessed using WISH against *lyz*. The decrease of neutrophils in *jagn1b* morphants was reversed to normal levels when embryos were co-injected with *jagn1b* mRNA. However, co-injection with *jagn1a* mRNA did not alleviate the neutropenia phenotype. In the *jagn1a* knockdown, the neutropenia phenotype was partially rescued by *jagn1a* overexpression, while the co-injection of *jagn1b* mRNA did not show any rescuing effect. Moreover, the overexpression of *jagn1a* or *jagn1b* in wild-type embryos did not affect the neutrophil numbers. These results suggest that the neutropenia phenotypes induced by *jagn1a* or *jagn1b* knockdown are specifically due to the interference with either *jagn1* paralog and argue for a non-redundant function of Jagn1a and Jagn1b in granulopoiesis.

For a more in-depth study of the impact of Jagn1a and Jagn1b downregulation on hematopoiesis, we performed WISH against hematopoietic cell-specific marker genes. First, we assessed the effect on *cmyb*$^{+}$ HSPCs and *spi1b*$^{+}$ early myeloid progenitors during definitive embryonic hematopoiesis. The interference with Jagn1a function influenced both immature hematopoietic cell types. Compared to the wild-type siblings, we saw a significant impairment in the expression pattern of *cmyb*$^{+}$ HSPCs and *spi1b*$^{+}$ myeloid progenitor cells. Contrarily, *jagn1b* morphants showed no effect on HSPCs or early myeloid progenitors. Next, we studied the impact on monopoiesis and erythropoiesis. We saw that *jagn1a*, but not *jagn1b* morphants, showed decreased *mpeg1.1*$^{+}$ macrophages compared to the wild type. Furthermore, the erythrocyte

marker *hbae1.1* was normally expressed, and circulating red blood cells were present in both morphants, indicating that *jagn1a* and *jagn1b* are not involved in erythropoiesis. These results strongly suggest that Jagn1a and Jagn1b play different non-redundant roles in hematopoiesis. While Jagn1a is involved in early hematopoiesis, monopoiesis, and granulopoiesis, Jagn1b's role is restricted to granulopoiesis. Both paralogs play a direct or indirect role in granulopoiesis. However, the phenotype induced by interfering with Jagn1b function mimics the phenotype of *JAGN1*-associated CN patients better. Thus, we decided to focus our further studies on Jagn1b.

Multiple mutations in the *JAGN1* gene can cause *JAGN1*-associated CN. The most frequent mutation affects the first Methionine (p.Met1Ile), which either eliminates or truncates the protein due to an alternative start codon at position 75 of the human *JAGN1* gene[41]. Thus far, *jagn1b* morpholino has successfully disrupted the start codon, mimicking this mutation. However, we also used a CRISPR/Cas9 approach targeting the ATG in the tg(mpo:*gfp*) reporter line. The transient knockout significantly reduced the number of mpo:*gfp*$^{+}$ neutrophils (data from publication **D**), reproducing the phenotype obtained from the morpholino-induced *jagn1b* knockdown. CN can also be caused by small deletions, nonsense or missense mutations in *JAGN1*. To mimic mutations targeting the transmembrane domain (TM), we used a CRISPR/Cas9 approach and injected guideRNA/Cas9 ribonucleoproteins (RNP) into the blastomere of tg(mpo:*gfp*) reporter embryos. The efficiency of the transient knockout (hereafter called TM crispants) varied between 62% and 92%. These TM crispants showed a reduced number of mpo:*gfp*$^{+}$ neutrophils compared to the wild type. Furthermore, we analyzed the effect of TM mutation on hematopoiesis. The neutropenia phenotype was confirmed using WISH against the neutrophil marker *lyz* without showing any impact on other hematopoietic cells, including *cmyb*$^{+}$ HSPCs, *spi1b*$^{+}$ myeloid progenitors, *mpeg1.1*$^{+}$ macrophages and *hbae1.1*$^{+}$ erythrocytes, mimicking the *JAGN1*-associated CN patients' phenotype.

Next, we tried to generate a stable mutant line targeting the TM domain. However, we could only identify heterozygous and no homozygous mutants through breeding the first (F1) and second (F2) generations. Two different genotypes, c.347_351del and c.351_357del, were discovered. These genotypes resulted in truncated Jagn1b proteins with 134 and 133 amino acids, respectively. The embryonic lethality of the

mutants was much higher than in the wild type. This led to the hypothesis that the homozygous mutation of *jagn1b* could be embryonically lethal, similar to *Jagn1*$^{-/-}$ mice[89] and *jagn* mutant *D. melanogaster*[38]. To study this more in-depth, we monitored the development from one-cell stage until 1dpf. Interestingly, these embryos were not able to enter gastrulation and displayed either an asymmetric cell division or a complete cell division arrest within the first two hours of development, resulting in embryonic lethality. Our data suggests that Jagn1b is essential for cell division during early embryonic development. Therefore, the development of stable *jagn1b*$^{c.347\_351del}$ and *jagn1b*$^{c.351\_357del}$ mutants was not possible. In *D.melanogaster,* Jagunal plays a critical role in the asymmetric division of the ER, which occurs just before the start of gastrulation, and an alteration of Jagunal leads to an impairment in the ER distribution[39]. Furthermore, this protein is also described as crucial for vesicular trafficking and cell growth[38]. A defect of those processes, e.g., cell growth, could explain the phenotype in Jagn1b mutant embryos. To exclude that the caused phenotype was due to a mutagenic off-target effect, we tested 13 predicted potential off-targets for our designed guide RNA. None of the potentially affected genes showed any alteration, confirming that a *jagn1b* mutation induced the phenotype. Although we were unable to generate stable mutants, we successfully mimicked the neutropenia phenotype with other approaches. We need to take into consideration that the morpholino-based *jagn1b* downregulation does not lead to the complete loss of protein, and transient knockouts contain maternal wild-type *jagn1b* transcripts until gastrulation, enabling normal embryonic development.

Another JAGN1 mutation that causes CN is the deletion of amino acids 12 to 14 (ΔT12-G14). To mimic this mutation, we overexpressed full-length *jagn1b* carrying the CN-inducing deletion from amino acid 12 to 14, hereafter called *jagn1b*$^{\Delta T12\text{-}G14}$. To study the effect of this mutation on granulopoiesis, we quantified *lyz*$^{+}$ neutrophils using WISH. The overexpression of *jagn1b*$^{\Delta T12\text{-}G14}$ led to impaired neutrophil development and significantly reduced the number of neutrophils compared to wild-type embryos. When co-injected with *jagn1b* morpholino, *jagn1b*$^{\Delta T12\text{-}G14}$ mRNA could not rescue the neutropenia and even pronounced the neutropenia phenotype. These results suggest that Jagn1b$^{\Delta T12\text{-}G14}$ has a negative dominant effect on wild-type Jagn1b, affecting neutrophil development. Furthermore, we analyzed the impact of the deletion in Jagn1b on other hematopoietic cells. We saw no significant effects on *cmyb*$^{+}$ HSPCs,

spi1b^{+} myeloid progenitors, *mpeg1.1*$^{+}$ macrophages, or *hbae1.1*$^{+}$ erythrocytes compared to wild-type siblings. These results are compatible with the *JAGN1*-associated CN patients' phenotype. Altogether, we showed, using various approaches, that the different mutations described in *JAGN1*-CN patients also induce neutropenia in zebrafish. These results argue for the conservation of the function between human JAGN1 and zebrafish Jagn1b, making the zebrafish an ideal model to study the underlying pathomechanism downstream of mutated JAGN1.

After defining Jagn1b's conserved function in zebrafish, we determined its subcellular localization. JAGN1 is knowingly an ER-membrane-binding protein[37]. To study the subcellular localization of wild-type Jagn1b we tagged the protein with GFP at the N-terminal domain and analyzed possible changes in localization upon mutation. As proof of the protein's functionality, despite the GFP-tagging, we overexpressed full-length wild-type GFP-tagged *jagn1b* mRNA in *jagn1b* morphants. This overexpression rescued the neutropenia phenotype, arguing for the preserved function. To study the subcellular localization in HSPCs, we injected GFP-labelled wild-type and *jagn1b*$^{\Delta T12\text{-}G14}$ mRNA into the HSPC-specific reporter line tg(draculin:*mCherry*). With confocal imaging of 1dpf injected embryos, we discovered a symmetric distribution of Jagn1b^{WT} around the nucleus, most likely the ER, while Jagn1b$^{\Delta T12\text{-}G14}$ was asymmetrically distributed in some HSPCs. The asymmetric distribution of the mutated Jagn1b could be explained by an altered binding to the ER, aggregation of the protein, or an altered ER structure, resembling ER-related abnormalities described in neutrophils from *JAGN1*-CN patients' cells[41]. Our observations of the abnormally distributed Jagn1b$^{\Delta T12\text{-}G14}$, together with the altered cell division during early embryonic development of the Jagn1b mutants, suggest that Jagn1b may play an essential role in cell division and ER organization. The mutations in Jagn1b may affect its structure, leading to alterations in the interaction with binding partners important for cell division, and a complete loss of Jagn1b is incompatible with normal embryonic development.

There are different hypotheses about the underlying mechanism causing defective granulocytic differentiation downstream of *JAGN1* mutations. The unfolded protein response (UPR) is described as one potential cause of neutropenia development in other CN-related genes, e.g. G6PC3[91], *SEC61A1*[92] and *ELANE*[93,94]. JAGN1-deficient granulocytes exhibit increased levels of binding immunoglobulin protein, suggesting

the activation of ER stress which normally activates the UPR[41]. Hence, we studied the UPR activation in our model by measuring the expression levels of different UPR players by RT-qPCR after interfering with the Jagn1b function. First, we quantified the expression level of *DNA damage-inducible transcript 3* (*ddit3*), encoding the UPR marker C/EBP homologous protein (Chop). The expression of *ddit3* can be activated by the three UPR pathways (Atf6, Perk, and Ire1)[95]. We observed a significant upregulation of the *ddit3* expression in *jagn1b* morphants and after *jagn1b*$^{\Delta T12\text{-}G14}$ mRNA overexpression compared to the wild-type expression level. However, *ddit3* expression was not activated upon overexpressing full-length wild-type *jagn1b* or control morpholino injection. Therefore, the expression of *ddit3* is upregulated explicitly upon Jagn1b alteration. Next, we analyzed the expression level of *activating transcription factor 4* (*atf4)*, which has a direct activating effect on *ddit3* expression. We observed a significant increase in the expression of *atf4,* compared to wild-type expression levels, after *jagn1b*$^{\Delta T12\text{-}G14}$ overexpression but not in *jagn1b* morphants or control morpholino-injected embryos. Furthermore, we quantified the expression levels of the Chop targets, *endoplasmic reticulum oxidoreductase 1-alpha* (*ero1a*) and *-beta* (*ero1b*), as well as *protein phosphatase 1 regulatory subunit 15A* (*ppp1r15a*) encoding growth arrest and DNA damage-inducible protein 34 (Gadd34)[96]. Whereas all Chop target genes were significantly upregulated upon *jagn1b*$^{\Delta T12\text{-}G14}$ overexpression, their expression levels were unaffected in *jagn1b* morphants or control morpholino-injected embryos when compared to the wild-type expression. Surprisingly, the expression level of *ppp1r15a* was slightly decreased in the morphants. These results suggest that Jagn1b$^{\Delta T12\text{-}G14}$ induced UPR through the Perk/Atf4/Chop pathway. However, *ddit3* induction in *jagn1b* morphants was independent from Atf4. Therefore, we analyzed the expression levels of additional UPR-related genes. The expression levels of *eukaryotic translation initiation factor 2 alpha kinase 3* (*eif2ak3*, encoding Perk), *ER to nucleus signaling 1* (*ern1*, encoding Ire1), *activating transcription factor 6* (*atf6*), were unaffected upon *jagn1b* downregulation. However, the expression of the Atf6 downstream target *X-box binding protein 1* (*xbp1*) was significantly upregulated in *jagn1b* morphants, arguing for the activation of the Atf6 pathway upon *jagn1b* downregulation. Moreover, *jagn1b* morphants also showed a non-significant trend of spliced *xbp1* (*sxbp1*) induction, suggesting potential crosstalk between UPR pathways and the activation of the Ire1 pathway. The variations in the expression levels of Chop

targets could be explained by the strength or state of UPR activation induced by the different Jagn1b alterations at the time of measurement, which may not have captured or reflected the time-dependent expression pattern of all UPR players. Moreover, different mutations can likely lead to the activation of different UPR pathways. This is consistent with previous results described in experimental settings of *ELANE*-associated CN[97]. Mutations in JAGN1 can alter its protein structure differently, leading to a variable degree of misfolding and potential protein accumulation. Further experiments are needed to define *JAGN1* mutation-specific activated UPR pathways. However, our data suggest the activation of UPR upon Jagn1b impairment.

After confirming that an impaired Jagn1b function led to UPR, we proceeded to study whether this mechanism could be the cause of neutropenia development. For this purpose, we chemically induced UPR and analyzed its effect on neutrophil numbers. To induce UPR, we treated the embryos with two different compounds: Dithiothreitol (DTT) and tunicamycin. DTT induces UPR by disrupting protein folding due to the reduction of disulfide bonds and tunicamycin by inhibiting N-linked glycosylation[98]. After 24 hours of treatment, we measured the expression of *ddit3,* which is activated by all UPR pathways, and *sxbp1*, where *xbp1* expression is induced by Atf6 pathway and spliced by Ire1[99]. The expression levels of both UPR markers were upregulated upon treatment. Furthermore, the treatment with DTT or tunicamycin of *jagn1b* morphants increased the UPR response. However, the injection of control morpholino or DMSO treatment did not affect their expression when compared to wild-type expression levels. To study the effect of the UPR induction on neutrophil counts, we quantified *lyz*$^{+}$ neutrophils after the UPR-inducing treatment of wild-type embryos and *jagn1b* morphants using WISH. The number of *lyz*$^{+}$ neutrophils in wild-type embryos after UPR induction with DTT or Tunicamycin did not vary significantly in comparison with untreated wild-type siblings. As a control treatment, we used DMSO, which did not affect neutrophil counts when compared to untreated littermates. Moreover, the number of *lyz*$^{+}$ neutrophils in the *jagn1b* morphants was not affected by the UPR-inducing treatment. Altogether, neutrophil counts did not vary in the conditions with or without treatment, regardless of the genetic background. These results suggest that the UPR induction alone is not sufficient to induce neutropenia.

The chronic ER stress and UPR, the activation of CHOP, and its targets are directly linked to apoptosis[96,100]. Moreover, an alternative suggested pathomechanism of neutropenia is the induction of apoptosis of myeloid progenitors[101]. To investigate this hypothesis, we assessed apoptosis upon *jagn1b* morpholino-induced KD and *jagn1b*$^{\Delta T12\text{-}G14}$ overexpression using the TUNEL assay. Interestingly, we saw a significant increase in apoptotic cells in *jagn1b* morphants, whereas the overexpression of *jagn1b*$^{\Delta T12\text{-}G14}$ showed no differences compared to the wild-type control embryos. The increase in apoptotic cells in the morphants was confirmed by acridine orange staining. However, the induction of apoptosis was not restricted to the hematopoietic tissue; apoptotic cells were distributed all over the morphants. The differences in apoptosis induction between *jagn1b* morphants and *jagn1b*$^{\Delta T12\text{-}G14}$ could be explained by their degree of ER stress, activated UPR pathways, or crosstalk between the different UPR pathways. The downregulation of *ppp1r15a* was previously associated with an increased apoptosis[102]. Interestingly, we saw a downregulation of this gene expression in *jagn1b* morphants but not in *jagn1b*$^{\Delta T12\text{-}G14}$, consistent with the increased apoptosis in *jagn1b* morphants. Further analyses at different time points are needed to study whether the presence of Jagn1b$^{\Delta T12\text{-}G14}$ also leads to apoptosis. However, we need to consider that after overexpressing *jagn1b*$^{\Delta T12\text{-}G14}$, the embryos still express wild-type *jagn1b,* which could distort the results. Nevertheless, our data suggest that *jagn1b* downregulation activates UPR response and leads to apoptosis, but not in a hematopoietic cell-specific manner.

To assess whether apoptosis induction can lead to neutropenia, we treated wild-type embryos and *jagn1b* morphants with the kinase inhibitor staurosporine and quantified *lyz*$^{+}$ neutrophils. Staurosporine-induced apoptosis was proven with acridine orange staining and TUNEL assay, where we observed that *jagn1b* morphants were more susceptible to staurosporine treatment than wild-type embryos. Next, we quantified the *lyz*$^{+}$ neutrophils after staurosporine treatment to test the effect on granulopoiesis. We saw that the chemical induction of apoptosis did not affect neutrophil numbers in either wild-type embryos or *jagn1b* morphants compared to their untreated controls. These results contradict previously published data showing that JAGN1-deficient neutrophils from CN patients were more susceptible to apoptosis induction with staurosporine than healthy neutrophils[41]. However, we showed a general increase in apoptosis susceptibility in *jagn1b* morphants, but not in a cell-specific manner. Altogether, our

data showed that the induction of apoptosis alone had no effect on the neutrophil counts, and the deficiency of Jagn1b in zebrafish did not make the neutrophils more susceptible to enter apoptosis. Nevertheless, it is worth noting that another study showed neutropenia development after prolonged staurosporine treatment at early stages of embryonic development. The time point of staurosporine treatment probably affected primitive granulopoiesis and normal development[103]. To avoid the effect on primitive granulopoiesis and possible side effects on the development, our studies started at 24hpf with staurosporine treatment. Further studies are needed to analyze the impact of apoptosis on granulopoiesis, depending on the stage of development. The pathomechanism behind neutropenia development downstream from mutated JAGN1 is a complex process where UPR activation and apoptosis are probably only two of several responses and not the primary cause.

Another potential cause of neutropenia development, described in CN with different genetic backgrounds, e.g., *HAX1*[31,88] or *ELANE*[88], is an impaired G-CSFR signaling pathway. Several experimental observations indicate that JAGN1 plays a role in the G-CSFR-triggered granulopoiesis. *JAGN1*-CN patients' neutrophils showed a reduced expression and altered glycosylation of G-CSFR[41]. The G-CSFR signaling pathway was also impaired in G-CSF-treated neutrophils from *Jagn1*-deficient mice despite normal G-CSFR levels[89]. From previous experiments in the *hax1*-CN model, we already knew that G-CSFR-triggered granulopoiesis is highly conserved between zebrafish and humans. Using two approaches, we assessed whether the overexpression of *g-csfa* rescued the neutropenia phenotype induced by Jagn1b alterations. First, we overexpressed *g-csfa* mRNA in wild-type and *jagn1b* morphants, allowing the translation of the protein at early stages of embryonic development. Second, we injected a heat-inducible plasmid carrying the coding sequence of *g-csfa* into wildtype and *jagn1b* morphants and induced the expression at 44hpf. In both cases, the quantification of neutrophils showed that the overexpression of *g-csfa* induced granulopoiesis. In wild-type embryos, the *g-csfa* overexpression significantly increased the number of neutrophils compared to uninjected siblings. Meanwhile, in the *jagn1b* morphants, the overexpression of *g-csfa* induced neutrophil development at wild-type levels. Similarly, the neutropenia phenotype induced by Jagn1b$^{\Delta T12\text{-}G14}$, on tg(mpo:*gfp*) background, was rescued by *g-csfa* overexpression. Comparable to rhG-CSF-treated CN patients, the *g-csfa* overexpression rescued the neutropenia

phenotype regardless of the type of *jagn1b* alteration. We proceeded with studying the downstream G-csfr signal transduction pathway upon Jagn1b impairment. For this purpose, we analyzed the G-csfr-triggered steady-state granulopoiesis by assessing the effect on the master regulator Cebpa by quantifying the number of *cebpa*-expressing cells and *cebpa* expression levels in *jagn1b* morphants and wild-type embryos using WISH and RT-qPCR, respectively. Compared to wild-type siblings, the number of *cebpa*$^{+}$ cells and the expression level of *cebpa* were significantly reduced upon *jagn1b* knockdown. We also analyzed the expression levels of the Cebpa targets, *hcls1 and csf3r* (encoding zebrafish G-CSFR*),* which both were significantly downregulated upon interfering with the Jagn1b function. The reduced expression of *csf3r* is consistent with previous results in *JAGN1*-CN neutrophils[41]. Altogether, these results suggest an impaired G-csfr pathway upon Jagn1b alteration. To explain how the overexpression of *g-csfa* induced granulopoiesis in *jagn1b* morphants despite impaired G-csfr signaling, we assessed emergency granulopoiesis. For this purpose, we first studied Cebpb, the primary regulator of emergency granulopoiesis, and analyzed its expression level after *g-csfa* overexpression. We observed that the *cebpb* expression was not significantly altered in wild-type embryos upon *g-csfa* overexpression. In contrast, the *g-csfa* overexpression in *jagn1b* morphants led to a significantly increased *cebpb* expression compared to wild-type levels. This observation argues for the activation of emergency granulopoiesis in *jagn1b* morphants upon *g-csfa* overexpression. To assess whether the rescue of the neutropenia phenotype is induced through Cebpb-regulated emergency granulopoiesis, we interfered with the Cebpb function using a morpholino knockdown strategy. First, we injected *cebpb* morpholino in tg(mpo:*gfp*) embryos and quantified the mpo:*gfp*$^{+}$ neutrophils at 2dpf. We observed that the interference with Cebpb had no effect on the neutrophil counts in wild-type embryos, where the G-csfr-triggered steady-state granulopoiesis is intact. Meanwhile, the number of mpo:*gfp*$^{+}$ neutrophils was significantly reduced in *jagn1b* morphants following *cebpb* knockdown compared to *jagn1b* morphants, and a *g-csfa* rescue was inefficient. However, the overexpression of wild-type *cebpb* mRNA rescued these effects. Altogether, these results suggest that the increase in neutrophil counts in *jagn1b* morphants upon *g-csfa* overexpression is induced by emergency granulopoiesis. Interestingly, we observed a significant induction of *cebpb* expression and the number of *cebpb*-expressing cells in *jagn1b*

morphants. Similarly, we saw an increase in the expression level of *g-csfa* but not *g-csfb* (second G-CSF ortholog) upon *jagn1b* knockdown compared to wild-type expression levels. These data suggest that the untreated *jagn1b* morphants activate a compensatory mechanism to counterbalance the reduced *cebpa* expression, making an effort to kickstart granulopoiesis even in the absence of Jagn1b. The induced *g-csfa* probably activates Cebpb-triggered emergency granulopoiesis, although the induction level is insufficient to rescue neutropenia. Consistent with the data observed in *jagn1b* morphants, we saw a decrease in *cebpa*- and an increase in *cebpb*-expressing cells in embryos with Jagn1b$^{\Delta T12\text{-}G14}$. Our results argue for an altered steady-state granulopoiesis and active emergency granulopoiesis upon Jagn1b alteration. Similar observations were made in CN patients[104] and our *hax1*-associated zebrafish CN model. However, we need to consider that the candidate genes' expression level measurements were performed on mRNA samples obtained from the whole embryo. To ensure our conclusions, it would be essential to analyze the expression levels in promyelocytic cells. Yet, the developmental stages in zebrafish are not as defined as in humans. Therefore, we concluded that our results at least partially recapitulate the situation observed in promyelocytic cells. Furthermore, we confirmed some of the expression data using the independent method WISH, focusing solely on the hematopoietic tissue.

In summary, we have established a promising *JAGN1*-associated experimental CN model in zebrafish, which has allowed us to gain insight into the pathomechanism of neutropenia downstream of mutated *JAGN1*. Altered Jagn1b led to UPR activation and apoptosis. However, the chemical induction of UPR or apoptosis processes did not lead to neutropenia in zebrafish embryos. These results suggest neither UPR nor apoptosis as the sole underlying mechanism leading to neutropenia downstream of mutated *JAGN1*. Similar to CN patients, we also observed an impaired G-csfr signaling pathway leading to an altered steady-state and an active emergency granulopoiesis in zebrafish embryos with altered Jagn1b function. This could be considered a possible pathomechanism. However, the development of neutropenia is a complex combination of different affected mechanisms and pathways. Further studies are needed to uncover the complete and detailed mechanism of neutropenia development behind mutated *JAGN1*, and our zebrafish model is ideal for this investigation. It can also be used to test potential drug candidates for neutropenia treatment.

3.3. DEVELOPMENT OF A *COPZ1*-ASSOCIATED CN ZEBRAFISH MODEL

Covered in the published manuscript:

C. N. Borbarán Bravo, E. Deordieva*, **L. Doll***, M. ElGamacy*, B. Dannenmann*, J. Azevedo*, S. Bräuning, V. Zakharova, C. Lengerke, M. Sturm, O. Rieß, C. Zeidler, K. Welte, A. Shcherbina, M. Klimiankou, J. Skokowa, *'A New Severe Congenital Neutropenia Syndrome Associated with Autosomal Recessive COPZ1 Mutations*.' *Blood* 2025*;* 145 (20): 2317-2335.

Severe congenital neutropenia is a genetically very heterogeneous disease; mutations in more than 25 genes are described in CN patients, and still, some cases can't be classified. The discovery of the CN-causing mutations is essential to better understand the underlying mechanism of neutropenia development in each case and find a therapeutic solution. Our lab discovered novel mutations in the *COPZ1* gene, encoding the COPI Coat Complex Subunit Zeta 1 protein, in three CN patients from two independent families. Two patients carry a homozygous nonsense mutation leading to truncated protein at amino acid position 141 (p.Gln141Ter), and the other patient carries a missense mutation at position 132 (p.Gly132Arg). There is no known mouse model of COPZ1-deficiency. However, an *in vivo* model is always useful and essential to study a protein's function and its mutation's effect on particular pathophysiological processes, including granulopoiesis.

COPZ1 is a component of the COPI complex, essential for the retrograde protein transport from the Golgi to the ER[105]. This process is highly conserved among species, and so is COPZ1. After multiple protein alignment, phylogenic, and gene syntenic analyses, we confirmed that COPZ1 is an evolutionarily highly conserved protein, also present in zebrafish. To study the expression pattern of *copz1* in zebrafish, we performed whole-mount *in situ* hybridization at different developmental stages. At 1dpf, we saw a hematopoietic tissue-specific expression pattern, suggesting that *copz1* is expressed in the hematopoietic cells. Furthermore, at 5dpf, *copz1* was also expressed in the optic tectum of the brain, thymus, gills, and lens. In a previous publication, Copz1 was discovered essential for normal early embryonic development. Insertional mutagenesis resulted in a narrower head, smaller eyes, and underdeveloped liver and gut [106]. These results show that Copz1 plays essential roles in different organs where

it is expressed, and its impairment has various consequences. However, for our approach to address the role of COPZ1 in granulopoiesis, we tried to mimic the truncating mutation in the zebrafish Copz1 protein. For this purpose, we used a CRISPR/Cas9 approach targeting the conserved amino acid glutamine (Gln) at position 161 of Copz1. We microinjected CRISPR/Cas9 RNPs into tg(mpo:*gfp*) transgenic embryos and grew them until adulthood. The gene manipulated generation 0 (F0), and their offspring were genotyped. Zebrafish from F0 with high KO scores, which inherited the truncated Copz1 to their offspring, were selected for further studies. The resulting Copz1 protein was truncated, but we obtained different variants from 163 to 167 amino acids.

Next, we proceeded to analyze the effect of truncated Copz1 on granulopoiesis. To assess the impact on granulopoiesis, we used three different approaches. First, we quantified the mpo:*gfp*$^{+}$ neutrophils in the Copz1 gene-edited embryos and compared them to wild-type tg(mpo:*gfp*) 2dpf embryos. Second, we stained the Copz1 gene-edited and wild-type embryos with neutrophil-specific Sudan Black (SB) staining. Third, we stained Copz1 gene-edited embryos with WISH against the neutrophil marker *lyz*. All approaches showed a significant reduction in either mpo:*gfp*$^{+}$ neutrophils, SB^{+} neutrophils, or *lyz*$^{+}$ neutrophils, respectively when comparing embryos with Copz1 truncation and their wild-type counterparts. These results suggest that Copz1 plays an essential role in neutrophil development, and its truncation leads to neutropenia. Next, we proceeded to analyze the effect on other hematopoietic cells. To assess whether stem or progenitor cells were affected, we studied the expression pattern of the HSPC marker *cmyb* and myeloid progenitor marker *spi1b* in Copz1 gene-edited embryos and wild type. No significant differences regarding the more immature hematopoietic cells were found between Copz1 mutants and wild-type embryos. Furthermore, we studied the effect on other mature myeloid cells. The impact on monocytes/macrophages was studied using WISH for the macrophage marker *mpeg1.1*. In this type of myeloid cells, we observed a significant reduction in Copz1 gene-edited embryos compared to wild-type littermates. Moreover, we studied erythropoiesis using the erythroid marker *hbae1.1* without alterations induced by Copz1 truncation. Altogether, this data showed that Copz1 truncation did not affect early steps of definitive granulopoiesis, including stem and progenitor cells or the erythroid lineage. However, Copz1 truncation led to impaired neutrophil and macrophage development in zebrafish. These results only

partially mimic the phenotype of the *COPZ1*-associated CN patients, who show neutropenia with average to high monocyte counts. However, we need to take into consideration that the developmental stages of monocytes/macrophages are not as defined in zebrafish as in humans, and we are looking at embryonic definitive hematopoiesis. Therefore, the effect on monocytes/macrophages may vary during development and adult definitive hematopoiesis in zebrafish. Thus, a possible explanation for this phenotype could be an impaired common progenitor. Consistently, *in vitro* colony-forming unit (CFU) assays of iPSC-derived cells with truncated COPZ1 showed a reduction in CFU-GM (granulocyte-monocyte) colonies. Intracellularly, our *in vitro* analyses showed downregulation of *CEBPE* upon COPZ1 truncation. Previous studies using human and mouse myeloid cells deficient in *CEBPE* described an essential role of C/EBPε in normal neutrophil and macrophage development[107]. To conclusively explain the cause of the phenotype induced by truncated Copz1, we need further studies, including the effect on the G-csfr pathway and *cepb1* (zebrafish ortholog of *CEBPE*) expression.

CN patients harboring truncating *COPZ1* mutation also displayed skeletal abnormalities, including scoliosis and foot deformities. Therefore, we examined the bone formation in zebrafish with truncated Copz1. First, we studied the craniofacial cartilage skeleton of 4 dpf embryos using Alcian blue staining without seeing any significant differences in the structures in Copz1 gene-edited embryos compared to the wild type. However, older larvae (30 dpf) showed malformations in the vertebral column consistent with scoliosis. This alteration was not confirmed in adults since the skin pigmentation prevented the visibility of the skeleton, and there were no obvious malformations. Apparently, Copz1 also plays a role in bone formation, but further investigations are needed to elucidate the exact mechanism.

We have established an *in vivo COPZ1*-associated CN zebrafish model that will allow us to understand better the downstream of mutated COPZ1 leading to neutropenia. This model can and will also be used to investigate the role of Copz1 in granulopoiesis. The effect of truncated Copz1 on, e.g., the G-csfr signaling pathway can be assessed, as well as the impact on other organs, including the brain or bones. Furthermore, the interaction of components of the COPI complex with JAGN1 was previously described[41]. However, the direct interaction of JAGN1 with COPZ1 was not detected in co-immunoprecipitation experiments in HEK293T cells. Nevertheless, the interaction

with similar components involved in the same processes may indicate common altered pathways and processes to be studied. Additionally, this model is ideal for testing new therapeutic approaches for neutropenia.

3.4. USING THE ZEBRAFISH CN MODELS FOR NEW DRUG DISCOVERY AND REPURPOSING

Covered in the published manuscripts:

C. N. Borbarán Bravo, E. Deordieva*, **L. Doll***, M. ElGamacy*, B. Dannenmann*, J. Azevedo*, S. Bräuning, V. Zakharova, C. Lengerke, M. Sturm, O. Rieß, C. Zeidler, K. Welte, A. Shcherbina, M. Klimiankou, J. Skokowa, *'A New Severe Congenital Neutropenia Syndrome Associated with Autosomal Recessive COPZ1 Mutations'*. *Blood* 2025*;* 145 (20): 2317-2335*.*

D. M. Nasri*, B. Dannenmann*, **L. Doll**, B. Findik, F. Bernhard, S. Kandabarau, M. Klimiankou, M. Gawaz, C. Lengerke, C. Zeidler, K. Welte, J. Skokowa. *'Flavopiridol restores granulopoiesis in experimental models of severe congenital neutropenia*.' *Mol Ther* 2025; 33 (6): 2851-2871.

To date, neutropenia patients, independently of the CN-causing mutation, are treated with daily subcutaneous administration of rhG-CSF. Without treatment, the majority of CN patients die from severe infections at a very young age[27]. Nevertheless, the treatment is daily and frequently causes side effects such as bone pain, headache, and fatigue, among others[24]. Furthermore, some CN patients are poor- or non-responders to rh-GCSF, and the only alternative treatment known is stem cell transplantation. CN patients who are treated with rhG-CSF are at high risk of developing MDS or AML, in particular, those who display a poor response to the treatment[24,27,28]. Therefore, discovering new therapeutic approaches and alternative treatments is essential to reduce leukemogenesis risk and increase the possibility of treating G-CSF poor- or non-responders. To this end, it is crucial to understand the underlying mechanism of neutropenia downstream of each mutated gene, allowing a more specific therapeutic approach for each CN case or therapeutically targeting a common altered pathway.

We have established three CN zebrafish models, which are ideal for studying the effect of potential drug candidates on granulopoiesis in an *in vivo* model. We tried to identify treatment options for the newly discovered CN-causing gene *COPZ1* using the

connectivity map tool (CMAP)[108]. This tool allows the comparison of gene expression profiles induced by various drugs and small molecules with the transcriptomic profiles of *COPZ1*-mutated and control HSPCs. Among the significantly enriched compounds, we found IOX2, an activator of the master transcriptional regulator of cellular and developmental responses to hypoxia, HIF1α (Hypoxia-Inducible Factor 1-alpha), and evaluated its therapeutic potential. To assess the effect of IOX2 treatment on *in vivo* granulopoiesis, we defined its potential toxicity and treated the *COPZ1*-mutated CN zebrafish embryos with non-toxic concentrations of IOX2. Zebrafish embryos absorb small molecules from their surrounding media, so the drugs were dissolved in zebrafish media to treat them. To establish the toxicity of IOX2, we incubated 1dpf zebrafish embryos in zebrafish media with different concentrations of IOX2, starting from 0.1 up to 100µM. After two days of incubation, we assessed the phenotype and survival of embryos. We found that 10µM of IOX2 was the highest non-toxic dose, where the embryos showed no negative phenotypes such as edema, curved tail, or death. We proceeded with studying the effect of IOX2 treatment on defective granulopoiesis and treated 1dpf embryos with truncated Copz1 for two days. As a control, we treated wild-type and Copz1 gene-edited embryos with DMSO. After two days of treatment, we quantified the mpo:*gfp*$^{+}$ neutrophils and found that the IOX2 treatment rescued the neutropenia phenotype of Copz1 gene-edited embryos. These promising results could hint at the suitability of the hypoxia signaling as a therapeutically targetable pathway. Furthermore, it was previously described that G-CSF can activate HIF1α expression[109], and HIF1α subsequently activates *CEBPA*[110]. These findings suggest a possible involvement of HIF1α in G–CSFR–triggered granulopoiesis, which should be further elucidated. The *COPZ1*-associated CN zebrafish model is an ideal tool to study further the hypoxia pathway's druggability and the relationship between hypoxia and the G-CSFR pathway.

Moreover, we have identified the small molecule flavopiridol using the transcriptomic profiling of HSPCs generated from *ELANE*-CN-patient-derived isogenic iPSC lines in which *ELANE* mutations were corrected using CRISPR/Cas9 gene editing. Differently expressed genes between two isogenic conditions (ELANE mutated vs ELANE mutation corrected) were analyzed using the L1000 Characteristic Direction Signatures (L1000CDS)[111] search engine and the Connectivity Map database[108]. These tools generate functional associations between drugs, genes, and diseases using gene

expression signatures. Flavopiridol was one of the suggested candidate drugs that could reverse the expression signature downstream of ELANE mutations and thus potentially can be used to treat CN patients.

Flavopiridol is an FDA-approved drug described as a cyclin-dependent kinase inhibitor used for acute myeloid leukemia treatment. *In vitro*, 40nM flavopiridol, a concentration ten times lower than that used in cancer treatment, showed a promising effect on inducing granulopoiesis in primary *ELANE*-CN cells, but also in CN cells with different mutations, including *HAX1*-CN, *JAGN1*-CN, and *SRP54*-CN. Most CN patients harbor a mutation in the *ELANE* gene coding for neutrophil elastase (NE). Unfortunately, the zebrafish has no *ELANE* paralog, and its function can't be studied directly. However, as proof of principle, we used our *HAX1*- and *JAGN1*-associated CN zebrafish models to assess the effect of flavopiridol on granulopoiesis. However, the toxicity of this drug is a concern. Therefore, we first studied the effect of flavopiridol treatment on the development of zebrafish embryos. We incubated 1dpf embryos at different concentrations of flavopiridol, starting from 0.1µM to 100µM for two days. In our hands, single doses of flavopiridol up to 10 µM for two days showed no toxic effects on the embryos. However, higher concentrations and prolonged exposure induced phenotypes such as curved tails and cardiac edema or led to embryonic lethality. Previous studies in zebrafish embryos showed similar side effects, including reduced length, already at lower concentrations, but with repeated dosing[112]. Nevertheless, we proceeded to study the impact of our highest, non-toxic concentration of flavopiridol, 10µM, on healthy hematopoietic stem cells and neutrophils. We used two approaches to assess the effect on hematopoietic stem cells. First, we treated embryos of the transgenic reporter line tg(CD41:*gfp*), where *gfp* is expressed under the control of the CD41 (coded by *itga2b*) promotor. CD41 is one of the earliest markers for hematopoietic commitment. However, it is not only expressed in early HSPCs but also in thrombocytes[113,114]. To reduce the effect of mature thrombocytes on the analyses, we quantified the CD41:*gfp*$^{+}$ cells in the caudal hematopoietic tissue at 2dpf after one day of flavopiridol treatment. We saw no significant differences in the number of CD41:*gfp*$^{+}$ cells after flavopiridol treatment compared to DMSO-treated controls. Additionally, we studied the effect of flavopiridol on the expression pattern of the HSPC-specific marker gene *cmyb* in wild-type embryos treated for two days. The analysis of the WISH staining in the embryos treated with flavopiridol and DMSO

controls showed no significant differences. In line with previous studies[115], these results showed that flavopiridol treatment did not affect the development of HSPCs at these developmental stages. Similarly, we studied the effect of flavopiridol on healthy neutrophils by incubating 1dpf tg(mpo:*gfp*) embryos with flavopiridol and DMSO as a control for two days. The quantification of the mpo:*gfp*$^{+}$ neutrophils showed no significant differences between the zebrafish embryos treated with flavopiridol or DMSO. Previous publications also described the absence of toxic effects on *mpo*$^{+}$ neutrophils[115,116] upon flavopiridol treatment. However, a negative impact on *lyz*-expressing cells was described[115]. Further analyses of *lyz* expression levels and *lyz*-expressing cells upon flavopiridol treatment need to be done to elucidate the meaning of these results. Nevertheless, we can conclude that flavopiridol has no adverse effect on the neutrophil population expressing *mpo*. Next, to study the effect on impaired granulopoiesis, we treated 1dpf *hax1* morphants and *jagn1b* crispants on tg(mpo:*gfp*) background with flavopiridol and DMSO as control. After two days of treatment with flavopiridol, the numbers of mpo:*gfp*$^{+}$ neutrophils were restored to wild-type levels in both zebrafish CN models. Thus, our data suggest that flavopiridol may be an appropriate new treatment for CN, regardless of the CN-causing mutation.

Flavopiridol has been described as a pan-CDK inhibitor, and at the concentration used in the *in vitro* experiments, it inhibits CDK1, 2, 4, and 9[117]. We wanted to elucidate the mechanism of action of this drug on granulopoiesis. A direct link between CDKs and granulopoiesis has been described previously. It is known that C/EBPα has an inhibitory effect on CDK2 and CDK4, limiting cell proliferation and inducing myeloid differentiation[17]. Flavopiridol also inhibits CDK2 and CDK4, mimicking the function of C/EBPα. Interestingly, in myeloid progenitor cells of CN patients[31] and also in our *HAX1*- and *JAGN1*-associated CN zebrafish models, we saw a severely reduced expression of C/EBPα, which could be the underlying reason for the maturation arrest of granulopoiesis. To study whether the inhibitory activity of flavopiridol is enough to mimic the function of C/EBPα, we interfered with the function of C/ebpα in zebrafish embryos and treated them with flavopiridol. The *cebpa* knock-down in tg(mpo:*gfp*) embryos, induced by morpholino injection, led to impaired granulopoiesis, similar to previously described *cebpa* zebrafish mutants[87]. However, the reduction in mpo:*gfp*$^{+}$ neutrophil after *cebpa* knock-down was rescued by flavopiridol treatment. These results suggest that flavopiridol can mimic the function of C/EBPα and induce

granulopoiesis even upon reduced C/EBPα. Altogether, flavopiridol is an interesting candidate for treating neutropenia regardless of the CN-causing mutation. Its mechanism of action appears to target a common defect, downregulation of *CEBPA* expression, which is caused by several mutations, including those in *HAX1* and *JAGN1*. Furthermore, our CN zebrafish models are ideal for further investigations of flavopiridol's mechanism of action and the discovery of alternative druggable pathways or proteins.

In summary, our *in vivo* CN zebrafish models are valuable tools for the discovery of new drug candidates and druggable pathways. These models can be used to test a drug candidate's toxicity, effect on specific cell types, and underlying mechanism of action.

4. Outlook

In this work, we aimed to **(1)** establish *HAX1*-CN, *JAGN1*-CN, and *COPZ1*-CN zebrafish models, use them to uncover the underlying pathomechanism, and **(2)** discover new therapeutic approaches for CN.

We successfully established all three CN zebrafish models and studied the underlying pathomechanism of neutropenia. Our studies mainly focused on the hematopoietic phenotypes. However, CN patients, in addition to neutropenia, show different extra-hematopoietic syndromes, including neurological and skeletal defects, and have a high risk of developing MDS or AML. Our models are suitable for studying the effects of *HAX1*, *JAGN1*, and *COPZ1* mutations on other organs, e.g., the brain or bones. Furthermore, by introducing additional leukemia-driving mutations in genes like *CSF3R* or *RUNX1*, these models can also be used to study leukemogenesis on a CN background.

The established CN zebrafish models were also successfully used to test the potential drug candidates IOX2 and flavopiridol for their potency in restoring defective granulopoiesis *in vivo*. Our CN zebrafish models could be further used to elucidate the underlying mechanism of these compounds' beneficial effects on granulopoiesis and study their impact on extra-hematopoietic symptoms seen in CN patients. Additionally, it would be interesting to examine the relationship between the response to hypoxia through HIF1α and the G-CSFR/CEBPA pathway in regulating granulopoiesis and discover further druggable targets.

5. Acknowledgements

First, I would like to express my heartfelt gratitude to Prof. Julia Skokowa. Your thoughtful insights and encouragement have greatly influenced my work, helping me navigate challenges and grow as a female researcher. I am also deeply thankful to Prof. Karl Welte, whose wisdom and insights have been a guiding influence.

I would also like to extend my sincere thanks to Prof. Rita Triebskorn for your valuable feedback and diverse perspectives that have enriched my research.

A special thank you to Dr. Baubak Bajoghli, whose extensive knowledge has profoundly impacted my work. Your ability to break down complex concepts, combined with your encouraging words, helped me navigate challenges with confidence and curiosity. I am also grateful to Dr. Narges Aghaallaei, whose patience and enthusiasm in teaching made every learning moment enjoyable and fulfilling. I would also like to thank Dr. Thomas Dickmeis, who made my initial exposure to zebrafish research possible. That early experience laid the foundation for my journey and opened my eyes to the fascinating world of zebrafish.

I'd like to recognize the essential role of the zebrafish in my research, as well as the dedicated animal care staff.

I am also very grateful to all my colleagues and fellow PhD students for fostering a supportive and friendly environment. Your camaraderie and collaboration made this journey not only productive but also filled with laughter and shared experiences that I will cherish. I would especially like to thank Adi, Anna, and Natalia for your unwavering support and encouragement throughout this process.

Finally, I would like to express my deepest appreciation to my family and friends. Your support during both the highs and lows has made this journey all the more meaningful. A heartfelt thank you to my parents for your unwavering encouragement and belief in me. To my partner, Nghi, your love and support have been my greatest source of strength, and I truly couldn't have done this without you. I would also like to extend my gratitude to Kristie for your meticulous proofreading and invaluable feedback. This dissertation is not just my achievement; it is a reflection of the incredible people who have supported me along the way. Thank you all for being such an important part of this journey.

6.BIBLIOGRAPHY

1. Akashi, K., Traver, D., Miyamoto, T. & Weissman, I.L. A clonogenic common myeloid progenitor that gives rise to all myeloid lineages. *Nature* **404**, 193-197 (2000).
2. Galy, A., Travis, M., Cen, D. & Chen, B. Human T, B, natural killer, and dendritic cells arise from a common bone marrow progenitor cell subset. *Immunity* **3**, 459-473 (1995).
3. Mestas, J. & Hughes, C.C. Of mice and not men: differences between mouse and human immunology. *J Immunol* **172**, 2731-2738 (2004).
4. Deng, Q., Yoo, S.K., Cavnar, P.J., Green, J.M. & Huttenlocher, A. Dual roles for Rac2 in neutrophil motility and active retention in zebrafish hematopoietic tissue. *Dev Cell* **21**, 735-745 (2011).
5. Summers, C.*, et al.* Neutrophil kinetics in health and disease. *Trends Immunol* **31**, 318-324 (2010).
6. Cowland, J.B. & Borregaard, N. Granulopoiesis and granules of human neutrophils. *Immunol Rev* **273**, 11-28 (2016).
7. Lawrence, S.M., Corriden, R. & Nizet, V. The Ontogeny of a Neutrophil: Mechanisms of Granulopoiesis and Homeostasis. *Microbiol Mol Biol Rev* **82**(2018).
8. Radomska, H.S.*, et al.* CCAAT/enhancer binding protein alpha is a regulatory switch sufficient for induction of granulocytic development from bipotential myeloid progenitors. *Mol Cell Biol* **18**, 4301-4314 (1998).
9. Ma, O., Hong, S., Guo, H., Ghiaur, G. & Friedman, A.D. Granulopoiesis requires increased C/EBPalpha compared to monopoiesis, correlated with elevated Cebpa in immature G-CSF receptor versus M-CSF receptor expressing cells. *PLoS One* **9**, e95784 (2014).
10. Friedman, A.D. C/EBPalpha in normal and malignant myelopoiesis. *Int J Hematol* **101**, 330-341 (2015).
11. Barreda, D.R., Hanington, P.C. & Belosevic, M. Regulation of myeloid development and function by colony stimulating factors. *Dev Comp Immunol* **28**, 509-554 (2004).
12. Rawat, K., Syeda, S. & Shrivastava, A. Neutrophil-derived granule cargoes: paving the way for tumor growth and progression. *Cancer Metastasis Rev* **40**, 221-244 (2021).
13. Malech, H.L., Deleo, F.R. & Quinn, M.T. The role of neutrophils in the immune system: an overview. *Methods Mol Biol* **1124**, 3-10 (2014).
14. Amulic, B., Cazalet, C., Hayes, G.L., Metzler, K.D. & Zychlinsky, A. Neutrophil function: from mechanisms to disease. *Annu Rev Immunol* **30**, 459-489 (2012).
15. Liew, P.X. & Kubes, P. The Neutrophil's Role During Health and Disease. *Physiol Rev* **99**, 1223-1248 (2019).
16. Hirai, H.*, et al.* C/EBPbeta is required for 'emergency' granulopoiesis. *Nat Immunol* **7**, 732-739 (2006).
17. Wang, H.*, et al.* C/EBPalpha arrests cell proliferation through direct inhibition of Cdk2 and Cdk4. *Mol Cell* **8**, 817-828 (2001).
18. Mehta, H.M. & Corey, S.J. G-CSF, the guardian of granulopoiesis. *Semin Immunol* **54**, 101515 (2021).
19. Palmblad, J., Dufour, C. & Papadaki, H.A. How we diagnose neutropenia in the adult and elderly patient. *Haematologica* **99**, 1130-1133 (2014).
20. Gibson, C. & Berliner, N. How we evaluate and treat neutropenia in adults. *Blood* **124**, 1251-1258; quiz 1378 (2014).
21. Denic, S.*, et al.* Prevalence of neutropenia in children by nationality. *BMC Hematol* **16**, 15 (2016).
22. Donadieu, J., Fenneteau, O., Beaupain, B., Mahlaoui, N. & Chantelot, C.B. Congenital neutropenia: diagnosis, molecular bases and patient management. *Orphanet J Rare Dis* **6**, 26 (2011).
23. Carlsson, G.*, et al.* Incidence of severe congenital neutropenia in Sweden and risk of evolution to myelodysplastic syndrome/leukaemia. *Br J Haematol* **158**, 363-369 (2012).

24. Skokowa, J., Dale, D.C., Touw, I.P., Zeidler, C. & Welte, K. Severe congenital neutropenias. *Nat Rev Dis Primers* **3**, 17032 (2017).
25. Bonilla, M.A.*, et al.* Effects of recombinant human granulocyte colony-stimulating factor on neutropenia in patients with congenital agranulocytosis. *N Engl J Med* **320**, 1574-1580 (1989).
26. Nasri, M.*, et al.* CRISPR/Cas9-mediated ELANE knockout enables neutrophilic maturation of primary hematopoietic stem and progenitor cells and induced pluripotent stem cells of severe congenital neutropenia patients. *Haematologica* **105**, 598-609 (2020).
27. Rosenberg, P.S.*, et al.* The incidence of leukemia and mortality from sepsis in patients with severe congenital neutropenia receiving long-term G-CSF therapy. *Blood* **107**, 4628-4635 (2006).
28. Rosenberg, P.S.*, et al.* Stable long-term risk of leukaemia in patients with severe congenital neutropenia maintained on G-CSF therapy. *Br J Haematol* **150**, 196-199 (2010).
29. Trebinska-Stryjewska, A., Wakula, M., Chmielarczyk, M. & Grzybowska, E.A. HAX1: A versatile, intrinsically disordered regulatory protein. *Biochim Biophys Acta Mol Cell Res* **1870**, 119538 (2023).
30. Suzuki, Y.*, et al.* HAX-1, a novel intracellular protein, localized on mitochondria, directly associates with HS1, a substrate of Src family tyrosine kinases. *J Immunol* **158**, 2736-2744 (1997).
31. Skokowa, J.*, et al.* Interactions among HCLS1, HAX1 and LEF-1 proteins are essential for G-CSF-triggered granulopoiesis. *Nat Med* **18**, 1550-1559 (2012).
32. Chao, J.R.*, et al.* Hax1-mediated processing of HtrA2 by Parl allows survival of lymphocytes and neurons. *Nature* **452**, 98-102 (2008).
33. Gallagher, A.R., Cedzich, A., Gretz, N., Somlo, S. & Witzgall, R. The polycystic kidney disease protein PKD2 interacts with Hax-1, a protein associated with the actin cytoskeleton. *Proc Natl Acad Sci U S A* **97**, 4017-4022 (2000).
34. Klein, C.*, et al.* HAX1 deficiency causes autosomal recessive severe congenital neutropenia (Kostmann disease). *Nat Genet* **39**, 86-92 (2007).
35. Carlsson, G.*, et al.* Kostmann syndrome or infantile genetic agranulocytosis, part two: Understanding the underlying genetic defects in severe congenital neutropenia. *Acta Paediatr* **96**, 813-819 (2007).
36. Germeshausen, M.*, et al.* Novel HAX1 mutations in patients with severe congenital neutropenia reveal isoform-dependent genotype-phenotype associations. *Blood* **111**, 4954-4957 (2008).
37. VanWinkle, P.E., Parish, F., Edwards, Y.J.K. & Sztul, E. JAGN1, tetraspanins, and Erv proteins: is common topology indicative of common function in cargo sorting? *Am J Physiol Cell Physiol* **319**, C667-C674 (2020).
38. Lee, S. & Cooley, L. Jagunal is required for reorganizing the endoplasmic reticulum during Drosophila oogenesis. *J Cell Biol* **176**, 941-952 (2007).
39. Eritano, A.S.*, et al.* The endoplasmic reticulum is partitioned asymmetrically during mitosis before cell fate selection in proneuronal cells in the early Drosophila embryo. *Mol Biol Cell* **28**, 1530-1538 (2017).
40. Ascencio, G.*, et al.* A deficiency screen of the 3rd chromosome for dominant modifiers of the Drosophila ER integral membrane protein, Jagunal. *G3 (Bethesda)* (2023).
41. Boztug, K.*, et al.* JAGN1 deficiency causes aberrant myeloid cell homeostasis and congenital neutropenia. *Nat Genet* **46**, 1021-1027 (2014).
42. Khandagale, A.*, et al.* JAGN1 is required for fungal killing in neutrophil extracellular traps: Implications for severe congenital neutropenia. *J Leukoc Biol* **104**, 1199-1213 (2018).
43. Cosson, P., Demolliere, C., Hennecke, S., Duden, R. & Letourneur, F. Delta- and zeta-COP, two coatomer subunits homologous to clathrin-associated proteins, are involved in ER retrieval. *EMBO J* **15**, 1792-1798 (1996).

44. de Jong, J.L. & Zon, L.I. Use of the zebrafish system to study primitive and definitive hematopoiesis. *Annu Rev Genet* **39**, 481-501 (2005).
45. Bertrand, J.Y.*, et al.* Definitive hematopoiesis initiates through a committed erythromyeloid progenitor in the zebrafish embryo. *Development* **134**, 4147-4156 (2007).
46. Myllymaki, H., Yu, P.P. & Feng, Y. Opportunities presented by zebrafish larval models to study neutrophil function in tissues. *Int J Biochem Cell Biol* **148**, 106234 (2022).
47. Jin, H.*, et al.* Definitive hematopoietic stem/progenitor cells manifest distinct differentiation output in the zebrafish VDA and PBI. *Development* **136**, 647-654 (2009).
48. Le Guyader, D.*, et al.* Origins and unconventional behavior of neutrophils in developing zebrafish. *Blood* **111**, 132-141 (2008).
49. Gore, A.V., Pillay, L.M., Venero Galanternik, M. & Weinstein, B.M. The zebrafish: A fintastic model for hematopoietic development and disease. *Wiley Interdiscip Rev Dev Biol* **7**, e312 (2018).
50. Jing, L. & Zon, L.I. Zebrafish as a model for normal and malignant hematopoiesis. *Dis Model Mech* **4**, 433-438 (2011).
51. Howe, K.*, et al.* The zebrafish reference genome sequence and its relationship to the human genome. *Nature* **496**, 498-503 (2013).
52. Koparir, A.*, et al.* Zebrafish as a model to investigate a biallelic gain-of-function variant in MSGN1, associated with a novel skeletal dysplasia syndrome. *Hum Genomics* **18**, 23 (2024).
53. Clark, K.J., Urban, M.D., Skuster, K.J. & Ekker, S.C. Transgenic zebrafish using transposable elements. *Methods Cell Biol* **104**, 137-149 (2011).
54. Bajoghli, B., Aghaallaei, N., Heimbucher, T. & Czerny, T. An artificial promoter construct for heat-inducible misexpression during fish embryogenesis. *Dev Biol* **271**, 416-430 (2004).
55. Summerton, J. & Weller, D. Morpholino antisense oligomers: design, preparation, and properties. *Antisense Nucleic Acid Drug Dev* **7**, 187-195 (1997).
56. Blum, M., De Robertis, E.M., Wallingford, J.B. & Niehrs, C. Morpholinos: Antisense and Sensibility. *Dev Cell* **35**, 145-149 (2015).
57. Hoshijima, K.*, et al.* Highly Efficient CRISPR-Cas9-Based Methods for Generating Deletion Mutations and F0 Embryos that Lack Gene Function in Zebrafish. *Dev Cell* **51**, 645-657 e644 (2019).
58. Patton, E.E., Zon, L.I. & Langenau, D.M. Zebrafish disease models in drug discovery: from preclinical modelling to clinical trials. *Nat Rev Drug Discov* **20**, 611-628 (2021).
59. Renshaw, S.A.*, et al.* A transgenic zebrafish model of neutrophilic inflammation. *Blood* **108**, 3976-3978 (2006).
60. Hall, C., Flores, M.V., Storm, T., Crosier, K. & Crosier, P. The zebrafish lysozyme C promoter drives myeloid-specific expression in transgenic fish. *BMC Dev Biol* **7**, 42 (2007).
61. Dai, Z.X.*, et al.* [Forward genetic screening for zebrafish mutants defective in myelopoiesis]. *Nan Fang Yi Ke Da Xue Xue Bao* **30**, 1230-1233 (2010).
62. Quiring, R.*, et al.* Large-scale expression screening by automated whole-mount in situ hybridization. *Mech Dev* **121**, 971-976 (2004).
63. Zhang, Y., Jin, H., Li, L., Qin, F.X. & Wen, Z. cMyb regulates hematopoietic stem/progenitor cell mobilization during zebrafish hematopoiesis. *Blood* **118**, 4093-4101 (2011).
64. North, T.E.*, et al.* Prostaglandin E2 regulates vertebrate haematopoietic stem cell homeostasis. *Nature* **447**, 1007-1011 (2007).
65. Ward, A.C.*, et al.* The zebrafish spi1 promoter drives myeloid-specific expression in stable transgenic fish. *Blood* **102**, 3238-3240 (2003).
66. Chung, H.Y.*, et al.* Meis1, Hi1alpha, and GATA1 are integrated into a hierarchical regulatory network to mediate primitive erythropoiesis. *FASEB J* **35**, e21915 (2021).

67. Ellett, F., Pase, L., Hayman, J.W., Andrianopoulos, A. & Lieschke, G.J. mpeg1 promoter transgenes direct macrophage-lineage expression in zebrafish. *Blood* **117**, e49-56 (2011).
68. Pazhakh, V., Clark, S., Keightley, M.C. & Lieschke, G.J. A GCSFR/CSF3R zebrafish mutant models the persistent basal neutrophil deficiency of severe congenital neutropenia. *Sci Rep* **7**, 44455 (2017).
69. Basheer, F., Rasighaemi, P., Liongue, C. & Ward, A.C. Zebrafish Granulocyte Colony-Stimulating Factor Receptor Maintains Neutrophil Number and Function throughout the Life Span. *Infect Immun* **87**(2019).
70. Carapito, R.*, et al.* Mutations in signal recognition particle SRP54 cause syndromic neutropenia with Shwachman-Diamond-like features. *J Clin Invest* **127**, 4090-4103 (2017).
71. Schurch, C.*, et al.* SRP54 mutations induce congenital neutropenia via dominant-negative effects on XBP1 splicing. *Blood* **137**, 1340-1352 (2021).
72. Venkatasubramani, N. & Mayer, A.N. A zebrafish model for the Shwachman-Diamond syndrome (SDS). *Pediatr Res* **63**, 348-352 (2008).
73. Zhang, C.Y.*, et al.* Transforming growth factor-beta1 regulates the nascent hematopoietic stem cell niche by promoting gluconeogenesis. *Leukemia* **32**, 479-491 (2018).
74. Khuchua, Z., Yue, Z., Batts, L. & Strauss, A.W. A zebrafish model of human Barth syndrome reveals the essential role of tafazzin in cardiac development and function. *Circ Res* **99**, 201-208 (2006).
75. Peckl-Schmid, D.*, et al.* HAX1 deficiency: impact on lymphopoiesis and B-cell development. *Eur J Immunol* **40**, 3161-3172 (2010).
76. Morishima, T.*, et al.* Genetic correction of HAX1 in induced pluripotent stem cells from a patient with severe congenital neutropenia improves defective granulopoiesis. *Haematologica* **99**, 19-27 (2014).
77. Pittermann, E.*, et al.* Gene correction of HAX1 reversed Kostmann disease phenotype in patient-specific induced pluripotent stem cells. *Blood Adv* **1**, 903-914 (2017).
78. Tang, Q.*, et al.* Dissecting hematopoietic and renal cell heterogeneity in adult zebrafish at single-cell resolution using RNA sequencing. *J Exp Med* **214**, 2875-2887 (2017).
79. Athanasiadis, E.I.*, et al.* Single-cell RNA-sequencing uncovers transcriptional states and fate decisions in haematopoiesis. *Nat Commun* **8**, 2045 (2017).
80. Carlsson, G.*, et al.* Central nervous system involvement in severe congenital neutropenia: neurological and neuropsychological abnormalities associated with specific HAX1 mutations. *J Intern Med* **264**, 388-400 (2008).
81. Boulanger-Weill, J. & Sumbre, G. Functional Integration of Newborn Neurons in the Zebrafish Optic Tectum. *Front Cell Dev Biol* **7**, 57 (2019).
82. Cavnar, P.J., Berthier, E., Beebe, D.J. & Huttenlocher, A. Hax1 regulates neutrophil adhesion and motility through RhoA. *J Cell Biol* **193**, 465-473 (2011).
83. Carlsson, G.*, et al.* Kostmann syndrome: severe congenital neutropenia associated with defective expression of Bcl-2, constitutive mitochondrial release of cytochrome c, and excessive apoptosis of myeloid progenitor cells. *Blood* **103**, 3355-3361 (2004).
84. Stachura, D.L.*, et al.* The zebrafish granulocyte colony-stimulating factors (Gcsfs): 2 paralogous cytokines and their roles in hematopoietic development and maintenance. *Blood* **122**, 3918-3928 (2013).
85. Liongue, C., Hall, C.J., O'Connell, B.A., Crosier, P. & Ward, A.C. Zebrafish granulocyte colony-stimulating factor receptor signaling promotes myelopoiesis and myeloid cell migration. *Blood* **113**, 2535-2546 (2009).
86. Park, S.D.*, et al.* A review of granulocyte colony-stimulating factor receptor signaling and regulation with implications for cancer. *Front Oncol* **12**, 932608 (2022).
87. Dai, Y.*, et al.* Cebpalpha is essential for the embryonic myeloid progenitor and neutrophil maintenance in zebrafish. *J Genet Genomics* **43**, 593-600 (2016).
88. Skokowa, J. & Welte, K. Defective G-CSFR signaling pathways in congenital neutropenia. *Hematol Oncol Clin North Am* **27**, 75-88, viii (2013).

89. Wirnsberger, G.*, et al.* Jagunal homolog 1 is a critical regulator of neutrophil function in fungal host defense. *Nat Genet* **46**, 1028-1033 (2014).
90. Mosimann, C.*, et al.* Chamber identity programs drive early functional partitioning of the heart. *Nat Commun* **6**, 8146 (2015).
91. Boztug, K.*, et al.* A syndrome with congenital neutropenia and mutations in G6PC3. *N Engl J Med* **360**, 32-43 (2009).
92. Van Nieuwenhove, E.*, et al.* Defective Sec61alpha1 underlies a novel cause of autosomal dominant severe congenital neutropenia. *J Allergy Clin Immunol* **146**, 1180-1193 (2020).
93. Kollner, I.*, et al.* Mutations in neutrophil elastase causing congenital neutropenia lead to cytoplasmic protein accumulation and induction of the unfolded protein response. *Blood* **108**, 493-500 (2006).
94. Grenda, D.S.*, et al.* Mutations of the ELA2 gene found in patients with severe congenital neutropenia induce the unfolded protein response and cellular apoptosis. *Blood* **110**, 4179-4187 (2007).
95. Yang, Y.*, et al.* Transcription Factor C/EBP Homologous Protein in Health and Diseases. *Front Immunol* **8**, 1612 (2017).
96. Marciniak, S.J.*, et al.* CHOP induces death by promoting protein synthesis and oxidation in the stressed endoplasmic reticulum. *Genes Dev* **18**, 3066-3077 (2004).
97. Nustede, R.*, et al.* ELANE mutant-specific activation of different UPR pathways in congenital neutropenia. *Br J Haematol* **172**, 219-227 (2016).
98. Kaufman, R.J. Stress signaling from the lumen of the endoplasmic reticulum: coordination of gene transcriptional and translational controls. *Genes Dev* **13**, 1211-1233 (1999).
99. Yoshida, H., Matsui, T., Yamamoto, A., Okada, T. & Mori, K. XBP1 mRNA is induced by ATF6 and spliced by IRE1 in response to ER stress to produce a highly active transcription factor. *Cell* **107**, 881-891 (2001).
100. Li, G.*, et al.* Role of ERO1-alpha-mediated stimulation of inositol 1,4,5-triphosphate receptor activity in endoplasmic reticulum stress-induced apoptosis. *J Cell Biol* **186**, 783-792 (2009).
101. Dale, D.C. & Link, D.C. The many causes of severe congenital neutropenia. *N Engl J Med* **360**, 3-5 (2009).
102. Krokowski, D.*, et al.* GADD34 Function in Protein Trafficking Promotes Adaptation to Hyperosmotic Stress in Human Corneal Cells. *Cell Rep* **21**, 2895-2910 (2017).
103. Mojicevic, M.*, et al.* Streptomyces sp. BV410 isolate from chamomile rhizosphere soil efficiently produces staurosporine with antifungal and antiangiogenic properties. *Microbiologyopen* **9**, e986 (2020).
104. Skokowa, J.*, et al.* NAMPT is essential for the G-CSF-induced myeloid differentiation via a NAD(+)-sirtuin-1-dependent pathway. *Nat Med* **15**, 151-158 (2009).
105. Rout, M.P. & Field, M.C. The Evolution of Organellar Coat Complexes and Organization of the Eukaryotic Cell. *Annu Rev Biochem* **86**, 637-657 (2017).
106. Amsterdam, A.*, et al.* Identification of 315 genes essential for early zebrafish development. *Proc Natl Acad Sci U S A* **101**, 12792-12797 (2004).
107. Gombart, A.F.*, et al.* Aberrant expression of neutrophil and macrophage-related genes in a murine model for human neutrophil-specific granule deficiency. *J Leukoc Biol* **78**, 1153-1165 (2005).
108. Lamb, J. The Connectivity Map: a new tool for biomedical research. *Nat Rev Cancer* **7**, 54-60 (2007).
109. Liu, S.P.*, et al.* Granulocyte colony-stimulating factor activating HIF-1alpha acts synergistically with erythropoietin to promote tissue plasticity. *PLoS One* **5**, e10093 (2010).
110. Jia, A.*, et al.* Hippo Kinase MST1-Mediated Cell Metabolism Reprograms the Homeostasis and Differentiation of Granulocyte Progenitor Cells. *J Immunol* **211**, 91-102 (2023).

111. Duan, Q.*, et al.* L1000CDS(2): LINCS L1000 characteristic direction signatures search engine. *NPJ Syst Biol Appl* **2**, 16015- (2016).
112. Matrone, G., Mullins, J.J., Tucker, C.S. & Denvir, M.A. Effects of Cyclin Dependent Kinase 9 inhibition on zebrafish larvae. *Cell Cycle* **15**, 3060-3069 (2016).
113. Bertrand, J.Y., Kim, A.D., Teng, S. & Traver, D. CD41+ cmyb+ precursors colonize the zebrafish pronephros by a novel migration route to initiate adult hematopoiesis. *Development* **135**, 1853-1862 (2008).
114. Lin, H.F.*, et al.* Analysis of thrombocyte development in CD41-GFP transgenic zebrafish. *Blood* **106**, 3803-3810 (2005).
115. Belt, A.J., Grant, S., Tombes, R.M. & Rothschild, S.C. Myeloid Targeted Human MLL-ENL and MLL-AF9 Induces cdk9 and bcl2 Expression in Zebrafish Embryos. *PLoS Genet* **20**, e1011308 (2024).
116. Hoodless, L.J.*, et al.* Genetic and pharmacological inhibition of CDK9 drives neutrophil apoptosis to resolve inflammation in zebrafish in vivo. *Sci Rep* **5**, 36980 (2016).
117. Montagnoli, A.*, et al.* A Cdc7 kinase inhibitor restricts initiation of DNA replication and has antitumor activity. *Nat Chem Biol* **4**, 357-365 (2008).

7. APPENDIX I: PUBLISHED MANUSCRIPTS

A. **L. Doll**, N. Aghaallaei, A.M. Dick, K. Welte, J. Skokowa, B. Bajoghli, '*A zebrafish model for HAX1-associated congenital neutropenia*'. *Haematologica* 2021; 106 (5): 1311-1320.

B. **L. Doll**, K. Welte, J. Skokowa, B. Bajoghli, *'A JAGN1-associated severe congenital neutropenia zebrafish model revealed an altered G-CSFR signaling and UPR activation.*' *Blood Adv* 2024; 8 (15): 4050–4065.

C. N. Borbarán Bravo, E. Deordieva*, **L. Doll***, M. ElGamacy*, B. Dannenmann*, J. Azevedo*, S. Bräuning, V. Zakharova, C. Lengerke, M. Sturm, O. Rieß, C. Zeidler, K. Welte, A. Shcherbina, M. Klimiankou, J. Skokowa, *'A New Severe Congenital Neutropenia Syndrome Associated with Autosomal Recessive COPZ1 Mutations'*. *Blood* 2025*;* 145 (20): 2317-2335*.*

D. M. Nasri*, B. Dannenmann*, **L. Doll**, B. Findik, F. Bernhard, S. Kandabarau, M. Klimiankou, M. Gawaz, C. Lengerke, C. Zeidler, K. Welte, J. Skokowa. *'Flavopiridol restores granulopoiesis in experimental models of severe congenital neutropenia*.' *Mol Ther* 2025; 33 (6): 2851-2871.

A. L. Doll, N. Aghaallaei, A.M. Dick, K. Welte, J. Skokowa, B. Bajoghli, '*A zebrafish model for HAX1-associated congenital neutropenia*'. *Haematologica* 2021; 106 (5): 1311-1320.

ARTICLE

A zebrafish model for HAX1-associated congenital neutropenia

Larissa Doll,[1] Narges Aghaallaei,[1] Advaita M. Dick,[1] Karl Welte,[2] Julia Skokowa[1] and Baubak Bajoghli[1]

[1]Department of Oncology, Hematology, Immunology and Rheumatology, University Hospital, University of Tübingen and [2]University Children's Hospital Tübingen, Tübingen, Germany

Ferrata Storti Foundation

Haematologica 2021
Volume 106(5):1311-1320

ABSTRACT

Severe congenital neutropenia is a rare heterogeneous group of diseases, characterized by an arrest of granulocyte maturation. Autosomal recessive mutations in the *HAX1* gene are frequently detected in affected individuals. However, the precise role of HAX1 during neutrophil differentiation is poorly understood. To date, no reliable animal model has been established to study *HAX1*-associated congenital neutropenia. Here we show that knockdown of zebrafish *hax1* impairs neutrophil development without affecting other myeloid cells and erythrocytes. Furthermore, we found that interference with Hax1 function decreases the expression level of key target genes of the granulocyte colony-stimulating factor signaling pathway. The reduced neutrophil numbers in the morphants could be reversed by granulocyte colony-stimulating factor, which is also the main therapeutic intervention for patients who have congenital neutropenia. Our results demonstrate that the zebrafish is a suitable model for *HAX1*-associated neutropenia. We anticipate that this model will serve as an *in vivo* platform to identify new avenues for developing tailored therapeutic strategies for patients with congenital neutropenia, particularly for those individuals who do not respond to granulocyte colony-stimulating factor treatment.

Introduction

Severe congenital neutropenia (CN) is a rare hematologic disorder, which is characterized by impaired maturation of neutrophil granulocytes.[1-6] Mutations in various genes, including *ELANE, HAX1, G6PC3, CXCR4* and *G-CSFR* are associated with CN.[1] Affected individuals are prone to life-threatening infections that begin in their first months of life unless treated by human granulocyte colony-stimulating factor (G-CSF, encoded by the *CSF3* gene) or bone marrow transplantation.[1,2] CN is also a preleukemic syndrome and patients are predisposed to develop myelodysplasia or acute myeloid leukemia after a long period of time.[7,8] However, the severity of neutropenia and the risk of leukemia vary between individuals with distinct genetic aberrations, and a group of CN patients do not respond to the G-CSF therapy. The cumulative incidence of leukemia in less responsive patients is 40% after 15 years, in comparison to 20% in responsive patients,[9] although, the underlying mechanisms are poorly understood.

HAX1 is ubiquitously expressed among human tissues.[10,11] It acts as a binding partner of multiple proteins and is involved in various signaling pathways and cellular processes.[12-14] For example, HAX1 interacts with the mitochondrial proteases PARL and HTRA2 and is involved in anti-apoptotic signaling.[15] It interacts with PKD2 protein and is associated with the actin cytoskeleton.[16] HAX1 plays a role in BCR-mediated internalization through binding to the cytoplasmic domain of B-cell receptors.[17] In hematopoietic progenitors, upon activation of the G-CSF receptor (G-CSFR), the cytoplasmic HAX1 binds to the HCSL1 and LEF-1 proteins, transporting LEF-1 into the nucleus. This transcription factor then activates target genes of the G-CSF signaling pathway including *CEBPA* and *HCLS1*.[18] Taking into account that HAX1 is involved in diverse subcellular processes, it remains unclear why patients who lack functional HAX1 display predominantly impaired neutrophil differentiation.

Our current knowledge on the role of HAX1 in granulopoiesis is predominantly derived from *in vitro* studies and clinical observations.[1,2] To date, no faithful animal

Correspondence:

BAUBAK BAJOGHLI
baubak.bajoghli@med.uni-tuebingen.de

Received: October 11, 2019.

Accepted: April 9, 2020.

Pre-published: April 23, 2020.

https://doi.org/10.3324/haematol.2019.240200

model has been established and, therefore, the experimental model system is based on in vitro neutrophil differentiation of induced pluripotent stem cells from patients with *HAX1*-associated CN.[19,20] Mice lacking *Hax1* display normal granulopoiesis and their predominant phenotype is post-natal lethality due to neuronal apoptosis.[15] Hence, there is an urgent need for an *in vivo* model to study the role of HAX1 in granulopoiesis and leukemogenesis. Here, we chose to use zebrafish (*Danio rerio*) as a vertebrate model because cellular and molecular mechanisms underlying granulopoiesis are largely conserved between zebrafish and humans,[21-25] and 82% of disease-causing human genes have an orthologue in zebrafish.[26,27] For example, zebrafish harboring mutations in *g-csfr,*[23,24] *cxcr4*,[28] and *g6pc3*[29] display impaired neutrophil development, mimicking CN patients who lack the corresponding orthologue gene. Thus far, it was unknown whether *hax1* is involved in zebrafish granulopoiesis. Here, we show that this gene is expressed in zebrafish hematopoietic cells and is indispensable for neutrophil development, which makes zebrafish a suitable model for studying *HAX1*-associated neutropenia.

Methods

Zebrafish

Zebrafish lines were maintained according to standard protocols and handled in accordance with European Union animal protection directive 2010/63/EU and approved by the local government (Tierschutzgesetz §11, Abs. 1, Nr. 1, husbandry permit 35/9185.46/Uni TÜ). All experiments described in the present study were conducted on embryos younger than 5 days post-fertilization (dpf). In this study, we used the wild-type TE strain of zebrafish. The transgenic (tg) reporter lines tg(*mpo:gfp*) and tg(*lyz:dsRED*) have been described previously.[30,31]

Injection of morpholino, single-guide RNA and messenger RNA

Three morpholinos (GeneTools) targeting the *hax1* gene were used in this study (*Online Supplementary Table S1*). For the rescue experiment, full-length complementary DNA (cDNA) of zebrafish *hax1* was isolated and cloned into the pMC vector.[32] Capped messenger RNA (mRNA) was synthesized using the mMESSAGE mMACHINE SP6 kit (Ambion). Morpholino and 5-10 ng/µL of *hax1* mRNA were co-injected into one-cell stage zebrafish embryos. To perform transient CRISPR-Cas9 targeting of the *hax1* gene, single guide RNA (sgRNA) target site (5'-GGGTTTTTCGGGATTCCCGG-3') was predicted and evaluated for off-target site by using the CCTop web tool.[33] sgRNA (15 ng/µL) and 150 ng/µL of Cas9 mRNA (a kind gift from J. Wittbrodt, Heidelberg University) were co-injected into one-cell stage transgenic tg(*mpo:gfp*) embryos.

Heat-inducible *g-csfa* construct

The full-length cDNA of zebrafish *g-csfa* (or *csf3a*) was isolated and cloned into the pTGH2 plasmid containing a bi-directional heat-inducible promoter[34] flanked by Tol2 binding sites. The resulting plasmids were then injected at a dose of 20 ng/µL with 10 ng/µL mRNA of *Tol2* transposase into one-cell-stage embryos. Injected embryos at 1 dpf were heat treated at 39°C for 1 h. Green fluorescent protein-positive (GFP^+) embryos were selected for subsequent whole mount *in situ* hybridization (WISH) analysis.

Whole mount *in situ* hybridization

RNA *in situ* hybridization of zebrafish embryos was performed as described previously[35] using digoxigenin-labeled RNA antisense probes, which are listed in *Online Supplementary Table S2*.

Statistical analysis

GraphPad Prism software (version 8) was used to produce graphs and for the statistical analysis. In this study, an unpaired, two-tailed Wilcoxon-Mann-Whitney test was used to compare the means of different data sets.

Additional details of the material and methods are available in the *Online Supplementary Material* and *Methods*.

Results

Zebrafish *hax1* is expressed in hematopoietic cells

An *in silico* analysis was carried out to characterize zebrafish *hax1*. A high degree of synteny was found between human and zebrafish *hax1* with the *upab2l* and *pygo2* genes upstream, and *aqp10b* and *cks1b* genes downstream in the corresponding genomic loci (Figure 1A). Multiple alignment and phylogenetic analysis revealed strong amino acid similarities over the entire coding region of Hax1 protein between zebrafish and its orthologues in other vertebrates (Figure 1B, *Online Supplementary Figure S1*). To elucidate whether *hax1* is expressed in zebrafish hematopoietic cells, we first searched for *hax1* in two single-cell RNA-sequencing databases[36,37] of adult zebrafish whole kidney marrow (akin to mammalian bone marrow). In both databases, *hax1* was found to be expressed in neutrophils, macrophages, and erythrocytes, albeit at low levels (*data not shown*). WISH was performed to determine the *hax1* spatial expression patterns during embryonic development, revealing that *hax1* is ubiquitously expressed throughout gastrulation and early embryonic segmentation (Figure 1C). At later stages, the *hax1* transcript was detected in the posterior intermediate cell mass and caudal hematopoietic tissue (Figure 1C-F, black arrows), which are the sites of primitive and definitive hematopoiesis, respectively, in zebrafish embryos.[21] The expression of *hax1* in hematopoietic cells was also confirmed by double fluorescent *in situ* hybridization analysis, revealing co-localization of *hax1* and *cmyb*, a marker of hematopoietic stem cells (Figure 1D). Notably, *hax1* transcript was also detected in the brain at 4 dpf (Figure 1G, arrow).

Loss-of-function of Hax1 leads to reduced neutrophil numbers in zebrafish embryos

To determine whether *hax1* has a role in zebrafish hematopoiesis, a morpholino (MO)-mediated gene knockdown strategy was used. Specifically, three MO targeting the *hax1* gene were used (*Online Supplementary Figure S2A*). One MO was designed against the ATG start codon site (hereafter named atg-MO), whereas the other two blocked the correct splicing of either exon 1 (hereafter named e1-MO) or exon 2 (hereafter named e2-MO), leading to a truncated Hax1 protein (*Online Supplementary Figure S2B-E*). Quantitative analysis showed that wild-type *hax1* transcript levels decreased to 90% and 70% in the embryos injected with e1-MO and e2-MO, respectively (Figure 2A, *Online Supplementary Figure S2F* and *G*). Notably, injection of MO did not result in embryonic mal-

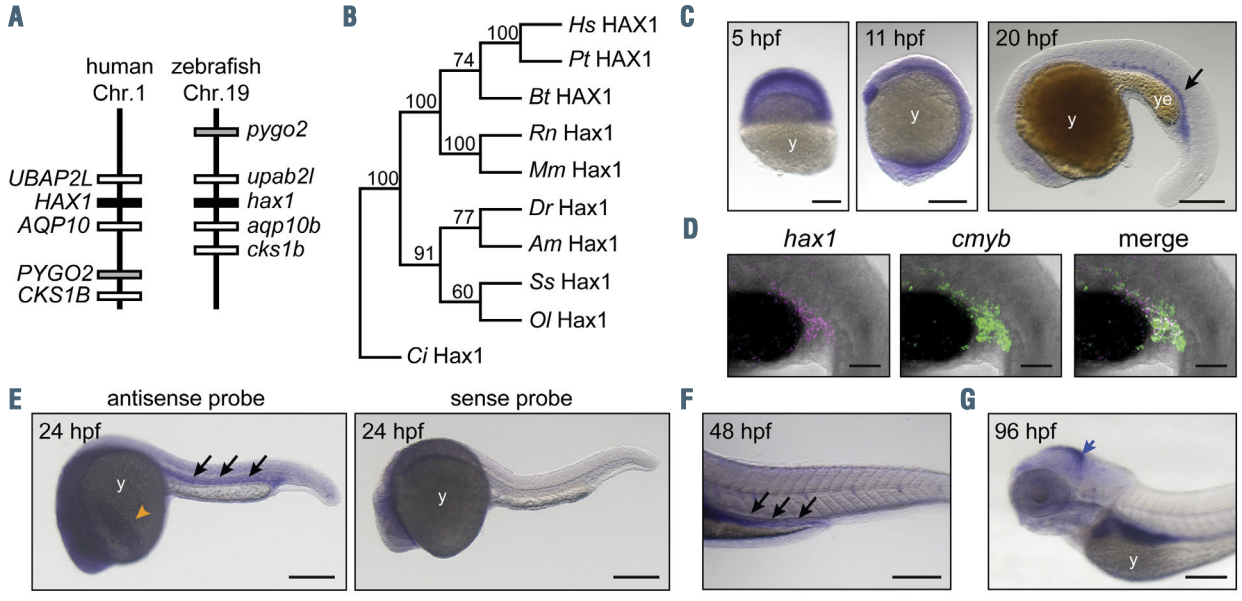

Figure 1. Characterization of zebrafish *hax1*. (A) Schematic comparison showing syntenic conservation of the *hax1* loci in humans and zebrafish. (B) A neighbor-joining phylogenetic tree of Hax1 proteins, which was performed with 1,000 bootstrap replications. *Am, Astyanax mexicanus; Bt, Bos taurus; Ci, Ciona intestinalis; Dr, Danio rerio; Hs, Homo sapiens; Mm, Mus musculus; Ol, Oryzias latipes; Pt, Pan troglodytes; Rn, Rattus norvegicus; Ss, Salmo salar*. (C) Spatial *hax1* expression by whole mount *in situ* hybridization analysis from 5 to 20 hours post-fertilization (hpf). (D) Confocal image of double fluorescent *in situ* hybridization of *hax1* (magenta) and *cmyb* (green) at 20 hpf. (E-G) Spatial *hax1* expression at 24 (E), 48 (F) and 96 (G) hpf. Arrows in C, E, and F indicate *hax1* expression in the hematopoietic site. A sense probe was used as a negative control (E, right panel). Note that the images shown in E are two images stitched together. y: yolk; ye: yolk extension. Scale bars: 100 μm (C, E-G), 50 μm (D).

formation (*Online Supplementary Figure S3*). To determine whether *hax1* knockdown impairs neutrophil development, two different approaches were used. First, cells expressing the neutrophil-specific marker *myeloid peroxidase (mpo)* were stained in MO-injected embryos (hereafter called morphants) using WISH. Compared to wild-type embryos, the number of *mpo*$^+$ cells was significantly reduced in all three morphants (Figure 2B). As a second approach, MO were injected separately into the zebrafish transgenic tg(*mpo:gfp*) embryos in which GFP is expressed under the control of *mpo* promoter.[30] Consistent with WISH data, in all three morphants, the numbers of GFP$^+$ cells were reduced in comparison to the numbers in uninjected siblings (Figure 2C) and no significant difference was observed when a control MO was injected (*Online Supplementary Figure S4*). To test the specificity of the MO, full-length mRNA of zebrafish *hax1* was co-injected with either e1-MO or e2-MO, showing that overexpression of *hax1* rescued the reduced neutrophil numbers in both morphants (Figure 2D). In addition to MO-mediated gene knockdown, transient CRISPR-Cas9 targeting of the *hax1* gene in the tg(*mpo:gfp*) line was performed. Compared with the non-injected siblings, *hax1* crispants showed significantly fewer GFP$^+$ cells in the trunk region at 2 dpf (*Online Supplementary Figure S5*). Collectively, our findings suggest that *hax1* has a role in zebrafish neutrophil development.

Normal phagocytic activity and migratory behavior of neutrophils in *hax1* morphants

Given that Hax1 is able to interact with proteins associated with cytoskeleton machinery and is involved in the migration of cancer cells *in vitro*,[38] we tested to what extent Hax1 loss-of-function impairs the migratory behavior of neutrophils *in vivo*. One way to induce an inflammatory response and chemotaxis is to inject bacteria into the notochord of zebrafish embryos.[35] We, therefore, injected Alexa 594-conjugated *Staphylococcus aureus* debris into this region (Figure 3A) and then embryos were analyzed using confocal microscopy. We found a similar accumulation of neutrophils in the infected site between wild-type (Figure 3B, top panels) and *hax1* morphants (Figure 3B, bottom panels). Time-lapse *in vivo* imaging revealed that *hax1* knockdown did not substantially affect the migration or phagocytic activity of neutrophils (Figure 3C).

Normal erythropoiesis and monopoiesis in *hax1* morphants

Based on single-cell RNA sequencing databases of zebrafish hematopoietic cells,[36,37] *hax1* is also expressed in erythrocytes and macrophages. We, therefore, performed tests to determine whether loss-of-function of Hax1 could affect erythropoiesis or the development of macrophages. WISH analysis showed that there were no detectable differences in the expression patterns of *gata1* and *hemoglobin alpha embryonic 1.1 (hbae1.1)* in the morphants when compared to wild-type embryos at 1 dpf (Figure 4A and B). These results and the presence of circulating red blood cells in the morphants (*data not shown*) suggest that *hax1* is dispensable for embryonic erythropoiesis.

We next examined to what extent the development of myeloid cells was affected in *hax1* morphants. We tested the expression of *pu.1*, a regulator of monocytic differentiation.[39] In 2 dpf *hax1* MO-injected embryos, the number of *pu.1*$^+$ cells appeared comparable with that in the wild-type fish (Figure 4C), which mimics data from CN patients.[40] Analysis with markers of mature myeloid cells demonstrated a substantial decrease in *l-plastin*$^+$ leukocytes (Figure 4D), *lyz*$^+$ neutrophils (Figure 4E) and *g-csfr*$^+$

cells (Figure 4F). The last gene is expressed in monocytes and neutrophils. In contrast, *mpeg1.1*$^{+}$ macrophages[41] were not affected (Figure 4G). With regard to definitive hematopoiesis, no difference was observed in the expression of the hematopoietic stem cell marker *cmyb* between wild-type and *hax1* morphants at 2 dpf (Figure 4H). Together, these results indicate that *hax1* is dispensable for embryonic erythropoiesis and monopoiesis.

Interference with Hax1 function enhances apoptosis in embryos but not in neutrophils

We next sought to determine the underlying molecular basis for the role of Hax1 in neutrophil development. To date, two main observations associated with HAX1 deficiency in CN patients are increased apoptosis of myeloid progenitors,[6] and decreased activity of the G-CSF signal transduction pathway.[18] Based on these findings, we examined to what extent cellular viability and the G-CSF signaling pathway were affected in *hax1* morphants. We used three approaches to identify apoptotic cells. First, a terminal deoxynucleotidyl transferase dUTP nick end labeling (TUNEL) assay was performed to detect apoptotic cells. Compared to their wild-type counterparts, *hax1* morphants exhibited increased apoptosis at 1 dpf (Figure 5A and B). The increased apoptosis at 1 dpf was specific to the *hax1* knockdown fish because no significant difference was observed when a control MO was injected (Figure 5B). By 2 dpf, the number of apoptotic cells was comparable between morphants and uninjected embryos (Figure 5C, *Online Supplementary Figure S6*). As a second approach, we stained wild-type embryos and *hax1* morphants with the fluorescent dye acridine orange (Figure 5D). Similar to the TUNEL assay, this showed that the number of apoptotic cells was increased in the *hax1* morphants at 1 dpf (Figure 5E), but not at 2 dpf (Figure 5F). Strikingly, apoptotic cells stained with acridine orange as well as TUNEL were scattered throughout the embryo and not preferentially associated with sites of hematopoiesis. In support of this notion, we incubated wild-type and *hax1*-injected tg(*lyz:dsRED*) embryos with a caspase 3/7 reporter, which produces a green fluorogenic response upon cleavage by activated caspase-3 or caspase-7. Confocal imaging of 2 dpf transgenic tg(*lyz:dsRED*) embryos (Figure 5G) showed that the frequency of dsRED^{+} cells stained with the caspase 3/7 reporter was comparable in the wild-type and *hax1* morphants at 2 dpf (Figure 5H). It is also worth noting that interference with Hax1 function did not affect cell proliferation in embryos (*Online Supplementary Figure S7*). These findings, therefore, indicate that *hax1* knockdown enhances apoptosis in zebrafish embryos at early stages, but not in neutrophils.

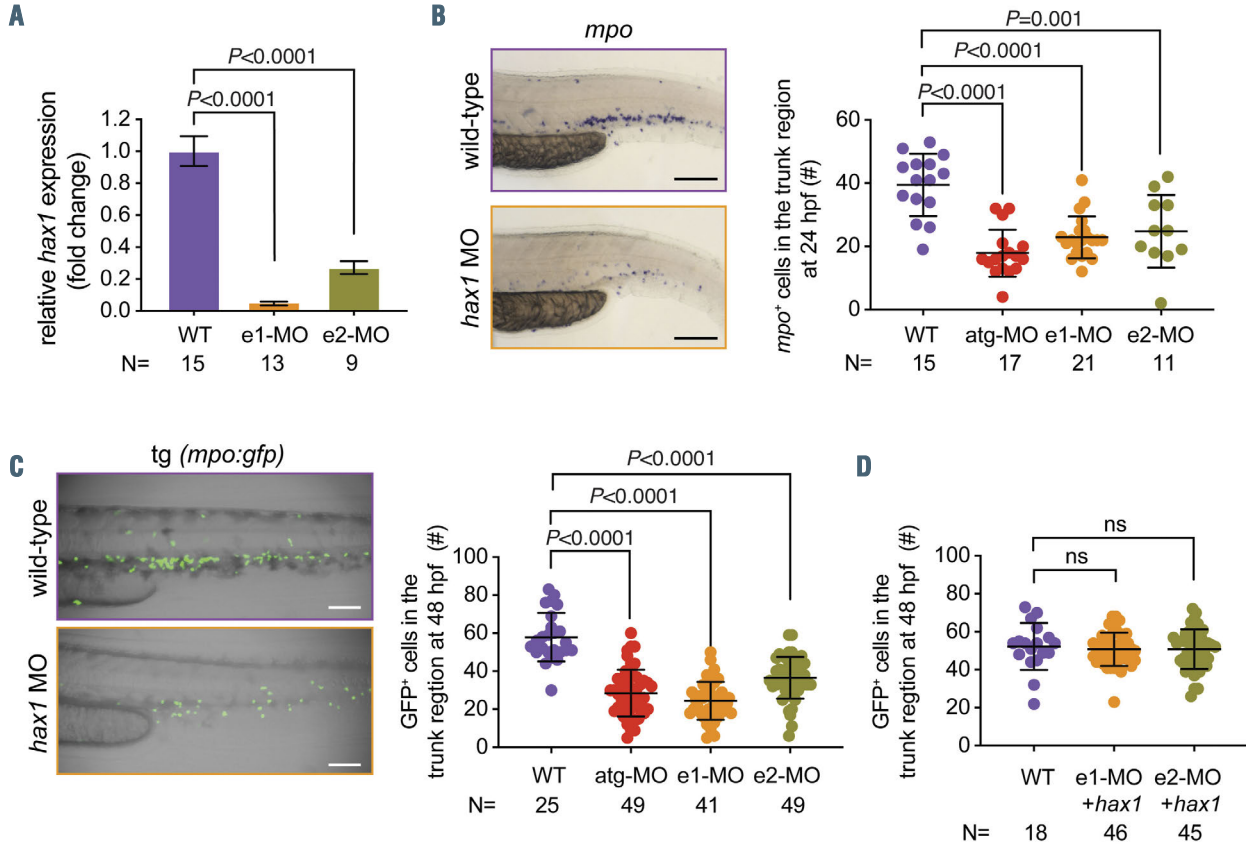

Figure 2. Knockdown of *hax1* impairs neutrophil development. (A) Relative change of wild-type *hax1* transcript in the *hax1* morphants compared with wild-type (WT) using quantitative polymerase chain reaction. N indicates number of biological replicates. (B) Representative images of *mpo*-stained cells in WT and e1-MO injected embryos (left panel). Note that each stained cell represents a neutrophil. The right panel shows numbers of *mpo* stained cells in the trunk region at 24 hours post-fertilization (hpf). (C) Injection of *hax1* morpholinos (MO) in the tg(*mpo:gfp*) line. The left panel shows representative images of uninjected (WT) and *hax1* e1-MO injected transgenic embryos at 48 hpf. The right panel shows numbers of green fluorescent protein-positive cells in the trunk region. (D) Co-injection of e1-MO or e2-MO morpholinos with *hax1* mRNA rescued the reduced neutrophil numbers in the tg(*mpo:gfp*) line. Scale bars indicate 100 μm. Each dot represents an individual embryo. Data are means ± standard deviation.

Granulocyte colony-stimulating factor rescues reduced neutrophil numbers in the *hax1* morphants

Next, two approaches were used to evaluate the expression of *hcls1, cebpa* and *cebpb*, which are activated by G-CSF. First, total RNA was isolated from morphants and uninjected embryos at 2 dpf. Quantitative reverse transcriptase polymerase chain reaction analysis was performed to determine the levels of expression of *hcls1, cebpa* and *cebpb*. This revealed a downregulation of the expression levels of *hcls1* and *cebpa*, while the expression of *cebpb* was upregulated in the *hax1* morphants (Figure 6A). As a second approach, cells expressing *cebpa* or *cebpb* were stained using WISH. Similarly, the number of *cebpa*$^{+}$ cells was reduced (Figure 6B), while the number of *cebpb*$^{+}$ cells was increased (Figure 6C) in the *hax1* morphants. These findings raised the question of whether overexpression of *g-csf* is sufficient to rescue the reduced number of neutrophils in *hax1* morphants. To address this question, a heat-inducible promoter[34] was used to ectopically express zebrafish *g-csfa* at 1 dpf (Figure 6D).

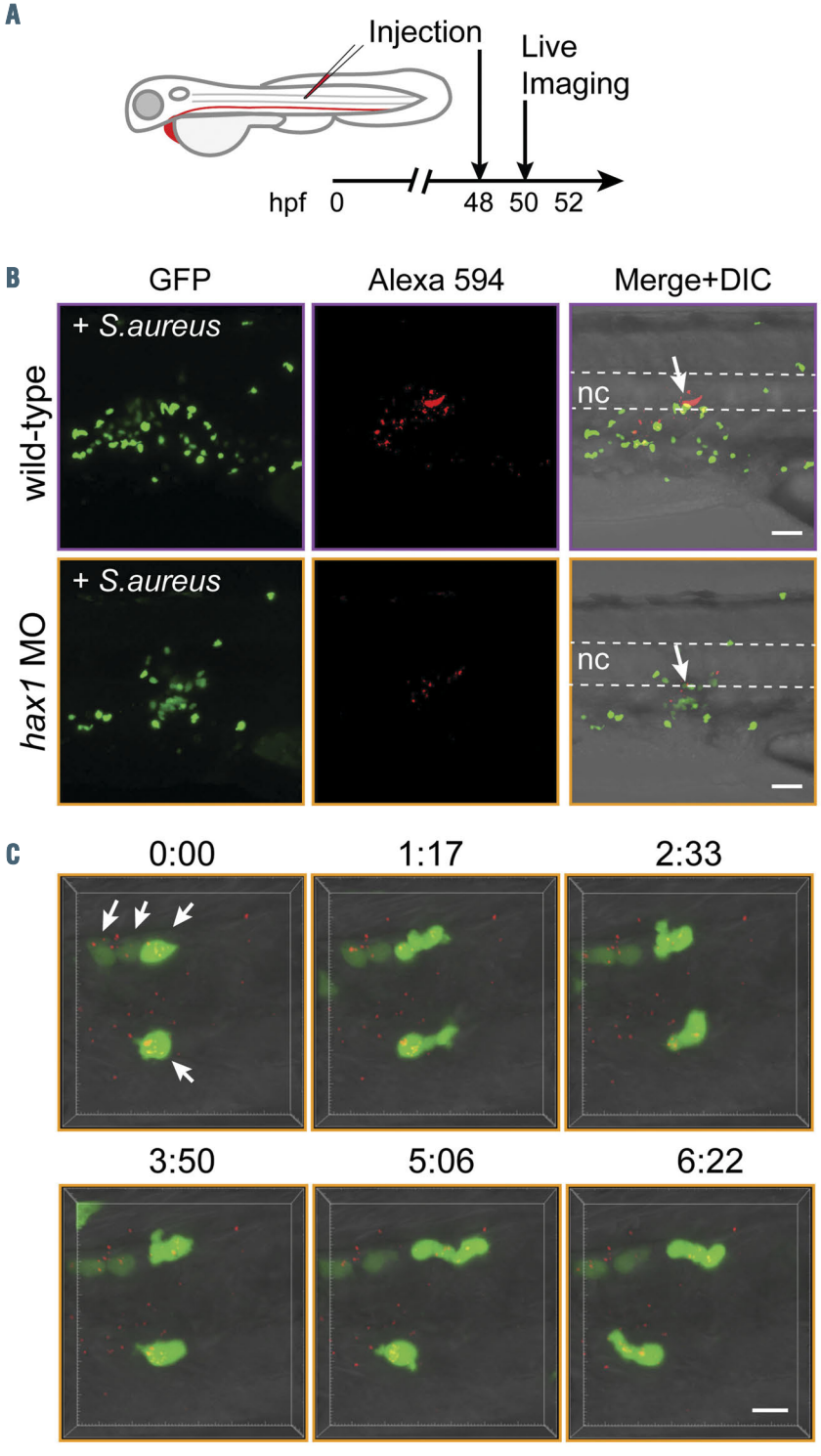

Figure 3. Migration and phagocytosis of neutrophils in the *hax1* morphants. (A) Experimental design. (B) Injection of Alexa-594 conjugated *Staphylococcus aureus* debris into the notochord of tg(*mpo:gfp*) embryos at 2 days post-fertilization (dpf). Arrows indicate the injected site. Dashed lines indicate the position of the notochord. (C) Still photographs from a time-lapse recording illustrating the migration and phagocytic activity of neutrophils (arrows) in the *hax1* morphants. Numbers indicate time in minutes. Scale bars, 40 μm (B) and 10 μm (C). GFP: green fluorescent protein; nc: notochord.

Consistent with a previous study,[22] an average 1.7-fold increase of *mpo*$^+$ cells was observed when *g-csfa* was ectopically expressed in wild-type embryos (Figure 6E). Next, the *g-csfa* inducible construct was co-injected with *hax1* e1-MO into embryos. Heat shock was performed at 1 dpf and GFP$^+$ embryos were selected for WISH analysis. As expected, embryos injected with e1-MO displayed reduced neutrophil numbers. However, when *g-csfa* was induced in the morphants, we observed that the number of neutrophils was increased to a level which was compa-

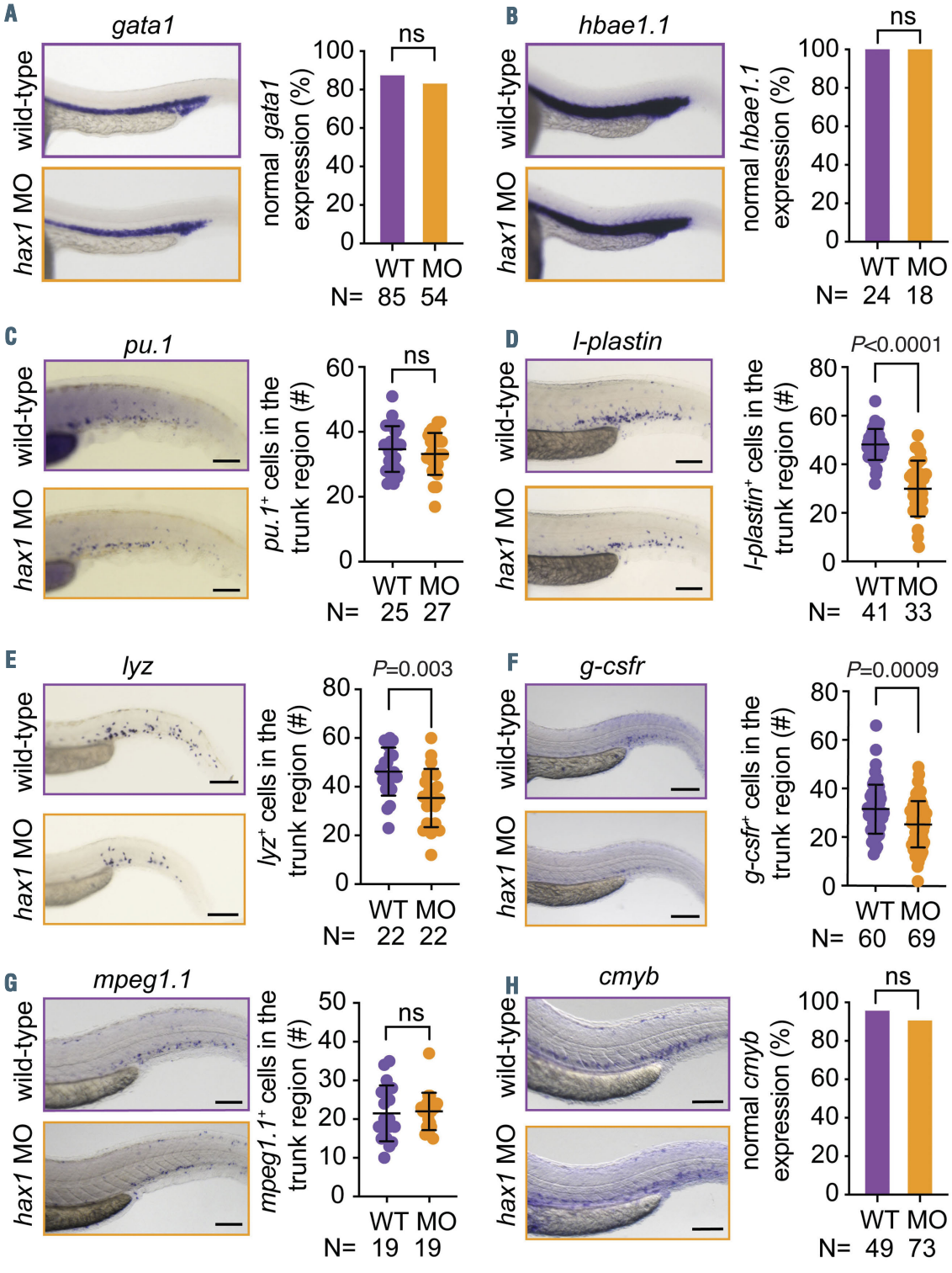

Figure 4. Normal development of erythrocytes, macrophages and hematopoietic stem cells in the *hax1* morphants. (A-H) Left panels show representative images of whole mount *in situ* hybridization for *gata1* (A), *hbae1.1* (B), *pu.1* (C), *l-plastin* (D), lyz (E), *g-csfr* (F), *mpeg1.1* (G) and *cmyb* (H) expression in uninjected (WT) and *hax1* e1-MO injected embryos at 24 hours post-fertilization (hpf) (A,B) or 48 hpf (C-H). Right panels show quantitative numbers of stained cells in the trunk region. Scale bars indicate 100 μm. Each dot in C-G represents an individual embryo. Data are means ± standard deviation.

rable with that in the control group (Figure 6E), indicating that *g-csfa* is sufficient to reverse the reduced neutrophil numbers in *hax1* morphants.

Discussion

In this study, we show that *hax1* is indispensable for zebrafish granulopoiesis. This is the first study demonstrating that *hax1* is required for neutrophil development in a vertebrate other than humans. Our data revealed that knockdown of *hax1* reduces the expression of *cebpa* and *hcls1* genes, two downstream target genes of the G-csf signaling pathway. This result is in agreement with our previous *in vitro* study, in which knockdown of HAX1 in $CD34^+$ progenitor cells impaired granulocytic differentiation by reducing the levels of *CEBPA* and *HCLS1* expression.[18] Similarly, *CEBPA* expression is severely diminished in CN patients with *HAX1* deficiency. C/EBPα is a transcription factor involved in steady-state granulopoiesis, and regulates *G-CSFR* expression through a positive feedback loop.[25] This regulatory relationship between C/EBPα and G-CSFR appears to be evolutionarily conserved between zebrafish and humans because zebrafish *cebpa* mutants also display reduced *g-csfr* expression.[42] Although we did not provide a direct assessment of G-CSF signaling in zebrafish *hax1*-deficient neutrophils, the reduced levels of expression of *hcls1* and *cebpa*, two direct target genes of G-CSF signaling, together with decreased *g-csfr*$^+$ cells in the morphants support the notion that *hax1* has a role in G-CSF signaling, which is in agreement with previous *in vitro* data.[18] It is, however, important to stress that our data do not rule out the possibility that *hax1* knockdown reduced the number of *cebpa*-expressing cells rather than decreasing the *cebpa* expression level in each myeloid cell. Nevertheless, the expression of *cebpb* was increased in the *hax1* morphants. C/EBPβ functions as the main transcriptional regulator for emergency granulopoiesis,[43] and CN patients with *HAX1* deficiency also show an elevated level of *CEBPB* expression.[18,44]

Previous studies have shown that HAX1 has an anti-apoptotic function and interacts with a variety of intracel-

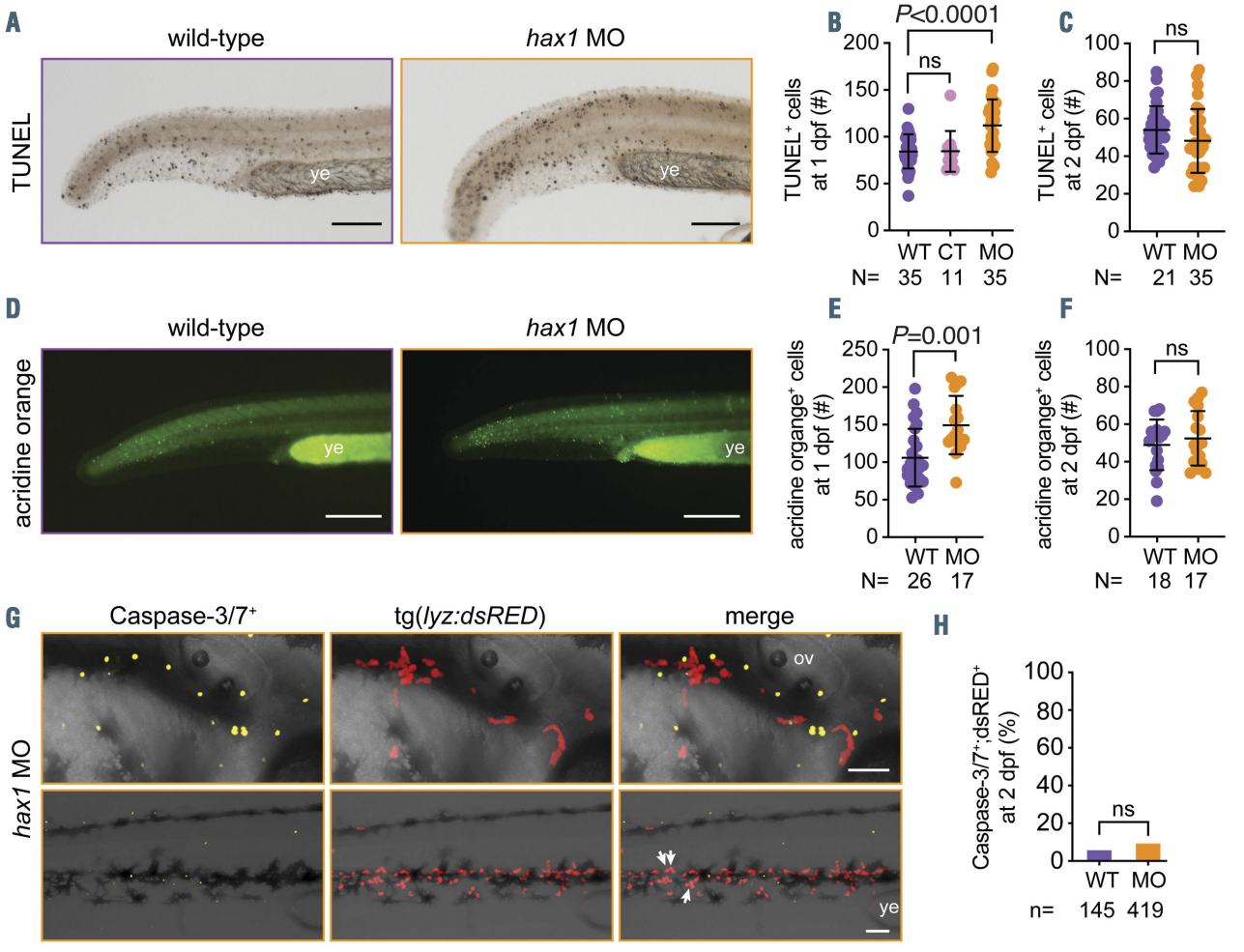

Figure 5. Enhanced apoptosis by *hax1* knockdown. (A) Representative images of TUNEL-positive cells in wild-type (WT) and *hax1* morphants (MO) at 1 day post-fertilization (dpf). (B, C) Quantitative numbers of TUNEL-positive cells in the trunk region at 1 dpf (B) and 2 dpf (C). Note injection of control (CT) morpholino did not significantly increase the number of TUNEL-positive cells. (D) Representative images of acridine orange-stained cells in WT and *hax1* MO at 1 dpf. (E, F) Quantitative numbers of acridine orange-stained cells in the trunk region at 1 dpf (E) and 2 dpf (F). (G) Representative images from the head (top panel) and trunk region (bottom panel) of the tg(*lyz:dsRED*) embryos injected with *hax1* MO showing cells stained with caspase-3/7 reporter (yellow) and neutrophils (red) at 2 dpf. (H) Frequency of caspase-3/7 and dsRED double positive cells in WT and *hax1* morphants. n indicates number of $dsRED^+$ cells counted from three wild-type embryos (WT) and 10 morphants (MO) at 2 dpf. Each dot in B, C, E and F represents an individual embryo. Data are means ± standard deviation. Scale bars: 100 μm (A, D) and 50 μm (G). ov: otic vesicle; ye: yolk extension.

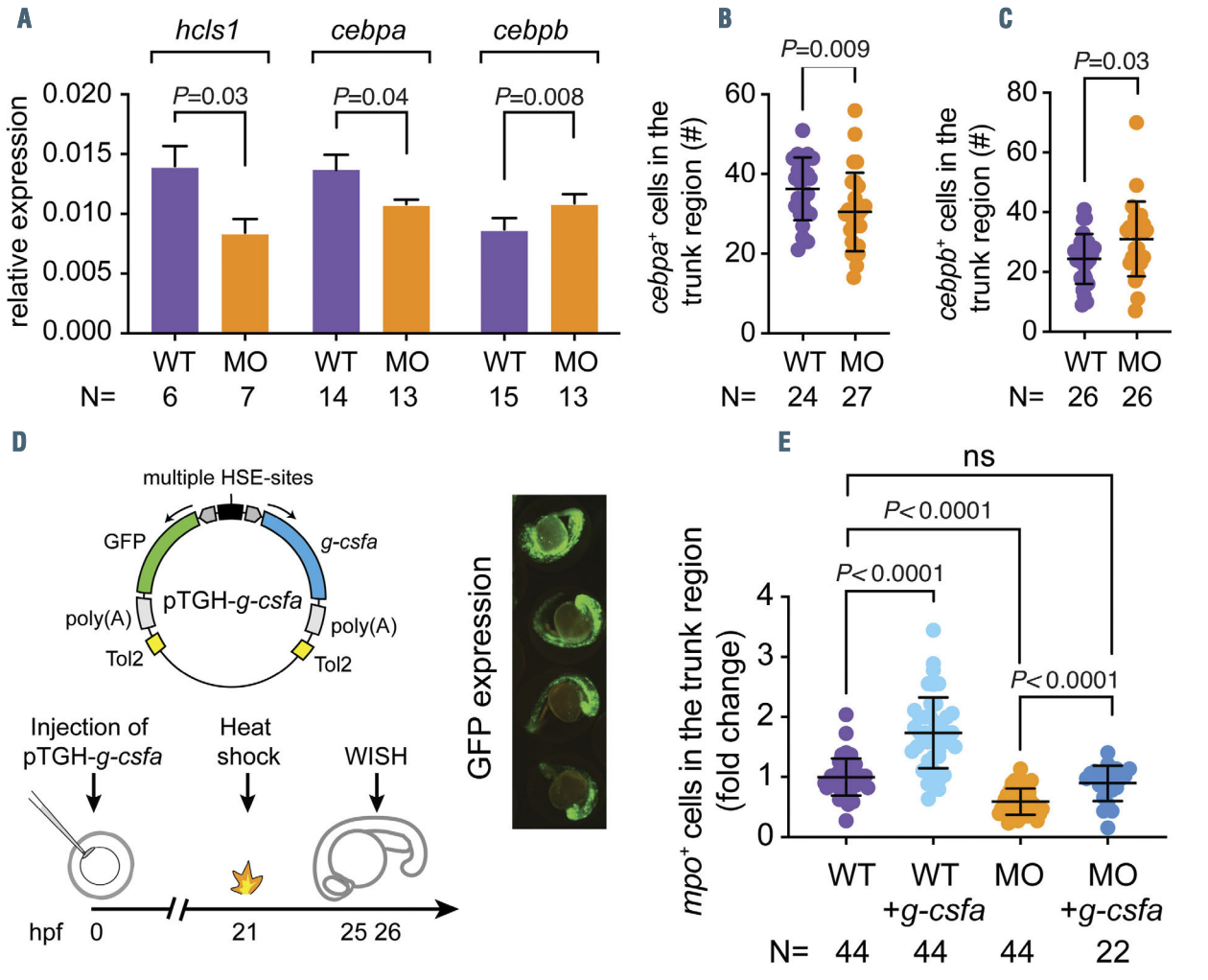

Figure 6. G-csfa induction rescued the reduced neutrophil numbers in the *hax1* morphants. (A) Relative expression of *hcls1, cebpa, cebpb* in wild-type (WT) and morphants (MO) at 2 days post-fertilization (dpf). The *β-actin* gene was used as an internal control for normalization. N indicates number of biological replicates. (B, C) Quantitative numbers of *cebpa*- and *cebpb*-expressing cells in the trunk region of WT and MO at 2 dpf. (D) The top panel illustrates the bi-directional construct (pTGH-*g-csfa*) used to ectopically induce the zebrafish *g-csfa* cDNA. Note that green fluorescent protein (GFP) expression was used as a positive control for induction (4 representative embryos are shown in the right panel). The lower panel outlines the timing of the experiment. (E) Fold change of *mpo*$^+$ cells in the trunk region of embryos at 25 hours post-fertilization (hpf). Each dot represents an individual embryo. N indicates number of embryos. Data are means ± standard deviation.

lular apoptosis-related proteins.[15,45] Consequently, Hax1-deficient mice display neuronal apoptosis.[15] Increased apoptosis was also observed in the bone marrow myeloid progenitor cells of CN patients with a HAX1 mutation.[46] Knockdown of zebrafish *hax1* increased apoptosis at 1 dpf, as determined by a TUNEL assay and acridine orange staining. However, cell death was not associated with the hematopoietic tissue. Furthermore, knockdown of *hax1* did not enhance apoptosis in neutrophils. Hence, zebrafish Hax1 has an anti-apoptotic role during early embryonic development, but increased cell death is most likely not the main reason for the reduced neutrophil numbers. These results contradict previous data indicating that autosomal recessive mutations in the human *HAX1* gene are associated with increased apoptosis in myeloid cells.[6]

In human, two alternatively spliced isoforms of *HAX1* have been identified.[4] Patients with *HAX1* mutations affecting the full-length transcript or the splice variant I develop CN, whereas patients with mutations affecting the splice isoforms I and II develop CN with neurological abnormalities.[5,10] The isoform II uses an alternate in-frame splice site producing a shortened exon 2, and is expressed in the brain but not in the bone marrow.[10] In zebrafish, a sole *hax1* transcript was identified by amplification from the embryonic cDNA. Interestingly, *hax1* transcript was also detected in a brain region where newborn neurons are continuously added and contribute to sensory information processing, akin to the superior colliculus in mammals.[47] Nevertheless, the role of Hax1 in zebrafish neurogenesis remains to be elucidated.

Collectively, our data have established zebrafish as an *in vivo* model for HAX1-associated neutropenia, filling the gap between *in vitro* models and clinical assessment. Given that the zebrafish is a valuable model for studying driver mutations underlying disease pathogenesis in acute myeloid leukemia and myelodysplastic syndromes,[48] a stable *hax1*-deficient zebrafish line will help investigations into the leukemogenic role of Hax1, alone and in combination with other gene mutations.[49] Besides being an important cancer model, the zebrafish also represents a reliable platform to perform screens of large compounds and assess their therapeutic relevance.[50] Therefore, we

anticipate that our model will serve as a platform to identify new avenues for developing tailored therapeutic strategies for patients with CN.

Disclosures

No conflicts of interest to disclose.

Contributions

LD and BB made initial observations; LD performed most of the experiments and contributed to the design of the work; NA performed experiments in the transgenic lines; AMD performed quantitative polymerase chain reaction, immunostaining and fluorescence in situ hybridization analysis; KW and JS provided useful insights and interpreted the data. BB supervised and supported the study and wrote the manuscript. All authors read and edited the manuscript.

Acknowledgments

The authors would like to thank Patrick Müller (Fredrich Miescher Laboratory, Tübingen) for providing the wild-type TE strain of zebrafish and transgenic lines, Jochen Wittbrodt (Center for Organismal Studies, Heidelberg University) for providing the Cas9 construct, Annisa Claasen and Christine Gottschalk for technical help, and the Institute of Medical Virology and Microbiology for continuous support in confocal microscopy.

Funding

The work in BB's laboratory is supported by the Deutsche Forschungsgemeinschaft (BA 5766/3-1), Deutsche José Carreras Leukämie-Stiftung (DJCLS11 R/2018), and Wilhelm-Sander-Stiftung.

References

1. Skokowa J, Dale DC, Touw IP, Zeidler C, Welte K. Severe congenital neutropenias. Nat Rev Dis Primers. 2017;3:17032.
2. Klein C. Kostmann's disease and HCLS1-associated protein X-1 (HAX1). J Clin Immunol. 2017;37(2):117-122.
3. Boztug K, Ding XQ, Hartmann H, et al. HAX1 mutations causing severe congenital neuropenia and neurological disease lead to cerebral microstructural abnormalities documented by quantitative MRI. Am J Med Genet A. 2010;152A(12):3157-3163.
4. Fadeel B, Grzybowska E. HAX-1: a multifunctional protein with emerging roles in human disease. Biochim Biophys Acta. 2009;1790(10):1139-1148.
5. Germeshausen M, Grudzien M, Zeidler C, et al. Novel HAX1 mutations in patients with severe congenital neutropenia reveal isoform-dependent genotype-phenotype associations. Blood. 2008;111(10):4954-4957.
6. Klein C, Grudzien M, Appaswamy G, et al. HAX1 deficiency causes autosomal recessive severe congenital neutropenia (Kostmann disease). Nat Genet. 2007; 39(1):86-92.
7. Yetgin S, Olcay L, Koc A, Germeshausen M. Transformation of severe congenital neutropenia to early acute lymphoblastic leukemia in a patient with HAX1 mutation and without G-CSF administration or receptor mutation. Leukemia. 2008; 22(9):1797.
8. Zeidler C, Germeshausen M, Klein C, Welte K. Clinical implications of ELA2-, HAX1-, and G-CSF-receptor (CSF3R) mutations in severe congenital neutropenia. Br J Haematol. 2009;144(4):459-467.
9. Rosenberg PS, Zeidler C, Bolyard AA, et al. Stable long-term risk of leukaemia in patients with severe congenital neutropenia maintained on G-CSF therapy. Br J Haematol. 2010;150(2):196-199.
10. Carlsson G, van't Hooft I, Melin M, et al. Central nervous system involvement in severe congenital neutropenia: neurological and neuropsychological abnormalities associated with specific HAX1 mutations. J Intern Med. 2008;264(4):388-400.
11. Hippe A, Bylaite M, Chen M, et al. Expression and tissue distribution of mouse Hax1. Gene. 2006;379:116-126.
12. Grzybowska EA, Zayat V, Konopinski R, et al. HAX-1 is a nucleocytoplasmic shuttling protein with a possible role in mRNA processing. FEBS J. 2013;280(1):256-272.
13. Suzuki Y, Demoliere C, Kitamura D, Takeshita H, Deuschle U, Watanabe T. HAX-1, a novel intracellular protein, localized on mitochondria, directly associates with HS1, a substrate of Src family tyrosine kinases. J Immunol. 1997;158(6):2736-2744.
14. Yap SV, Vafiadaki E, Strong J, Kontrogianni-Konstantopoulos A. HAX-1: a multifaceted antiapoptotic protein localizing in the mitochondria and the sarcoplasmic reticulum of striated muscle cells. J Mol Cell Cardiol. 2010;48(6):1266-1279.
15. Chao JR, Parganas E, Boyd K, Hong CY, Opferman JT, Ihle JN. Hax1-mediated processing of HtrA2 by Parl allows survival of lymphocytes and neurons. Nature. 2008;452(7183):98-102.
16. Gallagher AR, Cedzich A, Gretz N, Somlo S, Witzgall R. The polycystic kidney disease protein PKD2 interacts with Hax-1, a protein associated with the actin cytoskeleton. Proc Natl Acad Sci U S A. 2000; 97(8):4017-4022.
17. Wolkerstorfer S, Schwaiger E, Rinnerthaler M, et al. HAX1 deletion impairs BCR internalization and leads to delayed BCR-mediated apoptosis. Cell Mol Immunol. 2016;13(4):451-461.
18. Skokowa J, Klimiankou M, Klimenkova O, et al. Interactions among HCLS1, HAX1 and LEF-1 proteins are essential for G-CSF-triggered granulopoiesis. Nat Med. 2012;18(10):1550-1559
19. Morishima T, Watanabe K, Niwa A, et al. Genetic correction of HAX1 in induced pluripotent stem cells from a patient with severe congenital neutropenia improves defective granulopoiesis. Haematologica. 2014;99(1):19-27.
20. Pittermann E, Lachmann N, MacLean G, et al. Gene correction of HAX1 reversed Kostmann disease phenotype in patient-specific induced pluripotent stem cells. Blood Adv. 2017;1(14):903-914.
21. Avagyan S, Zon LI. Fish to learn: insights into blood development and blood disorders from zebrafish hematopoiesis. Hum Gene Ther. 2016;27(4):287-294.
22. Stachura DL, Svoboda O, Campbell CA, et al. The zebrafish granulocyte colony-stimulating factors (Gcsfs): 2 paralogous cytokines and their roles in hematopoietic development and maintenance. Blood. 2013;122(24):3918-3928.
23. Pazhakh V, Clark S, Keightley MC, Lieschke GJ. A GCSFR/CSF3R zebrafish mutant models the persistent basal neutrophil deficiency of severe congenital neutropenia. Sci Rep. 2017;7:44455.
24. Basheer F, Rasighaemi P, Liongue C, Ward AC. Zebrafish granulocyte colony-stimulating factor receptor maintains neutrophil number and function throughout the life span. Infect Immun. 2019;87(2):e00793-18.
25. Liongue C, Hall CJ, O'Connell BA, Crosier P, Ward AC. Zebrafish granulocyte colony-stimulating factor receptor signaling promotes myelopoiesis and myeloid cell migration. Blood. 2009;113(11):2535-2546.
26. Howe K, Clark MD, Torroja CF, et al. The zebrafish reference genome sequence and its relationship to the human genome. Nature. 2013;496(7446):498-503.
27. Oyarbide U, Topczewski J, Corey SJ. Peering through zebrafish to understand inherited bone marrow failure syndromes. Haematologica. 2019;104(1):13-24.
28. Walters KB, Green JM, Surfus JC, Yoo SK, Huttenlocher A. Live imaging of neutrophil motility in a zebrafish model of WHIM syndrome. Blood. 2010;116(15):2803-2811.
29. Zhang CY, Yin HM, Wang H, et al. Transforming growth factor-beta1 regulates the nascent hematopoietic stem cell niche by promoting gluconeogenesis. Leukemia. 2018;32(2):479-491.
30. Renshaw SA, Loynes CA, Trushell DM, Elworthy S, Ingham PW, Whyte MK. A transgenic zebrafish model of neutrophilic inflammation. Blood. 2006;108(13):3976-3978.
31. Hall C, Flores MV, Storm T, Crosier K, Crosier P. The zebrafish lysozyme C promoter drives myeloid-specific expression in transgenic fish. BMC Dev Biol. 2007;7:42.
32. Fink M, Flekna G, Ludwig A, Heimbucher T, Czerny T. Improved translation efficiency of injected mRNA during early embryonic development. Dev Dyn. 2006; 235(12):3370-3378.
33. Stemmer M, Thumberger T, Del Sol Keyer M, Wittbrodt J, Mateo JL. CCTop: an intuitive, flexible and reliable CRISPR/Cas9 target prediction tool. PLoS One. 2015; 10(4):e0124633.
34. Bajoghli B, Aghaallaei N, Heimbucher T, Czerny T. An artificial promoter construct for heat-inducible misexpression during fish embryogenesis. Dev Biol. 2004; 271(2):416-430.
35. Kuri P, Ellwanger K, Kufer TA, Leptin M, Bajoghli B. A high-sensitivity bi-directional reporter to monitor NF-kappaB activity in cell culture and zebrafish in real time. J Cell Sci. 2017;130(3):648-657.

36. Tang Q, Iyer S, Lobbardi R, et al. Dissecting hematopoietic and renal cell heterogeneity in adult zebrafish at single-cell resolution using RNA sequencing. J Exp Med. 2017;214(10):2875-2887.
37. Athanasiadis EI, Botthof JG, Andres H, Ferreira L, Lio P, Cvejic A. Single-cell RNA-sequencing uncovers transcriptional states and fate decisions in haematopoiesis. Nat Commun. 2017;8(1):2045.
38. Cavnar PJ, Berthier E, Beebe DJ, Huttenlocher A. Hax1 regulates neutrophil adhesion and motility through RhoA. J Cell Biol. 2011;193(3):465-473.
39. Tenen DG, Hromas R, Licht JD, Zhang DE. Transcription factors, normal myeloid development, and leukemia. Blood. 1997; 90(2):489-519.
40. Skokowa J, Welte K. Dysregulation of myeloid-specific transcription factors in congenital neutropenia. Ann N Y Acad Sci. 2009;1176:94-100.
41. Ellett F, Pase L, Hayman JW, Andrianopoulos A, Lieschke GJ. mpeg1 promoter transgenes direct macrophage-lineage expression in zebrafish. Blood. 2011;117(4):e49-56.
42. Dai Y, Zhu L, Huang Z, et al. Cebpalpha is essential for the embryonic myeloid progenitor and neutrophil maintenance in zebrafish. J Genet Genomics. 2016; 43(10):593-600.
43. Manz MG, Boettcher S. Emergency granulopoiesis. Nat Rev Immunol. 2014; 14(5):302-314.
44. Skokowa J, Welte K. Defective G-CSFR signaling pathways in congenital neutropenia. Hematol Oncol Clin North Am. 2013; 27(1):75-88, viii.
45. Yap SV, Koontz JM, Kontrogianni-Konstantopoulos A. HAX-1: a family of apoptotic regulators in health and disease. J Cell Physiol. 2011;226(11):2752-2761.
46. Carlsson G, Aprikyan AA, Tehranchi R, et al. Kostmann syndrome: severe congenital neutropenia associated with defective expression of Bcl-2, constitutive mitochondrial release of cytochrome c, and excessive apoptosis of myeloid progenitor cells. Blood. 2004;103(9):3355-3361.
47. Boulanger-Weill J, Sumbre G. Functional integration of newborn neurons in the zebrafish optic tectum. Front Cell Dev Biol. 2019;7:57.
48. Baeten JT, de Jong JLO. Genetic models of leukemia in zebrafish. Front Cell Dev Biol. 2018;6:115.
49. Skokowa J, Steinemann D, Katsman-Kuipers JE, et al. Cooperativity of RUNX1 and CSF3R mutations in severe congenital neutropenia: a unique pathway in myeloid leukemogenesis. Blood. 2014;123(14):2229-2237.
50. MacRae CA, Peterson RT. Zebrafish as tools for drug discovery. Nat Rev Drug Discov. 2015;14(10):721-731.

A zebrafish model for HAX1-associated congenital neutropenia

Larissa Doll,[1] Narges Aghaallaei,[1] Advaita M. Dick,[1] Karl Welte,[2] Julia Skokowa[1] and Baubak Bajoghli[1]

[1]Department of Oncology, Hematology, Immunology and Rheumatology, University Hospital, University of Tübingen and [2]University Children's Hospital Tübingen, Tübingen, Germany

 doi:10.3324/haematol.2019.240200

Received: October 11, 2019.

Accepted: April 9, 2020.

Pre-published: April 23, 2020.

Correspondence: *BAUBAK BAJOGHLI* - baubak.bajoghli@med.uni-tuebingen.de

Supplementary Data:

Supplementary Material and Methods

Quantitative RT-PCR

Total RNA was extracted from pools of 8 zebrafish embryos at 48 hpf using TRIzol (Life Technologies) following the manufacturer's protocol. RNA samples were then treated with RQ1 RNAse-Free DNase (Promega) before first-strand cDNA synthesis with random hexamer primers and Superscript III Reverse Transcriptase (ThermoFischer) following the manufacturer's protocol. Quantitative PCR (qPCR) was carried out using the SYBR Green Kit (Applied Biosystems) on the Light Cycler 480 (ROCHE). The data was analyzed in Microsoft Excel using the ΔCT method with *β-actin* as a reference gene for normalization. Primers are listed in the *Supplementary Table 3*.

Fluorescent *in situ* hybridization (FISH)

High resolution double FISH was performed utilizing standard digoxigenin- and fluorescein-labeled RNA antisense probes along with tyramide signal amplification (TSA) as described previously [1]. Briefly, after hybridization and removal of both probes, samples were incubated with 1:500 diluted Anti-Fluorescein-POD antibody in blocking solution for overnight at 4°C and then stained with the TSA Plus Fluorescein solution for 60 minutes in the dark. Samples were treated with 1% H_2O_2 in Methanol for 30 minutes. After stepwise rehydration and blocking, samples were incubated with 1:1000 diluted Anti-DIG-POD antibody in blocking solution for overnight at 4°C. The TSA Plus Cy3 solution (1:50 dilution) was used for the second staining. Images were taken using LSM 710 microscope.

Whole-mount immunostaining

Immunostaining was performed as described previously [2]. Briefly, zebrafish embryos at 2 dpf were fixed with 4% paraformaldehyde in 2xPBS, 0.1% Tween-20 for at least 24 hours at 4°C. For permeabilization, samples were treated with 100% Acetone at -20°C for 20 minutes. After wash steps, samples were incubated with blocking solution (10% FCS, 0.8% Triton X-100, 1% BSA, 0.1% Tween in 1xPBS) at 4°C for 3 hours with a gentle agitation on a turning wheel. For primary Antibody incubation, rabbit anti-phosphohistone 3 antibody (Ser10, Millipore 06-570, 1:500 dilution) was incubated with the sample in the incubation buffer (1% FCS, 0.8% Triton X-100, 1% BSA, 0.1% Tween in 1xPBS) at 4°C in the dark for 3 days. As secondary antibody, the Cy3-donkey anti-rabbit IgG (Jakson laboratories, 711-165-152, 1:500) was used for the

incubation with samples in the incubation buffer at 4°C in the dark for 2.5 days. To remove residual secondary antibody, samples were washed 3 times for 1 hour with PBS-TS (10% FCS, 1% Triton X-100 in PBS).

TUNEL assay

TUNEL staining in whole-mount embryos was performed using the In situ Cell Death Detection kit (Roche) according to manufacturer's protocol. Briefly, zebrafish embryos were fixed in 4% PFA/2xPBS and 0.1% Tween at 4°C overnight. Embryos were then permeabilized in 10µg/ml Proteinase K in PBS and 0.1% Tween for 20 min without shaking. For positive control, embryos were first incubated with DNase I at 25°C for 30 min. For negative control, embryos were incubated only with the labeling solution.

Acridine Orange staining

Zebrafish embryos at 2 dpf were stained for 30 minutes in a 50µg/ml acridine orange (Enzo, ENZ-52405) solution prepared with E3 media. After incubation in the dark, the embryos were washed 10 times for 5 minutes with E3 and imaged directly afterward.

Caspase-3/7 green detection assay

Transgenic tg(*lyz:dsRED*) were stained in 1:100 diluted Caspase-3/7 detection reagent (IncuCyte, 4440) with E3 media. After overnight incubation, embryos were washed five times for 5 minutes with E3 media and imaged directly afterward.

Microscopy and cell enumeration

A Nikon stereo-fluorescent microscope SMZ18 fitted with a Nikon DS-Fi3 camera and NIS-Elements software was used for imaging and manual counting. Confocal images were taken using a Zeiss LSM 710 NLO microscope. Z-stacks of 60-70µm spanning the trunk region (z-space 1µm) were acquired using 10x and 20x objectives. Confocal images were analyzed with Imaris software. The number of GFP-positive cells was automatically quantified using the fast spot tool (diameter: 8 µm, quality >1.25). Single cells detected by Imaris software were then examined manually. In this work, quantification of cell numbers was restricted to the cells that were located in the trunk region caudal to the yolk extension.

Supplementary Figures

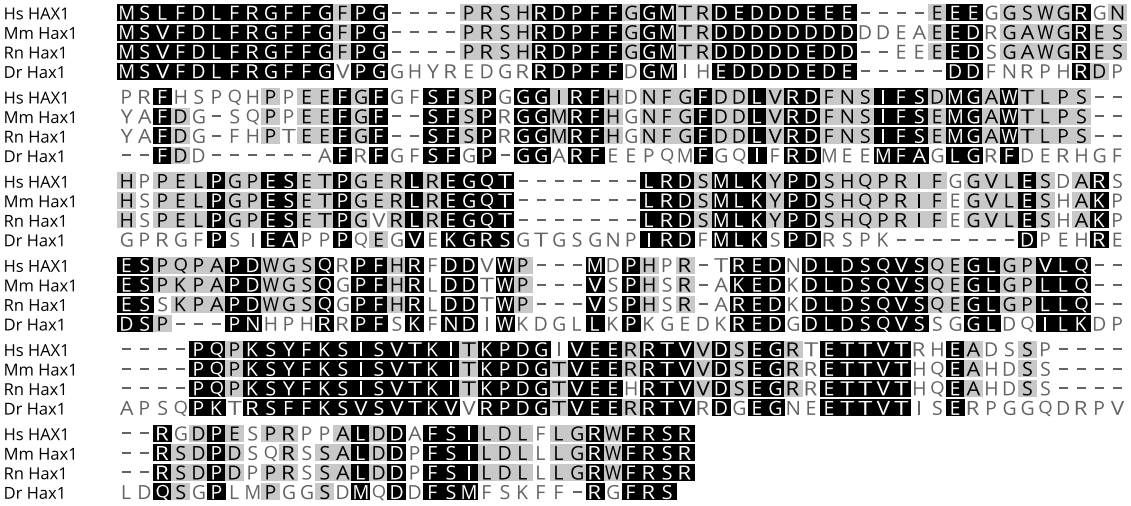

Supplementary Figure 1. Multiple alignment of the Hax1 amino acids sequences. The alignment was produced using Clustal W. Shading indicates conservation, with more strongly conserved positions shaded in darker colors. Hax1 protein from mouse (*Mus musculus*, Mm; Ensebml ID ENSMUSG00000027944), human (*Homo sapiens*, Hs; Accession number NM172219), rat (*Rattus norvegicus*, Rn; Ensebml ID ENSRNOG00000045647), and zebrafish (*Danio rerio*, Dr; ID ENSDARP00000053379), were used for the alignment.

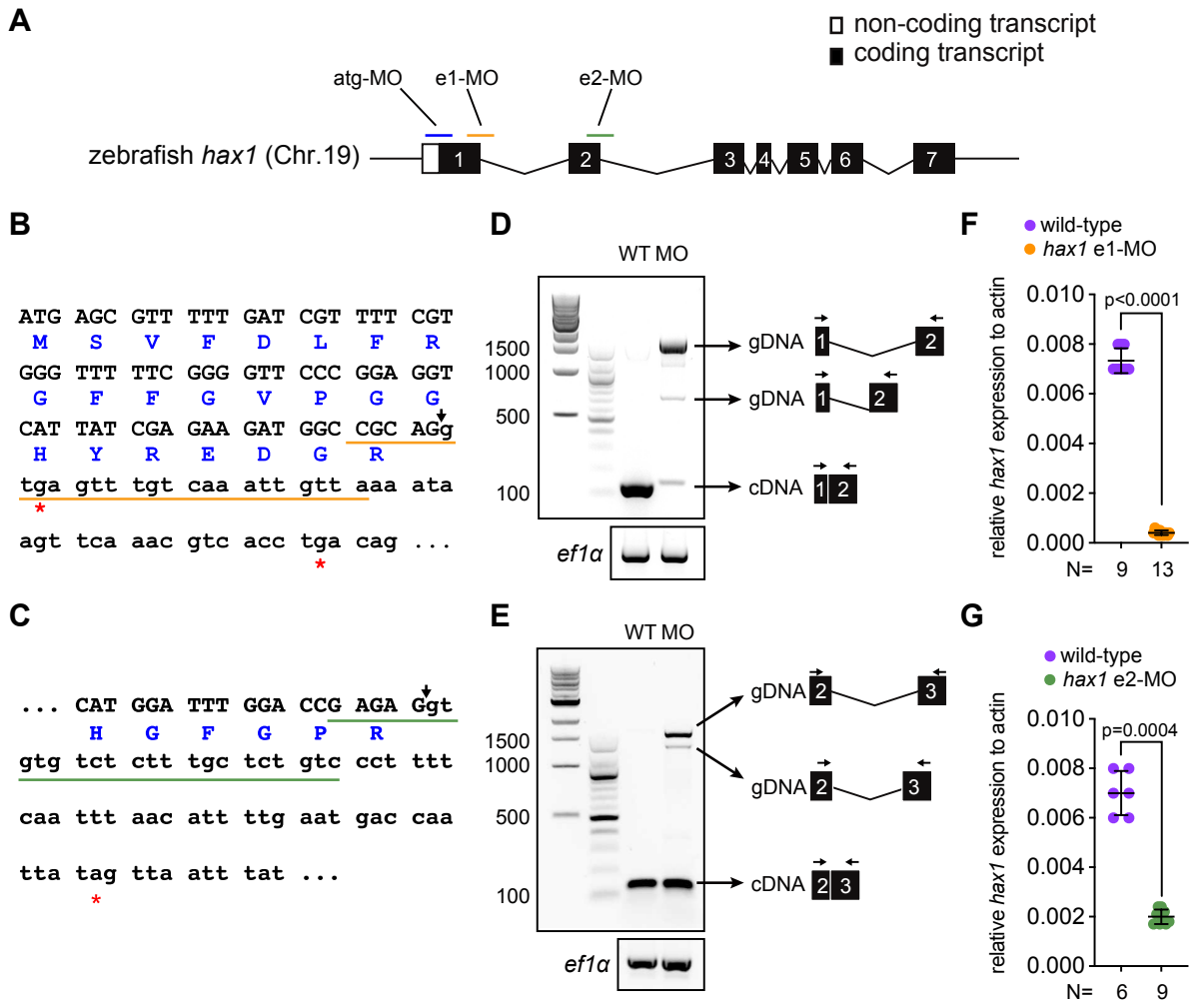

Supplementary Figure 2. Efficiency of *hax1* knockdown by using morpholinos. (**A**) Schematic diagram of zebrafish *hax1* gene organization. The binding sites of three morpholinos (MO) are highlighted by blue, orange and green lines. (**B, C**) The e1-MO and e2-MO target the splice donor site of exon 1-intron 1 (**B**) and exon 2- intron 2 (**C**), respectively. The coding sequences are shown in upper case and intronic sequences in lower cases. The blue letters indicate the amino acid sequences. Arrow indicates the splice donor site. Asterisks mean stop codon. (**D, E**) RT-PCR analysis of *hax1* transcript in wild-type (WT) and *hax1* e1-MO (**D**) or e2-MO (**E**) injected embryos at 48 hpf. (**F**, **G**) Relative expression level of normal *hax1* in WT and e1-MO (**F**) or e2-MO (**G**) injected embryos at 48 hpf. The *β-actin* gene was used as a reference for normalization. N indicates number of biological replicates.

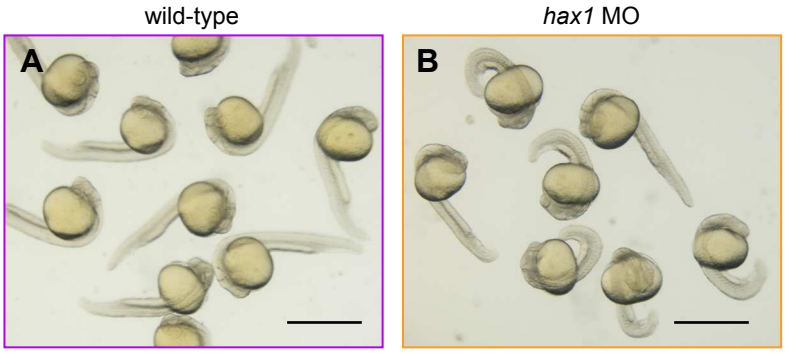

Supplementary Figure 3. No embryonic malformation in the *hax1* morphants. (A) Wild-type embryos at 1 dpf. (B) Embryos injected with e1-MO at 1 dpf. Scale bars indicate 500μm.

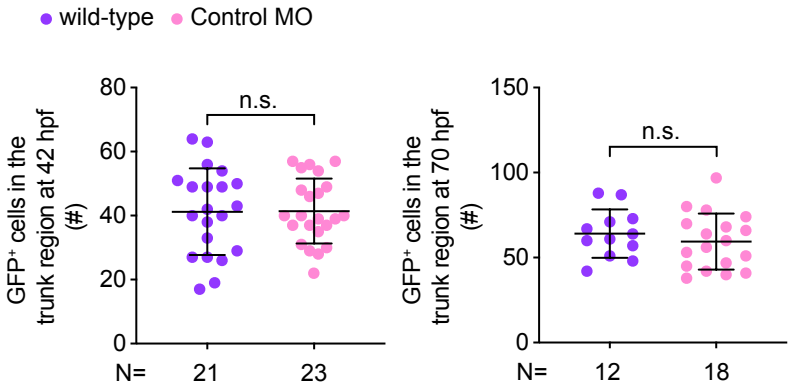

Supplementary Figure 4. Injection of control morpholino does not impair neutrophil development in the tg(*mpo:gfp*) embryos. Numbers of GFP-positive cells in the trunk region in uninjected (WT) and embryos injected with control MO at 42 hpf (left panel) and 70 hpf (right panel). Each dot represents an individual embryo. N indicates number of embryos. Data are means ± SD.

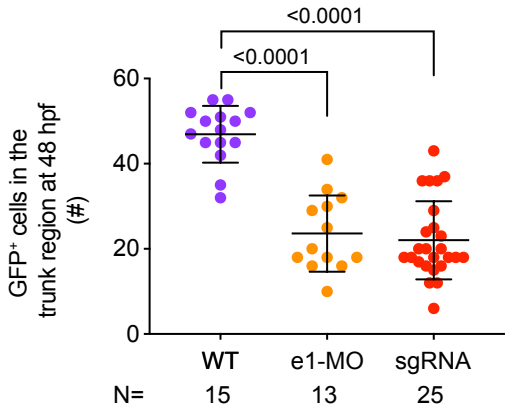

Supplementary Figure 5. Reduced neutrophil numbers in the *hax1* crispants. A sgRNA targeting *hax1* gene with mRNA of Cas9 were co-injected into the tg(*mpo:gfp*) embryos. Number of GFP-positive cells were counted in the trunk region in wild-type (WT) and crispants (sgRNA) at 48 hpf. For comparison, *hax1* e1-MO was also injected. Each dot represents an individual embryo. N indicates number of embryos. Data are means ± SD.

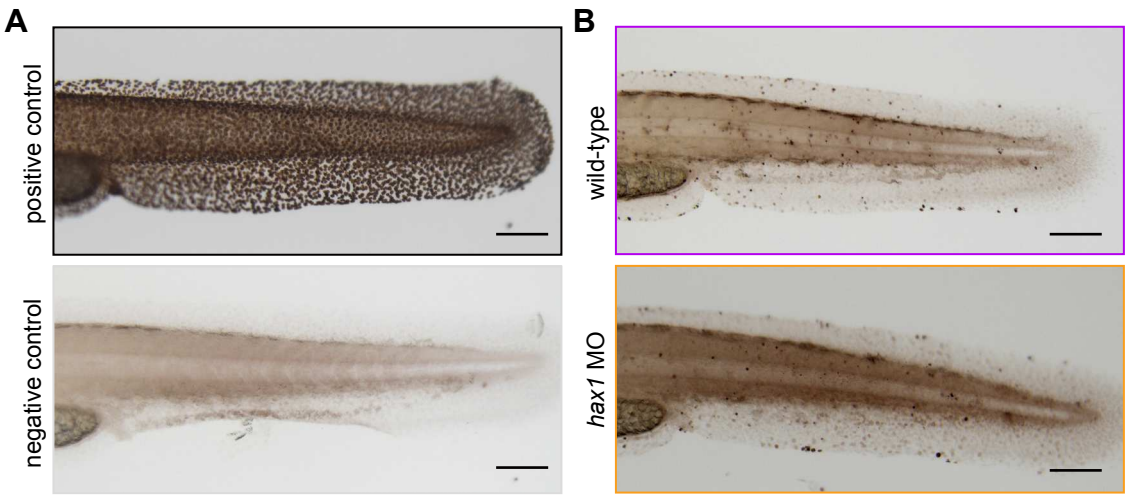

Supplementary Figure 6. TUNEL staining of zebrafish embryos at 2 dpf. (A) Top panel shows a representative image of a TUNEL staining in wild type pretreated with DNase I, as a positive control. Bottom panel shows a representative image of a TUNEL staining in wild type that were incubated with the labeling solution, as a negative control. (B) Representative images of TUNEL-positive cells in wild-type (top panel) and *hax1* morphants (bottom panel) at 2 dpf. Scale bars indicate 100 µm.

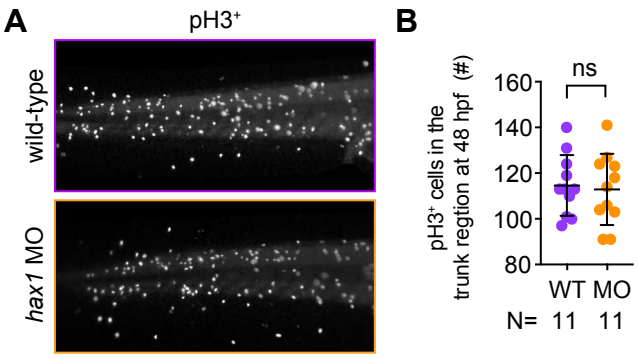

Supplementary Figure 7. Knockdown of *hax1* does not impair embryonic proliferation. (A) Representative images of pH3-positive cells in wild-type and *hax1* morphants at 2 dpf. (B) Number of pH3-positive cells counted in the trunk region in wild-type (WT) and morphant (MO) at 48 hpf. Each dot represents an individual embryo. N indicates number of embryos. Data are means ± SD.

Supplementary Table 1: Morpholinos used in this study

Name	Sequence (5‘>3‘)
hax1 atg-MO	AACGCTCATTTATGGACAGAATCCT
hax1 e1-MO	TAACAATTTGACAAACTCACCTGCG
hax1 e2-MO	GACAGAGCAAAGAGACACACCTCTC
Scrambled-MO	CCTCTTACCTCAGTTACAATTTATA

Supplementary Table 2: Gene-specific *in situ* hybridization probes used in this study

Gene	Accession Number/Eensembl ID	Nucleotides X to X
hax1	ENSDARG00000036764	164-755
mpo	BC056287	225-938
l-plastin	NM131320	404-1029
runx1	NM131603	542-1204
cmyb	NM131266	346-966
csf1ra	ENSDARG00000102986	2116-2755
csf3r	NM001113377	124-737
mpeg1.1.	ENSDARG00000055290	859-1417
pu.1 (spi1b)	ENSDARG00000000767	67-614
cebpa	ENSDARG00000036074	323-919
cebpb	ENSDARG00000042725	345-923
hbae1.1	ENSDARG00000088330	45-323

Supplementary Table 3: Primers for quantitative RT-PCR used in this study

Gene	Forward primer (5‘>3‘)	Reverse primer (5‘>3‘)
b-actin	GATCTTCACTCCCCTTGTTCA	GGCAGCGATTTCCTCATC
cebpa	GCTCCATGAAGATTGGCGATCG	CATTTTCGCCTTGTCCCGACTC
cebpb	CTCAAGCGGGAAAGGCAAGAAG	TGCGCATTTTGGCTTTGTCTCT
hcls1	AGAGAACGAGAAGAGGCACGAC	GGGAATTTCCGGCAGTTTCCTG
hax1 [a]	GTTCCCGGAGGTCATTATCGAGAAG	CTGGACCGAAACTGAATCCAAACC
hax1 [b]	CAGATCTTCAGAGACATGGAGG	CTCCTGCCTTTCTCAACTCCTTCC

[a] Primers bind to the exon 1 and 2 of *hax1* gene and were used to validate the efficiency of e1-MO.
[b] Primers bind to the exon 2 and 3 of *hax1* gene and were used to validate the efficiency of e2-MO.

Supplementary References:

1. Brend T, Holley SA. Zebrafish whole mount high-resolution double fluorescent in situ hybridization. J Vis Exp. 2009;25):
2. Bajoghli B, Kuri P, Inoue D, et al. Noninvasive In Toto Imaging of the Thymus Reveals Heterogeneous Migratory Behavior of Developing T Cells. J Immunol. 2015;195(5):2177-2186.

B. L. Doll, K. Welte, J. Skokowa, B. Bajoghli, *'A JAGN1-associated severe congenital neutropenia zebrafish model revealed an altered G-CSFR signaling and UPR activation.*' *Blood Adv* 2024; 8 (15): 4050–4065.

REGULAR ARTICLE

blood advances

A *JAGN1*-associated severe congenital neutropenia zebrafish model revealed an altered G-CSFR signaling and UPR activation

Larissa Doll,[1] Karl Welte,[1,2] Julia Skokowa,[1,3,*] and Baubak Bajoghli[1,4,*]

[1]Department of Oncology, Hematology, Clinical Immunology, and Rheumatology and [2]Department of Pediatric Hematology, Oncology and Bone Marrow Transplantation, Children's Hospital, University Hospital Tuebingen, Tuebingen, Germany; [3]Gene and RNA Therapy Center, Tuebingen University, Tuebingen, Germany; and [4]Austrian BioImaging/CMI, Vienna, Austria

Key Points

- Deregulation of zebrafish Jagn1 disrupts neutrophil development, affecting steady-state granulopoiesis.
- Activation of unfolded protein response and apoptosis alone is insufficient to induce neutropenia in zebrafish.

A variety of autosomal recessive mutations in the *JAGN1* gene cause severe congenital neutropenia (CN). However, the underlying pathomechanism remains poorly understood, mainly because of the limited availability of primary hematopoietic stem cells from *JAGN1*-CN patients and the absence of animal models. In this study, we aimed to address these limitations by establishing a zebrafish model of *JAGN1*-CN. We found 2 paralogs of the human *JAGN1* gene, namely *jagn1a* and *jagn1b*, which play distinct roles during zebrafish hematopoiesis. Using various approaches such as morpholino-based knockdown, CRISPR/Cas9–based gene editing, and misexpression of a *jagn1b* harboring a specific human mutation, we successfully developed neutropenia while leaving other hematopoietic lineages unaffected. Further analysis of our model revealed significant upregulation of apoptosis and genes involved in the unfolded protein response (UPR). However, neither UPR nor apoptosis is the primary mechanism that leads to neutropenia in zebrafish. Instead, Jagn1b has a critical role in granulocyte colony-stimulating factor receptor signaling and steady-state granulopoiesis, shedding light on the pathogenesis of neutropenia associated with *JAGN1* mutations. The establishment of a zebrafish model for *JAGN1*-CN represents a significant advancement in understanding the specific pathologic pathways underlying the disease. This model provides a valuable in vivo tool for further investigation and exploration of potential therapeutic strategies.

Introduction

Severe congenital neutropenia (CN) is a preleukemia bone marrow failure syndrome that is characterized by impaired neutrophil development and more than 20 associated mutated genes, including *JAGN1*.[1] Different types of *JAGN1* mutations have been reported in patients with CN, including deletions, missense, and, nonsense mutations. The majority of the mutations are located in the cytoplasmic N-terminal part of JAGN1. The severity and symptoms of neutropenia vary among patients. The pathophysiological mechanism in defective granulopoiesis remains poorly understood because of the lack of suitable animal models. The current understanding of *JAGN1*-associated CN is mostly based on clinical observations and in vitro studies.

Submitted 11 September 2023; accepted 2 May 2024; prepublished online on *Blood Advances* First Edition 13 May 2024; final version published online 31 July 2024. https://doi.org/10.1182/bloodadvances.2023011656.

*J.S. and B.B. contributed equally to this study.

Data are available on reasonable request from the corresponding authors, Julia Skokowa (Julia.skokowa@med.uni-tuebingen.de) and Baubak Bajoghli (Baubak.bajoghli@vbcf.ac.at).

The full-text version of this article contains a data supplement.

JAGN1 encodes an endoplasmic reticulum (ER)-resident protein with 4 transmembrane domains and cytoplasmic N- and C-terminal regions.[2] This membrane topology resembles that of 2 known cargo transporters, tetraspanins and endoplasmic reticulum vesicle (Erv) proteins.[3] Despite its evolutionary conservation, the precise function of JAGN1 remains to be fully elucidated. In *Drosophila melanogaster*, the *JAGN1* orthologous gene, *jagunal*, is involved in ER reorganization and vesicular trafficking during oogenesis[2] and in the proper asymmetric partitioning of the ER and spindle orientation in embryonic neuroblasts.[4] In addition, Jagunal plays a role in signaling and distribution of ER membranes in *Drosophila melanogaster* stem cells as they adopt their fate.[5] In human cells, JAGN1 interacts with tubulin and the coat protein I complex components that are essential for retrograde vesicular trafficking from the Golgi complex to the ER and within the Golgi.[6] These interactions occur through the highly conserved N-terminal region of JAGN1. The impact of mutations in JAGN1 on protein stability or its interaction with other binding partners remains unclear. Notably, electron microscopy images have shown ultrastructural ER defects and a lack of granules in neutrophils isolated from patients with *JAGN1*-CN.[6] In vitro studies have demonstrated a connection between *JAGN1* deficiency and defective NETs formation,[7] reduced myeloperoxidase (MPO) levels,[7] and abnormal protein N-glycosylation.[6,8] Moreover, transduction experiments with CN-associated *JAGN1* mutants in HL-60 cells have suggested the activation of calpain-dependent cell death.[9] Furthermore, there are indications of JAGN1 involvement in granulocyte colony-stimulating factor receptor (G-CSFR)-mediated STAT3 phosphorylation in the HeLa cell line and *Jagn1*$^{-/-}$ mouse neutrophils.[6,10] However, it remains uncertain whether these intracellular processes also affect the granulocytic differentiation of bone marrow myeloid progenitor cells, which is impaired in patients with *JAGN1*-CN. Most studies have been conducted in nonhematopoietic cell lines, artificial in vitro expression systems, terminally differentiated neutrophils, or immortalized lymphocytes of patients with *JAGN1*-CN.[6-9,11] The limited availability of primary bone marrow cells for experimentation hinders our understanding of the disease. Hence, there is an urgent need for suitable animal models to study the role of JAGN1 in granulopoiesis. Complete *Jagn1* knockout in mice leads to embryonic lethality, whereas mice with a conditional knockout in hematopoietic cells display normal neutrophil counts.[10] Over the past decade, zebrafish has emerged as a promising alternative model system for studying CN in humans.[12] Zebrafish deficient in *g-csfr*,[13,14] *hax1*,[15] *srp54*,[16,17] *sbds*,[18] *g6pc3*,[19] or *taz*[20] recapitulate phenotypes similar to those observed in CN. In addition, the response to G-CSF is comparable between the zebrafish models and patients with CN.[15]

In this study, we established a zebrafish model of *JAGN1*-CN. We demonstrated that either downregulation of *jagn1b* or misexpression of CN-associated mutated *jagn1b* induces isolated neutropenia. At the molecular level, we found a robust activation of the unfolded protein response (UPR) upon Jagn1b deregulation, but neither UPR activation nor increased cell death alone hindered neutrophil development in zebrafish. We therefore propose a mechanism through which Jagn1b contributes to the G-CSFR signaling pathway and steady-state granulopoiesis, and its neutropenia phenotype can be rescued by emergency granulopoiesis activation.

Material and methods

Zebrafish maintenance

Zebrafish wild-type (WT) Tübingen TE strain and transgenic reporter lines (tg(mpo:*gfp*), tg(drl:*mCherry*)[21,22]) were maintained according to standard protocols and handled in accordance with the European Union Animal Protection Directive (2010/63/EU). Maintenance and generation of *jagn1b* mutants, using CRISPR/Cas9 gene editing, was approved by the local government (Tierschutzgesetz§11, Abs.1, Nr.1, husbandry permit 35/9185.46/UniTÜ; Tierschutzgesetz§8, Abs.1, permit M08/20G).

Genetic manipulation

Zebrafish embryos were genetically modified by microinjection of morpholinos (0.5 mM), CRISPR/Cas9 ribonucleoproteins (5 μM), and/or messenger RNAs (mRNAs) (20-50 ng/μL) into the 1 cell-stage.

Whole-mount in situ hybridization

Whole-mount in situ hybridization (WISH) was performed as previously described.[23] The antisense probes that were used in this study are listed in supplemental Table 1.

In silico analysis

Genomic synteny was studied by analyzing neighboring genes of human and zebrafish *JAGN1* orthologs using ENSEMBL. Multiple protein (supplemental Table 2) alignments and neighbor-joining phylogenetic tree of JAGN1 proteins were performed with 1000 bootstrap replications using Geneious.

Statistical analysis

For statistical analysis, GraphPad Prism (version 8.0.2) was used. The normal distribution was characterized using the Kolmogorov-Smirnov test. When normal distribution was confirmed, an unpaired *t* test was used for single comparisons between 2 groups and analysis of variance was used for multiple comparisons. When normal distribution was not confirmed, a Mann-Whitney test was used for single comparisons and a Kruskal-Wallis test was used for multiple comparisons.

Additional methods are available online.

Results

Two paralogs of the human *JAGN1* gene in zebrafish

Zebrafish has 2 paralogs of the human *JAGN1* gene, namely *jagn1a* and *jagn1b*. Multiple alignments showed high similarities between the different JAGN1 orthologs (supplemental Figure 1A). Phylogenetic (Figure 1A) and genomic synteny (Figure 1B) analyses indicated that the presence of zebrafish *jagn1a* and *jagn1b* was the consequence of species-specific gene duplication.

Expression levels of *jagn1a* and *jagn1b* were explored in 2 available single-cell RNA sequencing data sets of whole kidney marrow, corresponding to mammalian hematopoietic tissue.[24,25] Macrophages expressed low levels of *jagn1a*, but *jagn1b* was detected in hematopoietic progenitors, macrophages, erythrocytes, and neutrophils (data not shown). A comparison of the transcriptome data set (GSE70881[26]) of zebrafish *draculin*-expressing cells, which mark hematopoietic stem and progenitor cells (HSPCs), with niche

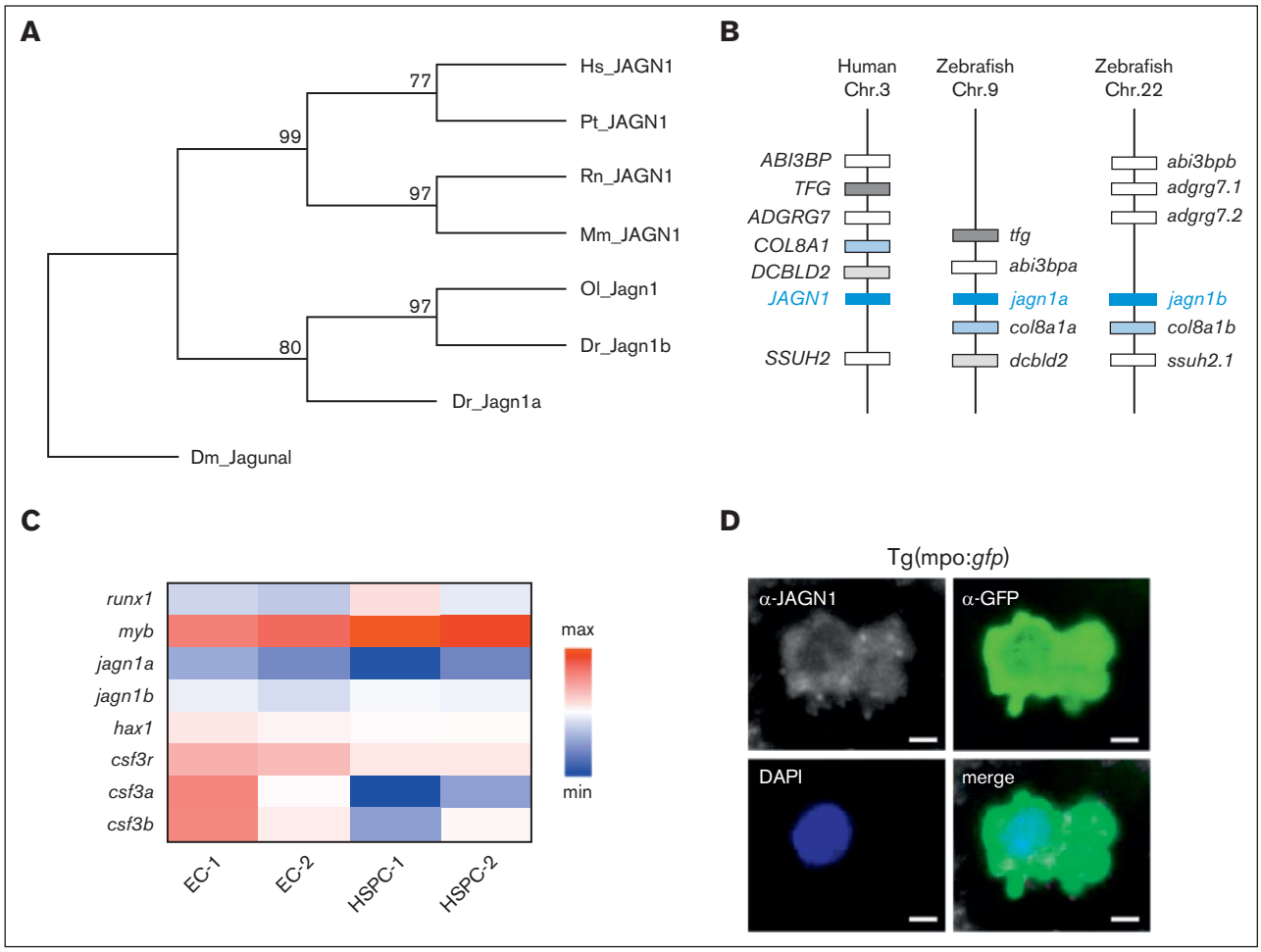

Figure 1. The evolution of *JAGN1* gene and the expression patterns of its homologs in zebrafish. (A) A neighbor-joining phylogenetic tree of JAGN1 proteins performed with 1000 bootstrap replications. Branch labels represent consensus support in percentage. (B) Schematic comparison of genomic synteny between human *JAGN1* and zebrafish *jagn1a* and *jagn1b* loci. (C) Heat map representing gene expression levels in sorted endothelial (EC-1, EC-2) and HSPCs (HSPC-1, HSPC-2) of draculin:*mCherry* embryos. (D) Representative picture of a GFP$^+$ neutrophil with JAGN1 detection and DAPI staining after immunostaining against JAGN1 and GFP on a 2 dpf transgenic tg(mpo:*gfp*) reporter embryo. DAPI, 4′,6-diamidino-2-phenylindole; Dm, *Drosophila melanogaster*; Dr, *Danio rerio*; Hs, *Homo sapiens*; Mm, *Mus musculus*; Ol, *Oryzias latipes*; Pt, *Pan troglodytes*; Rn, *Rattus norvegicus*.

cells (endothelial cells) showed that *jagn1a* was not expressed in the niche cells or the HSPCs, whereas *jagn1b* RNA was present in both cell types (Figure 1C). Whole-mount immunostaining of transgenic (tg) tg(mpo:*gfp*) zebrafish embryos using the human α-JAGN1 antibody demonstrated co-localization between green fluorescent protein (GFP) (marking neutrophils) and α-JAGN1 staining (Figure 1D; supplemental Figure 1B).

Jagn1a and Jagn1b have distinct, nonredundant functions in zebrafish hematopoiesis

To investigate the importance of Jagn1a and Jagn1b in hematopoiesis, we employed an antisense morpholino (MO)-knockdown strategy. Antisense oligos were designed to bind to the ATG of *jagn1a* or *jagn1b* mRNA, thereby preventing their protein translation. We first confirmed the specificity of both morpholinos in zebrafish embryos by injecting them with a GFP mRNA construct containing the ATG of *jagn1a* or *jagn1b* (supplemental Figure 2A-B) and used WISH to examine the number of cells that expressed the neutrophil marker *lysozymeC* (*lyz*) in the MO-injected embryos (hereafter called morphants). Both *jagn1a* and *jagn1b* morphants exhibited a significant reduction in the number of *lyz*$^+$ neutrophils when compared with the WT embryos (Figure 2A-B). Similar results were obtained when the morpholinos were injected in the transgenic tg(mpo:*gfp*) reporter line (supplemental Figure 2C). A control MO at the same concentration did not affect neutrophil numbers (supplemental Figure 2D).

We also performed rescue experiments by coinjecting morpholinos with full-length wild-type *jagn1a* or *jagn1b* mRNA containing different sequences around the ATG region, which cannot be targeted by the morpholinos. The neutropenia phenotype induced by *jagn1a* knockdown was partially rescued by *jagn1a* mRNA coinjection, but not by coinjection of *jagn1b* mRNA (Figure 2A; supplemental Figure 2E). Conversely, the neutropenia in *jagn1b* knockdown embryos were completely restored in embryos coinjected with *jagn1b* mRNA, but not *jagn1a* mRNA (Figure 2B; supplemental Figure 2E). The injection of wild-type *jagn1a* or

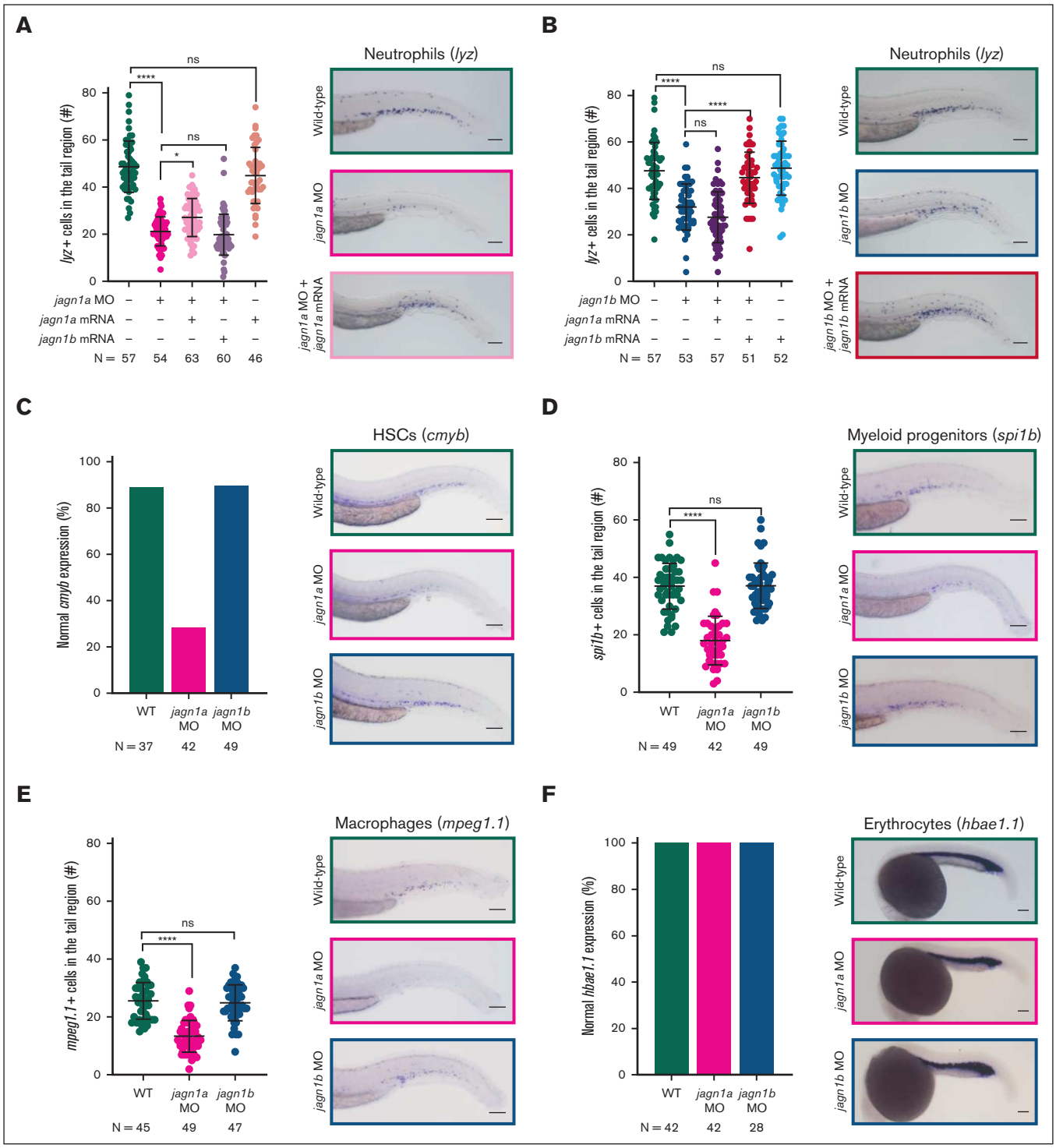

Figure 2. Jagn1a and Jagn1b have distinct and nonredundant functions in zebrafish hematopoiesis. (A-B) Effect of *jagn1a* (A) or *jagn1b* (B) downregulation on neutrophil counts and the rescue with *jagn1a* and *jagn1b* mRNA. The left panels show a quantitative analysis of the cells expressing the neutrophil marker *lysozyme C* (*lyz*), stained using WISH. The neutrophils were quantified after interfering with *jagn1a* (*jagn1a* MO) or *jagn1b* function (*jagn1*b MO), the subsequent rescue with full-length *jagn1a* or *jagn1b* mRNA, and *jagn1a* or *jagn1b* mRNA overexpression alone. The right panels show representative images of WISH for *lysozyme C* (*lyz*) in 2.25 dpf wild-type embryos or *jagn1a* and *jagn1b* morphants with or without overexpression of *jagn1a* or *jagn1b* mRNA. (C-F) Effect of *jagn1a* and *jagn1b* downregulation on other hematopoietic cells. The left panels show quantitative analyses of stained cells with WISH against hematopoietic cell-specific markers. The right panels show representative images of the WISH-stained embryos. The cells were stained against (C) *cmyb*, staining HSCs, (D) *spi1b*, staining myeloid progenitors, (E) *mpeg1.1*, staining macrophages in 2.25 dpf embryos and (F) *hbae1.1* staining erythrocytes in 1 dpf embryos. (C,F) Comparison of the percentage (%) of normal gene expression pattern between wild-type, *jagn1a* and *jagn1b* morphants. (D-E) Numbers of stained cells in the hematopoietic region. Each dot in panels A-B,D-E represents the number of cells in the hematopoietic tissue of an individual 2.25 dpf embryo.

jagn1b mRNA alone did not affect neutrophil numbers (Figure 2A-B; supplemental Figure 2E). These results indicate that Jagn1a and Jagn1b have nonredundant functions in hematopoiesis.

To explore other hematopoietic cells in *jagn1a* or *jagn1b* morphants, we analyzed *cmyb*$^{+}$ hematopoietic stem cells (HSCs) and *spi1b*$^{+}$ myeloid precursors using WISH (Figure 2C-D). The *jagn1a*, but not *jagn1b* morphants exhibited a significant reduction in these cell numbers when compared with their WT counterparts. Moreover, we observed a significant reduction in macrophages (positive for *macrophage-expressed gene 1.1* [*mpeg1.1*]) in *jagn1a* morphants, but not in *jagn1b* morphants (Figure 2E). The unchanged expression of the erythrocyte marker *hemoglobin, alpha embryonic 1.1* (*hbae1.1*) (Figure 2F) and the presence of circulating red blood cells (data not shown) in the morphants indicate that *jagn1a* and *jagn1b* are not involved in erythropoiesis. These findings strongly suggest that Jagn1a and Jagn1b are regulating distinct mechanisms that might directly or indirectly influence granulopoiesis. Although Jagn1a is involved in early hematopoiesis and myelopoiesis, Jagn1b specifically plays a role in granulopoiesis. Therefore, we decided to focus on Jagn1b in this study.

JAGN1-CN–associated mutations in zebrafish *jagn1b* cause neutropenia

Thus far, our *jagn1b* MO has successfully disrupted the start codon, preventing the translation of Jagn1b protein. However, only a subset of patients with *JAGN1*-CN have mutations in the start codon (p.Met1Ile). Patients with *JAGN1*-CN also have deletions and missense and nonsense mutations (Figure 3A). To mimic these types of *JAGN1*-CN, we employed 2 different strategies. In the first approach, we designed and tested a guide RNA targeted to the TM domain (Figure 3A). By using CRISPR/Cas9 gene editing (supplemental Figure 3A-B), we detected a significantly reduced number of *lyz*-expressing neutrophils in 2.25 days postfertilization (dpf) *jagn1b* crispants when compared with the control group (Figure 3B,D). We also confirmed the reduction of neutrophils in tg(mpo:*gfp*) reporter embryos (supplemental Figure 3C). Furthermore, similar to the *jagn1b* morphants, the *jagn1b* crispants did not show any differences in *cmyb*$^{+}$ HSCs, *spi1b*$^{+}$ myeloid progenitors, *mpeg1.1*$^{+}$ macrophages, and *hbae1.1*$^{+}$ erythrocytes when compared with their WT counterparts (supplemental Figure 3D-G).

Through breeding the F1 and F2 generations to generate stable zebrafish *jagn1b* mutants, we were only able to identify adult heterozygous *jagn1b* mutants (supplemental Figure 3H) with 2 different genotypes, c.347_351del and c.351_357del, which led to truncated Jagn1b proteins with 134 and 133 amino acids, respectively (supplemental Figure 3K). To determine whether homozygous *jagn1b* mutants were embryonic lethal, we crossed *jagn1b* heterozygote fish and monitored the development of the offspring from the 1-cell stage until 1 dpf. Interestingly, many embryos exhibited either asymmetrical blastomere division or complete arrest in cell division within the first 2 hours of embryonic development (supplemental Figure 3I). These embryos were unable to proceed to gastrulation, leading to high embryonic lethality (supplemental Figure 3J), which could explain the absence of adult homozygous *jagn1b* mutants. To confirm that the observed effects were specific to *jagn1b* mutations, we predicted 13 potential off-target regions for our designed gRNAs using the CCTop tool[27] (supplemental Table 10), but none of them was confirmed by Sanger sequencing. These results indicate that Jagn1b is crucial for the correct and symmetrical division of zebrafish blastomeres, and stable *jagn1b*$^{c.347\_351del}$ and *jagn1b*$^{c.351\_357del}$ mutants cannot be generated.

As an alternative strategy to mimic *JAGN1*-associated CN in zebrafish, we introduced deletion mutation ΔT12-G14 into zebrafish *jagn1b* full-length mRNA. We aimed to assess the impact of the mutation on its subcellular localization by tagging *jagn1b*^{WT} or *jagn1b*$^{\Delta T12\text{-}G14}$ with GFP at the N-terminal region. Overexpression of GFP-tagged *jagn1b*^{WT} did not affect the number of neutrophils in WT embryos and rescued the *jagn1b* morphants (supplemental Figure 4A-B). Interestingly, *gfp-jagn1b*$^{\Delta T12\text{-}G14}$ overexpression significantly reduced the number of neutrophils when compared with the wild-type siblings. This effect was even more pronounced after *jagn1b* knockdown (Figure 3C,E), suggesting a dominant negative effect of mutated Jagn1b. Moreover, we found that the overexpression of *jagn1b*$^{\Delta T12\text{-}G14}$ had no effect on *cmyb*$^{+}$ HSCs, *spi1b*$^{+}$ myeloid progenitors, *mpeg1.1*$^{+}$ macrophages, or *hbae1.1*$^{+}$ erythrocytes when compared with WT siblings (Figure 3F-I). To determine the subcellular localization of the WT and mutated proteins, we injected the GFP-tagged *jagn1b* mRNAs into the tg(draculin:*mCherry*) HSPCs reporter line. Confocal images of injected tg(draculin:*mCherry*) embryos revealed a symmetric distribution of GFP-Jagn1b^{WT}, most likely in the ER (Figure 3J). In contrast, GFP-Jagn1b$^{\Delta T12G14}$ exhibited asymmetric distribution within some HSPCs (arrowheads in Figure 3J; supplemental Videos 1 and 2). This observation suggests that the Jagn1b$^{\Delta T12G14}$ could lead to protein aggregation within the ER, resembling the ER-related abnormalities described in patients with *JAGN1*-CN.[6]

Deregulation of Jagn1b leads to UPR activation, but UPR induction alone is not sufficient to induce neutropenia in zebrafish

Next, we examined whether UPR was activated upon injection of WT and mutated *jagn1b* mRNA and *jagn1b* MO. To assess this, we quantified the expression levels of *DNA damage-inducible transcript 3* (*ddit3*), which encodes the UPR marker C/EBP homologous protein (Chop), activated by the 3 different UPR pathways (ATF6, PERK, and IRE1).[28] We observed a significant increase in *ddit3* expression in embryos injected with either *jagn1b*$^{\Delta T12\text{-}G14}$ or *jagn1b* MO. However, the expression level of *ddit3* remained unchanged in embryos injected with *jagn1b*^{WT} mRNA or control MO (Figure 4A), suggesting that the misexpression of Jagn1b^{WT} or the injection of a nonspecific MO is not sufficient to induce UPR. Because *ddit3* expression can be induced by activating transcription factor 4 (ATF4),[29] we also quantified the expression levels of the zebrafish ortholog *atf4* in embryos injected with *jagn1b*$^{\Delta T12\text{-}G14}$ or *jagn1b* MO. The

Figure 2 (continued) Data are presented as mean ± standard deviation. The data represent the combined results from 2 to 3 independent experiments. N represents the total number of analyzed embryos. (A-E) Images were taken with 10× magnification. Scale bars represent 100 μm. (F) Images were taken with 8× magnification. Scale bars represent 100 μm. ns, not significant; *$P < .05$; ****$P < .0001$.

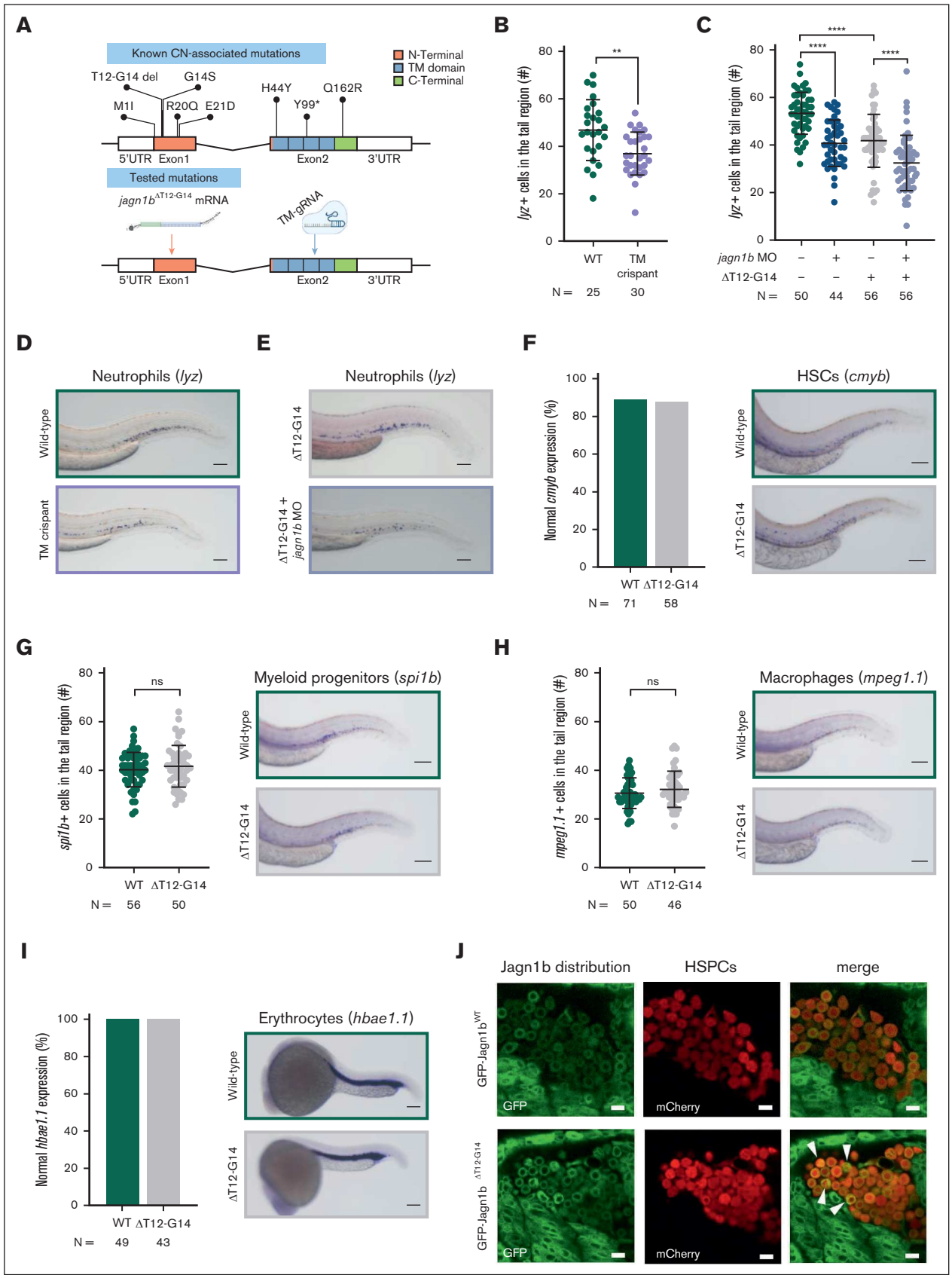

Figure 3.

overexpression of mutated *jagn1b*, but not the downregulation of *jagn1b*, led to a significant increase in *atf4* expression (Figure 4B). In addition, we analyzed the expression levels of zebrafish orthologs of the Chop target genes, *endoplasmic reticulum oxidoreductase 1-alpha* (*ero1a*) and *-beta* (*ero1b*) and *protein phosphatase 1 regulatory subunit 15A* (*ppp1r15a* encoding Gadd34).[30] We found a significant increase in the expression levels of *ero1a*, *ero1b*, and *ppp1r15a* in embryos injected with *jagn1b*$^{\Delta T12G14}$ mRNA but not with *jagn1b* MO (Figure 4C-D) or control MO (supplemental Figure 5A). Thus, these results suggest that Jagn1b$^{\Delta T12G14}$ can induce UPR through the activation of the PERK/ATF4/CHOP pathway. In *jagn1b* morphants, we saw an increase in the expression of *ddit3*, which was not induced by Atf4. However, the expression of *ddit3* can be induced by several UPR pathways, including the ATF6 pathway. Therefore, we quantified the expression level of unspliced *X-box binding protein 1* (*xbp1*), another downstream ATF6 target. Indeed, the expression levels of unspliced *xbp1* were significantly increased in *jagn1b* morphants when compared with their WT siblings, but not in *jagn1b*$^{\Delta T12\text{-}G14}$ overexpressed embryos (Figure 4E). The spliced *xbp1* (*sxbp1*) showed a trend of induction that was not significant (supplemental Figure 5B). However, the upregulation of *ddit3* and *xbp1* is consistent with the activation of the ATF6 pathway. Although UPR was also induced in *jagn1b* morphants, the expression of Chop target genes remained unchanged. Interestingly, the *jagn1b* morphants group showed a slight decrease in *ppp1r15a* expression (Figure 4D). In addition, mRNA expression of *ER to nucleus signaling 1* (*ern1*) (encoding Ire1), *eukaryotic translation initiation factor 2α kinase 3* (*eif2ak3*) (encoding Perk), and *activating transcription factor 6* (*atf6*) was unaffected upon *jagn1b* downregulation (supplemental Figure 5B).

Previous studies have proposed that ER stress and UPR activation are involved in diminished granulocytic differentiation downstream of CN-associated mutations such as *ELANE*[31,32] or *G6PC3*.[33] Elevated ER-stress was also described in *JAGN1*-mutant granulocytes.[6] Therefore, we aimed to investigate whether UPR activation could impair granulopoiesis in our zebrafish model. To induce UPR in vivo, we treated embryos with dithiothreitol (DTT) or tunicamycin, 2 compounds known to disrupt protein folding by reducing disulfide bonds and inhibiting N-linked glycosylation, respectively.[34] These reagents have been used previously to induce UPR in cell-based,[35] zebrafish,[17] and mice neutropenia models[31] and the zebrafish UPR reporter.[36,37] To confirm the activation of UPR in zebrafish embryos, we treated WT embryos with DTT or tunicamycin from 24 to 48 hours postfertilization (hpf) and quantified the expression levels of *ddit3* (Figure 4F) and *sxbp1* (Figure 4G) using reverse transcriptase polymerase chain reaction (RT-PCR) at 48 hpf. As a negative control, we used dimethylsulfoxide (DMSO) treatment. Our results showed that both, DTT and tunicamycin treatments were sufficient to induce UPR as evidenced by an increased expression of *ddit3* and *sxbp1* in treated WT embryos (Figure 4F-G). However, there was no significant difference in the number of neutrophils between DTT-treated, tunicamycin-treated, DMSO-treated, and untreated embryos (Figure 4H-I). Next, we treated *jagn1b* morphants. Despite the strong UPR activation (Figure 4F-G), we did not observe any additional decrease in neutrophil numbers in *jagn1b* morphants after treatment with tunicamycin or DTT (Figure 4H-I).

Together, we detected UPR activation after the interference with Jagn1b function. However, the implicated UPR pathways varied depending on whether *jagn1b* was downregulated or upon overexpression of *jagn1b*$^{\Delta T12\text{-}G14}$. Nevertheless, the chemically induced UPR response alone did not affect the number of neutrophils, arguing that UPR induction alone is insufficient to cause neutropenia in zebrafish.

Apoptosis is increased upon *jagn1b* knockdown, but it is insufficient to induce neutropenia

There are several connections between chronic ER stress, CHOP activation, its targets, and apoptosis.[28,30,38] Therefore, we investigated apoptosis in embryos injected with *jagn1b*$^{\Delta T12\text{-}G14}$ mRNA and *jagn1b* MO using the terminal deoxynucleotidyltransferase-mediated dUTP nick end labeling (TUNEL) assay. Surprisingly, we found that the number of apoptotic cells was increased only in *jagn1b* morphants and not with *jagn1b*$^{\Delta T12\text{-}G14}$ (Figure 5A). TUNEL-positive cells were distributed throughout the body, including the tail region. However, we did not observe a significant increase in apoptotic cells within the hematopoietic tissue (data not shown). This finding was further confirmed by acridine orange (AO) staining (Figure 5B).

Next, we investigated whether induced apoptosis could cause neutropenia by treating WT embryos and *jagn1b* morphants with the protein kinase inhibitor staurosporine (STS) for 24 hours.

Figure 3. Expression of zebrafish Jagn1b$^{\Delta T12\text{-}G14}$ results in neutropenia, without affecting other hematopoietic cells. (A) Top panel shows a schematic representation of identified CN-associated mutations in human *JAGN1* gene. The bottom panel shows the tested mutations with the corresponding approach in this study. Note, to mimic the deletion (ΔT12-G14) we overexpressed *jagn1b*$^{\Delta T12\text{-}G14}$ mRNA. Further, we targeted the transmembrane domain using CRISPR/Cas9 gene editing to introduce a truncating mutation. (B-C) Quantitative analysis of the cells expressing the neutrophil marker *lysozyme C* (*lyz*), stained with WISH in (B) *jagn1b* TM crispants and (C) after *jagn1b*$^{\Delta T12\text{-}G14}$ overexpression alone or in combination with *jagn1b* morpholino. Each dot represents the number of cells in the hematopoietic tissue of a 2.25 dpf individual embryo. Data are presented as mean ± standard deviation. The data represent combined results from 2 independent experiments. N represents the total number of analyzed embryos. (D-E) Representative images of *lyz*$^{+}$ neutrophils in (D) TM crispants and (E) after overexpression of *jagn1b*$^{\Delta T12\text{-}G14}$ alone or in combination with *jagn1b* morpholino. Images were taken with 10× magnification. Scale bars represent 100 μm. (F-I) Effect of overexpression of *jagn1b*$^{\Delta T12\text{-}G14}$ on other hematopoietic cells. The left panels show quantitative analyses of stained cells with WISH against hematopoietic cell-specific marker. The right panels show representative images of the WISH-stained embryos. The cells were stained against (F) *cmyb*, (G) *spi1b*, (H) *mpeg1.1* all 3 in 2.25 dpf embryos and (I) *hbae1.1* in 1 dpf embryos. (F,I) Comparison of the percentage (%) of normal gene expression pattern between wild-type embryos compared to that carrying *jagn1b*$^{\Delta T12\text{-}G14}$ mutation. (G-H) Numbers of stained cells in the hematopoietic region. Each dot represents the number of cells in the hematopoietic tissue of an individual 2.25 dpf embryo. Data are presented as mean ± standard deviation. The data represent combined results from 2 independent experiments. N represents the total number of analyzed embryos. Pictures were taken with 8× to 10× magnification. Scale bars represent 100 μm. (J) Representative images of intracellular Jagn1 protein localization (GFP signal) after overexpression of *gfp-jagn1b*^{WT} and *gfp-jagn1b*$^{\Delta T12\text{-}G14}$ mRNA in draculin:*mCherry*-positive HSPCs at 20 hours postfertilization (hpf). ns, not significant; $^{**}P < .01$; $^{****}P < .0001$.

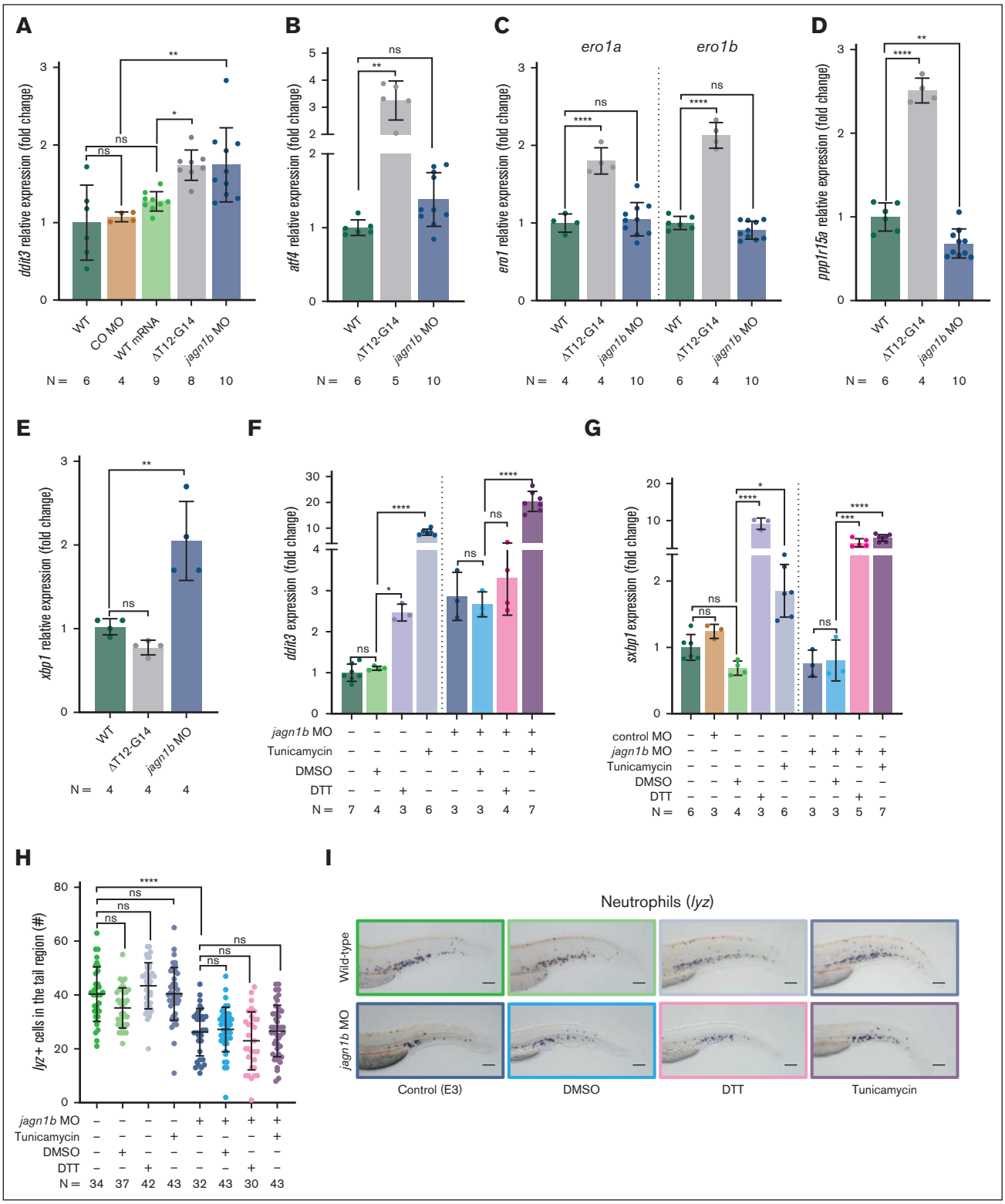

Figure 4. Deregulation of Jagn1b results in UPR activation, but UPR induction alone is not sufficient to induce neutropenia in zebrafish. (A-E) Relative expression levels (fold change) of UPR-associated genes measured with quantitative RT-PCR after interference with *jagn1b* by overexpressing *jagn1b*$^{\Delta T12\text{-}G14}$ mRNA or inhibiting *jagn1b* with morpholino. Relative expression levels of (A) *ddit3*, coding the UPR marker Chop, (B) *atf4*, (C) *ero1a* and *ero1b*, (D) *ppp1r15a*, and (E) *xbp1* were measured, corresponding groups are indicated. Expression levels were normalized to the housekeeping gene *b-actin* and fold change was calculated with respect to the expression levels of wild-type embryos. Each dot represents the value of the relative expression of 1 sample. Data are presented as mean ± standard deviation. The data represent combined results from 2 to 3 independent experiments. N represents the total number of analyzed complimentary DNA samples. (F-G) Relative expression (fold change) quantified by quantitative RT-PCR,

Apoptosis was evaluated using AO staining (Figure 5B) and the TUNEL assay (supplemental Figure 5C-D). We found that the *jagn1b* morphants were more susceptible to the STS treatment than the WT embryos. The *jagn1b* morphants already showed an increased number of AO^+ apoptotic cells in the tail region at a low STS concentration (2.5 µM) (Figure 5B) when compared with the DMSO-treated *jagn1b* morphants, whereas the WT embryos only showed an increased number of AO^+ apoptotic cells at the high concentration (5 µM) when compared with DMSO-treated WT siblings (Figure 5B). To investigate whether apoptosis led to neutropenia, we quantified the lyz^+ neutrophils in WT and morphants treated with 5 µM STS. Interestingly, the induction of apoptosis did not affect the number of neutrophils in either WT embryos or *jagn1b* morphants (Figure 5C-D).

Deregulation of Jagn1b affects steady-state and emergency granulopoiesis.

We also tested whether *JAGN1* is involved in G-CSFR-triggered steady-state and emergency granulopoiesis because several indications support this hypothesis.[6,10] It was previously shown that the G-CSFR pathway and the relationship between its activation and *CCAAT/enhancer-binding protein alpha* (*CEBPA*) induction is evolutionarily conserved between human and zebrafish.[15,39] To investigate whether overexpression of *g-csfa* rescues neutropenia in *jagn1b* morphants, we used 2 different approaches. First, we injected *g-csfa* mRNA into zebrafish embryos, allowing for protein translation at an early embryonic stage, and quantified lyz^+ neutrophils (Figure 6A). Second, we induced *g-csfa* expression in 44 hpf embryos using a heat-inducible construct[15,40] and quantified mpo^+ neutrophils (supplemental Figure 6A). Both approaches showed a significantly increased number of neutrophils in *jagn1b* morphants when compared with WT embryos at 2.25 dpf and successfully rescued the neutropenia induced by *jagn1b* knockdown (Figure 6A; supplemental Figure 6A). Similarly, overexpression of *g-csfa* in transgenic tg(mpo:*gfp*) reporter embryos, together with $jagn1b^{\Delta T12\text{-}G14}$ mRNA, rescued neutropenia induced by $Jagn1b^{\Delta T12\text{-}G14}$ (Figure 6B).

To assess the impact of Jagn1b alterations on steady-state granulopoiesis, we examined the zebrafish ortholog of *CEBPA*.[41,42] Indeed, we found a significant reduction in *cebpa*-expressing cells (supplemental Figure 6B) and *cebpa* expression level (Figure 6C) in *jagn1b* morphants when compared to control siblings. Furthermore, we found that the expression levels of *CEBPA* targets, *hematopoietic cell-specific lyn substrate 1* (*hcls1*) and *csf3r* (encoding zebrafish G-CSFR), were significantly reduced in *jagn1b* morphants when compared with WT embryos (Figure 6C). These results strongly suggest impaired G-CSF signaling upon *jagn1b* downregulation.

Given that steady-state granulopoiesis was impaired, the rescue observed upon *g-csfa* induction in *jagn1b* morphants is likely explained by the activation of emergency granulopoiesis. To examine this hypothesis, we measured the expression level of *CCAAT/enhancer-binding protein beta* (*cebpb*), a key regulator of emergency granulopoiesis[43,44] and found a substantial increase in its expression in *jagn1b* morphants upon *g-csfa* induction (Figure 6D). To further confirm the essential role of *cebpb* in emergency granulopoiesis activation, we interfered with *cebpb* function in the *g-csfa*-rescued embryos using a MO knockdown strategy. As a control, we injected *cebpb* MO into WT embryos. As expected, *cebpb* knockdown alone did not affect the number of neutrophils in WT embryos, confirming that *cebpb* does not play a vital role in steady-state granulopoiesis.[43] However, in sharp contrast, *cebpb* knockdown further decreased the number of neutrophils in *jagn1b* morphants, and *g-csfa* overexpression was no longer sufficient to rescue the neutropenia phenotype when *cebpb* was downregulated (Figure 6E). These effects were rescued by overexpressing *cebpb* mRNA (supplemental Figure 6C-D). Together, our results demonstrate that *g-csfa* induction rescues neutrophil development in *jagn1b* morphants by activating the emergency granulopoiesis.

We also noticed a significant increase in the expression level of *cebpb* (Figure 6F) and the number of *cebpb*-expressing cells (supplemental Figure 6E) in *jagn1b* morphants when compared with WT counterparts. The same trend was observed for the expression of endogenous *g-csfa*, but not *g-csfb* (Figure 6F), the second ortholog of human G-CSF.[39] This suggests that *jagn1b* knockdown alone is capable of elevating the expression of *g-csfa* and *cebpb*, although the level of induction is insufficient to completely rescue neutropenia. Similarly, embryos injected with $jagn1b^{\Delta T12\text{-}G14}$ mRNA showed a decrease in *cebpa*-(supplemental Figure 6B) and an increased number of *cebpb*-expressing cells (supplemental Figure 6E). These observations suggest that, consistent with the results obtained in *jagn1b* morphants, the steady-state granulopoiesis is impaired and the emergency granulopoiesis is activated downstream of mutated Jagn1b.

Discussion

Thus far, the main focus of research on the mechanism of *JAGN1*-associated CN has been restricted to clinical observation and in vitro studies.[6-10,45,46] In this study, we report the successful establishment of a zebrafish model of *JAGN1*-associated CN, demonstrating neutropenia induction by interfering with JAGN1 function using *jagn1b*-specific MO, CRISPR/Cas9, or misexpression of a *JAGN1*-CN specific mutation. Our analyses revealed 4 new findings. First, JAGN1 is required for cell division. It was initially discovered to be essential for *Drosophila* oocyte

Figure 4 (continued) normalized to the housekeeping gene *b-actin* and fold changes were calculated respect the expression levels of wild-type embryos of (F) UPR-marker *ddit3* (G) and spliced *xbp1* after UPR induction with tunicamycin (1 µg/mL), DTT (0.7 mM) or DMSO control (0.7%) alone or in combination with *jagn1b* morpholino. Data are presented as mean ± standard deviation. Each dot represents the value of relative expression of one sample. The data represent combined results from 2 to 3 independent experiments. N represents the total number of analyzed complimentary DNA samples. (H-I) Effect of chemically induced UPR on neutrophil counts. (H) Quantification of lyz^+ neutrophils stained with WISH after UPR induction with tunicamycin (1 µg/mL), DTT (0.7 mM) or DMSO control (0.7%) alone or in combination with *jagn1b* morpholino. Each dot represents the number of cells in the hematopoietic tissue of a 2 dpf individual embryo after 24 hours of treatment. Data are presented as mean ± standard deviation. The data represent the combined results from 2 to 3 independent experiments. N represents the total number of analyzed embryos. (I) Representative images were taken with 10× magnification. Scale bars represents 100 µm. ns, not significant; $^*P < .05$; $^{**}P < .01$; $^{***}P < .001$; $^{****}P < .0001$.

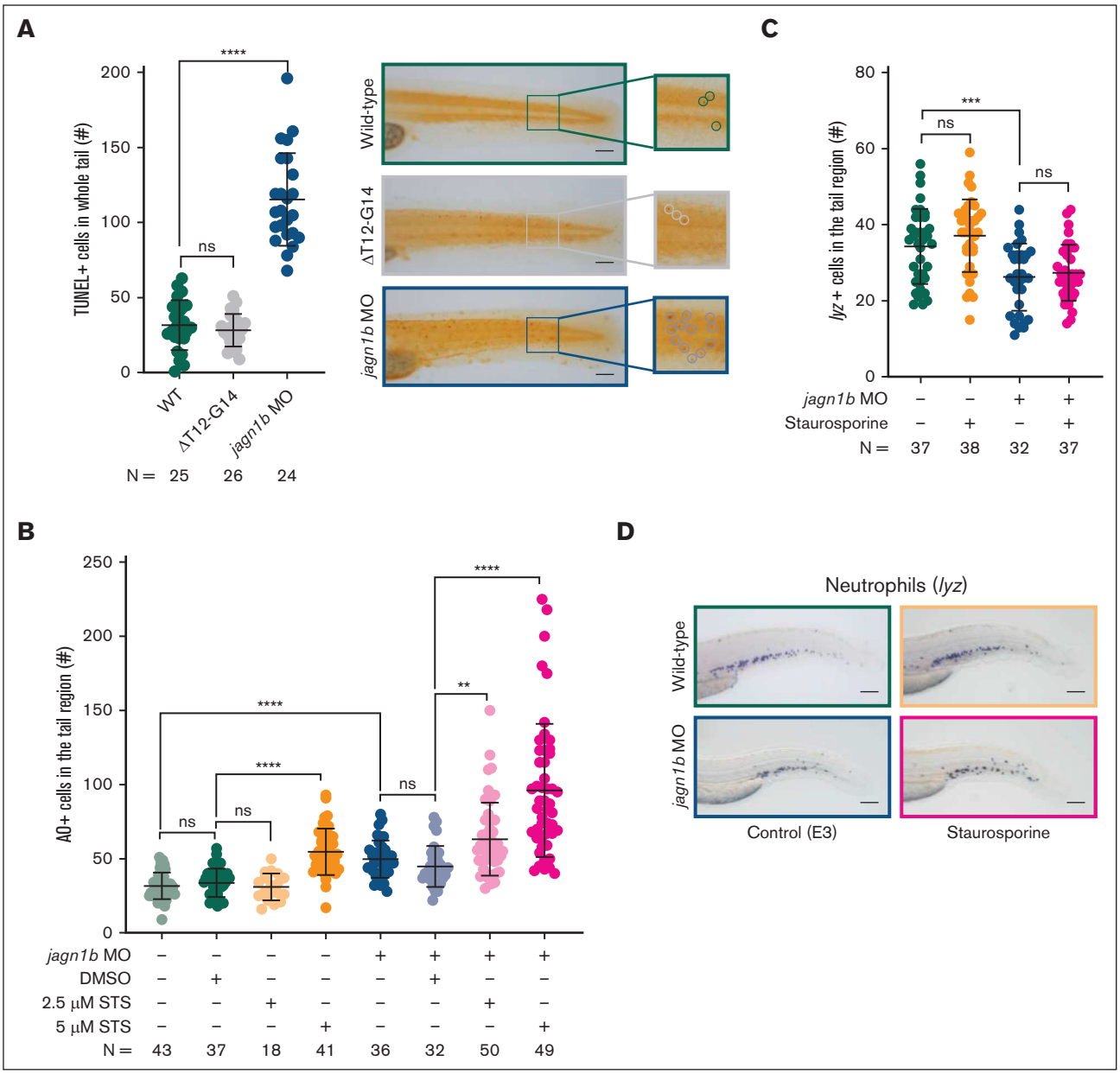

Figure 5. Apoptosis is increased upon *jagn1b* knockdown, but it is not sufficient to induce neutropenia. (A) Assessment of TUNEL$^+$ apoptotic cells upon *jagn1b* interference. The left panel shows the quantification of the TUNEL$^+$ cells in the whole trunk region of 2.25 dpf embryos after overexpression of *jagn1b*$^{\Delta T12\text{-}G14}$ or *jagn1b* morpholino. Data shows mean and standard deviation. Each dot represents the number of TUNEL$^+$ cells in the tail region of an individual embryo. The data represent the combined results from 2 independent experiments. N represents the total number of analyzed embryos. The right panel shows representative images of the tail region of wild-type, *jagn1b*$^{\Delta T12\text{-}G14}$ embryos, and *jagn1b* morphants. Images were taken with 10× magnification. Scale bars represent 100 μm. The square at the right of each image represents a magnification of the marked tail region where each apoptotic cell is encircled. (B) Apoptosis induction in staurosporine-treated embryos using AO staining. Quantification of AO-positive apoptotic cells in the tail region of 2 dpf wild-type embryos and *jagn1b* morphants treated with DMSO, or staurosporine (STS). Each dot represents the number of AO$^+$ cells in the tail region of an individual 2 dpf embryo. Data are presented as mean ± standard deviation. The data represent the combined results from 3 independent experiments. N represents the total number of analyzed embryos. (C-D) Effect of staurosporine-induced apoptosis on the neutrophil count. (C) Quantification of *lyz*$^+$ neutrophils stained with WISH after apoptosis induction with staurosporine (5 μM) alone or combined with *jagn1b* morpholino. Data are presented as mean ± standard deviation. Each dot represents the number of stained cells in the hematopoietic region of an individual 2 dpf embryo. The data represent the combined results from 2 independent experiments. N represents the total number of analyzed embryos. (D) Representative images were taken with 10× magnification. Scale bars represent 100 μm. ns, not significant; $^{**}P < .01$; $^{***}P < .001$; $^{****}P < .0001$.

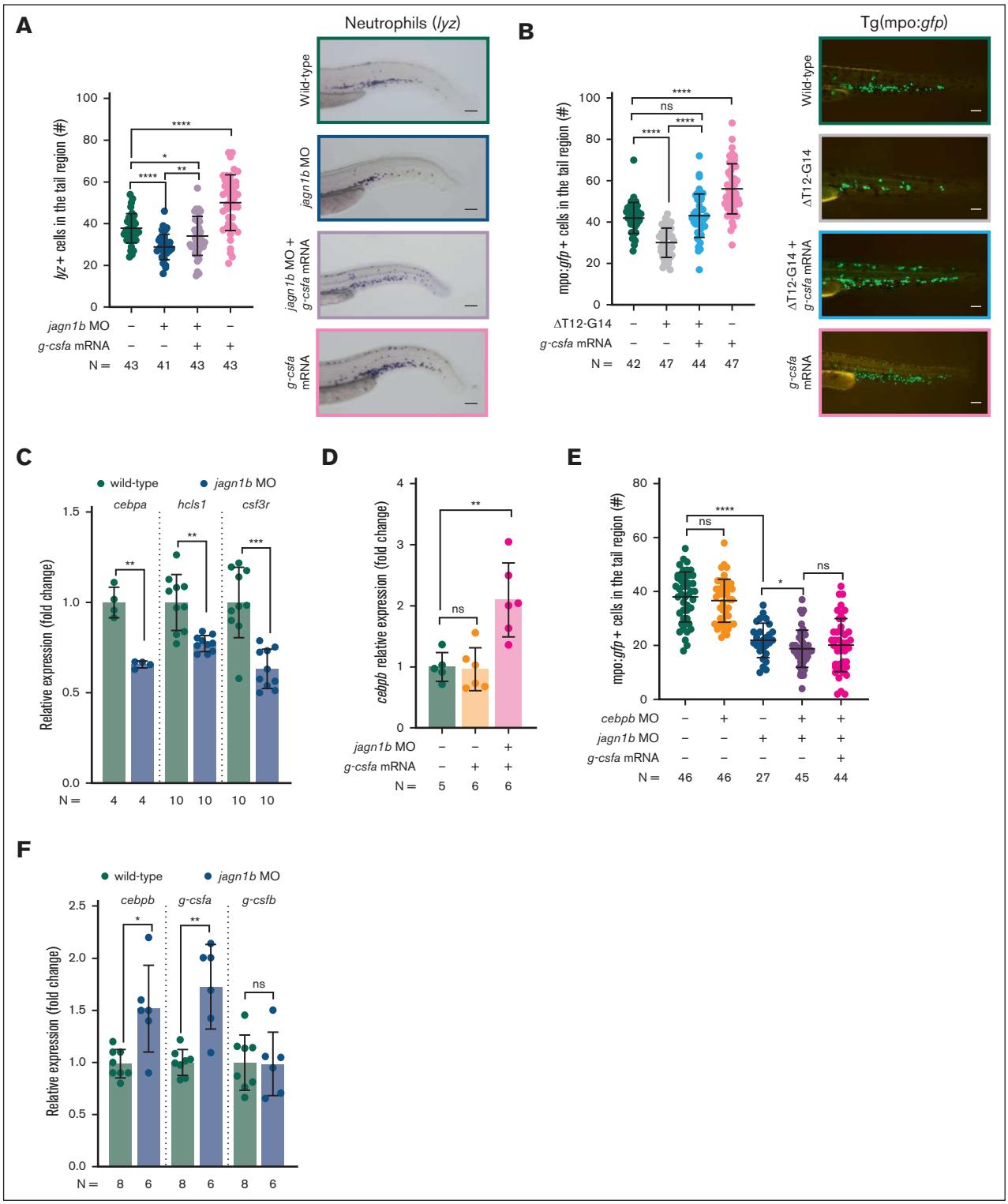

Figure 6. Jagn1b deregulation affects steady-state and emergency granulopoiesis. (A-B) G-csfa rescue after *jagn1b* interference. (A) G-csfa rescue in *jagn1b* morphants. The left panel shows the quantification of *lyz*$^{+}$ neutrophils stained with WISH after *g-csfa* overexpression in 2.25 dpf wild-type embryos and *jagn1b* morphants. Right panel shows representative images taken with 10× magnification. Scale bars represent 100 µm. (B) G-csfa rescue in *jagn1b*$^{\Delta T12\text{-}G14}$ embryos. The left panel shows the quantification of mpo:*gfp*$^{+}$neutrophils after *g-csfa* overexpression in 2.25 dpf wild-type and *jagn1b*$^{\Delta T12\text{-}G14}$ embryos. Right panel shows representative images taken with 8× magnification. Scale bars represent 100 µm. (C) Relative expression (fold change) of *cebpa*, *hcls1* and *csf3r* in wild-type embryos and *jagn1b* morphants, quantified by quantitative RT-PCR, normalized to the housekeeping gene *b-actin*. Fold change was calculated in respect to the wild-type expression. (D) Relative expression (fold change) of *cebpb* after g-*csfa* overexpression in wild-type embryos and *jagn1b* morphants, quantified by quantitative RT-PCR, normalized to the housekeeping gene *b-actin*. Fold change was calculated in

development by controlling ER reorganization, vesicular trafficking, and asymmetric ER partitioning during cell mitosis.[2,4] Similarly, we observed a strong disruption in the cell division of blastomeres during early zebrafish development in the Jagn1b CRIPSR/Cas9-mutant model. Therefore, a JAGN1 deficiency in the whole organism during early embryonic development is lethal, as shown in zebrafish (this study) and mice.[10] It is worth noting that knockdown of *jagn1b* using MO does not usually lead to complete loss of protein, and crispants (transient knockout) contain maternal WT transcripts until gastrulation, which enable normal embryonic development. The mutations in *JAGN1* may alter the protein's structure, leading to impaired ER-membrane binding or altered interactions between JAGN1 and its interaction partners, which seems important for cell division.

Second, our results suggest that ER stress and UPR pathways are not the primary and sole cause of neutropenia downstream of mutated Jagn1b because UPR induction alone did not cause neutropenia in WT embryos, and it did also not lead to a further decrease in neutrophil numbers in *jagn1b* morphants. It was described previously that specific mutations in *SEC61A1* can cause CN through dysregulation of the UPR.[35] Furthermore, the expression of mutant *ELANE* in human primary granulocytic precursors or myeloid cell lines led to UPR activation and apoptosis.[47,48] In addition, myeloid cell lines that express mutant *ELANE*[48] and granulocytic precursors of G193X *Elane* mice showed increased susceptibility to tunicamycin treatment.[31] These results show that there is a direct link between ER stress and neutropenia. In vitro, JAGN1-deficient granulocytes also exhibit increased levels of binding immunoglobulin protein, suggesting the activation of ER stress.[6] In addition, under conditions of ER stress, *JAGN1* was induced in insulinoma cells and the sperm proteome of men with obesity, contributing to alleviating protein folding load in the ER and restoring ER homeostasis.[49,50] These findings also suggest a connection between ER stress and JAGN1. Nevertheless, UPR activation is not the primary cause of *JAGN1*-associated neutropenia. In this study, we observed elevated expression levels of the UPR-associated genes *atf4* and *ddit3* and the Chop targets *ero1a*, *ero1b*, and *ppp1r15a* following overexpression of *jagn1b*$^{\Delta T12\text{-}G14}$. The upregulation of these genes is consistent with the activation of the PERK/ATF4/CHOP pathway. In *jagn1b* morphants, we saw upregulation of *ddit3* and unspliced *xbp1*, downstream targets of the ATF6 pathway.[51,52] However, there was no significant increase in *atf4* expression. These results are consistent with the activation of the ATF6 pathway. Furthermore, we saw a trend of induction of spliced *xbp1* in *jagn1b* morphants, which could be a hint for the activated IRE1 pathway. Surprisingly, the Chop target genes *ero1a* and *ero1b* were unaffected upon *jagn1b* knockdown. However, we need to consider that the chosen time point for UPR measurement may not have captured or reflected the expression of these target genes. Our results indicate that different *JAGN1* mutations activate different UPR pathways. These data are consistent with our previous observations of *ELANE* mutant-specific activation of different UPR pathways.[32] The different mutations may also alter the structure of JAGN1 differently, leading to various degrees of accumulation of misfolded proteins inducing UPR. JAGN1 has also been described as essential for proper protein trafficking.[3] Its absence or mutation can affect the interaction with transport-related proteins, for example components of the coat protein I complex,[6] and affect the transport of different proteins, leading to stagnation and subsequent activation of UPR. Further experiments are required to elucidate *JAGN1* mutation-specific activated UPR pathways. In addition, functional inhibition of the UPR pathways is required to demonstrate conclusively that the activation is not responsible for neutropenia. Based on our results, however, we would expect that the inhibition of PERK/ATF4/CHOP or ATF6 pathway would not restore granulopoiesis. It is, therefore, very likely that UPR activation is one of the multiple affected processes downstream of mutated *JAGN1*.

Third, our experiments revealed that cell death alone cannot induce neutropenia in zebrafish. The mechanism proposed for neutropenia in CN-associated genes, such as *HAX1*,[53] *G6PC3*,[54] *WAS*,[55] *SBDS*,[56] *GFI1*,[57] and *ELANE*,[48] converge in a final common process involving apoptosis of granulocytic precursors. Similarly, there is evidence that suggests that JAGN1 plays a role in apoptosis. Experiments conducted with *JAGN1*-CN–associated mutations in HL-60 cells demonstrated calpain-dependent cell death activation.[9] In addition, JAGN1 promotes the expression of TRAIL-R1 in primary effusion lymphoma cell lines.[11] When apoptosis was induced with STS in JAGN1-deficient neutrophils, a higher frequency of susceptibility was observed when compared with neutrophils from healthy individuals.[6] In line with these findings, we observed enhanced apoptosis in *jagn1b* morphants and a higher susceptibility to apoptosis induction with STS. However, it did not affect neutrophil development when we induced apoptosis pharmacologically by treating WT or *jagn1b* morphants from 24 to 48 hpf with STS. It is worth noting that a previous study has shown that continuous administration of STS from 6 hpf to 72 hpf in zebrafish embryos lead to neutropenia.[58] The induction of apoptosis at very early stages of embryonic development affects granulopoiesis and impairs organogenesis (eg, heart, liver, and vascularization).[58] The main reason for selecting the 24 hpf time window for our treatment was to minimize the side-effects on early embryonic development and primitive granulopoiesis. The fact that apoptosis was induced in *jagn1b* morphants but not in embryos injected with *jagn1b*$^{\Delta T12\text{-}G14}$ mRNA can be explained by their degree of UPR response and ER stress. For example, the downregulation of *ppp1r15a*, as seen in *jagn1b* morphants, but not in *jagn1b*$^{\Delta T12\text{-}G14}$ mRNA-injected embryos, has been associated with increased apoptosis.[59] Whether Jagn1b$^{\Delta T12\text{-}G14}$ leads to apoptosis at a later time point of granulopoiesis needs to be elucidated. Our

Figure 6 (continued) respect to the WT expression. (E) Quantification of mpo:*gfp*$^{+}$ neutrophils after interfering with the function of *jagn1b* (*jagn1b* MO), *cebpb* (*cebpb* MO) and overexpression of *g-csfa* (*g-csfa* mRNA) alone or in combination. (F) Relative expression (fold change) of *cebpb*, *g-csfa* and *g-csfb* in wild-type embryos and *jagn1b* morphants, quantified by quantitative RT-PCR and normalized to *b-actin*. The fold change difference was calculated respective to the wild-type expression. (A-B,E) Each dot represents the number of cells in the hematopoietic tissue of a 2.25 dpf individual embryo. Data are presented as mean ± standard deviation. The data represent combined results from 2-3 independent experiments. N represents the total number of analyzed embryos. (C,D,F) Each dot represents the relative expression of 1 analyzed sample. Data are presented as mean ± standard deviation. The data represent combined results from 2 to 3 independent experiments. N represents the total number of analyzed biological samples. ns, not significant; *$P < .05$; **$P < .01$; ***$P < .001$; ****$P < .0001$.

observations suggest that it is likely that the activation of UPR and subsequent cell death following *jagn1b* impairment is not the primary mechanism that leads to neutropenia in zebrafish. Nevertheless, further studies are required to evaluate the implication of apoptosis in neutrophil development conclusively.

Fourth, there is valid evidence of deregulated G-CSFR signaling in patients with *JAGN1*-CN. Boztug et al demonstrated a significant reduction in G-CSFR expression on neutrophils among patients with *JAGN1*-CN, indicating potential G-CSFR glycosylation defects.[6] Wirnsberger et al found reduced phosphorylation of the signal transducer and activator 3 (STAT3) in G-CSF–treated *Jagn1*-deficient neutrophils, despite normal G-CSFR levels. Consistent with the findings of Boztug et al, we observed a substantial decrease in *csf3r* mRNA expression following *jagn1b* downregulation. This coincided with the downregulation of *cebpa* mRNA levels and an increase in *cebpb* expression. The elevated expression of the latter factor in untreated *jagn1b* morphants is likely a compensatory mechanism employed by hematopoietic cells to counterbalance the reduced *cebpa* expression and to attempt to initiate granulopoiesis in the absence of *jagn1b*, albeit with limited efficiency. Interestingly, the induced expression of *cebpb* correlates with activated *csf3a* but not *csf3r* expression. These findings confirm the differential signaling outcomes between emergency granulopoiesis triggered by Cebpb- and Cebpa-regulated steady-state granulopoiesis. These data align with our previous observations that showed a diminished steady-state and enhanced emergency granulopoiesis in patients with CN.[44]

Notably, the expression levels of the studied candidate genes in this study were quantified from whole embryo mRNA and not specifically in hematopoietic cells. Granulopoiesis in patients with CN is known to arrest at the promyelocytic stage, and sorting of promyelocytic cells would be essential to analyze the effects of Jagn1b alteration on granulopoiesis. However, the corresponding developmental stages of neutrophils in zebrafish are not as distinct as in humans. Therefore, we hypothesized that the changes in expression levels seen in the whole embryo would, at least, partially recapitulate the situation in promyelocytic cells. Additional WISH examination, solely focusing our analysis on the hematopoietic tissue, also confirmed some of the RT-PCR results.

Despite the evolutionary conservation of granulopoiesis among vertebrates,[60-62] there might be species-specific adaption during the evolution. In mice, conditional knockout of *Jagn1* or transgenic expression of *JAGN1*-CN–specific mutations had no effect on neutrophil development.[10] Similarly, mice deficient in *Hax1*[63] or *G6pc3*[64] or *Elane* (p.G193X) transgenic mice[31] displayed either no or mild neutropenia. In contrast, zebrafish are a suitable model organisms to study neutropenia. One potential limitation of the zebrafish model is the challenge of identifying orthologs of human genes within its genome. There are 2 zebrafish homologs of human *JAGN1*, namely *jagn1a* and *jagn1b,* with high sequence similarity but nonredundant functions in hematopoiesis. Although *jagn1a* plays a role in immature HSCs, *jagn1b* expression and its specific involvement in granulopoiesis strongly support its function as the ortholog of human *JAGN1*.

Acknowledgments

The authors thank Advaita Dick and Anna-Sophia Hellmuth (University Hospital Tuebingen) for technical support, Patrick Mueller (University of Konstanz) for providing the draculin:*mCherry* reporter line, Daniel Capek (University of Konstanz) for technical help, and the Institute of Medical Virology and Microbiology for continuous support in confocal microscopy. The authors also acknowledge Euro-BioImaging for providing access to Zeiss LSM880 and services at the Austrian BioImaging/CMI node. This research was supported using resources of the VetCore Facility (VetImaging) of the University of Veterinary Medicine Vienna.

This work was supported by the German Research Foundation, Madeleine Schickedanz Kinderkrebsstiftung, and EuNet-INNOCHRON COST action.

Some of the graphs, including the visual abstract, were created using BioRender.com.

Authorship

Contribution: L.D. and B.B. made initial observations; L.D. designed the work, performed the experiments, and analyzed the data; J.S. and K.W. provided useful insights and interpreted the data; B.B. supervised the work and interpreted the data; and B.B., L.D., and J.S. wrote the manuscript.

Conflict-of-interest disclosure: The authors declare no competing financial interests.

The current affiliation for B.B. is Austrian BioImaging/CMI, Vienna, Austria.

ORCID profiles: L.D., 0000-0002-0121-011X; J.S., 0000-0002-4399-2324; B.B., 0000-0002-7368-7523.

Correspondence: Julia Skokowa, Department of Oncology, Hematology, Clinical Immunology and Rheumatology, University Hospital Tuebingen, Otfried-Mueller Str 10, Tuebingen 72076, Germany; email: Julia.skokowa@med.uni-tuebingen.de; and Baubak Bajoghli, Austrian Bioimaging/CMI, Vienna Biocenter Campus, Dr Bohr-Gasse-3, 1030-Vienna, Austria; email: Baubak.bajoghli@vbcf.ac.at.

References

1. Skokowa J, Dale DC, Touw IP, Zeidler C, Welte K. Severe congenital neutropenias. *Nat Rev Dis Primers*. 2017;3:17032.
2. Lee S, Cooley L. Jagunal is required for reorganizing the endoplasmic reticulum during Drosophila oogenesis. *J Cell Biol*. 2007;176(7):941-952.
3. VanWinkle PE, Parish F, Edwards YJK, Sztul E. JAGN1, tetraspanins, and Erv proteins: is common topology indicative of common function in cargo sorting? *Am J Physiol Cell Physiol*. 2020;319(4):C667-C674.
4. Eritano AS, Altamirano A, Beyeler S, Gaytan N, Velasquez M, Riggs B. The endoplasmic reticulum is partitioned asymmetrically during mitosis before cell fate selection in proneuronal cells in the early Drosophila embryo. *Mol Biol Cell*. 2017;28(11):1530-1538.

5. Ascencio G, de Cruz MA, Abuel J, et al. A deficiency screen of the 3rd chromosome for dominant modifiers of the Drosophila ER integral membrane protein, Jagunal. *G3 (Bethesda)*. 2023;13(7):jkad059.
6. Boztug K, Jarvinen PM, Salzer E, et al. JAGN1 deficiency causes aberrant myeloid cell homeostasis and congenital neutropenia. *Nat Genet*. 2014;46(9):1021-1027.
7. Khandagale A, Lazzaretto B, Carlsson G, et al. JAGN1 is required for fungal killing in neutrophil extracellular traps: Implications for severe congenital neutropenia. *J Leukoc Biol*. 2018;104(6):1199-1213.
8. Hagelkruys A, Wirnsberger G, Stadlmann J, et al. A crucial role for Jagunal homolog 1 in humoral immunity and antibody glycosylation in mice and humans. *J Exp Med*. 2021;218(1):e20200559.
9. Khandagale A, Holmlund T, Entesarian M, et al. Severe congenital neutropenia-associated JAGN1 mutations unleash a calpain-dependent cell death programme in myeloid cells. *Br J Haematol*. 2021;192(1):200-211.
10. Wirnsberger G, Zwolanek F, Stadlmann J, et al. Jagunal homolog 1 is a critical regulator of neutrophil function in fungal host defense. *Nat Genet*. 2014;46(9):1028-1033.
11. Kuehnle N, Osborne SM, Liang Z, Manzano M, Gottwein E. CRISPR screens identify novel regulators of cFLIP dependency and ligand-independent, TRAIL-R1-mediated cell death. *Cell Death Differ*. 2023;30(5):1221-1234.
12. Konantz M, Schurch C, Hanns P, Muller JS, Sauteur L, Lengerke C. Modeling hematopoietic disorders in zebrafish. *Dis Model Mech*. 2019;12(9):dmm040360.
13. Pazhakh V, Clark S, Keightley MC, Lieschke GJ. A GCSFR/CSF3R zebrafish mutant models the persistent basal neutrophil deficiency of severe congenital neutropenia. *Sci Rep*. 2017;7:44455.
14. Basheer F, Rasighaemi P, Liongue C, Ward AC. Zebrafish granulocyte colony-stimulating factor receptor maintains neutrophil number and function throughout the life span. *Infect Immun*. 2019;87(2):e00793-18.
15. Doll L, Aghaallaei N, Dick AM, Welte K, Skokowa J, Bajoghli B. A zebrafish model for HAX1-associated congenital neutropenia. *Haematologica*. 2021;106(5):1311-1320.
16. Carapito R, Konantz M, Paillard C, et al. Mutations in signal recognition particle SRP54 cause syndromic neutropenia with Shwachman-Diamond-like features. *J Clin Invest*. 2017;127(11):4090-4103.
17. Schurch C, Schaefer T, Muller JS, et al. SRP54 mutations induce congenital neutropenia via dominant-negative effects on XBP1 splicing. *Blood*. 2021;137(10):1340-1352.
18. Venkatasubramani N, Mayer AN. A zebrafish model for the Shwachman-Diamond syndrome (SDS). *Pediatr Res*. 2008;63(4):348-352.
19. Zhang CY, Yin HM, Wang H, et al. Transforming growth factor-beta1 regulates the nascent hematopoietic stem cell niche by promoting gluconeogenesis. *Leukemia*. 2018;32(2):479-491.
20. Khuchua Z, Yue Z, Batts L, Strauss AW. A zebrafish model of human Barth syndrome reveals the essential role of tafazzin in cardiac development and function. *Circ Res*. 2006;99(2):201-208.
21. Renshaw SA, Loynes CA, Trushell DM, Elworthy S, Ingham PW, Whyte MK. A transgenic zebrafish model of neutrophilic inflammation. *Blood*. 2006;108(13):3976-3978.
22. Sanchez-Iranzo H, Galardi-Castilla M, Minguillon C, et al. Tbx5a lineage tracing shows cardiomyocyte plasticity during zebrafish heart regeneration. *Nat Commun*. 2018;9(1):428.
23. Quiring R, Wittbrodt B, Henrich T, et al. Large-scale expression screening by automated whole-mount in situ hybridization. *Mech Dev*. 2004;121(7-8):971-976.
24. Tang Q, Iyer S, Lobbardi R, et al. Dissecting hematopoietic and renal cell heterogeneity in adult zebrafish at single-cell resolution using RNA sequencing. *J Exp Med*. 2017;214(10):2875-2887.
25. Athanasiadis EI, Botthof JG, Andres H, Ferreira L, Lio P, Cvejic A. Single-cell RNA-sequencing uncovers transcriptional states and fate decisions in haematopoiesis. *Nat Commun*. 2017;8(1):2045.
26. Mosimann C, Panakova D, Werdich AA, et al. Chamber identity programs drive early functional partitioning of the heart. *Nat Commun*. 2015;6:8146.
27. Stemmer M, Thumberger T, Del Sol Keyer M, Wittbrodt J, Mateo JL. CCTop: an intuitive, flexible and reliable CRISPR/Cas9 target prediction tool. *PLoS One*. 2015;10(4):e0124633.
28. Yang Y, Liu L, Naik I, Braunstein Z, Zhong J, Ren B. Transcription factor C/EBP homologous protein in health and diseases. *Front Immunol*. 2017;8:1612.
29. Fawcett TW, Martindale JL, Guyton KZ, Hai T, Holbrook NJ. Complexes containing activating transcription factor (ATF)/cAMP-responsive-element-binding protein (CREB) interact with the CCAAT/enhancer-binding protein (C/EBP)-ATF composite site to regulate Gadd153 expression during the stress response. *Biochem J*. 1999;339(Pt 1):135-141.
30. Marciniak SJ, Yun CY, Oyadomari S, et al. CHOP induces death by promoting protein synthesis and oxidation in the stressed endoplasmic reticulum. *Genes Dev*. 2004;18(24):3066-3077.
31. Nanua S, Murakami M, Xia J, et al. Activation of the unfolded protein response is associated with impaired granulopoiesis in transgenic mice expressing mutant Elane. *Blood*. 2011;117(13):3539-3547.
32. Nustede R, Klimiankou M, Klimenkova O, et al. ELANE mutant-specific activation of different UPR pathways in congenital neutropenia. *Br J Haematol*. 2016;172(2):219-227.

33. Boztug K, Appaswamy G, Ashikov A, et al. A syndrome with congenital neutropenia and mutations in G6PC3. *N Engl J Med*. 2009;360(1):32-43.
34. Kaufman RJ. Stress signaling from the lumen of the endoplasmic reticulum: coordination of gene transcriptional and translational controls. *Genes Dev*. 1999;13(10):1211-1233.
35. Van Nieuwenhove E, Barber JS, Neumann J, et al. Defective Sec61alpha1 underlies a novel cause of autosomal dominant severe congenital neutropenia. *J Allergy Clin Immunol*. 2020;146(5):1180-1193.
36. Clark EM, Nonarath HJT, Bostrom JR, Link BA. Establishment and validation of an endoplasmic reticulum stress reporter to monitor zebrafish ATF6 activity in development and disease. *Dis Model Mech*. 2020;13(1):dmm041426.
37. Li J, Chen Z, Gao LY, et al. A transgenic zebrafish model for monitoring xbp1 splicing and endoplasmic reticulum stress in vivo. *Mech Dev*. 2015;137:33-44.
38. Li G, Mongillo M, Chin KT, et al. Role of ERO1-alpha-mediated stimulation of inositol 1,4,5-triphosphate receptor activity in endoplasmic reticulum stress-induced apoptosis. *J Cell Biol*. 2009;186(6):783-792.
39. Stachura DL, Svoboda O, Campbell CA, et al. The zebrafish granulocyte colony-stimulating factors (Gcsfs): 2 paralogous cytokines and their roles in hematopoietic development and maintenance. *Blood*. 2013;122(24):3918-3928.
40. Bajoghli B, Aghaallaei N, Heimbucher T, Czerny T. An artificial promoter construct for heat-inducible misexpression during fish embryogenesis. *Dev Biol*. 2004;271(2):416-430.
41. Ma O, Hong S, Guo H, Ghiaur G, Friedman AD. Granulopoiesis requires increased C/EBPalpha compared to monopoiesis, correlated with elevated Cebpa in immature G-CSF receptor versus M-CSF receptor expressing cells. *PLoS One*. 2014;9(4):e95784.
42. Zhang DE, Zhang P, Wang ND, Hetherington CJ, Darlington GJ, Tenen DG. Absence of granulocyte colony-stimulating factor signaling and neutrophil development in CCAAT enhancer binding protein alpha-deficient mice. *Proc Natl Acad Sci U S A*. 1997;94(2):569-574.
43. Hirai H, Zhang P, Dayaram T, et al. C/EBPbeta is required for 'emergency' granulopoiesis. *Nat Immunol*. 2006;7(7):732-739.
44. Skokowa J, Lan D, Thakur BK, et al. NAMPT is essential for the G-CSF-induced myeloid differentiation via a NAD(+)-sirtuin-1-dependent pathway. *Nat Med*. 2009;15(2):151-158.
45. Baris S, Karakoc-Aydiner E, Ozen A, et al. JAGN1 deficient severe congenital neutropenia: two cases from the same family. *J Clin Immunol*. 2015;35(4):339-343.
46. Cifaldi C, Serafinelli J, Petricone D, et al. Next-generation sequencing reveals A JAGN1 mutation in a Syndromic child with intermittent neutropenia. *J Pediatr Hematol Oncol*. 2019;41(4):e266-e269.
47. Kollner I, Sodeik B, Schreek S, et al. Mutations in neutrophil elastase causing congenital neutropenia lead to cytoplasmic protein accumulation and induction of the unfolded protein response. *Blood*. 2006;108(2):493-500.
48. Grenda DS, Murakami M, Ghatak J, et al. Mutations of the ELA2 gene found in patients with severe congenital neutropenia induce the unfolded protein response and cellular apoptosis. *Blood*. 2007;110(13):4179-4187.
49. Nosak C, Silva PN, Sollazzo P, et al. Jagn1 is induced in response to ER stress and regulates proinsulin biosynthesis. *PLoS One*. 2016;11(2):e0149177.
50. Pini T, Parks J, Russ J, et al. Obesity significantly alters the human sperm proteome, with potential implications for fertility. *J Assist Reprod Genet*. 2020;37(4):777-787.
51. Yoshida H, Okada T, Haze K, et al. ATF6 activated by proteolysis binds in the presence of NF-Y (CBF) directly to the cis-acting element responsible for the mammalian unfolded protein response. *Mol Cell Biol*. 2000;20(18):6755-6767.
52. Yoshida H, Matsui T, Yamamoto A, Okada T, Mori K. XBP1 mRNA is induced by ATF6 and spliced by IRE1 in response to ER stress to produce a highly active transcription factor. *Cell*. 2001;107(7):881-891.
53. Carlsson G, Aprikyan AA, Tehranchi R, et al. Kostmann syndrome: severe congenital neutropenia associated with defective expression of Bcl-2, constitutive mitochondrial release of cytochrome c, and excessive apoptosis of myeloid progenitor cells. *Blood*. 2004;103(9):3355-3361.
54. Jun HS, Lee YM, Song KD, Mansfield BC, Chou JY. G-CSF improves murine G6PC3-deficient neutrophil function by modulating apoptosis and energy homeostasis. *Blood*. 2011;117(14):3881-3892.
55. Moulding DA, Moeendarbary E, Valon L, Record J, Charras GT, Thrasher AJ. Excess F-actin mechanically impedes mitosis leading to cytokinesis failure in X-linked neutropenia by exceeding Aurora B kinase error correction capacity. *Blood*. 2012;120(18):3803-3811.
56. Rujkijyanont P, Watanabe K, Ambekar C, et al. SBDS-deficient cells undergo accelerated apoptosis through the Fas-pathway. *Haematologica*. 2008;93(3):363-371.
57. Person RE, Li FQ, Duan Z, et al. Mutations in proto-oncogene GFI1 cause human neutropenia and target ELA2. *Nat Genet*. 2003;34(3):308-312.
58. Mojicevic M, D'Agostino PM, Pavic A, et al. Streptomyces sp. BV410 isolate from chamomile rhizosphere soil efficiently produces staurosporine with antifungal and antiangiogenic properties. *Microbiologyopen*. 2020;9(3):e986.
59. Krokowski D, Guan BJ, Wu J, et al. GADD34 function in protein trafficking promotes adaptation to hyperosmotic stress in human corneal cells. *Cell Rep*. 2017;21(10):2895-2910.
60. Elsaid R, Soares-da-Silva F, Peixoto M, et al. Hematopoiesis: a layered organization across chordate species. *Front Cell Dev Biol*. 2020;8:606642.
61. Robertson AL, Avagyan S, Gansner JM, Zon LI. Understanding the regulation of vertebrate hematopoiesis and blood disorders—big lessons from a small fish. *FEBS Lett*. 2016;590(22):4016-4033.

62. Jagannathan-Bogdan M, Zon LI. Hematopoiesis. *Development*. 2013;140(12):2463-2467.

63. Chao JR, Parganas E, Boyd K, Hong CY, Opferman JT, Ihle JN. Hax1-mediated processing of HtrA2 by Parl allows survival of lymphocytes and neurons. *Nature*. 2008;452(7183):98-102.

64. Cheung YY, Kim SY, Yiu WH, et al. Impaired neutrophil activity and increased susceptibility to bacterial infection in mice lacking glucose-6-phosphatase-beta. *J Clin Invest*. 2007;117(3):784-793.

A *JAGN1*-associated severe congenital neutropenia zebrafish model revealed an altered G-CSFR signaling and UPR activation

Larissa Doll, Karl Welte, Julia Skokowa and Baubak Bajoghli

Supplementary Data:

Supplementary Material and Methods

DNA constructs

For *in vitro* transcription full length sequences of *jagn1a*, *jagn1b* and *g-csfa* were cloned into pMC vector[1]. Full length *cebpb* with a SP6-binding site and polyA sequence was amplified without cloning into a vector. For morpholino-binding-efficiency test (*jagn1a* and *jagn1b* MO), the corresponding ATG-morpholino binding sequence was cloned preceding the GFP coding sequence. Detailed cloning strategies can be found in **Supplementary Table 3 and 4**. To introduce *jagn1b*$^{\Delta T12\text{-}G14}$ in the pMC-*gfp-jagn1b* construct, site directed mutagenesis was performed using the QuikChange II XL Site-Directed Mutagenesis Kit (Agilent, Cat. No. #200521). Primers are listed in **Supplementary Table 5**. The generated plasmids were linearized and transcribed using mMESSAGE mMACHINE SP6 (Invitrogen, Cat. No. AM1340) kit following the manufacturer's instructions. The final capped mRNA product was purified using the RNeasy Mini kit (Qiagen, Cat. No. 74104).

Knock-down and rescue experiments

We designed and ordered morpholinos (GeneTools) targeting the translational sites of *jagn1a*, *jagn1b*, and *cebpb* (previously described[2]). Sequences found in **Supplementary Table 6**. Approximately 2 nl of 0.5 mM morpholino was injected into the blastomere of one-cell stage embryos. For rescue experiments, 50 ng/µl of *jagn1a*, *jagn1b*, *g-csfa* or *cebpb* mRNA was injected into the blastomere alone or in combination with morpholinos. For the rescue experiment with the heat inducible *g-csfa* expressing plasmid[3,4], 20ng/µl was injected together with 10ng/µL mRNA of Tol2 transposase into one-cell-stage embryos. Injected embryos were heat-treated (39°C) for 1h, at 44hpf. GFP-positive embryos were selected for subsequent WISH analysis.

CRISPR/Cas9-based transient and stable mutation of zebrafish *jagn1b*

To develop transient gene-edited embryos (crispants), 2 nl RNPs (5µM) with *jagn1b* specific gRNA and Cas9 protein (Alt-R® S.p. Cas9 nuclease, v.3, IDT) were co-injected into the blastomere of tg(mpo:*gfp*) zebrafish embryos. To quantify the knock-out efficiency, the targeted sequence of *jagn1b* was amplified (gRNA and primer sequences in **Supplementary Table 7**), sequenced and analyzed with TIDE assay (https://ice.synthego.com/#/). The injected embryos were raised to adulthood for the generation of a stable mutant line (F0), genotyped and crossed to obtain zebrafish with homozygous *jagn1b* c.347_351del and c.351_357del mutants. Note, the incross of heterozygous *jagn1b* mutants did not lead

to homozygous adult fish. Genomic regions with predicted off-targets were amplified using PCR (primer in **Supplementary Table 8**) and sequenced.

Embryonic apoptosis staining: TUNEL and acridine orange

The TUNEL assay *in situ* cell death detection kit POD (Roche, Cat. No. 11684817910) was used to detect and quantify apoptotic cells in zebrafish embryos at 2.25dpf following manufacturer's instructions. To visualize apoptotic cells in live, embryos were incubated in a 50µg/ml Acridine orange (Enzo, Cat. No. ENZ-52405) solution in E3 for 30 minutes in the dark.

Quantitative RT-PCR

Total RNA was isolated from 3dpf embryos. The embryos were homogenized in Triazol (QIAzol Lysis Reagent, Qiagen, Cat. No. 79306) and chloroform. RNA phase was separated by centrifugation. To complete the RNA isolation, we used the RNeasy Mini kit (Qiagen, Cat. No. 74104) following the manufacturer's protocol. After cDNA synthesis (SuperScript III Reverse Transcriptase kit, Invitrogen, Cat. No. 18080093), RT-PCR was performed using SYBR Green I (ROCHE, Cat. No. 04707516001) kit with the LightCycler 480. The results were normalized to the level of the internal control *b-actin* and calculated using the ΔΔCt method, being represented in fold changes. Primers used in this study are listed in **Supplementary Table 9**.

Whole mount immunostaining

Immunostaining of GFP and Jagn1 was performed in tg(mpo:*gfp*) embryos at 2dpf, as described previously [5]. Briefly, we used the goat anti-GFP (Abcam, Cat. No. ab5450, 1:500 dilution) antibody and rabbit anti-JAGN1 (Invitrogen, Cat.No. PA5-98615, 1:250). As secondary antibodies Alexa488-donkey anti goat (Abcam, Cat. No. ab15129, 1:600) and Cy3-donkey anti-rabbit IgG (Jakson laboratories, Cat. No. 711-165-152, 1:500) were used.

Drug treatment

To induce UPR we treated dechorionized zebrafish embryos at 1 dpf, with 0.7 mM Dithiothreitol (Invitrogen, Cat. No. Y00147) or 1 µg/ml Tunicamycin (Sigma, Cat. No. T7765-1MG) in E3 media for 24 hours. Similarly, to induce apoptosis, the embryos were incubated in 5 µM Staurosporine (Sigma, Cat. No. S5921-1mg) in E3 media also for 24 hours. As control, embryos were incubated in 0,7% DMSO/E3. After treatment, embryos were fixed for WISH or RNA was isolated for RT-PCR analyses.

Microscopy and cell enumeration

Manual cell quantification after WISH, TUNEL and acridine orange staining, were performed with a Nikon stereo-fluorescent SMZ18 microscope. In this study, quantification of cell numbers was restricted to cells in the trunk region caudal to the yolk extension. Pictures were taken with the microscope-fitted Nikon DS-Fi3 camera and NIS Elements software. Brightness and contrast were adapted for better visualization. Confocal images from immunostaining and GFP-Jagn1b localization were taken using a

Zeiss LSM 710 NLO microscope. Z-stacks of 60-70µm spanning the trunk region (z space= 1 µm) were acquired using 10x and 20x objectives. Confocal images were analyzed with Imaris software.

Supplementary Tables:

Supplementary Table 1. Gene specific antisense RNA probes for *in situ* hybridization used in this study

Gene	Ensembl ID	Nucleotides (X to X)	Primer forward 5'-3'	Primer reverse 5'-3'
lyz	ENSDARG00000057789	25-412	TGTCTGGCGTGGATGTCCTC	AGCGGGACATCTTACGACCG
mpo	ENSDART00000043961	178-891	GTCATTAAGCCTTCTGACAAGC	CATGTAGGCAGTGTGCCCAGAACC
mpeg1.1	ENSDARG00000055290	820-1382	ATTCAGAGCCACGGAGGAGC	CGACGGACGTGGTAAGAATCACC
hbae1.1	ENSDARG00000088330	45-280	GCCAAGATCGCTGGAAAGGC	CGCAGCTGGAAAGCATGGAG
spi1b	ENSDARG00000000767	161-706	CAGAGATCTATCGACCACCAATGG	CTTTGTGCTTGGATGAGAACTGG
cmyb	ENSDART00000075730	176-819	GTTCTGAAGACTGGAAAGTCATCG	GTGTCTCTGGATAGCAGCAGTGCC
cebpα	ENSDARG00000036074	110-705	AGATCTGCGAGAACGAGAACTCC	CATTTTCGCCTTGTCCCGACTC
cebpβ	ENSDARG00000042725	137-715	CGAGAAAGCCATAGACTTCAGC	TGCGCATTTTGGCTTTGTCTCT

Supplementary Table 2. JAGN1 proteins from different species used for *in silico* analysis.

Protein	Organism	Accession code
JAGN1	Human (*Homo sapiens*)	NP_115881.3
JAGN1	Chimpanzee (*Pan troglotides*)	JAA39217.1
JAGN1	Rat (*Rattus norvegicus*)	NP_001037737.1
JAGN1	Mouse (*Mus musculus*)	NP_080641.1
Jagn1	Medaka (*Oryzias latipes*)	XP_004066598.1
Jagn1a	Zebrafish (*Danio rerio*)	NP_001005774.1
Jagn1b	Zebrafish (*Danio rerio*)	NP_001003584.2
Jagunal	Fruit fly (*Drosophila melanogaster*)	NP_731002.1

Supplementary Table 3. Templates for mRNA synthesis used in this study

Cloning strategies							
Created plasmid	**Original vector**	**Vector digest***	**Insert**	**Forward primer (5'-3')**	**Reverse primer (5'-3')**	**Insert digest***	**Comments**
pMC-*jagn1a*	pMC[1]	NcoI/BcuI	*jagn1a*	CTTGAATTCACCATGGCA TCTCGTGCAGG (1,2)	GCAACTGAGACATAAATA GCGG (1) ATCACTAGTTTTTATTTC TCTTCTTCTC (2)	EcoRI/BcuI	To amplify full-length *jagn1a* a nested PCR was needed. Forward and second reverse primer included cutting sites for restriction enzymes.
pMC-*jagn1b*	pMC[1]	BamHI/BcuI	*jagn1b*	TATGGATCCGCCATGG CATCACGAGCAGGACC	AGTACTAGTCACTAAACA TCCACCAGAAGTCC	BamHI/BcuI	The coding sequence corresponding to full-length *jagn1b* was amplified with primers containing cutting sites for the restriction enzymes.
pMC-*gfp-jagn1b*	pMC-*jagn1b* (vector)	NcoI/EcoRI	*gfp*	CTTGAATTCATCATGGTG AGCAAGGGCGAGGAG	ATGCCATGGTAGCTCCTG CACCGGCGCCAGCTCCTG CACCCAACTTGTACAGCT CGTCC	No digest	The coding sequence of *gfp* was introduced into the already cloned plasmid. The mRNA resulting from this plasmid has a *gfp* on the N-terminal part of *jagn1b* separated by a linker.
pMC-*g-csfa*	pMC[1] (vector) pTGH-zf-*g-csfa*[3,4]	EcoRI/BcuI	*g-csfa*	No primer	No primer	EcoRI/BcuI	Full length sequence of zebrafish *g-csfa* was cut from pTGH-zf-*g-csfa* and cloned into pMC.

Generation of template for mRNA synthesis without plasmid						
Template construct	**PCR 1**	**Primer (5'-3')**	**PCR 2**	**Primer (5'-3')**	**PCR 3: fusion PCR**	**Primer (5'-3')**
SP6-*cebpb*-polyA	SP6 (binding site) - *cebpb* (coding region) **Template**: cDNA	**Forward**: GACCATTTAGGTGACACTATAGAAGAACATGG AAGTGGCCGGTTTTTACGAG **Reverse**: GCTTTATCAGCACTGGCCGGTGG	*cebpb*-polyA **Template:** pCRII-TOPO®-SP6-*jagn1b*(ATG)-*gfp*-polyA	**Forward**: CAGTGCTGATAAAGCGGC CATCACTAGTGAC **Reverse**: GAATTAAAAAACCTCCCAC ACCTCCC	SP6-*cebpb*-polyA **Template**: PCR1 + PCR2	**Forward**: GACCATTTAGGTGACACTATAGAAG **Reverse**: GAATTAAAAAACCTCCCACACCTCCC

* All digests were performed with FastDigest restriction enzymes from ThermoFisher. BamHI (Cat. No. FD0054), BcuI (Cat. No FD1254), EcoRI (Cat. No. FD0274), NcoI (Cat. No. FD0574)

Supplementary Table 4. Cloning approach for morpholino-binding-efficiency tests used in this study

Created plasmid	Original vector	Vector digest*	Insert	Forward primer (5'-3')	Reverse primer (5'-3')	Insert digest*	Comments
pSA-*jagn1a*(ATG)-*gfp*-polyA	pSA-*gfp*-polyA	BshTI/NcoI	*jagn1a*(ATG)	TCGACGGATATTGGCAATG GCATCTCGTGCATA	CATGTATGCACGAGATGC CATTGCCAATATCCG	SalI/NcoI	The primers, containing *jagn1a* ATG MO binding sequence and flanked by SalI and NcoI cutting sites, were annealed to generate the insert. A plasmid containing SP6 promotor and *gfp*-polyA sequence was digested and ligated with the annealed and digested primers (insert).
pCRII-TOPO®-SP6-*jagn1b*(ATG)-*gfp*-polyA	pCR-BluntII-TOPO® (ThermoFisher, Cat. No 450245) (vector)	No digest	*jagn1b*(ATG)-*gfp*-polyA	GACCATTTAGGTGACACTAT AGAAGCGGTTGTCGACGGA GGTGGTTTGCCATGGTGAG CAAGGGCGAGGAGC	GTGGCGGCCGCGAATTAA AAAACC	No digest	To generate the insert, the *gfp* coding sequence was amplified with forward primer including SP6 site and *jagn1b* morpholino binding site from a template including a polyA sequence after the *gfp* coding sequence.

* All digests were performed with FastDigest restriction enzymes from ThermoFisher. SalI (Cat. No. FD0644), BshTI (Cat. No. FD1464), NcoI (Cat. No. FD0574).

Supplementary Table 5. Site-directed mutagenesis primer used in this study

Plasmid	Mutation	Forward primer 5'-3'	Reverse primer 5'-3'
pMC-*gfp-jagn1b*	ΔT12-G14	GGACCGCGGGCCACAGGTA GCGACTACCAGCACCGTGAG	CTCACGGTGCTGGTAGTCGCTA CCTGTGGCCCGCGGTCC

Supplementary Table 6. Morpholinos used in this study

Morpholino target gene	Sequence 5'-3'
jagn1a	GCACGAGATGCCATTGCCAATATCC
jagn1b	CATGGCAAACCACCTCCGTCGACAA
cebpb	GATCTTAACACCCGCCGGATTGCG

Supplementary Table 7. gRNA and genotyping primer sequences for *jagn1b* CRISPR/Cas9 gene-editing used in this study

Name	Sequence 5'-3'
jagn1b-TM-gRNA	CGGCCCTATTCTTTACGGG
jagn1b primer forward	TGGTCTGGTTTCTTGTCGCAGC
jagn1b primer reverse	GGTGAACCAGGCATCCAGCAGC

Supplementary Table 8. Primers to amplify genomic regions with predicted off-targets generated by *jagn1b*-TM-gRNA used in this study

Gene	Ensembl ID	Primer forward 5'-3'	Primer reverse 5'-3'
lama1	ENSDARG00000056043	GACGCAGCTCATAGAGAAGC	GGTATGATCGGCCCATTAAC
cacna1da	ENSDARG00000024004	GTAAGTTGCAGGCACAGGAC	TTCTGCTCTGCTGTGAAGGC
atp10a	ENSDARG00000061039	CAGAGCTTATGGAGAGCAGA	CACACAGTAGGTAGAAGAGCG
apbb3	ENSDARG00000053771	CCGAGGCTTCAAATGTCACAG	AGGACCTCTAAGGACATTGG
triob	ENSDARG00000000370	ATTCCAAGAGCGACAGTCGC	CTCAGCAGGTTAGTACAAAGC
lrp1b	ENSDARG00000029146	TGTTGTGAAGTGCAGGAAGC	AGTCAGTCATACCGCACTCC
cxcr5	ENSDARG00000010514	GACAACAACTCAACTAGGCTC	AAGCCGATACTCTCGGTCAC
lrrc47	ENSDARG00000053138	GCTGAAGGACAAGAGGCTTG	GGTCGGACATCTTTGACTGC
vmp1	ENSDARG00000012450	GTTGTCCCTAAATGCTTCAAG	TCATGGCTACTCTGAGGTCTG
dlgap2	ENSDARG00000076070	TGTAGAGAGCTGTGGGTCATG	CAGGGATGTAGATCTCTATGC
c6cast1	ENSDARG00000069216	AGCTCTGTGATGCACTATGG	TCCCTCTGTGTTGACGAAGC
jag1b	ENSDARG00000013168	GAGCGATTGAACTTCAGTCAG	TCCTGGGGTTGTAGATGAGG
tsc2	ENSDARG00000086415	TGGTCCTGCCTTCCTTCTAC	CTATGAGAGTCCTCTCTGGG

Supplementary Table 9. Primers for quantitative RT-PCR used in this study

Purpose	Gene	Ensembl ID	Primer forward 5'-3'	Primer reverse 5'-3'
G-csfr pathway analysis	*cebpα*	ENSDARG00000036074	GCTCCATGAAGATTGGCGATCG	CATTTTCGCCTTGTCCCGACTC
	cebpβ	ENSDARG00000042725	CTCAAGCGGGAAAGGCAAGAAG	TGCGCATTTTGGCTTTGTCTCT
	hcls1	ENSDARG00000012729	TCTGCCACATAGCTGTGTCC	CAGCATTGCAGATCTCAGGC
	csf3r	ENSDARG00000045959	TGAAGGATCTTCAACCACAC	GATGCACCAATGCATGCTGG
	g-csfa	ENSDARG00000102211	AACTACATCTGAACCTCCTG	GACTGCTCTTCTGATGTCTG
	g-csfb	ENSDARG00000098752	GGAGCTCTGCGCACCCAACA	GGCAGGGCTCCAGCAGCTTC
Unfolded protein response (UPR)	*atf4*	ENSDARG00000111939	CAGACCCGATCCTGAAGCATC	TCGCTGTTCAGCGACTCCTG
	ddti3 (Chop)	ENSDARG00000059836	AAGGAAAGTGCAGGAGCTGA	TCACGCTCTCCACAAGAAGA
	ero1a	ENSDARG00000015228	CGTCTCTGAGTTCCAGCAGAG	CCGCAGCTCAATGAGGTACAG
	ero1b	ENSDARG00000103915	GCGAACACTGTGAGTGAGATGC	CAGGAGCAGATCCACATACTCTG
	ppp1r15a (Gadd34)	ENSDARG00000069135	CGCAGTCCAGAACTACTGCATG	CAAGATGCCCATCATGGCTAC
	sxbp1	ENSDARG00000035622	TGTTGCGAGACAAGA	CCTGCACCTGCTGCGGACT
	ern1 (Ire1)	ENSDARG00000058475	TGACGTGGTGGAAGTTGGTA	ACGGATCACATTGGGATGTT
	eif2ak3 (Perk)	ENSDARG00000062139	TGGGCTCTGAAGAGTTCGAT	TGTGAGCCTTCTCCGTCTTT
	atf6	ENSDARG00000012656	CTGTGGTGAAACCTCCACCT	CATGGTGACCACAGGAGATG
	xbp1	ENSDART00000124467	GAGTCCGCAGTGAGCGATTTAGG	GCAGGAGATCAGACTCAGAGTCTG

Supplementary Table 10. Predicted off-targets of *jagn1b*-TM-gRNA

Predicted affected genes (off-target)	Chromosome	Strand	Missmatches	Target sequences	PAM	Sequenced genomic area
jagn1b	chr22	+	0	CGGCCCTATTCTTTACGG	GGG	Mutation identified
lama1	chr24	-	3	CGGCGCTGCTCTTTACGG	CGG	No mutation identified
cacna1da	chr11	-	4	CAGCCATCTTCTTAACGG	TGG	No mutation identified
atp10a	chr6	+	3	TGGCCCTCTTCTTTACTG	TGG	No mutation identified
APBB3	chr21	+	3	CGGCCCTCTGCTTTACTG	TGG	No mutation identified
triob	chr16	+	4	CGGTCCAACTCTTTACTG	TGG	No mutation identified
lrp1b	chr23	+	4	CGGCCTGAGTCTTTACAG	CGG	No mutation identified
CXCR5	chr18	+	4	TGGCCCTATTGGTTACAG	TGG	No mutation identified
lrrc47	chr8	-	4	CGGCACTTTTCTTTTTGG	AGG	No mutation identified
vmp1	chr15	-	4	TGGCCCTAGTCTTTTCTG	CGG	No mutation identified
dlgap2	chr20	+	4	CGGCCATTTTCTTTCCTG	AGG	No mutation identified
c6ast1	chr7	-	4	CGTCCCTATTCCTGACAG	TGG	No mutation identified
jag1b	chr13	-	4	CGGTCCTATTCTTCCAGG	TGG	No mutation identified
tsc2	chr1	-	4	CGGCCGTATTTTTTAATG	AGG	No mutation identified

Supplementary Figures:

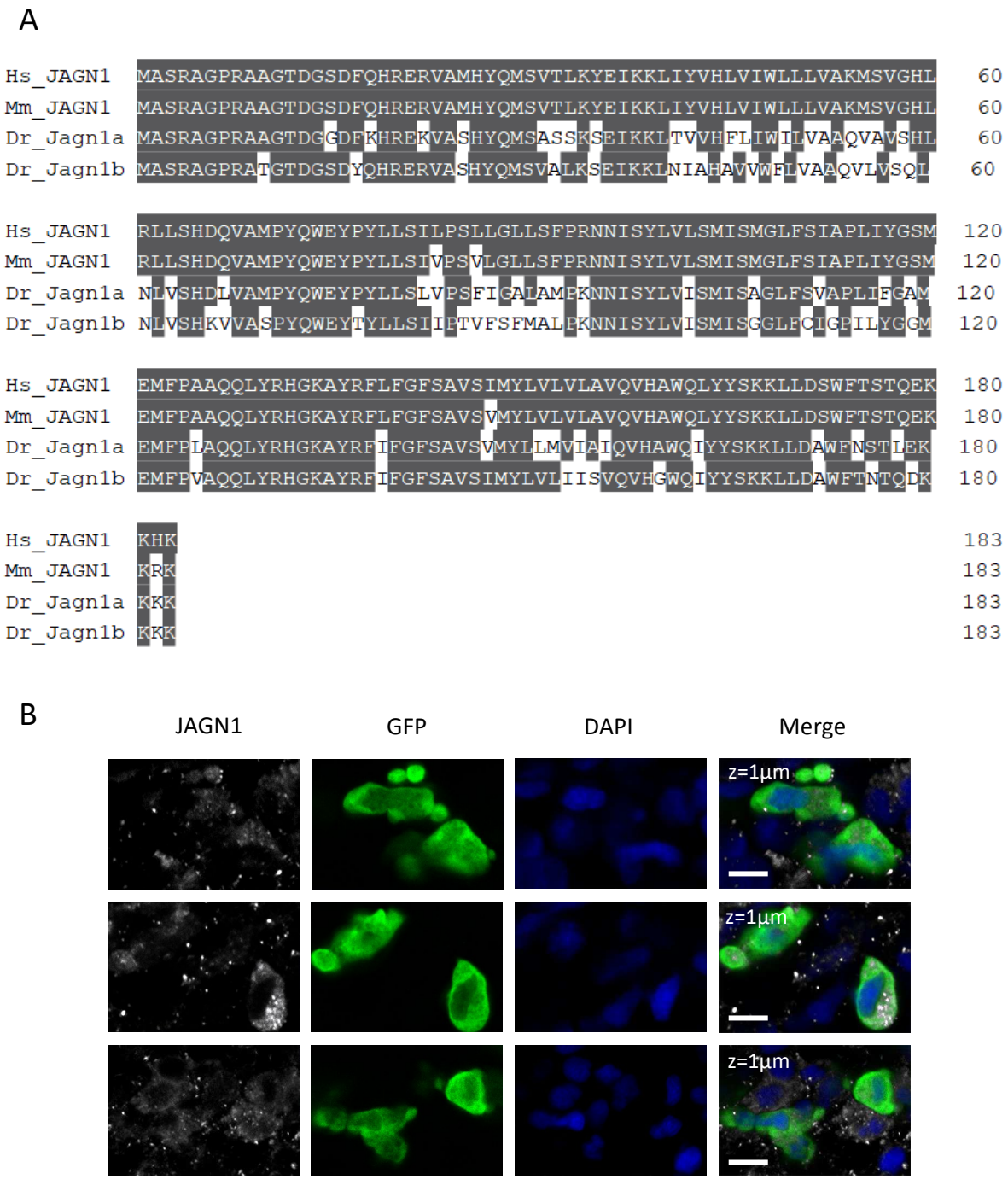

Supplementary Figure 1. The evolution of JAGN1 and the expression patterns of its homologs in zebrafish

(A) Multiple protein alignment for human (*Hs, Homo sapiens*), mouse (*Ms, Mus musculus*) and zebrafish (*Dr, Danio rerio*) JAGN1 orthologs. Human JAGN1 protein sequence was used as reference sequence. Dark highlighting represents sequence consensus. **(B)** Representative images of GFP-expressing neutrophils from various 2 dpf transgenic tg(mpo:*gfp*) embryos after double-immunostaining against GFP (neutrophils), JAGN1 and DAPI staining. Images were taken with 40x magnification. Scale bars represent 5µm.

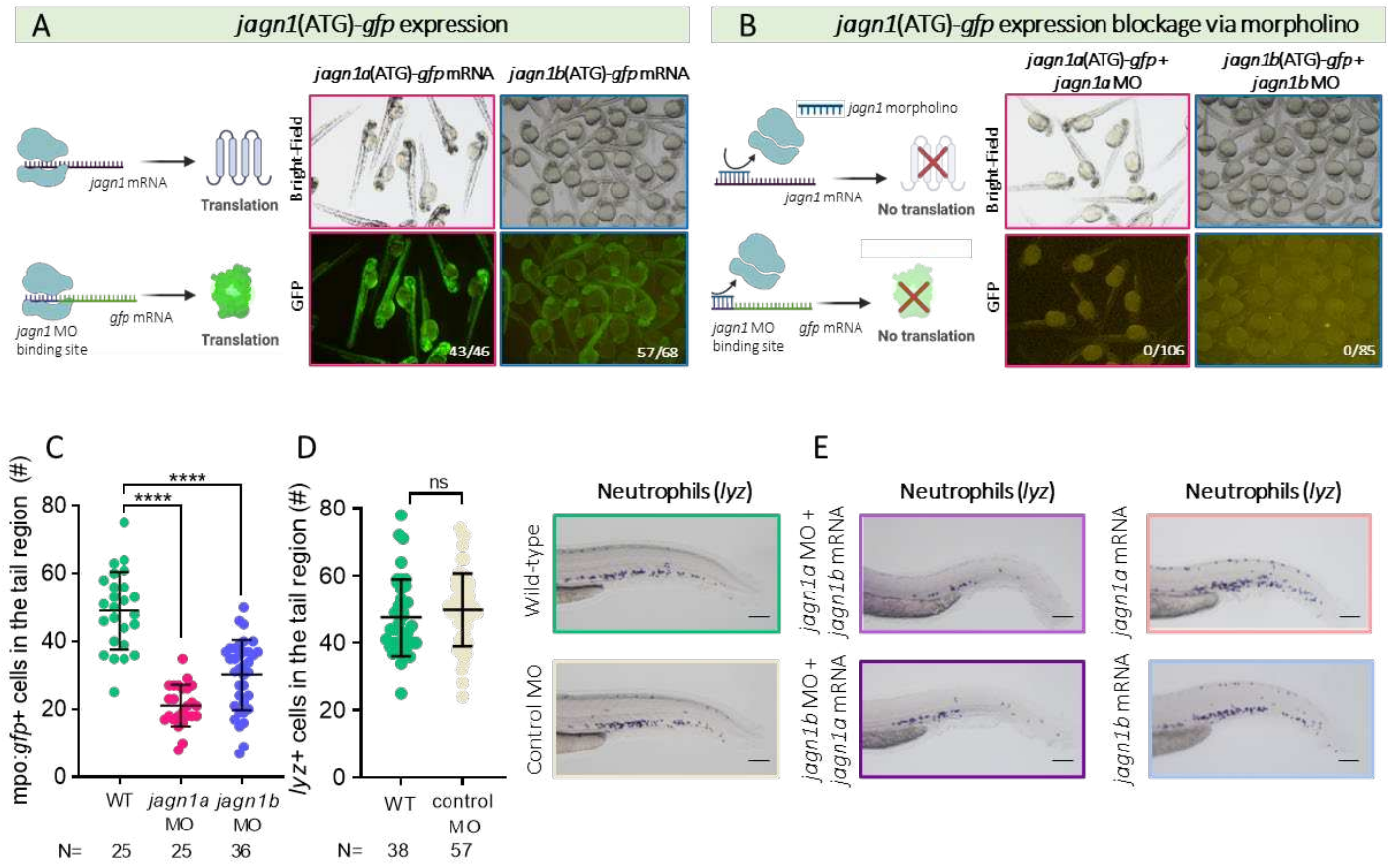

Supplementary Figure 2. Morpholino knock-down strategy and effect on neutrophils.

(A-B) Morpholino-binding-efficiency test. **(A)** The left panel shows a schematic representation of the translational process of *gfp* mRNA containing the start region of *jagn1a* or *jagn1b* (morpholino binding site). The right panel shows representative images of the GFP expression. At 2 dpf 43 out of 46 embryos were GFP-positive after *jagn1a*(ATG)-*gfp* overexpression and 57 out of 68 after *jagn1b*(ATG)-*gfp* overexpression. Created by BioRender.com. **(B)** The left panel shows a schematic representation of the translational process of *gfp* mRNA containing the start region of *jagn1a* or *jagn1b* (morpholino binding site) after co-injection with the corresponding morpholino. The right panel shows representative images of the GFP expression. At 2 dpf none of the embryos (0/106 and 0/85) showed GFP signal after co-injection of *jagn1*(ATG)-*gfp* mRNA and morpholino. Created by BioRender.com. **(C)** Quantification of mpo:*gfp*$^{+}$ neutrophils after *jagn1a* and *jagn1b* interference **(D)** Effect of control morpholino injection on *lyz*-expressing neutrophils. The left panel shows the quantification of *lyz*-positive neutrophils after control morpholino injection compared to uninjected siblings. The right panel shows representative images of 2.25 dpf wild-type and control morpholino injected embryos. **(C-D)** Data shows mean and standard deviation. Each dot represents the number of stained cells in the hematopoietic region of an individual 2.25dpf embryo. N represents number of analyzed embryos. **(E)** Representative images of *lyz*-stained (WISH) cells after co-injection of *jagn1a* morpholino with *jagn1b* mRNA, *jagn1b* morpholino with *jagn1a* mRNA and overexpression of *jagn1a* and *jagn1b* mRNA alone in 2.25dpf embryos. Images were taken with 10x magnification. Scale bars represent 100µm. ns, not significant; **** p_value < 0.0001.

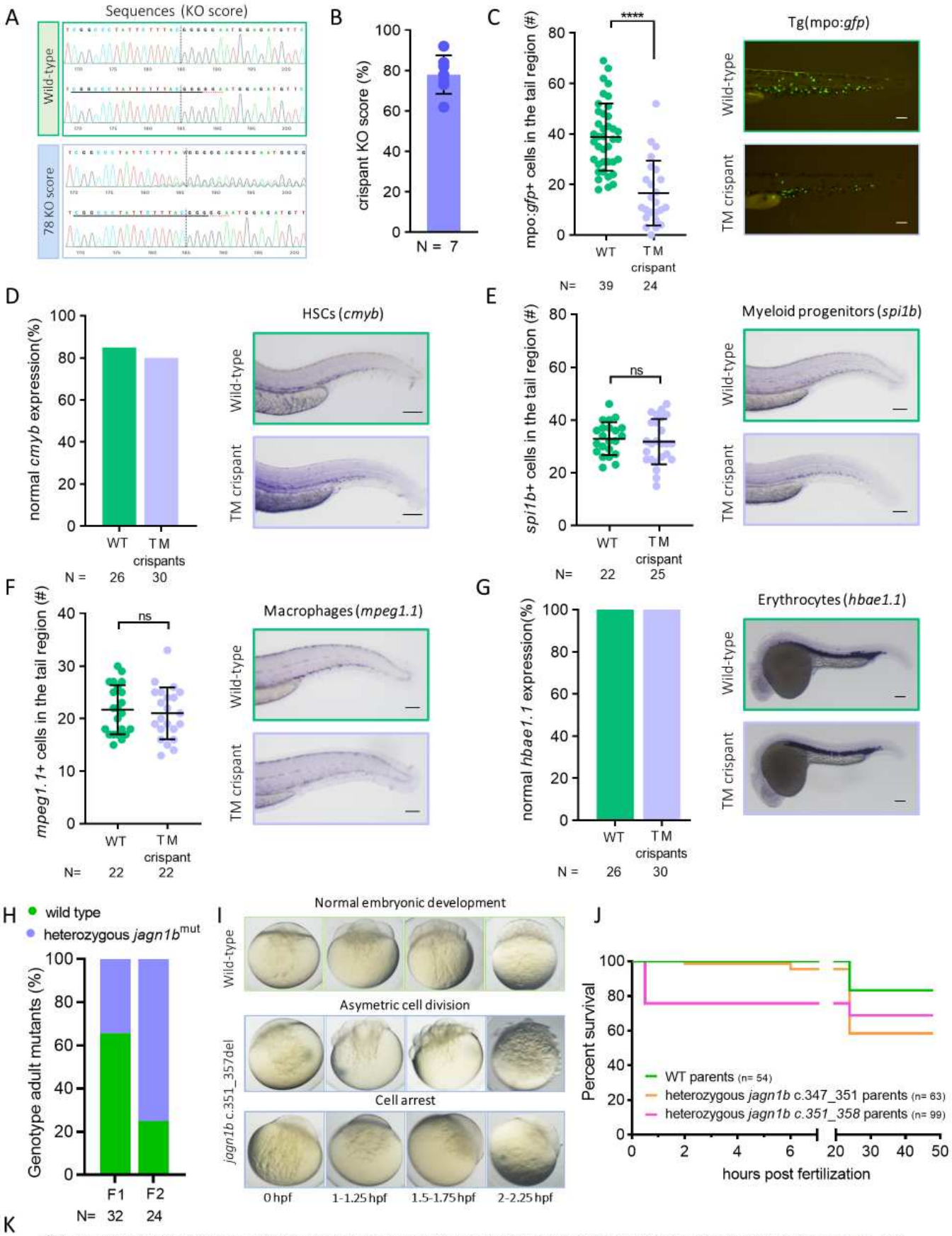
A
Sequences (KO score)
Wild-type
78 KO score
B
crispant KO score (%)
N = 7
C
mpo:gfp+ cells in the tail region (#)
****
WT
TM crispant
N= 39 24
Tg(mpo:gfp)
Wild-type
TM crispant
D
normal cmyb expression(%)
WT
TM crispants
N = 26 30
HSCs (cmyb)
Wild-type
TM crispant
E
spi1b+ cells in the tail region (#)
ns
WT
TM crispant
N= 22 25
Myeloid progenitors (spi1b)
Wild-type
TM crispant
F
mpeg1.1+ cells in the tail region (#)
ns
WT
TM crispant
N= 22 22
Macrophages (mpeg1.1)
Wild-type
TM crispant
G
normal hbae1.1 expression(%)
WT
TM crispants
N = 26 30
Erythrocytes (hbae1.1)
Wild-type
TM crispant
H
wild type
heterozygous jagn1b mut
Genotype adult mutants (%)
F1
F2
N= 32 24
I
Normal embryonic development
Wild-type
Asymetric cell division
jagn1b c.351_357del
Cell arrest
0 hpf
1-1.25 hpf
1.5-1.75 hpf
2-2.25 hpf
J
Percent survival
WT parents (n= 54)
heterozygous jagn1b c.347_351 parents (n= 63)
heterozygous jagn1b c.351_358 parents (n= 99)
hours post fertilization
K
wild type MASRAGPRATGTDGSDYQHRERVASHYQMSVALKSEIKKLNIAHAVVWFLVAAQVLVSQLNLVSHKVVASPYQWEYTYLLSIIPTVFSFMALPKNNISYLVISMISGGLFCIGPILYGGM 120
c.347_351 MASRAGPRATGTDGSDYQHRERVASHYQMSVALKSEIKKLNIAHAVVWFLVAAQVLVSQLNLVSHKVVASPYQWEYTYLLSIIPTVFSFMALPKNNISYLVISMISGGLFCIGPIRGNGD 120
c.351_358 MASRAGPRATGTDGSDYQHRERVASHYQMSVALKSEIKKLNIAHAVVWFLVAAQVLVSQLNLVSHKVVASPYQWEYTYLLSIIPTVFSFMALPKNNISYLVISMISGGLFCIGPILY-GD 119
wild type NLVSHKVVASPYQWEYTYLLSIIPTVFSFMALPKNNISYLVISMISGGLFCIGPILYGGMEMFPVAQQLYRHGKAYRFIFGFSAVSIMYLVLIISVQVHGWQIYYSKKLLDAWFTNTQDKKKK 183
c.347_351 NLVSHKVVASPYQWEYTYLLSIIPTVFSFMALPKNNISYLVISMISGGLFCIGPIRGNGDVPCGSAALSPRQSL---------- 134
c.351_358 NLVSHKVVASPYQWEYTYLLSIIPTVFSFMALPKNNISYLVISMISGGLFCIGPILY-GDVPCGSAALSPRQSL---------- 133

Supplementary Figure 3. Transient CRISPR/Cas9-induced truncation in Jagn1b led to neutropenia without affecting other hematopoietic cell types. The stable mutation altered embryonic development and lethality.

(A) Exemplary sequences of the region of *jagn1b,* coding the transmembrane domain, targeted by the guide RNA. Alignment between the wild-type and a crispant sequences with the corresponding KO score. **(B)** KO scores of 7 embryos injected with CRISPR/Cas9 targeting *jagn1b* transmembrane domain (TM crispants). **(C)** Effect of targeting *jagn1b* transmembrane domain, using CRISPR/Cas9, on neutrophils. Left panel shows the quantification of mpo:*gfp*$^{+}$ neutrophils of transgenic tg(mpo:*gfp*) uninjected reporter embryos compared to *jagn1b* TM crispants. Right panel shows representative images of mpo:*gfp*$^{+}$ neutrophils of a 2dpf wild-type transgenic mpo:*gfp* reporter embryo compared to a TM crispant. **(D-G)** Effect of *jagn1b* CRISPR/Cas9-induced mutation on other hematopoietic cells. The left panels show quantitative analyses of stained cells with WISH against hematopoietic cell-specific marker. The right panels show representative images of the WISH-stained embryos. The cells were stained against **(D)** *cmyb*, staining hematopoietic stem cells (HSC), **(E)** *spi1b*, staining myeloid progenitors, **(F)** *mpeg1.1*, staining macrophages in 2.25dpf embryos and **(G)** *hbae1.1* staining erythrocytes in 1dpf embryos. **(D,G)** Comparison of the percentage (%) of normal gene expression pattern between wild-type embryos and *jagn1b* crispants. **(E,F)** Numbers of stained cells in the hematopoietic region. Each dot represents the cell numbers of an individual embryo. Data shows mean and standard deviation. N represents the total number of analyzed embryos. Images were taken with 8x-10x magnification. Scale bars represent 100µm. **(H)** Genotype of adult mutants first (F1) and second (F2) generation in percentage (%). **(I)** Representative images of early stages of embryonic development from 0 to 2.25hpf of wild-type and offspring of *jagn1b* c.351_357 heterozygous mutants. The offspring of the mutants shows two phenotypes: an impaired cell division (dysmorphic) or the cell division arrest in the one-cell stage (arrested). **(J)** Embryonic survival in percentage (%) of wild-type embryos and offspring of heterozygous *jagn1b* c.347_351 and c.351_358 mutants. **(K)** Alignment of resulting Jagn1b protein upon mutation induced by CRISPR/Cas9. Two different mutations c.347_351, deletion of 5 nucleotides (light blue) and c.351_358, deletion of 8 nucleotides (dark blue) result in a truncated protein. The highlighted region represents the affected region of Jagn1b upon mutation. ns, not significant; **** p_value < 0.0001.

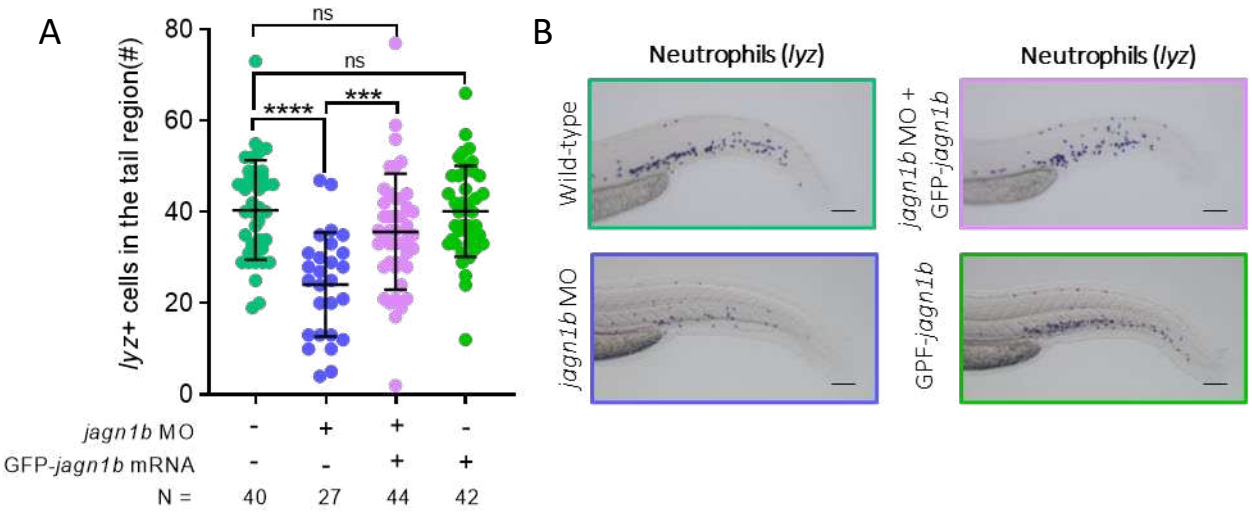

Supplementary Figure 4. GFP-tagged Jagn1b can rescue *jagn1b*-morpholino-induced neutropenia phenotype.

(A) Quantification of *lyz*$^{+}$ cells in *jagn1b* morphants (MO), after overexpression of GFP-tagged *jagn1b* mRNA alone and the combination of both, compared to uninjected 2.25dpf siblings. Data shows mean and standard deviation. Each dot represents the number of stained cells in the hematopoietic tissue of an individual 2.25dpf embryo. The data represents the combined results from 2 independent experiments. N represents the total number of analyzed embryos **(B)** Representative images of the rescue experiment of GFP-tagged *jagn1b*. Images were taken with 10x magnification. Scale bars represent 100µm. ns, not significant; *** p_value<0.001 **** p_value < 0.0001

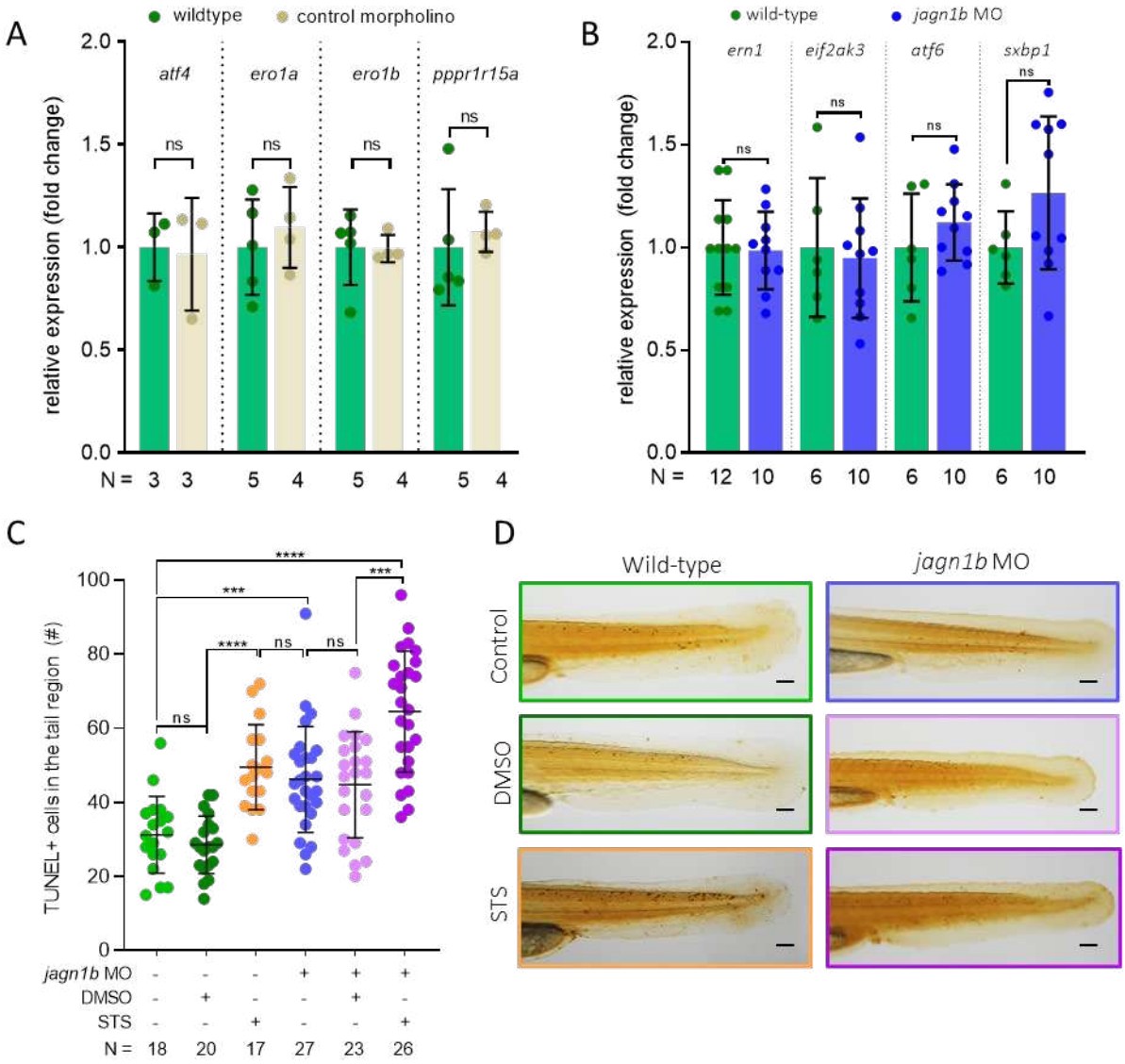

Supplementary Figure 5. Additional tested genes involved in unfolded protein response (UPR) and apoptosis activation upon staurosporine treatment.

(A) Relative expression levels of UPR-associated genes quantified with quantitative RT-PCR after control morpholino injection compared to wild-type. Values were normalized to the housekeeping gene *b-actin* and fold change were calculated respect wild-type expression. Data shows mean with standard deviation. Each dot represents the value of relative expression of one sample. N represents number of analyzed samples. **(B)** Relative expression levels of UPR-associated genes quantified with quantitative RT-PCR after *jagn1b* interference with morpholino compared to wild-type expression. Values were normalized to the housekeeping gene *b-actin* and fold change were calculated. Data shows mean with standard deviation. Each dot represents the value of relative expression of one sample. **(C)** Quantification of TUNEL-positive apoptotic cells in the tail region of 2dpf wild-type and *jagn1b* morphants without treatment (control), after DMSO or 5µM staurosporine (STS) treatment. The data shows mean, standard deviation and represents the combined results from 2 independent experiments. N represents the total number of analyzed embryos. **(D)** Representative images of the tail region of TUNEL-stained 2dpf wild-type and *jagn1b* morphants without treatment (control), after DMSO or 5µM staurosporine treatment. Images were taken with 8x magnification. Scale bars represent 100µm. ns, not significant; *** p_value<0.001;**** p_value < 0.0001.

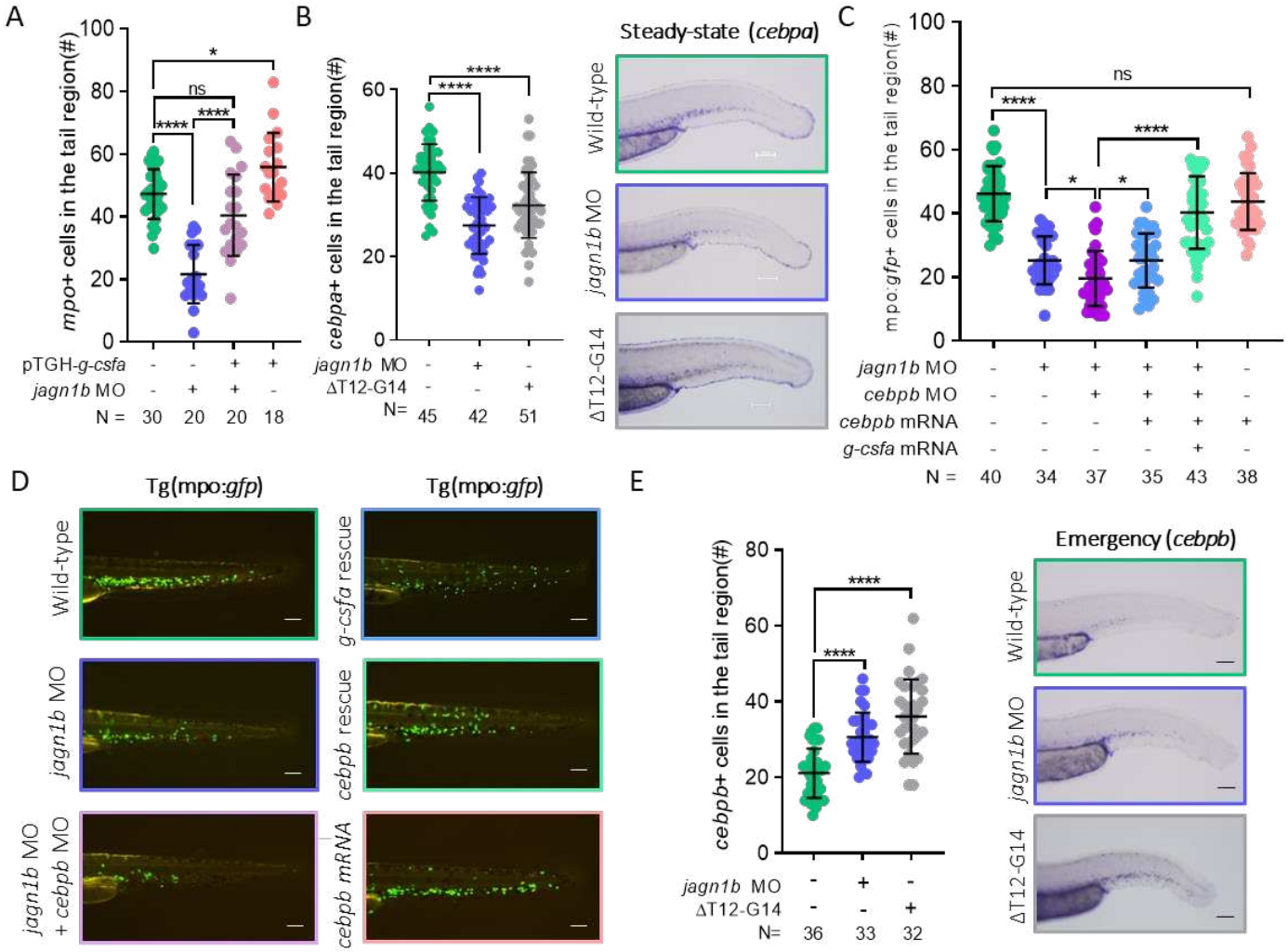

Supplementary Figure 6. Steady-state and emergency granulopoiesis were affected by *jagn1b* knockdown and overexpression of *jagn1b*$^{\Delta T12\text{-}G14}$.

(A) Quantification of *mpo*$^{+}$ neutrophils, in the hematopoietic tissue, stained with whole mount *in situ* hybridization after pTGH-*g-csfa* injection and heat activation in wild-type or *jagn1b* morphants**. (B)** The left panel shows the quantification of *cebpa*-positive cells, in the hematopoietic tissue, stained with whole mount *in situ* hybridization in wild-type, *jagn1b* morphants and after *jagn1b*$^{\Delta T12\text{-}G14}$ overexpression. The right panel shows representative images of 2.25dpf embryos. Images were taken with 10x magnification. Scale bars represent 100µm. **(C-D)** *cebpb* mRNA rescue of the phenotype induced by the combination of *cebpb* and *jagn1b* morpholino. **(C)** Quantification of mpo:*gfp*$^{+}$ neutrophils in the hematopoietic tissue of 2.25dpf transgenic tg(mpo:*gfp*) embryos after *jagn1b* knockdown (*jagn1b* MO) alone, together with *cebpb* morpholino, in combination with *cebpb* mRNA and *cebpb* mRNA alone. **(D)** Representative images of the tail region. Images were taken with 8x magnification. Scale bar represents 100 µm. **(E)** The left panel shows quantification of *cebpb*-positive cells, in the hematopoietic tissue, stained with whole mount *in situ* hybridization in wild-type, *jagn1b* morphants and after *jagn1b*$^{\Delta T12\text{-}G14}$ overexpression. The right panel shows representative images of 2.25dpf embryos. Images were taken with 10x magnification and scale bar represents 100µm. Data of **A**, **B**, **C** and **E** shows mean and standard deviation. Each dot represents the number of cells in the hematopoietic tissue of an individual 2.25dpf embryo. The data represents the combined results from 2-3 independent experiments. N represents the total number of analyzed embryos. ns, not significant; * p value < 0.05; **** p_value < 0.0001.

Supplementary Movies:

Supplementary Movie 1. Localization of GFP-Jagn1b$^{\Delta T12\text{-}G14}$ in hematopoietic cells. GFP signal represent the distribution of Jagn1b$^{\Delta T12\text{-}G14}$ in the cells found in the hematopoietic tissue, delineated by the white lines, of a 24 hpf embryo. The cells beyond the hematopoietic tissue are muscle cells.

Supplementary Movie 2. Alteration of the expression pattern of Jagn1b upon ΔT12-G14 mutation in hematopoietic cells. Close up of hematopoietic cells expressing GFP-Jagn1b$^{\Delta T12\text{-}G14}$.

Supplementary Bibliography

1. Fink M, Flekna G, Ludwig A, Heimbucher T, Czerny T. Improved translation efficiency of injected mRNA during early embryonic development. Dev Dyn. Dec 2006;235(12):3370-8. doi:10.1002/dvdy.20995

2. Powell C, Elsaeidi F, Goldman D. Injury-dependent Muller glia and ganglion cell reprogramming during tissue regeneration requires Apobec2a and Apobec2b. J Neurosci. Jan 18 2012;32(3):1096-109. doi:10.1523/JNEUROSCI.5603-11.2012

3. Doll L, Aghaallaei N, Dick AM, Welte K, Skokowa J, Bajoghli B. A zebrafish model for HAX1-associated congenital neutropenia. Haematologica. May 1 2021;106(5):1311-1320. doi:10.3324/haematol.2019.240200

4. Bajoghli B, Aghaallaei N, Heimbucher T, Czerny T. An artificial promoter construct for heat-inducible misexpression during fish embryogenesis. Dev Biol. Jul 15 2004;271(2):416-30. doi:10.1016/j.ydbio.2004.04.006

5. Inoue D, Wittbrodt J. One for all--a highly efficient and versatile method for fluorescent immunostaining in fish embryos. PLoS One. 2011;6(5):e19713. doi:10.1371/journal.pone.0019713

C. N. Borbarán Bravo, E. Deordieva, **L. Doll**, M. ElGamacy, B. Dannenmann, J. Azevedo, S. Bräuning, V. Zakharova, C. Lengerke, M. Sturm, O. Rieß, C. Zeidler, K. Welte, A. Shcherbina, M. Klimiankou, J. Skokowa, *'A New Severe Congenital Neutropenia Syndrome Associated with Autosomal Recessive COPZ1 Mutations*.' *Blood* 2025; 145 (20): 2317-2335.

blood®
Regular Article

HEMATOPOIESIS AND STEM CELLS

A new severe congenital neutropenia syndrome associated with autosomal recessive *COPZ1* mutations

Natalia Borbaran Bravo,[1] Ekaterina Deordieva,[2,*] Larissa Doll,[1,*] Mohammad ElGamacy,[1,3,*] Benjamin Dannenmann,[1,*] Joana Azevedo,[4,5,*] Alberto Iannuzzo,[6] Selket Delafontaine,[7,8] Moritz Lehners,[9] Marius Kolodziej,[10] Birte Hernandez Alvarez,[3] Anna-Sophia Hellmuth,[1] Malte Ritter,[1] Betül Findik,[1] Viktoria Zakharova,[11] Sandro Bräuning,[1] Sergey Kandabarau,[1] Claudia Lengerke,[1] Robert Feil,[9] Isabelle Meyts,[7,8] Jérôme Delon,[6] Markus Templin,[10] Marc Sturm,[12] Olaf Rieß,[12] Cornelia Zeidler,[1] Karl Welte,[1,13] Anna Shcherbina,[2] Maksim Klimiankou,[1,†] and Julia Skokowa[1,†]

[1]Department of Oncology, Hematology, Clinical Immunology, and Rheumatology, University Hospital Tuebingen, Tuebingen, Germany; [2]Department of Immunology, Dmitry Rogachev National Medical Research Center of Pediatric Hematology, Oncology and Immunology, Moscow, Russia; [3]Department of Protein Evolution, Max Planck Institute for Biology, Tuebingen, Germany; [4]Hematology Department, Coimbra Hospital and University Centre, Coimbra, Portugal; [5]Faculty of Medicine, University of Coimbra, Coimbra, Portugal; [6]Université Paris Cité, French National Centre for Scientific Research, INSERM, Institut Cochin, Paris, France; [7]Department of Microbiology, Immunology, and Transplantation, Laboratory for Inborn Errors of Immunity, KU Leuven, Leuven, Belgium; [8]Department of Pediatrics, University Hospital Leuven, Leuven, Belgium; [9]Interfaculty Institute of Biochemistry, University of Tuebingen, Tuebingen, Germany; [10]Natural and Medical Sciences Institute, University of Tuebingen, Reutlingen, Germany; [11]National Medical Research Center for Endocrinology, Clinical Data Analysis Department, National Medical Research Center for Endocrinology, Moscow, Russia; [12]Institute of Medical Genetics and Applied Genomics, University Hospital Tuebingen, Tuebingen, Germany; and [13]Department of Pediatric Hematology and Oncology, University Children's Hospital Tuebingen, Tuebingen, Germany

KEY POINTS

- **Autosomal recessive mutations in the *COPZ1* gene cause CN.**
- ***COPZ1* mutations lead to defective granulocytic differentiation, which can be rescued by the activation of HIF1α or *COPZ2* transduction.**

We have identified a new inherited bone marrow failure syndrome with severe congenital neutropenia (CN) caused by autosomal recessive mutations in the coatomer protein complex I (COPI) subunit zeta 1 (*COPZ1*) gene. A stop-codon *COPZ1* mutation and a missense (MS) mutation were found in 3 patients from 2 unrelated families. Although 2 affected siblings with a stop-codon *COPZ1* mutation suffered from CN that involves other hematologic lineages and nonhematologic tissues, the patient with a MS *COPZ1* mutation had isolated neutropenia. Both *COPZ1* mutations were localized to a highly evolutionarily conserved region. The resulting truncated (TR) COPZ1 protein was predicted to display diminished interaction with its COPI complex partner, COPG1. These findings were consistent with the observed block in retrograde protein transport from the Golgi apparatus to the endoplasmic reticulum (ER) in human fibroblasts carrying TR *COPZ1*. Human CD34$^+$ cells with TR or MS *COPZ1* had significantly impaired granulocytic differentiation, and in zebrafish embryos, TR Copz1 also resulted in defective myelopoiesis. Intracellularly, TR *COPZ1* downregulated JAK/STAT/CEBPE/G-CSFR signaling and hypoxia-responsive pathways, while inducing STING, interferon-stimulated genes, stimulating oxidative phosphorylation activity, and increasing reactive oxygen species levels in hematopoietic cells. MS *COPZ1* deregulated interferon and JAK/STAT signaling but less than the TR protein. Finally, treatment with the small molecule HIF1α stabilizer IOX2 or transduction of cells with *COPZ2* restored defective granulopoiesis in *COPZ1*-mutated human CD34$^+$ cells, offering potential therapeutic options.

Introduction

Severe congenital neutropenia (CN) represents complex heterogeneous syndromes with neutrophil differentiation defects of hematopoietic stem and progenitor cells (HSPCs), with or without the involvement of other blood cell lineages or nonhematologic tissues. Autosomal-dominant or -recessive mutations in over 25 genes have been described in patients with CN.[1] Several CN-associated mutated genes are involved in endoplasmic reticulum (ER) homeostasis, suggesting abnormal intracellular protein transport as a possible cause of CN.[1] For example, mutations in the *ELANE* gene, encoding neutrophil elastase, lead to ER stress and the unfolded protein response (UPR),[2-5] whereas mutations in the *SRP54* gene lead to dysregulation of protein transport and sorting.[6-8] Members of the coat protein complex I (COPI), COPA and COPB2, have been identified as potential interaction partners of another CN-associated gene, jagunal homolog 1 (*JAGN1*).[9] JAGN1 connects the Golgi apparatus with the nucleus and plays an essential role in protein maturation, sorting, and transport.[9,10] The COPI complex is crucial for protein trafficking within the Golgi complex and from the Golgi back to the ER.[11] CN-associated mutated proteins also cause dysregulation of signal transduction pathways essential for granulocytic

differentiation, such as severely diminished expression of transcription factors, C/EBPα and LEF1[12,13]; upregulation of PU.1[14]; dysregulated levels of antiapoptotic factors[9,15-17]; elevated levels of nicotinamide phosphoribosyltransferase (NAMPT)/silent information regulator sirtuin (SIRT) triggered protein deacetylation[18]; hyperphosphorylation of signal transducer and activator of transcription 5A (STAT5A)[19]; defective hematopoietic cell-specific Lyn substrate (HCLS1) activation via Lyn and Syk[20] and diminished levels of secretory leukocyte protease inhibitor (SLPI).[21] Recently, Touw et al provided important evidence linking inflammatory pathways, increased reactive oxygen species (ROS) levels, and suppression of canonical granulocyte colony-stimulating factor (G-CSFR)/Janus kinase (JAK)/STAT signaling in the pathogenesis of CN downstream of *ELANE* and *HAX1* mutations.[22-24]

In this study, we describe novel homozygous truncating and missense (MS) mutations in COPI subunit zeta 1 (*COPZ1*). We have demonstrated the essential role of *COPZ1* in the myeloid differentiation of human and zebrafish HSPCs, elucidated the mechanism of neutropenia downstream of mutated *COPZ1*, and identified potential therapeutic substances capable of restoring granulopoiesis in patients with CN carrying *COPZ1* mutations.

Material and methods

WES

Multisample analysis of affected children and their healthy parents was conducted using SureSelect Human All Exon V6 capture panel (Agilent Technologies), followed by sequencing on NovaSeq 6000 in 150 bp PE mode, resulting in a minimum of 12 Gb of raw data per sample. The raw data were analyzed using the megSAP pipeline developed by the Institute of Medical Genetics and Applied Genomics (Tübingen, Germany; https://github.com/imgag/megSAP/) and the reference genome build GRCh38. For comprehensive details on whole-exome sequencing (WES) analysis and variant prioritization, refer to the supplemental Information, available on the *Blood* website.

Statistical analysis

Statistical analysis was performed using GraphPad Prism (version 8.0.2). In cellular models, a paired, 2-tailed Student *t* test was used for single comparisons between related groups. Paired repeated measures one-way analysis of variance (ANOVA) with Dunnett test was used for comparing multiple groups against the control, and paired multiple *t* tests (with Holm-Sidak correction) were used for comparing multiple pairs of groups. A two-way ANOVA was used for the cholera toxin B subunit (CtxB) assay. The normal data distribution in zebrafish models was assessed with the Kolmogorov-Smirnov test. For normally distributed data, an unpaired Student *t* test was used for single comparisons between 2 groups and ANOVA for multiple comparisons.

Additional Materials and methods are available online.

The study was conducted according to the Declaration of Helsinki. Informed written consent was obtained from study participants. Study approval was obtained from the ethical review board of the Medical Faculty of the University of Tuebingen.

Results

Identification of *COPZ1* mutations in 3 patients with CN

By WES of 2 unrelated families, including 3 affected patients and symptom-free family members, we identified 2 novel *COPZ1* mutations. In family 1, affected siblings had a homozygous stop-codon mutation (*COPZ1*-TR), NM_016057:c.421C>T, NP_057141:p.Gln141Ter (Figure 1A). In the second family, the patient had a homozygous MS mutation (*COPZ1*-MS), NM_016057:c.394G>C, NP_057141:p.Gly132Arg (Figure 1B).

Clinical characteristics and blood/bone marrow counts for all patients are shown in Tables 1-4. Patients P1 and P2 are female siblings from nonconsanguineous White parents from Russia. Patient P1 (Figure 1A,C), 21 years old, suffered from severe infections from age 1 month. Her blood counts revealed severe persistent neutropenia, lymphopenia, 2 episodes of autoimmune hemolytic anemia, and thrombocytopenia. She required multiple transfusions and suffers from hepatosplenomegaly, atypical autism with mental retardation, dermatitis, severe scoliosis, and foot deformities. Ongoing therapy with recombinant human granulocyte colony-stimulating factor (rhG-CSF; 10 μg/kg per day), started at age 7 months, corrected her neutropenia.

Female patient P2, aged 13 years, exhibited neutropenia, lymphopenia, anemia, and episodic thrombocytopenia from the second day of life, alongside severe infections including pneumonia, sepsis, and osteomyelitis. At age 4 months, she began treatment with rhG-CSF (30 μg/kg per day) and IV immunoglobulin. Due to her severe condition, she underwent HSC transplantation at age 12 months from an unrelated HLA-compatible donor after T-cell receptor (TCR) α/β/CD19 lymphocyte depletion. Eleven years after HSC transplantation, she has full donor chimerism, complete immune reconstitution, and resolution of cytopenias but suffers from connective tissue dysplasia, neuromuscular syndrome, atopic dermatitis, chronic right-sided sensorineural hearing loss, clubfoot deformities, and severe autism with mental retardation.

Female patient P3 (Figure 1B,D), aged 11 years, from healthy, nonconsanguineous White parents from Portugal, with 2 healthy siblings, was diagnosed at age 3 years with isolated neutropenia (absolute neutrophil count 0.22 × 10^9/L - 1.04 × 10^9/L) and recurrent severe bacterial infections starting at age 4 months. At age 8 years, she developed cold-associated perniosis of the thighs. Treatment with rhG-CSF (5 μg/kg per day) yielded a good hematologic and clinical response. Before G-CSF therapy, a bone marrow evaluation showed low cellularity with trilinear hematopoietic representation, no excess blasts, and no fibrosis (Figure 1D).

Phylogenetic analysis revealed a strong similarity in the *COPZ1* coding region between humans and other vertebrates (Figure 1E; supplemental Figure 1A), including the region with both identified mutations (Figure 1F). Introducing *COPZ1* frameshift mutations near p.Gln141 using CRISPR/Cas9 gene editing, which led to the creation of 52% p.Gly150Ter, 29% p.His144Ter, and 3% p.Leu148Ter deletions in COPZ1 with a general knockout score of 84% (data not shown), in K562 cells

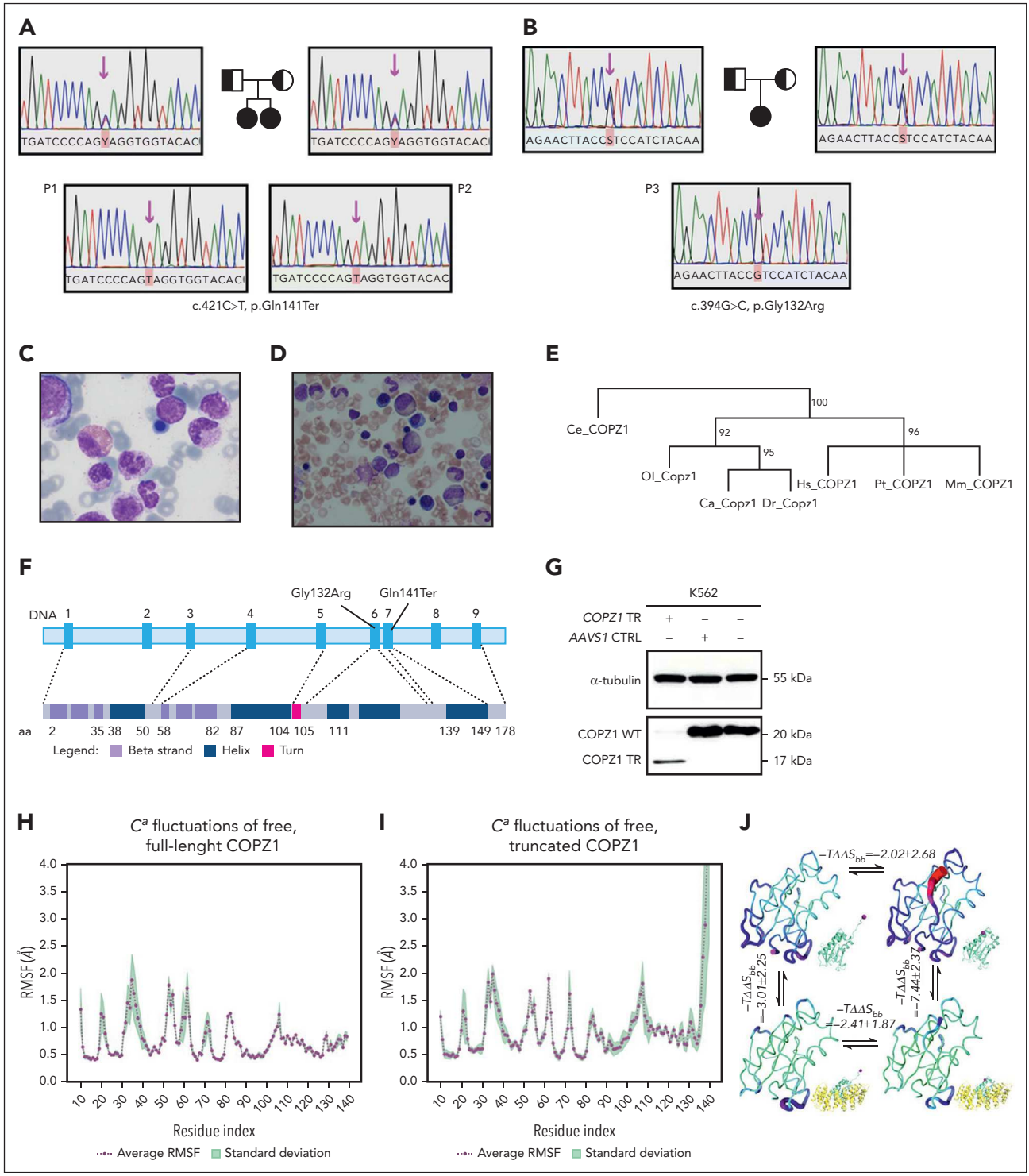

Figure 1. *COPZ1* mutations in 3 patients with CN. (A-B) Family trees and corresponding Sanger sequencing traces showing the inheritance of the homozygous stop-codon mutation c.445C>T:p.Gln141Ter (A) or MS mutation c.394G>C, p.Gly132Arg. (B) in *COPZ1* in patients (P1-P3) with CN. Red arrows indicate positions of mutations. (C-D) Bone marrow smears of patients P1 (×100 original magnification) and P3 (×50 original magnification). (E) Neighbor-joining phylogenetic tree of COPZ1 proteins, performed with 1000 bootstrap replications. (F) Schematic representation of the *COPZ1* gene (top) and COPZ1 protein (bottom) sequences highlighting protein domains, and positions of mutations. (G) Representative western blot images of COPZ1 protein in lysates of WT or *COPZ1*-TR K562 cells. α-tubulin staining was used to control protein loading. (H-I) RMSF plots of free full-length COPZ1 (H) and COPZ1-TR (I) show structural destabilization of the C-terminal segmented COPZ1 upon truncation. Purple dots and green shades represent the C^{α} RMSF averages and standard deviations from 3 independent simulations. (J) Estimation of backbone entropy change across the 4 states of free, full-length COPZ1 (upper left), free COPZ1-TR (upper right), bound COPZ1 full length (lower left), and bound COPZ1-TR (lower right) indicate a higher entropic penalty on the COPZ1-TR upon binding to COPG1. Large putty cartoons show the average C^{α} RMSF in tube width and color (in ascending order, cyan, blue, magenta, and red). Small cartoons show the whole model, in which COPZ1 is cyan, COPG1 is yellow, and the last backbone atom in COPZ1 is shown as a purple dot. (K) Quantifying the COPZ1:COPG1 interaction energies shows no difference in COPG1 binding by either COPZ1 or COPZ2. Moreover, an apparent loss of interaction energy is observed for COPZ1-TR, which is on par with previously described interaction mutants (COPZ1 mut1 and mut4).[25] (K-L) The *COPZ1*-MS mutation, however did not cause any difference in either binding interactions with COPG1 (K) or structural stability in the unbound form (L). Ca, *Carassius auratus*; Ce, *Caenorhabditis elegans*; Dr, *Danio rerio*; Hs, *Homo sapiens*; Mm, *Mus musculus*; Ol, *Oryzias latipes*; Pt, *Pan troglodytes*; RMSF, root mean square fluctuation.

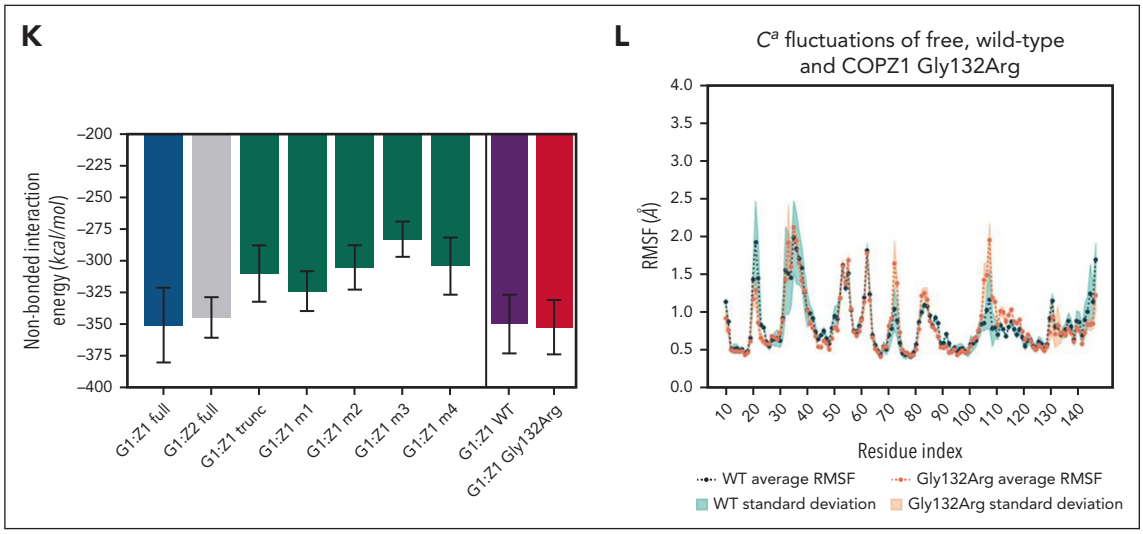

Figure 1 (continued)

resulted in truncated (TR) COPZ1 protein (Figure 1G). Most prediction algorithms confirmed the damaging effects of *COPZ1* p.Gly132Arg MS mutation (supplemental Tables 1 and 2).

Molecular dynamics simulations reveal the structural impact of *COPZ1* mutations on COPI complex formation

The 2 described *COPZ1* mutations lie at the binding interface between COPZ1 and COPG1 proteins, which is essential for the formation and function of COP-coated vesicles.[25-27] Therefore, we aimed to estimate the impact of the mutations on the COPZ1 structure and its binding to COPG1. We modeled the human COPZ1:COPG1 interaction structure using the available crystal structure of the bovine complex[26] as a template, which is highly conserved with human proteins (99% and 97% sequence identity, respectively).

Our first observation was the significant structural instability of the free COPZ1-TR protein compared with the wild type, with increased fluctuations in the contiguous segment from residue 100 to 140 (Figure 1H-I). Although the full-length structure ends with an α-β hairpin-α motif (a4-b5-b6-a5), the last helix (a5, residues 136-147) is missing in the truncated variant. The a5 helix forms stable interactions with helices a4 and a2 in the full-length protein, and its absence in the truncated form abolishes the stapling of the termini of the b5-b6 hairpin (residues 125-133). The missing interactions result in larger dynamic fluctuations at the C-terminal segment spanning a2-a3-a4-b5-b6 (Figure 1H-I; supplemental Figure 1B-C). This increased C-terminal flexibility of COPZ1-TR is, however, conformationally restrained in the COPG1-bound form, in which the binding event imparts a higher entropic penalty on the truncated variant (Figure 1J; supplemental Figures 1B-J and 2A-H). By estimating the backbone entropy change ($\Delta\Delta S_{bb}$) across these states, we obtain a binding free energy penalty ($-T\Delta\Delta S_{bb}$) of 4.43 ± 3.27 kcal/mol as a result of COPZ1 truncation (Figure 1J; supplemental Figure 2E-H). We also observed higher interaction energies across the COPZ1:COPG1 complex of the truncated form, pointing to worse binding enthalpy (Figure 1K). We applied the same analysis to the COPZ2:COPG1 complex and COPG1 in complex with 4 previously described *COPZ1* mutants (mut), mut1 through mut4, with successively weaker affinities[25] (supplemental Figure 1F-J). COPZ1-TR interactions fell within the range of the binding mutants, that is, COPZ1-TR interactions with COPG1 were weaker than COPZ1 mut1 but stronger than COPZ mut2. Meanwhile, the magnitude of COPZ2 interactions with COPG1 was not different from full-length COPZ1 (Figure 1K).

Longer simulations of COPZ1:COPG1 and COPZ1-p.G132R:COPG1, as well as unbound COPZ1 and COPZ1-p.G132R, were conducted to evaluate the potential impact of the p.Gly132Arg MS mutation on free and bound forms of COPZ1. In these simulations, analysis of the C^{α} root mean square deviation (RMSD) and root mean square fluctuation (RMSF) showed no clear difference between wild-type and COPZ1-MS variant (Figure 1L; supplemental Figure 2I-L). Furthermore, the interaction energies of the bound form indicated no difference between the wild-type and COPZ1-MS proteins (Figure 1K).

Taken together, COPZ1-TR appears to be less stable and to possess reduced binding interactions with COPG1 and incur a larger entropic penalty upon COPG1 binding, compared with full-length COPZ1. However, our analysis of the COPZ1-MS mutant shows no apparent difference from the wild type, at least within a simulation time frame of 600 ns.

COPZ1 mutations impair myeloid differentiation of human iPSCs and primary HSPCs

We next evaluated the impact of *COPZ1*-TR on neutrophilic differentiation. We first introduced *COPZ1* truncating mutation in induced pluripotent stem cell (iPSC) lines from a healthy donor using CRISPR/Cas9 gene editing. We generated 2 single-cell–derived iPSC lines: 1 carrying the patient-specific homozygous mutation, p.Gln141Ter (*COPZ1*-TR cl. C2); and the other harboring compound heterozygous p.Glu151Ter and p.Arg149Ter mutations (*COPZ1*-TR cl. G2; supplemental Figure 3A-B), applying previously established methods.[28,29] Using embryoid body–based myeloid differentiation (Figure 2A; supplemental Figure 3C),[29] we observed no significant

Table 1. Clinical and genetic characteristics of patients with *COPZ1* mutations

Patient	DOB	Sex	Age at diagnosis	Age at last follow-up (y)	ANCs (per μL) before G-CSF therapy	ANCs (per μL) on G-CSF therapy	Severe bacterial infections	Stomatitis gingivitis	Maturation arrest of bone marrow (before rhG-CSF therapy)	rhG-CSF therapy mean (or maximum) dose (μg/kg/d)	Neurological symptoms	Other extrahematological symptoms	*COPZ1* genotype cDNA and protein inheritance type
1	17 May 2003	F	1 mo of life	17	440	2620	Sepsis, purulent otitis, mucosal candidiasis, furuncle behind the ear, frequent acute respiratory infections, bronchitis, recurrent pneumonia, streptoderma, spleen microabscesses	Stomatitis, gingivitis	No	10	Atypical autism with intellectual disability	Atopic dermatitis, S-shaped scoliosis III-IV degree, varus deformity of both feet, chronic fibrous pulpitis	NM_016057: c.421C>T, NP_057141: p.Gln141Ter AR
2	9 October 2011	F	9 d of life	11	196	1320	Pneumonia, sepsis of mixed etiology, acute enteritis, meningitis, herpes simplex infection, enterocolitis, osteomyelitis of the right iliac bone	Stomatitis, gingivitis	No	30	Atypical autism with intellectual disability	Atopic dermatitis, myopia, chronic right-sided sensorineural hearing loss, planovalgus deformity of both feet, chronic fibrous pulpitis, postthrombotic syndrome	NM_016057: c.421C>T, NP_057141: p.Gln141Ter AR
3	4 November 2013	F	34 mo of life, reported neutropenia since 8 mo of life	9	400	1700	Otitis, cervical adenitis, laryngotracheitis, bacteriemia, *Staphylococcus aureus* facial cellulitis, EBV infection, gingivostomatitis, otitis, several upper respiratory and cutaneous infections	Stomatitis, 1 episode at young age	No	4 (5)	None	Skin: equestrian cold panniculitis of the tights	NM_016057: c.394G>C, NP_057141: p.Gly132Arg AR

ANC, absolute neutrophil count; AR, autosomal recessive; DOB, date of birth; EBV, Epstein-Barr virus; F, female.

Table 2. Peripheral blood parameters at diagnosis

Patient	Leu, $\times 10^9$/L	Neu, $\times 10^9$/L	Mo, $\times 10^9$/L	Ly, $\times 10^9$/L	T cells, $\times 10^9$/L	B cells, $\times 10^9$/L	IgG, g/L	IgA, g/L	IgM, g/L	IgE, UI/mL	NK cells, $\times 10^9$/L	RBC, $\times 10^{12}$/L	Hb, g/L	MCV, fL	MCH, pg	Plt, $\times 10^{12}$/L
1	3.65 (6.05-9.85)	0.99 (2-5.5)	1.02 (0.09-0.6)	1.46 (1.2-3)	0.73 (1.4-2)	0.5 (0.3-0.5)	40.7 (8.7-11.7)	6.45 (0.9-1.9)	1.5 (0.8-1.9)	4500 (<100)	0.27 (0.257-0.619)	3.55 (4.2-4.6)	86 (115-138)	NA	NA	147 (204-356)
2	2.3 (6.05-9.85)	0.27 (2.27-5.66)	0.62 (0.24-0.89)	1.058 (1.99-5.22)	0.51 (2.28-6.45)	0.33 (0.5-1.5)	24.8 (3.2-12.8)	4.04 (0.1-0.4)	1.03 (0.4-0.8)	NA	0.16 (0.381-0.971)	2.6 (4.2-4.6)	61 (115-138)	NA	NA	38 (204-356)
3	6.17 (5-15)	0.3 (1.5-8.0)	0.74 (0.2-1.0)	4.73 (6-9)	3.64 (NA)	0.8 (NA)	8.39 (4-12)	0.74 (0.24-2.32)	1.20 (0.41-2)	24 (<100)	0.1234 (NA)	4.89 (4.0-5.2)	115 (111-141)	73.3 (75-87)	23.6 (25-33)	NA

Blood parameter ranges related to patient age are given in parentheses.

Hb, hemoglobin; IgG, immunoglobulin G; Leu, leukocytes; Ly, lymphocytes; MCH, mean corpuscular hemoglobin; MCV, mean corpuscular volume of a red blood cell; Mo, monocytes; NA, not available; Neu, neutrophils; NK, natural killer cells; Plt, platelets; RBC, red blood cells.

Table 3. Peripheral blood parameters under rhG-CSF therapy

Patient	Leu, $\times 10^9$/L	Neu, $\times 10^9$/L	Mo, $\times 10^9$/L	Ly, $\times 10^9$/L	T cells, $\times 10^9$/L	B cells, $\times 10^9$/L	IgG, g/L	IgA, g/L	IgM, g/L	IgE, UI/mL	NK cells, $\times 10^9$/L	RBC, $\times 10^{12}$/L	Hb, g/L	MCV, fL	MCH, pg	Plt, $\times 10^{12}$/L
1	4.52 (6.05-9.85)	2.71 (1.5-8.5)	0.66 (0.09-0.6)	0.97 (1.5-7)	0.51 (1.1-2.4)	0.32 (0.1-0.4)	42.2 (7-16)	7.64 (1-2.3)	1.33 (0.6-2.6)	6440 (<100)	0.09 (0.1-0.4)	2.88 (4.2-4.6)	85 (115-138)	NA	NA	54 (204-356)
2	4.44 (6.05-9.85)	1.32 (2.27-5.66)	1.8 (0.24-0.89)	1.19 (1.99-5.22)	NA	NA	18.0 (3.2-12.8)	3.17 (0.1-0.4)	0.84 (0.4-0.8)	NA	NA	3.34 (4.2-4.6)	100 (115-138)	NA	NA	163 (204-356)
3	4.8 (4.5-13.5)	1.74 (1.5-8.0)	0.71 (0.1-0.95)	2.12 (1.5-6.8)	1.52 (NA)	0.58 (NA)	14.85 (5.52-16.31)	3.03 (0.21-2.82)	1.95 (0.47-2.40)	16 (<200)	NA	4.8 (4.0-5.2)	124 (115-155)	77.3 (77-95)	26.4 (25-33)	289 (180-450)

Blood parameter ranges related to patient age are given in parentheses.

Abbreviations explained in Table 2.

Table 4. Bone marrow parameters at diagnosis

Patient	Blasts, unclassified, %	Myeloblasts, %	Promyelocytes, %	Myelocytes, %	Metamyelocytes, %	Band neutrophils, %	Segmented neutrophils, %
1	0.8 (0.7-2.1)	0 (0.8-1.8)	3.2 (4.2-6.2)	18 (8.1-12.3)	11.6 (6.8-8.8)	13.6 (20.0-25.2)	23.2 (18.0-23.6)
2	1.0 (0.7-2.1)	0.5 (0.8-1.8)	3.5 (4.2-6.2)	36 (8.1-12.3)	15.5 (6.8-8.8)	16.5 (20.0-25.2)	9.5 (18.0-23.6)
3	4.5 (1.6-3.4)	2.8 (1.6-3.0)	12.5 (2.3-4.0)	12 (7.2-11.3)	17 (5.5-8.5)	22 (14.8-22.4)	21 (9.8-20.5)

Blood parameter ranges related to patient age are given in parentheses.
NA, not available.

differences in HSPCs generation on day 14 of differentiation (supplemental Figure 3D) but detected a marked decrease in the percentage of $CD15^+CD16^+CD45^+$ neutrophils on day 28 of culture in both *COPZ1*-TR iPSC lines compared with control iPSCs (Figure 2B-C). We also detected diminished numbers of colony-forming unit-granulocyte (CFU-G) and colony-forming unit granulocyte, macrophage (CFU-GM), but elevated colony-forming unit-macrophage (CFU-M) in the presence of COPZ1-TR compared with the control (Figure 2D). COPZ1-TR protein was expressed during all stages of myeloid differentiation (Figure 2E).

We further induced stop-codon mutations in *COPZ1* in human $CD34^+$ HSPCs at amino acid positions 137, 147, and 148, which are 4, 6, and 7 amino acids away from the patient-specific truncating mutation, using CRISPR/Cas9 system with the editing efficiency of approximately 80% (supplemental Figure 3E-F). As a control, the adeno-associated virus integration site 1 (*AAVS1*) gene locus was targeted with knockout (KO) scores ranging from 50% to 90% (supplemental Figure 3F). CRISPR/Cas9-edited HSPCs were differentiated into neutrophils using liquid culture differentiation (LCD) and CFU assay.[30] *COPZ1*-TR HSPCs showed a significant decrease in the total counts and percentage of neutrophils, as well as CFU-G, compared with *AAVS1* control (Figures 2F-I and 6D,G; supplemental Figure 4A-B).

Next, we introduced the *COPZ1*-MS mutation (p.Gly132Arg) into human $CD34^+$ HSPCs using CRISPR/Cas9 gene editing. A double-strand break was created at the mutation site with the single guide RNA (sgRNA) specific for *COPZ1* p.G132R (supplemental Table 3), followed by a knockin (KI) with a single-stranded oligodeoxynucleotide (ssODN) donor template containing the c.394G>C change and 3 silent mutations to prevent recutting by CRISPR/Cas9 (supplemental Table 4; supplemental Figure 4C). KI efficiencies for *COPZ1*-MS edited HSPCs ranged from 63% to 95% (supplemental Figure 4D). As a control, the same sgRNA was used with an identical ssODN carrying only the silent mutations, preserving the wild type (WT) form of the gene, achieving KI efficiencies of 80% to 96% (supplemental Figure 4D). *COPZ1*-MS HSPCs showed a significant decrease in granulocytic differentiation, as compated to controls (Figures 2F,J-L and 6H; supplemental Figure 4A,E).

Essential role of Copz1 during zebrafish myelopoiesis

Genomic synteny analyses indicated that *COPZ1* neighboring genes are highly conserved between human and zebrafish (Figure 3A). Therefore, we applied a zebrafish model to study the role of COPZ1 in granulopoiesis in vivo. We found that during early embryonic development (1 day post fertilization [dpf]), *copz1* expression was restricted to hematopoietic tissue (Figure 3B), and at day 5 dpf, it was expressed in the eyes, thymus, gills, and the optic tectum of the brain (Figure 3C-D). We next generated zebrafish that endogenously expressed Copz1-TR at a similar position as patients' specific mutation using the CRISPR/Cas9 approach in the transgenic reporter zebrafish line Tg (mpo:*gfp*), in which neutrophils express a green fluorescent protein (GFP). The resulting *copz1* gene-edited zebrafish were raised to adulthood (supplemental Figure 4G), and their offspring with Copz1-TR (amino acid positions 163-167; supplemental Figure 4F,H-I) was used for further analysis. We found that neutrophil numbers were significantly reduced at 2 dpf in Copz1-TR zebrafish embryos compared with wild-type littermates, as assessed by whole-mount in situ hybridization (WISH) of the neutrophil marker, *lysozyme C* (*lyz*; Figure 3E-F), quantification of mpo:gfp^+ cells (Figure 3F; supplemental Figure 4H), and Sudan black staining of neutrophils (Figure 3F). Primitive granulopoiesis was not affected (supplemental Figure 5A). To examine the effects of Copz1-TR on the development of HSCs and early myeloid progenitors, we analyzed the expression patterns of *cmyb* (marker of HSCs; Figure 3G) and *spi1b* (marker of myeloid progenitors; Figure 3H) in 2 dpf embryos using WISH. We found no significant differences in *cmyb* or *spi1b* expression patterns between Copz1-TR and wild-type controls (Figure 3G-H). We also analyzed the expression patterns of the erythrocyte- and macrophage cell–specific genes, *hbae1.1* (*hemoglobin, alpha embryonic 1.1*) and *mpeg1.1* (*macrophage-expressed gene 1.1*), respectively, and saw no significant alterations in *hbae1.1* expression (Figure 3I) but a significant *mpeg1.1* reduction in Copz1-TR embryos compared with in wild-type controls (Figure 3J).

Because *COPZ1*-TR patients have skeletal abnormalities, we next examined bone formation in Copz1-TR embryos by analyzing cartilage structures using Alcian blue staining. Analysis of the craniofacial cartilage skeleton showed no significant differences between the craniofacial structures of wild-type and Copz1-TR embryos at 4 dpf (supplemental Figure 5B-C). However, we observed malformation in the vertebral column in 3 of 3 adult (30 dpf) larvae examined (supplemental Figure 5D). We were not able to evaluate skeletal malformations in adult zebrafish, because skin pigmentation prevents clear visibility of the skeleton for microscopy.

Deregulated intracellular signaling downstream of *COPZ1* mutations

Next, we evaluated the mechanism of diminished neutrophil differentiation downstream of *COPZ1*-TR. After 4 days of

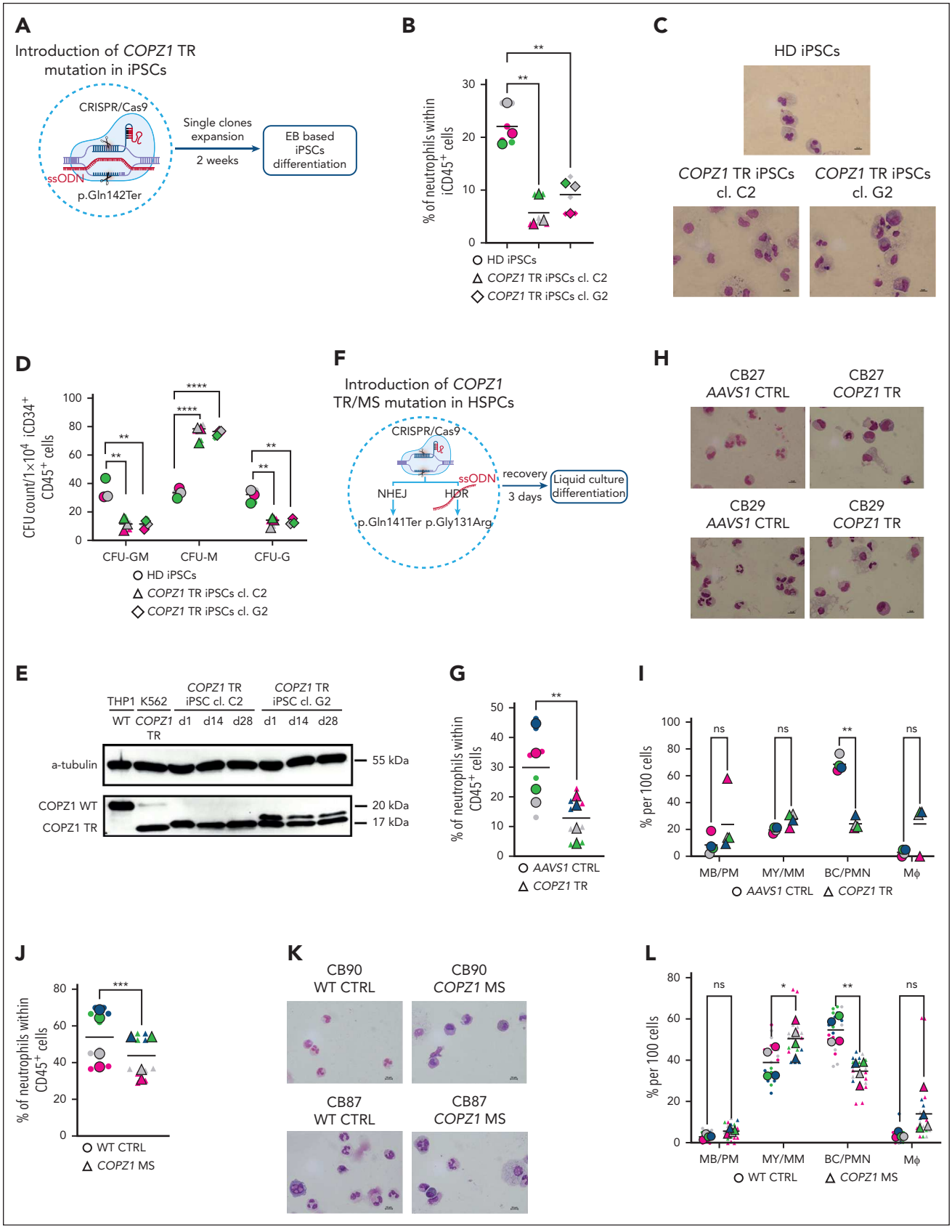

Figure 2. Mutated *COPZ1* suppressed granulocytic differentiation of human HSPCs in vitro. (A) Schematic representation of the experimental protocol for gene editing and granulocytic differentiation of iPSCs. Created with BioRender.com. (B) Flow cytometry analysis at day 28 of iPSC myeloid differentiation. The percentage of iPSC-derived $CD15^+CD16^+CD45^+$ neutrophils is shown. Means from 3 independent experiments (large symbols) performed in technical duplicates (small symbols) are plotted (pink, first experiment; gray, second experiment; green, third experiment). Statistical significance, $^{**}P < .01$. (C) Representative cytospin images of iPSC-derived hematopoietic cells at

myeloid differentiation, RNA sequencing (RNA-seq) analysis was performed on *COPZ1*-TR and *AAVS1* control-edited human HSPCs from 2 healthy donors. Editing efficiency averaged between 80% in *COPZ1*-TR cells and 77% in the *AAVS1* control group (supplemental Figure 6A). A principal component analysis of *COPZ1*-TR HSPCs captured 65% of the variation in PC1 and confirmed the difference between *COPZ1*-TR and *AAVS1* control cells (supplemental Figure 6B). Using the DeSeq2 package, we identified 1397 differentially expressed genes (DEGs; adjusted $P < .05$; Figure 4A; supplemental Table 5) between these groups. Gene set enrichment analysis (GSEA) demonstrated that, in line with known functions of the COPI complex in protein transport,[31-33] the introduction of *COPZ1*-TR led to upregulation of pathways associated with vesicle transport, especially endosomal and lysosomal transport (supplemental Figure 6C), which might be a compensatory response to defective COPI complex function. Pathways associated with other known genetic disorders of COPI complex (coatopathy; COPA syndrome), including "Interferon regulatory factor complex," "Hallmark Interferon Alpha Response," and "STING complex,"[34-37] were also enriched in *COPZ1*-TR HSPCs (Figure 4B; supplemental Figure 6D). GSEA using Kyoto encyclopedia of genes and genomes (KEGG) database further indicated that JAK/STAT signaling, a key pathway activated during G-CSFR–triggered myelopoiesis,[24,38,39] as well as hypoxia-responsive genes, including the target genes of hypoxia-inducible factor 1α (HIF1α), *PDK1*, *AK4*, and *ALDOC* were downregulated in *COPZ1*-TR cells compared with the control group (Figure 4C-E; supplemental Figure 6E). Pathways related to energy metabolism, such as glycolysis and oxidative phosphorylation (OXPHOS), were also significantly deregulated upon the introduction of *COPZ1*-TR mutation (Figure 4E; supplemental Figure 6E).

RNA-seq observations were confirmed by quantitative real-time transcription PCR in an independent experiment (supplemental Figure 6F-G). We found elevated messenger RNA (mRNA) expression levels of the interferon-stimulated genes (ISGs) *ISG15*, *IFIT1*, *IFNB1*, *TNF, USP18*, and the interferon alfa (IFN-α) response gene *MX1*[35] (supplemental Figure 6G) in *COPZ1*-TR HSPCs compared with the *AAVS1* control. The mRNA expression levels of CCAAT-enhancer binding protein ε (*CEBPE*), its target gene *CSF3R* (encoding G-CSFR), and the STAT5 target gene *PIM1* (encoding an oncogene serine/threonine kinase) were downregulated in *COPZ1*-TR HSPCs but not in control cells (Figure 4F). Reduced surface expression of G-CSFR in *COPZ1*-TR cells but not in *COPZ*1-MS was further confirmed by flow cytometry (Figure 4G; supplemental Figure 6H-I). mRNA expression of *PDK4,* the gatekeeper of the TCA cycle in OXPHOS,[40,41] was markedly increased in *COPZ1*-TR HSPCs compared with control cells (Figure 4H; supplemental Figure 6J). At the same time, the HIF1α targets, *ALDOC* and *BNIP3*,[42-44] were downregulated in *COPZ1*-TR HSPCs compared with controls (Figure 4H). Knowing that upregulation of ISGs[45] and elevated OXPHOS lead to increased ROS levels,[46-49] we investigated whether *COPZ1*-TR induces ROS. Indeed, we detected markedly elevated ROS levels in NB4 and HL-60 cell lines expressing *COPZ1*-TR compared with control cells (supplemental Figure 7A-B). Interestingly and unexpectedly, we observed no UPR deregulation downstream of *COPZ1*-TR (data not shown).

We also performed RNA-seq analysis of HSPCs genetically engineered to express *COPZ1*-MS and collected on day 4 of myeloid differentiation. The editing efficiency of cells was on average 80% for MS and 85% for control edited cells (supplemental Figure 4D). The distinct clustering and separation between *COPZ1*-MS and *COPZ1* WT groups were seen along PC3, which captured 11.4% of the variation (supplemental Figure 7C). Among DEGs (adjusted $P < .05$) were genes associated with immune response and its regulation (*MX1*, *IFIT1*, *IFIT2*, *IFIT3*, *IFI44*, *ARG1*, and *OASL)* and myeloid cell functions (*CEACAMs*, *FCN1*, and *NCF1*; Figure 4I; supplemental Figure 7D; supplemental Table 6). Pathway analysis using gene set enrichment analysis (preranked fgsea) and gene ontology gene sets in iDEP[50] showed downregulation of gene sets that play a role in neutrophil activation, degranulation, and neutrophil-mediated immunity and upregulation of type I interferon signaling pathway (Figure 4J). Although markedly fewer DEGs were detected in the *COPZ1*-MS group (supplemental Table 6), most DEGs (26/35 genes) were shared between *COPZ1*-MS and *COPZ1*-TR groups. This is consistent with clinical observations in which a patient with the *COPZ1*-MS mutation has a less severe disease course than those with the *COPZ1*-TR mutation.

We next evaluated the expression and phosphorylation of signaling proteins in primary HSPCs genetically modified to express either COPZ1-TR or COPZ1-MS protein. The cells were

Figure 2 (continued) day 28 of differentiation stained with May-Grünwald-Giemsa stain (×60 original magnification) for the indicated iPSC lines. (D) CFU assay of iPSC-derived $CD34^+CD45^+$ cells isolated at day 14 of iPSC differentiation. CFU counts are shown for the indicated iPSC lines. Data are represented as mean from 3 independent experiments (large symbols) performed in technical duplicates (small symbols). Pink represents the first experiment, gray is the second, and green is the third. CFU types included granulocytes, erythrocytes, monocytes, megakaryocytes (GEMM); granulocytes, monocytes (GM); granulocytes (G); monocytes (M). Statistical significance, $^{**}P < .01$; $^{****}P < .0001$. (E) Representative western blot images of lysates from iPSC clones C2 (lines 3 to 5) and G2 (lines 6 to 8) demonstrate a truncated (TR) COPZ1 protein at day 1, 14, and 28 of myeloid differentiation. The first lane on the left shows the control cell line THP1 (WT COPZ1) for comparison. (F) Schematic representation of gene editing and granulocytic differentiation of $CD34^+$ CB-HSPCs after introducing TR- or MS *COPZ1*. Created with BioRender.com. (G) Percentage of neutrophilic $CD45^+CD15^+CD66b^+CD11b^+CD16^+$ population at day 14 of LCD of *COPZ1*-TR or *AAVS1* edited $CD34^+$ CB-HSPCs from healthy donors. Data from 4 independent experiments are presented (pink, first experiment; gray, second experiment; green, third experiment; blue, fourth experiment). Large symbols represent the average value for each experiment, and small symbols represent technical replicates. Statistical significance, $^{**}P < .01$. (H) Representative images of Wright-Giemsa–stained cytospin preparations of differentiated cells on day 14 of LCD of 2 healthy donors (×60 original magnification). (I) Percentage of different cell populations on cytospin slides. 100 cells are counted per slide. Data are plotted as means from 4 independent experiments (color coded per experiment). Statistical significance, $^{**}P < .01$. (J) Percentage of $CD45^+CD15^+CD66b^+CD11b^+CD16^+$ neutrophils at day 14 of LCD of *COPZ1*-MS and WT control-edited $CD34^+$ CB-HSPCs from healthy donors. Data from 4 independent experiments are presented (pink, first experiment; gray, second experiment; green, third experiment; blue, fourth experiment). Large symbols represent the average value for each experiment, and small symbols represent technical replicates. Statistical significance: $^{***}P < .001$. (K) Representative images of Wright-Giemsa–stained cytospin preparations of cells on day 14 of LCD of 2 healthy donors (×60 original magnification). (L) Percentage of different cell populations on cytospin slides of in *COPZ1*-MS group compared with WT control-edited cells. Data are plotted as means from 4 independent experiments (large symbols: pink, gray, green, and blue), performed in 2 to 4 technical replicates (small symbols). Statistical significance, $^{*}P < .05$; $^{**}P < .01$. BC, band cell; EB, embryoid based; Mϕ, macrophage; MB, myeloblast; MM, metamyelocyte; MY, myelocyte; ns, not significant; PM, promyelocyte; PMN, polymorphonuclear cell.

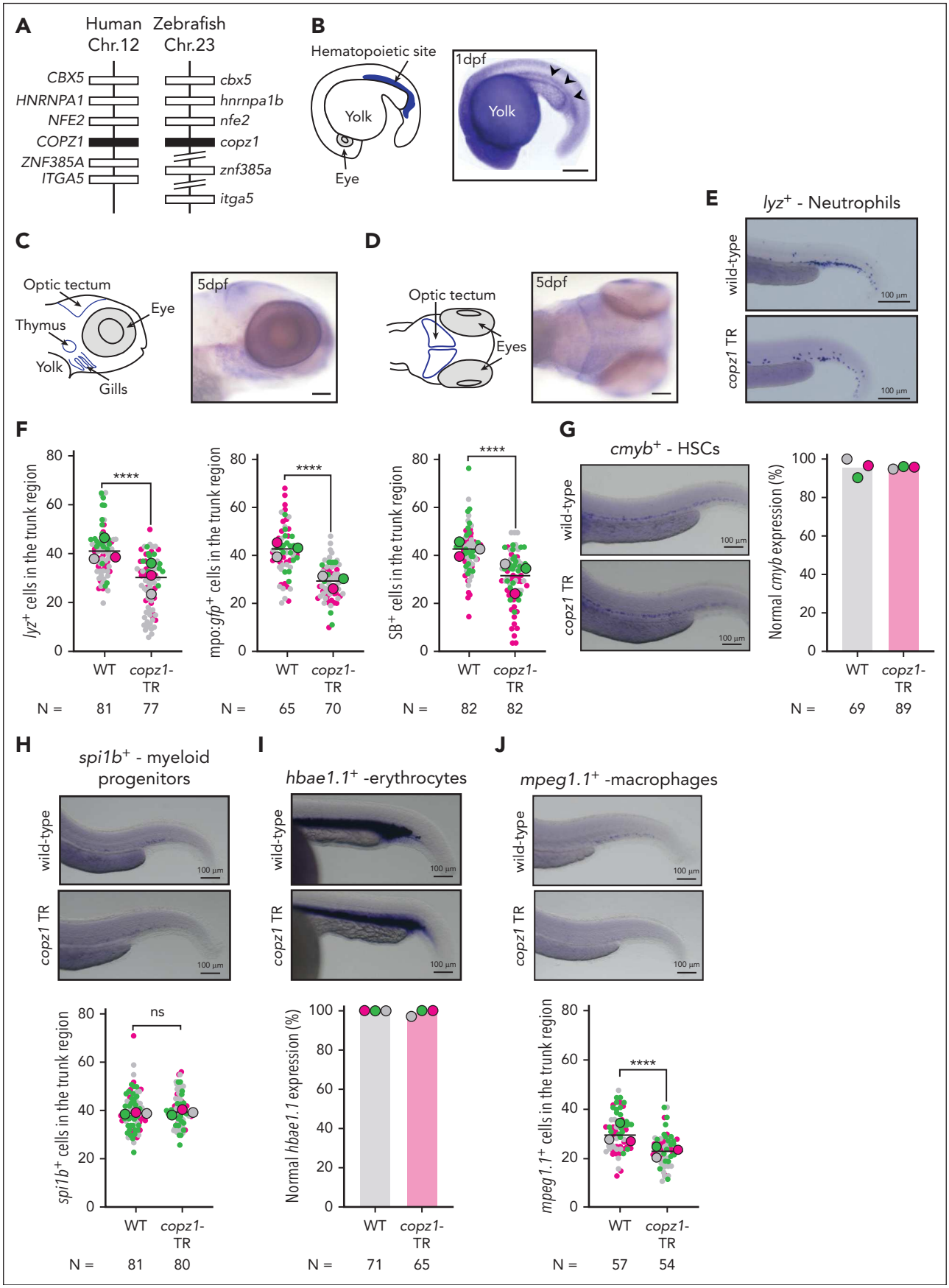

Figure 3.

starved overnight and then incubated with or without 1 ng/mL of G-CSF for 30 minutes. The editing efficiency was 91.8% for donor cord blood (CB) 86 and 96% for donor CB90 in the *COPZ1*-TR group and 62.9% and 79.1% for CB86 and CB90, respectively, in the *COPZ1*-MS group. We observed diminished G-CSF–triggered expression of Jak2, phospho-STAT3, phospho-Akt, and IκBα in both groups, with more severe defects in *COPZ1*-TR cells (Figure 5A). Additionally, introduction of *COPZ1*-TR led to severe defects in the G-CSF–mediated phosphorylation of STAT5, Erk2, p38 MAPK, MEK1/2, and mTOR. The levels of transcription factors C/EBPα, C/EBPβ, and c-myc, autophagy-related proteins LC3B, Beclin-1, and ATG5, hypoxia-related protein GLUT-1, NF-κB p50 subunit, and Bcl-xL were also reduced in the *COPZ1*-TR group (Figure 5B). Conversely, *COPZ1*-MS mutations resulted in elevated expression of SHP-2, FOXO3A, CD45, and acetylated STAT3 (Figure 5C). The milder signaling deregulation in *COPZ1*-MS than in *COPZ1*-TR can be attributed to the residual function of the COPZ1-MS protein, which is consistent with milder clinical phenotype in a patient carrying *COPZ1*-MS mutation. In addition, the lower gene editing efficiency of *COPZ1*-MS HSPCs, in comparison to *COPZ1*-TR group, may also partially explain the lower impact of *COPZ1*-MS on protein regulation.

Disruption of retrograde trafficking from Golgi to ER downstream of mutated *COPZ1*

Given that mutations in genes encoding other subunits of the COPI complex, such as those observed in COPA syndrome, lead to defective retrograde transport and subsequently trigger stress responses and inflammation,[37] we evaluated the retrograde transport of CtxB from the Golgi to the ER in human dermal fibroblasts after *COPZ1*-TR introduction using CRISPR/Cas9 gene editing (supplemental Figure 7E; Figure 5D). *COPZ1*-TR fibroblasts showed no differences in the amount of CtxB accumulated in the Golgi or ER at time 0 (supplemental Figure 7F). However, *COPZ1*-TR fibroblasts exhibited a block in Golgi-to-ER trafficking, with elevated levels of CtxB remaining in the Golgi for up to 8 hours, compared with *AAVS1*-edited fibroblasts, which exhibited a decrease in CtxB in the Golgi, concomitantly to an accumulation in the ER (Figure 5E; supplemental Figure 7G). The retention of CtxB in the Golgi of *COPZ1*-TR fibroblasts strongly indicates a disruption in retrograde COPI-dependent Golgi-to-ER transport, demonstrating clear evidence of COPI dysfunction. We were unable to generate *COPZ1* MS fibroblasts due to technical issues. Attempts to introduce the mutation via gene knock in failed due to a generally low homologous recombination rate in fibroblasts.[51] Fibroblasts also did not tolerate knock out of *COPZ1* followed by transgene *COPZ1*-MS expression.

Given established role of JAGN1 in protein trafficking, G-CSF receptor–mediated signaling, differentiation, and survival of neutrophils,[9] as well as its interaction with COPI proteins COPA and COPB2, we investigated the potential interaction between COPZ1 and JAGN1 proteins. We conducted a coimmunoprecipitation experiment by overexpressing FLAG-*JAGN1* and Myc-*COPZ1* in HEK293T cells and detected no interaction between these proteins (supplemental Figure 7H).

Ectopic *COPZ2* expression in COPZ1-deficient HSPCs rescues defective granulopoiesis in vitro

We next asked why patients' most severe symptoms are associated with hematopoietic and neuronal tissues. COPZ1, a ubiquitously expressed and evolutionarily conserved protein, has a paralog, COPZ2, that is highly similar, especially at the distal part of the protein, where both identified mutations are located[52,53] (supplemental Figure 8A). COPZ2 is expressed at low levels in hematological and neurological tissues (supplemental Figure 8B). We hypothesized that COPZ2 overexpression could rescue the functions of COPZ1-TR protein in HSPCs and transduced *COPZ1*-TR HSPCs of 4 healthy donors with lentiviral vectors expressing red fluorescent protein (RFP)–tagged *COPZ1*, *COPZ2*, or with control vector (Figure 6A; supplemental Figure 8C). Gene-editing efficiency averaged between 80% for *COPZ1*-TR and 65% for *AAVS1* (supplemental Figure 8D), and transduction efficiencies ranged between 58% and 98% (supplemental Figure 8E). Indeed, we found an increase in mature neutrophil numbers upon transgene expression of *COPZ1* or *COPZ2*, compared with control RFP-transduced *COPZ1*-TR cells (Figure 6B-D; supplemental Figure 8F-G).

The HIF1α stabilizer IOX2 induces granulocytic differentiation of *COPZ1*-mutated HSPCs

To identify new treatment options for patients with *COPZ1*-CN, we applied the connectivity map tool, which enables comparisons of gene expression profiles induced by various drug and small molecule treatments,[54,55] with the transcriptomic profiles of *COPZ1*-TR and *AAVS1* control HSPCs. Among the top, significantly enriched compounds was the HIF1α stabilizer, IOX2 (supplemental Figure 9A), which was in line with deregulated hypoxia pathway in HSPCs expressing *COPZ1*-TR mutant. Therefore, we evaluated the therapeutic potential of IOX2 in modulating myeloid differentiation of HSPCs carrying *COPZ1* mutations. We first tested the toxicity of IOX2 on healthy donor HSPCs and wild-type zebrafish embryos and found that IOX2 was not toxic at a concentration of 10 μM (supplemental Figure 9B and data not shown). We then treated *COPZ1*-TR and *COPZ1*-MS HSPCs (supplemental Figures 4D and 9C) with 10 μM of IOX2 or dimethyl sulfoxide (DMSO; vehicle control) and evaluated granulocytic differentiation in vitro. We found that IOX2 treatment activated granulopoiesis in *COPZ1*-TR HSPCs (Figure 6E-F; supplemental Figure 9C-D),

Figure 3. Truncated (TR) Copz1 inhibited myelopoiesis in zebrafish. (A) Comparison of human and zebrafish *COPZ1* loci synteny, showing syntenic conservation. (B-D) Spatial *copz1* expression in wild-type embryos stained using whole-mount in situ hybridization at 1 dpf (B), at 5 dpf lateral view (C), and 5 dpf top view (D). Arrows indicate the localization of the *copz1* expression. (E) Representative images of *lyz*-expressing neutrophils in *copz1* gene-edited zebrafish embryos compared with wild type. (F) Cell counts of *lyz*-expressing neutrophils, mpo:*gfp*–expressing neutrophils, and Sudan black (SB) B–stained neutrophils. (G-J) Effects of Copz1-TR on various hematopoietic cell lineages. The left panel show representative images of the whole-mount in situ hybridization for *cmyb* (HSCs) (G), *sp1b* (early myeloid progenitors) (H), *hbae1.1* (erythrocytes) (I), and *mpeg1.1* (macrophages) (J) in wild-type and *copz1* gene-edited embryos at 1 dpf (I) and 2dpf (G-H,J). The right (G) and lower (I) panels show a quantitative analysis of the stained cells in the trunk region, displaying the percentage (%) of normal gene expression patterns or (H,J) numbers of stained cells. In panels F,H,J, each of the small dots represents the number of cells of an individual embryo. Each of the big dots represents the mean of 1 of 3 independent experiments (pink, first; gray, second; green, third). Statistical significance: $^{**}P < .01$; $^{***}P \le .01$; $^{****}P \le .001$. Scale bars represent 100 μm. hbae1.1, hemoglobin, alpha embryonic 1.1; lyz, lysozyme C; mpo, myeloperoxidase; mpeg1.1, macrophage-expressed gene 1.1; ns, not significant.

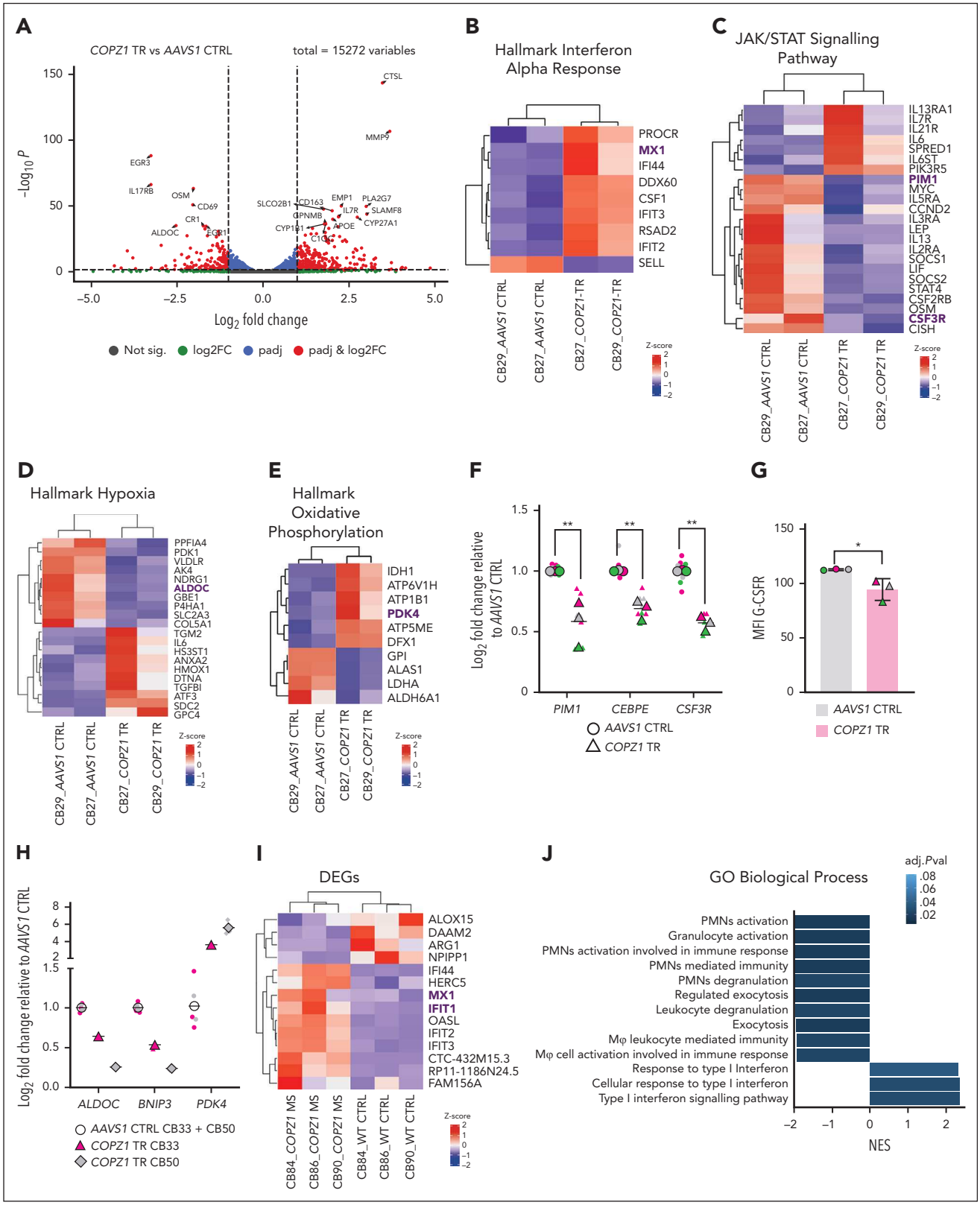

Figure 4. Deregulated signaling pathways downstream of *COPZ1* mutations. (A) Volcano plot of negative log10 transformed adjusted (adj.) *P* values against log2 fold change (log2FC) values, showing DEGs between *COPZ1*-TR vs *AAVS1* CTRL HSPCs. Red dots represent the DEGs with log2FC >1 or less than −1 and adj. *P* value <.05. Genes with −1 <log2FC <1 and adj. *P* value <.05 are shown in blue; genes with log2FC >1 or less than −1 and adj. *P* value >.05 are shown as green dots; gray dots are genes with −1 < log2FC <1 and adj. *P* value >.05. Horizontal dashed line marks gene expression with adj. *P* value of .05; vertical dashed lines represent log2FC of 1 (right line) and log2FC of −1 (left line). The names of the 20 top DEGs are displayed. (B-E) Supervised clustering of significantly upregulated or downregulated genes (adj. *P* < .05; |log2FC| > 1 [B,E] or adj. *P* < .05; |log2FC| > .5 [C-D]) from "Hallmark Interferon Alpha Response" (B), "JAK/STAT Signaling Pathway" (C), "Hallmark Hypoxia" (D), and "Hallmark Oxidative Phosphorylation" (E) gene sets of gene set enrichment analysis (GSEA). Gene expression heat maps were created using regularized logarithm transformation of read counts as an

albeit at levels lower than those observed in control-edited DMSO-treated samples. At the same time, IOX2 treatment restored the CFU-G–forming capacity in *COPZ1*-TR and *COPZ1*-MS HSPCs to the level of control cells (Figure 6G-H). As proof of principle, we treated CD34$^+$ bone marrow HSPCs from a patient with a *COPZ1*-MS mutation with IOX2 and detected a doubling of CFU-G numbers compared with DMSO-treated control (supplemental Figure 9F). Furthermore, treatment of *copz1* mutated zebrafish embryos with 10 μM IOX2 for 2 days revealed complete restoration of mpo:*gfp*$^+$ neutrophils in *copz1* mutated embryos compared with the DMSO-treated group (Figure 6I). Similarly, treatment of *hax1* morpholino-induced knockdown (KD) zebrafish embryos with 10 μM IOX2 for 2 days also showed a complete restoration of mpo:*gfp*$^+$neutrophils (Figure 6J).

Discussion

In this study, we identified homozygous truncating and MS mutations in *COPZ1* in 3 patients with CN from 2 unrelated families. *COPZ1*-TR mutation led to more severe phenotypes than the *COPZ1*-MS, affecting multiple hematological/immune cell lineages and nonhematological tissues. This aligns with previous studies showing that mutations in COPI complex components can disrupt cellular homeostasis[31,56] and trigger inflammatory responses.[57] Different clinical manifestations of the disease in patients carrying TR or MS *COPZ1* mutations are consistent with observations that the symptoms of patients with coatopathies vary according to the mutated COP protein[57,58] and the location of the mutation, depending on whether the mutation causes reduced COPI activity or affects cargo recognition sequences.[56,57]

The 2 identified mutations are located close to each other in a highly evolutionary conserved region of COPZ1 protein. The functional domains of human COPZ1 are still poorly defined. We studied the impacts of *COPZ1* mutations on COPI complex formation by modeling the human complexes between COPZ1 and COPG1 proteins. Our simulation results indicate a structurally destabilizing effect of the truncation that leads to weaker interaction between COPZ1-TR and COPG1 than WT COPZ1. However, no impact on COPG1 binding was observed for COPZ1-MS in the applied simulation settings, which might not be optimal for detecting the effects of the relatively "mild" COPZ1-MS on COPG1 interaction. Alternatively, *COPZ1*-MS mutation may have no impact on the COPG1 binding. Functional validation of the effects of *COPZ1* mutations on the stability of the COPI complex in HSPCs should be performed in future studies. Defective retrograde Golgi-to-ER trafficking in *COPZ1*-TR cells strongly supports its effect on the destabilization of the COPI complex.

Our study provides new insights into the role of COPZ1 protein in G-CSF–triggered granulopoiesis. RNA-seq and DigiWest analyses revealed suppressed JAK2-STAT3/5, Akt, MAPK, MEK1/2 signaling in *COPZ1*-TR HSPCs, a finding in line with diminished expression levels of *PIM1*, *C/EBPE*, *C/EBPA*, *C/EBPB*, and G-CSFR, downstream targets of JAK2/STAT3,5.[59-63] PIM1 regulates HSC expansion[64] and is a target of C/EBPε.[65] It would be interesting to investigate the role of PIM1 in granulopoiesis. It also remains unclear how mutant COPZ1 suppresses signaling proteins. It seems that COPZ1-MS has a much milder effect on signaling and disease severity than the truncated form. However, we also detected several proteins regulated by either TR- or MS *COPZ1* mutants, supporting the possibility of mutation-specific effects on granulopoiesis. Boztug et al described aberrant glycosylation of G-CSFR in neutrophils of patients with *JAGN1*-CN and diminished STAT3 phosphorylation in the presence of *JAGN1* mutations in HeLa cells.[9] Given that JAGN1 interacts with COPA and COPB2 proteins,[9] we investigated whether JAGN1 also interacts with COPZ1 and whether this interaction is affected by mutated COPZ1. We did not find any interaction between COPZ1 and JAGN1. It is still to be investigated whether JAGN1 interacts with the COPG1 protein and whether COPZ1, as a binding partner of COPG1, influences the JAGN1:COPG1 interaction. Knowing the key role of UPR activation in the pathogenesis of CN,[2-5] we examined the UPR in *COPZ1*-TR cells, but the UPR was not activated.

Pathways associated with vesicle transport, especially endosomal and lysosomal transport, were upregulated in *COPZ1*-TR cells, most likely as a compensatory response to deregulated retrograde Golgi-to-ER protein trafficking. Most disturbed pathways and cell functions in the case of *COPZ1*-MS were attributed to immune response, granulocyte activation, and secretory granules, whereas *COPZ1*-TR induced a much severe negative effect on cell pathways judged by dysregulation of the IFN-α regulatory pathway, STING complex, and NF-κB pathway. In both *COPZ1*-TR and *COPZ1*-MS cells, we observed increased expression of ISGs and related pathways. This aligns with findings in *ELANE*-CN, in which a proinflammatory state characterized by elevated IFN responses exists before the acquisition of *CSF3R* and *RUNX1* mutations.[23] Similarly, a proinflammatory state has been described in cells with *CSF3R* and *RUNXI* mutations.[66] These observations are consistent with the outcomes of *COPZ1* silencing in the human papillary thyroid carcinoma cell line TPC-1.[67]

The COPI complex regulates STING transport, mediating its retrieval from the Golgi to the ER and, importantly, keeping STING in its dormant state.[36,68] It is known that *COPA* mutations lead to a STING-dependent increase in the expression of ISGs.[34,68] *COPZ1*-mutant cells may also accumulate STING in the Golgi and activate ISGs, ultimately leading to reduced

Figure 4 (continued) input. (F) mRNA expression of JAK/STAT signaling-related genes *CSF3R*, *PIM1*, and *CEBPE*. The data are normalized to *ACTB* and *COPZ1*-TR group is compared with *AAVS1* control-edited group using the $2^{-\Delta\Delta Ct}$ method. Data are plotted as means (large symbols) from 3 independent experiments (color coded per experiment) performed in technical triplicates (small symbols). Statistical significance: $^{**}P < .01$. (G) Mean fluorescence intensity (MFI) of surface G-CSF3R expression in *COPZ1*-TR and *AAVS1* control-edited cells, measured by flow cytometry at day 4 of LCD. Data are presented as the mean ± standard deviation (SD) from 3 independent experiments, with each experiment color coded accordingly. Statistical significance: $^{*}P < .05$. (H) mRNA expression of *PDK4* and the hypoxia-related genes *ALDOC* and *BNIP3* in 2 *COPZ1*-TR HSPCs samples at day 4 of LCD. The data are normalized to *ACTB* and compared with the specific gene expression in *AAVS1* control-edited cells using the $2^{-\Delta\Delta Ct}$ method. (I) Supervised clustering of DEGs (|log2FC|>1 and adj. $P < .05$) in *COPZ1*-MS HSPCs compared with *COPZ1*-WT HSPCs. (J) Pathway analysis of *COPZ1*-MS vs *COPZ1*-WT RNA-seq data using GSEA (preranked fgsea) with gene sets from GO Biological Process in iDEP v96. The figure displays top upregulated and downregulated gene sets. Normalized enrichment score (NES) of the gene sets are plotted and bar colors represent adj. *P* values. GO, gene ontology.

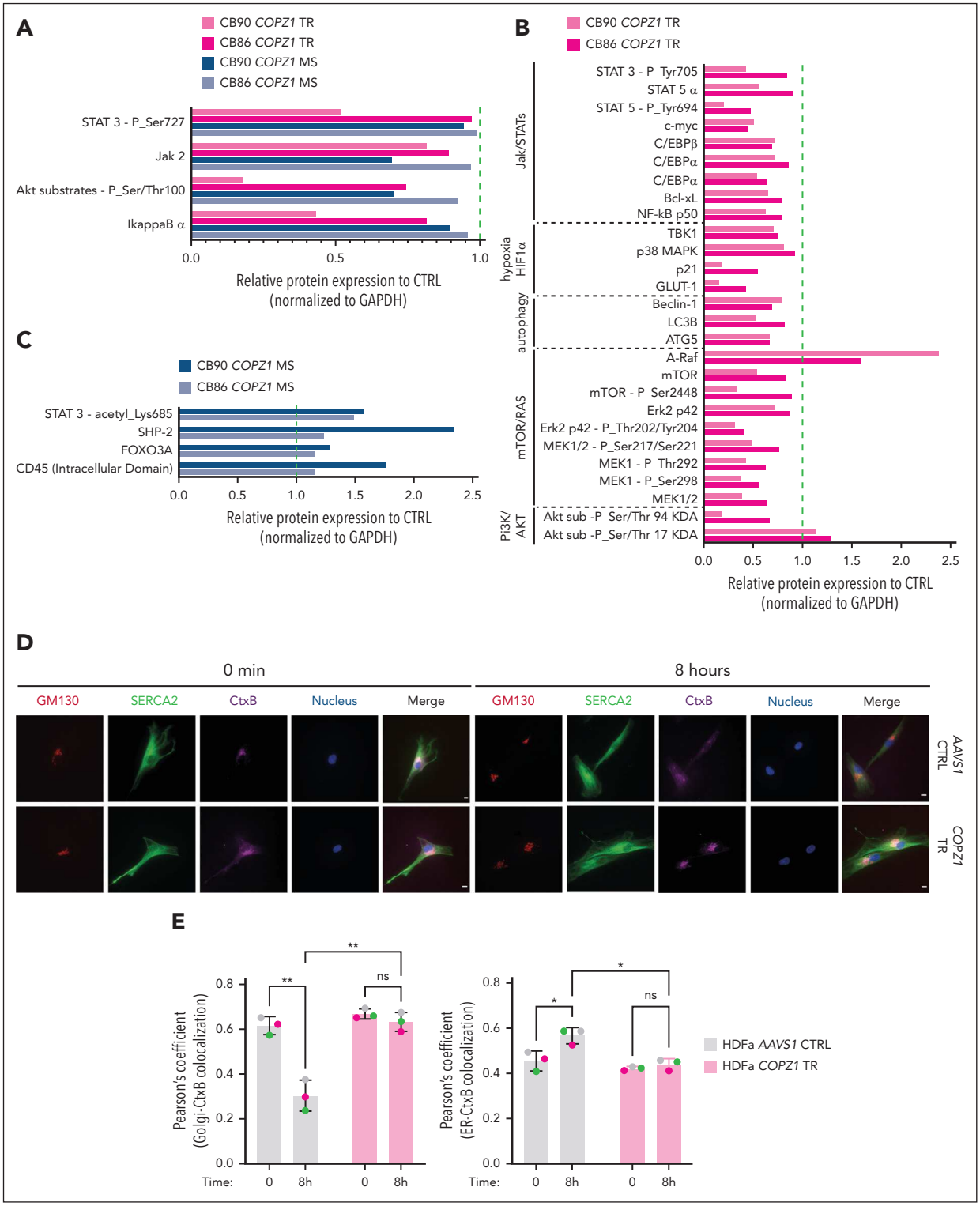

Figure 5. Mutant *COPZ1* caused deregulated protein expression, phosphorylation, and retrograde Golgi-to-ER trafficking. (A-C) Protein expression levels in *COPZ1* mutant samples relative to their corresponding *AAVS1*-edited controls, normalized to glyceraldehyde 3-phosphate dehydrogenase (GAPDH) protein loading control levels, as assessed by DigiWest assay. The green dotted line indicates the expression level in *COPZ1* WT samples (n = 2). (D) Immunofluorescence images of the CtxB transport assay in *AAVS1*-edited control and *COPZ1*-TR adult human primary dermal fibroblasts (HDFa), costained for GM130 (Golgi marker, red), SERCA2 (endoplasmic reticulum calcium pump, green), and nucleus (DAPI, blue). CtxB (cholera toxin subunitB, purple) was analyzed at 2 hours (time 0) and 10 hours (time 8 hours) postexposure to assess intracellular trafficking. The analysis was conducted at 2 hours (time 0) and 10 hours (time 8 hours) after CtxB exposure. Scale bars represent 10 μm. (E) Graphs depict the quantifications of the degree of CtxB colocalization with the Golgi (left) and the ER (right). Data are presented as means ± SD from 3 independent experiments. Statistical significance, *$P < .05$; **$P < .01$; ER, endoplasmic reticulum; ns, not significant.

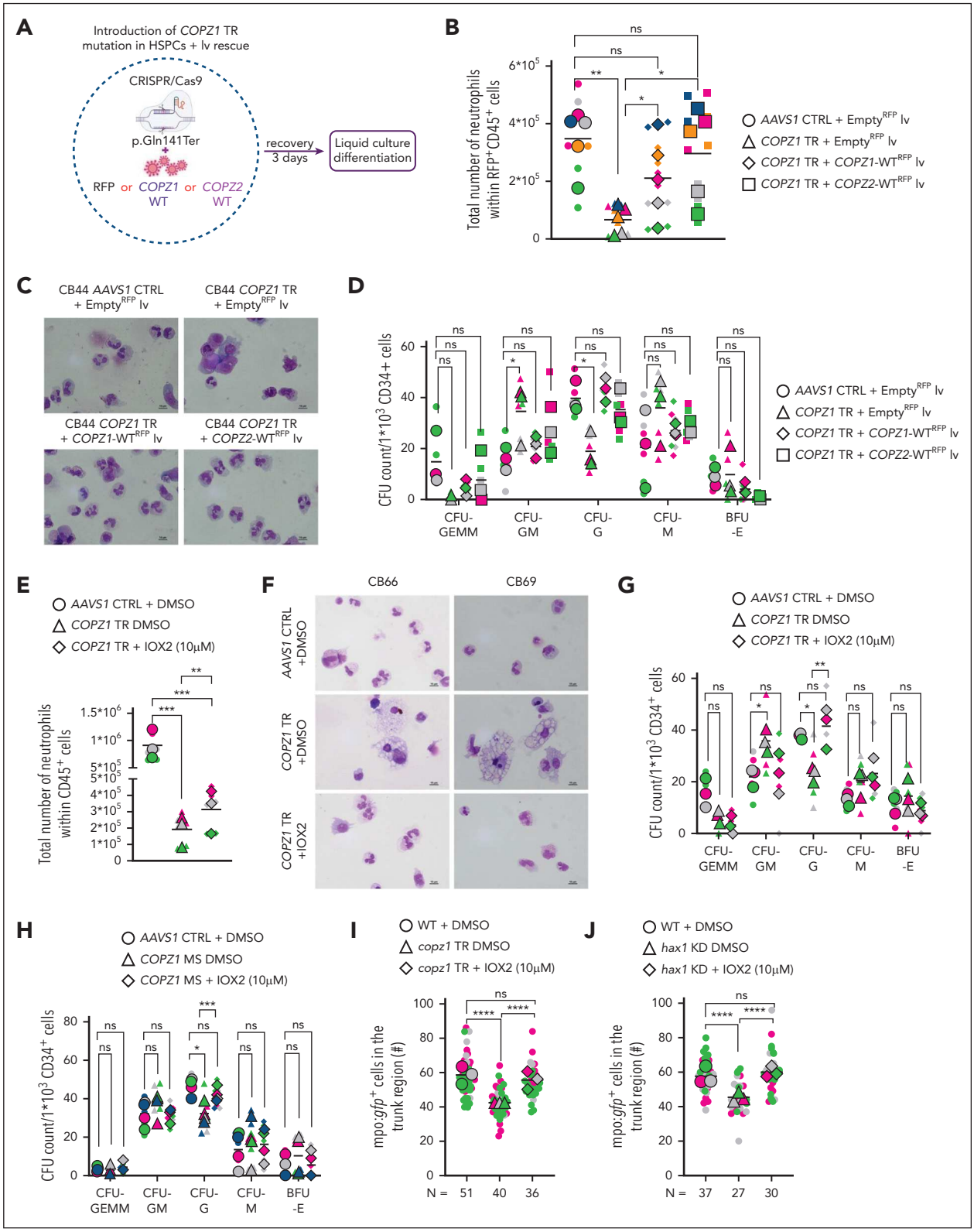

Figure 6. Restoration of defective granulopoiesis in *COPZ1* mutated HSPCs by *COPZ2* overexpression or HIF1α stabilizer IOX2. (A) Schematic of the in vitro *COPZ2* rescue experiment in *COPZ1*-TR CD34$^+$ cord blood (CB)-HSPCs. Created with BioRender.com. (B) Cell number for mature neutrophils (CD45$^+$CD15$^+$CD66b$^+$CD11b$^+$CD16$^+$) derived from 5 healthy donors on day 14 of LCD, after introduction of *COPZ1*-TR or *AAVS1* edited control, and overexpression of an RFP empty vector, *COPZ1* WT, or *COPZ2* WT, as assessed by flow cytometry. Data shown as means of total cell counts (large symbols) from 5 donors (color coded), with each donor's experiment performed in technical duplicates (small symbols). Statistical significance: $^{**}P < .01$; ns, not significant. (C) Representative May-Grünwald-Giemsa–stained images of indicated samples on day 14 of LCD; magnification ×60. (D) CFU assay of *COPZ1*-TR and *AAVS1* control-edited CD34$^+$ CB-HSPCs, transduced with lentiviral particles containing an RFP empty vector, *COPZ1* WT^{RFP}, or *COPZ2* WT^{RFP} (n = 3; color coded), on day 14 of LCD. CFU types included granulocytes, erythrocytes, monocytes, megakaryocytes (GEMM); granulocytes, monocytes (GM); granulocytes (G); monocytes (M); and burst-forming unit erythroid (BFU-E). Data represent means (large symbols) from 3 independent experiments in

granulopoiesis. Several lines of evidence link STING/ISGs-triggered inflammation to diminished hematopoiesis and granulopoiesis. For example, NF-κB activation reduces the number and repopulation capacity of HSPCs by inhibiting glycolysis and increasing ROS production.[69,70] IFN-α inhibits myeloid colony-forming capacity,[71] and treatment with IFN-α induces neutropenia in patients with hepatitis C.[72,73] These observations highlight a possible connection between COPZ1 and STING/ISGs/IFN-α signaling in regulating granulopoiesis that warrants further investigation. Interestingly, JAK/STAT signaling activates ISGs through STAT1 and STAT2.[74] In the context of COPZ1-disrupted granulopoiesis, the downregulation of STAT3 and STAT5 signaling may be a consequence of activated STING due to *COPZ1* mutations rather than the cause.

OXPHOS was also upregulated in *COPZ1*-TR cells, and neutrophil maturation is known to be OXPHOS driven.[75] However, OXPHOS can also simultaneously increase ROS, which can damage HSPCs.[47-49] We also observed downregulation of the hypoxia-responsive genes *ALDOC*, *PDK1*, and *BNIP3*.[42-44] In this case, HSPCs could not adequately counteract the increase in ROS levels, further enhancing susceptibility to oxidative stress.[76,77] Similarly, oxidative stress has been observed in certain experimental models of *ELANE*-CN and *HAX1*-CN.[22,23,78] Elevated ROS is also seen in iPSC models for reticular dysgenesis, characterized by myeloid maturation arrest at the promyelocyte stage due to AK2 mutations.[79] This further demonstrates how CN-related mutations can cause excessive oxidative stress in HSPCs and neutropenia. Consistent with these observations, there is a clear link between neutropenia-causing gene mutations, increased ROS, and hypoxia. The HIF1α signaling pathway has also been linked to G-CSF signaling. Thus, Liu et al showed that G-CSF stimulates HIF1α expression in human umbilical vein endothelial cells,[80] and Jia et al reported that HIF1α directly activates C/EBPA and synergizes with G-CSF to mobilize HSCs.[81] Additionally, the interaction between STAT3 and HIF1α is essential for HIF1α activity in both mouse embryonic stem cells and tumor-associated myeloid cells,[82] and STAT3 and HIF1α also cooperatively regulate genes involved in immune functions and developmental processes under oxidative stress.[83] Consequently, disruption of the G-CSFR signaling by *COPZ1* mutations may attenuate the HIF1α pathway, thereby linking COPZ1, the G-CSFR pathway, and HIF1α signaling in the common signaling cascade that regulates granulopoiesis. In line with this, we found that treatment of *COPZ1*-TR and *COPZ1*-MS HSPCs with IOX2 rescued the neutropenia phenotype. Thus, our data suggest the possible therapeutic potential of HIF1α stabilizers for treating patients with *COPZ1*-CN. Building on these findings and published data, we treated *hax1*-KD zebrafish embryos, recapitulating human *HAX1*-CN[84] with IOX2 to assess its generalizable potential therapeutic effects. Indeed, IOX2 treatment promoted granulocytic differentiation in *hax1*-KD zebrafish, suggesting a common pathomechanism of CN involving elevated ROS and disrupted hypoxia regulation.

Finally, our findings also reveal the compensatory role of COPZ2, particularly in hematopoietic and neuronal tissues in which its expression is low.[85] *COPZ2* induction could be a potential therapeutic strategy for mitigating the effects of *COPZ1* mutations. The feasibility of this approach for potential gene therapy may be the subject of future investigation.

Acknowledgments

The authors thank Olga Klimenkova, Regine Bernhard, and the Flow Cytometry Core Facility–Berg of the University Hospital Tuebingen for the excellent assistance. For the next-generation sequencing data storage and analysis, the authors used the service provided by the German Network for Bioinformatics Infrastructure (de.NBI), which is funded by the Federal Ministry of Education and Research of Germany. The simulations were performed on the High Performance Computing system Raven at the Max Planck Computing and Data Facility.

This work was supported by the Junior Research Group grant (Nr. 2627-0-0) of the Faculty of Medicine, University of Tuebingen; the German Federal Ministry of Education and Research (BMBF) funded consortium MyPred; the German Research Foundation (Deutsche Forschungsgemeinschaft [DFG]); M. Schickedanz Stiftung; the National Institutes of Health, National Institute of Allergy and Infectious Diseases grant (number 5 R24 AI162637-03); and the European Network for Innovative Diagnosis and Treatment of Chronic Neutropenias (EuNet-INNOCHRON, CA18233) action.

Authorship

Contribution: E.D., A.S., and J.A. identified patients; J.S. coordinated patients recruitment to the European branch of the Severe Chronic Neutropenia International Registry (SCNIR); M. Klimiankou, V.Z., and M.S. performed next-generation sequencing data analysis and made initial observations; J.S. and M. Klimiankou designed most experiments and supervised experimentation; N.B.B. performed most experiments and analyzed the data; A.I., S.D., M.L., N.B.B., A.-S.H., J.D., I.M., and R.F. performed endoplasmic reticulum−Golgi protein trafficking experiments; M. Kolodziej and M.T. conducted Digital Western Blot (Digi-West) assay; M. Klimiankou and S.K. conducted RNA-sequencing data analysis; M.E. performed molecular dynamics simulations; B.D., S.B., and B.F. performed experiments with induced pluripotent stem cells; B.H.A. performed immunoprecipitation of COPZ1 and JAGN1 proteins; L.D. conducted experimentation with zebrafish; J.S., N.B.B., and M. Klimiankou wrote the manuscript with assistance from L.D. and B.D.; K.W., C.Z., and C.L. provided patients' and healthy donors' material; and K.W., C.Z, A.S., M.R., O.R., and C.L. gave insightful comments.

Conflict-of-interest disclosure: The authors declare no competing financial interests.

ORCID profiles: N.B.B., 0000-0001-5987-3023; E.D., 0000-0002-8208-2075; M.E., 0000-0002-3446-8774; B.D., 0000-0001-9850-8854; J.A., 0000-0002-4172-4537; A.I., 0000-0001-8053-2362; S.D., 0000-0002-8985-8155; B.H.A., 0000-0003-0635-8698; M.R., 0000-0002-3670-7564; V.Z., 0000-0001-5949-5317; S.K., 0000-0002-1379-7974; C.L., 0000-0001-5442-2805; R.F., 0000-0002-7335-4841; I.M., 0000-0003-1214-0302; M.T., 0000-0002-6569-6489; M.S., 0000-0002-6552-8362; O.R., 0000-0002-7011-1369; C.Z., 0000-0002-8943-0984; K.W., 0000-0001-5178-3074; M. Klimiankou, 0009-0002-9193-0133; J.S., 0000-0002-4399-2324.

Figure 6 (continued) duplicates (small symbols). Statistical significance *$P < .05$. (E) Cell counts of $CD45^+CD15^+CD66b^+CD11b^+CD16^+$ neutrophils of *COPZ1*-TR and *AAVS1* edited control $CD34^+$ CB-HSPCs treated with 10 μM IOX2 or DMSO. Cell counts are derived from 3 donors on day 14 of LCD, as assessed by flow cytometry. Data show the mean counts from every experiment (large symbols), performed in technical duplicates (small symbols). Statistical significance, **$P < .01$; ***$P < .001$. (F) Representative May-Grünwald-Giemsa–stained images of indicated samples on day 14 of LCD. Original magnification ×60. (G-H) CFU assay of HSPCs treated with DMSO or IOX2 (10 μM). (G) *COPZ1*-TR and *AAVS1* control-edited $CD34^+$ CB-HSPCs (n = 3, in technical duplicates). (H) *COPZ1*-MS and WT control $CD34^+$ CB-HSPCs (n = 3, in technical duplicates). (I-J) Quantification of mpo:*gfp*$^+$ neutrophils after treatment with DMSO (control) or 10 μM IOX2 in wild-type and Copz1-TR zebrafish embryos (I) and wild-type and *hax1* morpholino-induced KD zebrafish embryos (J). Each of the small dots represents the number of cells of an individual embryo. Each big dot represents the mean of 1 of 3 independent experiments. (#) represents the number of stained cells. Statistical significance, ****$P < .0001$.

Correspondence: Julia Skokowa, Department of Oncology, Hematology, Clinical Immunology, and Rheumatology, University Hospital Tuebingen, Otfried-Mueller Str 10, Tuebingen 72076, Germany; email: julia.skokowa@med.uni-tuebingen.de; and Maksim Klimiankou, Department of Oncology, Hematology, Clinical Immunology, and Rheumatology, University Hospital Tuebingen, Otfried-Mueller Str 10, Tuebingen 72076, Germany; email: maksim.klimiankou@med.uni-tuebingen.de.

Footnotes

Submitted 19 September 2023; accepted 12 August 2024; prepublished online on *Blood* First Edition 6 December 2024. https://doi.org/10.1182/blood.2023022576.

*E.D., L.D., M.E., B.D., and J.A. contributed equally as second authors to this study.

†M. Klimiankou and J.S. contributed equally as senior authors to this study.

Presented in abstract form at the 66th annual meeting of the American Society of Hematology, San Diego, CA, 8 December 2024.

Original data are available on request from the corresponding authors, Julia Skokowa (julia.skokowa@med.uni-tuebingen.de) and Maksim Klimiankou (maksim.klimiankou@med.uni-tuebingen.de).

The online version of this article contains a data supplement.

There is a *Blood* Commentary on this article in this issue.

The publication costs of this article were defrayed in part by page charge payment. Therefore, and solely to indicate this fact, this article is hereby marked "advertisement" in accordance with 18 USC section 1734.

REFERENCES

1. Skokowa J, Dale DC, Touw IP, Zeidler C, Welte K. Severe congenital neutropenias. *Nat Rev Dis Primers*. 2017;3:17032.
2. Nustede R, Klimiankou M, Klimenkova O, et al. ELANE mutant-specific activation of different UPR pathways in congenital neutropenia. *Br J Haematol*. 2016;172(2):219-227.
3. Kollner I, Sodeik B, Schreek S, et al. Mutations in neutrophil elastase causing congenital neutropenia lead to cytoplasmic protein accumulation and induction of the unfolded protein response. *Blood*. 2006;108(2):493-500.
4. Nanua S, Murakami M, Xia J, et al. Activation of the unfolded protein response is associated with impaired granulopoiesis in transgenic mice expressing mutant Elane. *Blood*. 2011;117(13):3539-3547.
5. Grenda DS, Murakami M, Ghatak J, et al. Mutations of the ELA2 gene found in patients with severe congenital neutropenia induce the unfolded protein response and cellular apoptosis. *Blood*. 2007;110(13):4179-4187.
6. Bellanne-Chantelot C, Schmaltz-Panneau B, Marty C, et al. Mutations in the SRP54 gene cause severe congenital neutropenia as well as Shwachman-Diamond-like syndrome. *Blood*. 2018;132(12):1318-1331.
7. Juaire KD, Lapouge K, Becker MMM, et al. Structural and functional impact of SRP54 mutations causing severe congenital neutropenia. *Structure*. 2021;29(1):15-28.e7.
8. Schurch C, Schaefer T, Müller JS, et al. SRP54 mutations induce congenital neutropenia via dominant-negative effects on XBP1 splicing. *Blood*. 2021;137(10):1340-1352.
9. Boztug K, Järvinen PM, Salzer E, et al. JAGN1 deficiency causes aberrant myeloid cell homeostasis and congenital neutropenia. *Nat Genet*. 2014;46(9):1021-1027.
10. Lee S, Cooley L. Jagunal is required for reorganizing the endoplasmic reticulum during Drosophila oogenesis. *J Cell Biol*. 2007;176(7):941-952.
11. Rout MP, Field MC. The evolution of organellar coat complexes and organization of the eukaryotic cell. *Annu Rev Biochem*. 2017;86:637-657.
12. Skokowa J, Klimiankou M, Klimenkova O, et al. Interactions among HCLS1, HAX1 and LEF-1 proteins are essential for G-CSF-triggered granulopoiesis. *Nat Med*. 2012;18(10):1550-1559.
13. Skokowa J, Cario G, Uenalan M, et al. LEF-1 is crucial for neutrophil granulocytopoiesis and its expression is severely reduced in congenital neutropenia. *Nat Med*. 2006;12:1191-1197.
14. Skokowa J, Welte K. Dysregulation of myeloid-specific transcription factors in congenital neutropenia. *Ann N Y Acad Sci*. 2009;1176:94-100.
15. Aprikyan AA, Kutyavin T, Stein S, et al. Cellular and molecular abnormalities in severe congenital neutropenia predisposing to leukemia. *Exp Hematol*. 2003;31(5):372-381.
16. Carlsson G, Aprikyan AAG, Tehranchi R, et al. Kostmann syndrome: severe congenital neutropenia associated with defective expression of Bcl-2, constitutive mitochondrial release of cytochrome c, and excessive apoptosis of myeloid progenitor cells. *Blood*. 2004;103(9):3355-3361.
17. Cario G, Skokowa J, Wang Z, et al. Heterogeneous expression pattern of pro- and anti-apoptotic factors in myeloid progenitor cells of patients with severe congenital neutropenia treated with granulocyte colony-stimulating factor. *Br J Haematol*. 2005;129(2):275-278.
18. Skokowa J, Lan D, Thakur BK, et al. NAMPT is essential for the G-CSF-induced myeloid differentiation via a NAD(+)-sirtuin-1-dependent pathway. *Nat Med*. 2009;15(2):151-158.
19. Gupta K, Kuznetsova I, Klimenkova O, et al. Bortezomib inhibits STAT5-dependent degradation of LEF-1, inducing granulocytic differentiation in congenital neutropenia CD34(+) cells. *Blood*. 2014;123(16):2550-2561.
20. Skokowa J, Welte K. Defective G-CSFR signaling pathways in congenital neutropenia. *Hematol Oncol Clin North Am*. 2013;27(1):75-88. viii.
21. Klimenkova O, Ellerbeck W, Klimiankou M, et al. A lack of secretory leukocyte protease inhibitor (SLPI) causes defects in granulocytic differentiation. *Blood*. 2014;123(8):1239-1249.
22. Olofsen PA, Bosch DA, Roovers O, et al. PML-controlled responses in severe congenital neutropenia with ELANE-misfolding mutations. *Blood Adv*. 2021;5(3):775-786.
23. Touw IP. Congenital neutropenia: disease models guiding new treatment strategies. *Curr Opin Hematol*. 2022;29(1):27-33.
24. Touw IP, van de Geijn GJ. Granulocyte colony-stimulating factor and its receptor in normal myeloid cell development, leukemia and related blood cell disorders. *Front Biosci*. 2007;12:800-815.
25. Yu W, Lin J, Jin C, Xia B. Solution structure of human ζ-COP: direct evidences for structural similarity between COP I and clathrin-adaptor coats. *J Mol Biol*. 2009;386(4):903-912.
26. Yu X, Breitman M, Goldberg J. A structure-based mechanism for Arf1-dependent recruitment of coatomer to membranes. *Cell*. 2012;148(3):530-542.
27. Kuge O, Hara-Kuge S, Orci L, et al. zeta-COP, a subunit of coatomer, is required for COP-coated vesicle assembly. *J Cell Biol*. 1993;123(6 pt 2):1727-1734.
28. Dannenmann B, Klimiankou M, Oswald B, et al. iPSC modeling of stage-specific leukemogenesis reveals BAALC as a key oncogene in severe congenital neutropenia. *Cell Stem Cell*. 2021;28(5):906-922.e6.
29. Dannenmann B, Nasri M, Welte K, Skokowa J. CRISPR/Cas9 genome editing of human-induced pluripotent stem cells followed by granulocytic differentiation. *Methods Mol Biol*. 2020;2115:471-483.
30. Mir P, Ritter M, Welte K, Skokowa J, Klimiankou M. Gene knockout in hematopoietic stem and progenitor cells

followed by granulocytic differentiation. *Methods Mol Biol*. 2020;2115:455-469.

31. Arakel EC, Schwappach B. Formation of COPI-coated vesicles at a glance. *J Cell Sci*. 2018;131(5):jcs209890.
32. Beck R, Rawet M, Wieland FT, Cassel D. The COPI system: molecular mechanisms and function. *FEBS Lett*. 2009;583(17):2701-2709.
33. Luo PM, Boyce M. Directing traffic: regulation of COPI transport by post-translational modifications. *Front Cell Dev Biol*. 2019;7:190.
34. Lepelley A, Martin-Niclós MJ, Le Bihan M, et al. Mutations in COPA lead to abnormal trafficking of STING to the Golgi and interferon signaling. *J Exp Med*. 2020;217(11):e20200600.
35. Steiner A, Hrovat-Schaale K, Prigione I, et al. Deficiency in coatomer complex I causes aberrant activation of STING signalling. *Nat Commun*. 2022;13(1):2321.
36. Mukai K, Ogawa E, Uematsu R, et al. Homeostatic regulation of STING by retrograde membrane traffic to the ER. *Nat Commun*. 2021;12(1):61.
37. Delafontaine S, Iannuzzo A, Bigley TM, et al. Heterozygous mutations in the C-terminal domain of COPA underlie a complex autoinflammatory syndrome. *J Clin Invest*. 2024;134(4):e163604.
38. Rauprich P, Kasper B, Tidow N, Welte K. The protein tyrosine kinase JAK2 is activated in neutrophils from patients with severe congenital neutropenia. *Blood*. 1995;86(12):4500-4505.
39. Tian SS, Tapley P, Sincich C, Stein RB, Rosen J, Lamb P. Multiple signaling pathways induced by granulocyte colony-stimulating factor involving activation of JAKs, STAT5, and/or STAT3 are required for regulation of three distinct classes of immediate early genes. *Blood*. 1996;88(12):4435-4444.
40. Zhang S, Hulver MW, McMillan RP, Cline MA, Gilbert ER. The pivotal role of pyruvate dehydrogenase kinases in metabolic flexibility. *Nutr Metab*. 2014;11(1):10.
41. Sun Y, Daemen A, Hatzivassiliou G, et al. Metabolic and transcriptional profiling reveals pyruvate dehydrogenase kinase 4 as a mediator of epithelial-mesenchymal transition and drug resistance in tumor cells. *Cancer Metab*. 2014;2(1):20.
42. Guimaraes-Camboa N, Stowe J, Aneas I, et al. HIF1alpha represses cell stress pathways to allow proliferation of hypoxic fetal cardiomyocytes. *Dev Cell*. 2015;33(5):507-521.
43. Jian B, Wang D, Chen D, Voss J, Chaudry I, Raju R. Hypoxia-induced alteration of mitochondrial genes in cardiomyocytes: role of Bnip3 and Pdk1. *Shock*. 2010;34(2):169-175.
44. Wang V, Davis DA, Haque M, Huang LE, Yarchoan R. Differential gene up-regulation by hypoxia-inducible factor-1alpha and hypoxia-inducible factor-2alpha in HEK293T cells. *Cancer Res*. 2005;65(8):3299-3306.
45. Fan JB, Miyauchi-Ishida S, Arimoto Ki, et al. Type I IFN induces protein ISGylation to enhance cytokine expression and augments colonic inflammation. *Proc Natl Acad Sci U S A*. 2015;112(46):14313-14318.
46. Liemburg-Apers DC, Willems PH, Koopman WJ, Grefte S. Interactions between mitochondrial reactive oxygen species and cellular glucose metabolism. *Arch Toxicol*. 2015;89(8):1209-1226.
47. Zhao RZ, Jiang S, Zhang L, Yu ZB. Mitochondrial electron transport chain, ROS generation and uncoupling (review). *Int J Mol Med*. 2019;44(1):3-15.
48. Filippi MD, Ghaffari S. Mitochondria in the maintenance of hematopoietic stem cells: new perspectives and opportunities. *Blood*. 2019;133(18):1943-1952.
49. Nakamura-Ishizu A, Ito K, Suda T. Hematopoietic stem cell metabolism during development and aging. *Dev Cell*. 2020;54(2):239-255.
50. Ge SX, Son EW, Yao R. iDEP: an integrated web application for differential expression and pathway analysis of RNA-seq data. *BMC Bioinf*. 2018;19(1):534.
51. Howden SE, Thomson JA, Little MH. Simultaneous reprogramming and gene editing of human fibroblasts. *Nat Protoc*. 2018;13(5):875-898.
52. Moelleken J, Malsam J, Betts MJ, et al. Differential localization of coatomer complex isoforms within the Golgi apparatus. *Proc Natl Acad Sci U S A*. 2007;104(11):4425-4430.
53. Futatsumori M, Kasai K, Takatsu H, Shin HW, Nakayama K. Identification and characterization of novel isoforms of COP I subunits. *J Biochem*. 2000;128(5):793-801.
54. Lamb J, Crawford ED, Peck D, et al. The Connectivity Map: using gene-expression signatures to connect small molecules, genes, and disease. *Science*. 2006;313(5795):1929-1935.
55. Lamb J. The Connectivity Map: a new tool for biomedical research. *Nat Rev Cancer*. 2007;7(1):54-60.
56. Claerhout S, Dutta B, Bossuyt W, et al. Abortive autophagy induces endoplasmic reticulum stress and cell death in cancer cells. *PLoS One*. 2012;7(6):e39400.
57. Dell'Angelica EC, Bonifacino JS. Coatopathies: genetic disorders of protein coats. *Annu. Rev Cell Dev Biol*. 2019;35:131-168.
58. Macken WL, Godwin A, Wheway G, et al. Biallelic variants in COPB1 cause a novel, severe intellectual disability syndrome with cataracts and variable microcephaly. *Genome Med*. 2021;13(1):34.
59. Manz MG, Boettcher S. Emergency granulopoiesis. *Nat Rev Immunol*. 2014;14(5):302-314.
60. Hirai H, Zhang P, Dayaram T, et al. C/EBPbeta is required for 'emergency' granulopoiesis. *Nat Immunol*. 2006;7(7):732-739.
61. Avellino R, Delwel R. Expression and regulation of C/EBPalpha in normal myelopoiesis and in malignant transformation. *Blood*. 2017;129(15):2083-2091.
62. Shyamsunder P, Shanmugasundaram M, Mayakonda A, et al. Identification of a novel enhancer of CEBPE essential for granulocytic differentiation. *Blood*. 2019;133(23):2507-2517.
63. Verbeek W, Gombart AF, Chumakov AM, Müller C, Friedman AD, Koeffler HP. C/EBPepsilon directly interacts with the DNA binding domain of c-myb and cooperatively activates transcription of myeloid promoters. *Blood*. 1999;93(10):3327-3337.
64. Hu YL, Passegué E, Fong S, Largman C, Lawrence HJ. Evidence that the Pim1 kinase gene is a direct target of HOXA9. *Blood*. 2007;109(11):4732-4738.
65. Gombart AF, Krug U, O'Kelly J, An E, Vegesna V, Koeffler HP. Aberrant expression of neutrophil and macrophage-related genes in a murine model for human neutrophil-specific granule deficiency. *J Leukoc Biol*. 2005;78(5):1153-1165.
66. Olofsen PA, Fatrai S, van Strien PMH, et al. Malignant transformation involving CXXC4 mutations identified in a leukemic progression model of severe congenital neutropenia. *Cell Rep Med*. 2020;1(5):100074.
67. Di Marco T, Bianch F, Sfondrini L, et al. COPZ1 depletion in thyroid tumor cells triggers type I IFN response and immunogenic cell death. *Cancer Lett*. 2020;476:106-119.
68. Deng Z, Chong Z, Law CS, et al. A defect in COPI-mediated transport of STING causes immune dysregulation in COPA syndrome. *J Exp Med*. 2020;217(11):e20201045.
69. Nakagawa MM, Chen H, Rathinam CV. Constitutive activation of NF-kappaB pathway in hematopoietic stem cells causes loss of quiescence and deregulated transcription factor networks. *Front Cell Dev Biol*. 2018;6:143.
70. Sun Q, Fu Y, Zhu X, Tan WS, Cai H. Continuous NF-kappaB pathway inhibition promotes expansion of human phenotypical hematopoietic stem/progenitor cells through metabolism regulation. *Exp Cell Res*. 2021;399(2):112468.
71. Muller MR, Hofmann V, Cogoli M, Erni J, Arrenbrecht S. The effects of interferon on granulopoiesis in vitro. *Hematol Oncol*. 1984;2(2):199-208.
72. Sharvadze L, Gochitashvili N, Tophuria A, Bolokadze N, Tsertsvadze T. IFN/RBV treatment induced neutropenia and its

correction with neupogen in patients with hepatitis C. *Georgian Med News*. 2007;(147):52-55.

73. Soza A, Everhart JE, Ghany MG, et al. Neutropenia during combination therapy of interferon alfa and ribavirin for chronic hepatitis C. *Hepatology*. 2002;36(5):1273-1279.

74. Schindler C, Levy DE, Decker T. JAK-STAT signaling: from interferons to cytokines. *J Biol Chem*. 2007;282(28):20059-20063.

75. Riffelmacher T, Clarke A, Richter FC, et al. Autophagy-dependent generation of free fatty acids is critical for normal neutrophil differentiation. *Immunity*. 2017;47(3):466-480.e5.

76. Zhang CC, Sadek HA. Hypoxia and metabolic properties of hematopoietic stem cells. *Antioxid Redox Signal*. 2014;20(12):1891-1901.

77. Jakubison BL, Sarkar T, Gudmundsson KO, et al. ID2 and HIF-1alpha collaborate to protect quiescent hematopoietic stem cells from activation, differentiation, and exhaustion. *J Clin Invest*. 2022;132(13):e152599.

78. Fan Y, Murgia M, Linder MI, et al. HAX1-dependent control of mitochondrial proteostasis governs neutrophil granulocyte differentiation. *J Clin Invest*. 2022;132(9):e153153.

79. Rissone A, Weinacht KG, la Marca G, et al. Reticular dysgenesis-associated AK2 protects hematopoietic stem and progenitor cell development from oxidative stress. *J Exp Med*. 2015;212(8):1185-1202.

80. Liu SP, Lee SD, Lee HT, et al. Granulocyte colony-stimulating factor activating HIF-1alpha acts synergistically with erythropoietin to promote tissue plasticity. *PLoS One*. 2010;5(4):e10093.

81. Jia A, Wang Y, Yang Q, et al. Hippo kinase MST1-mediated cell metabolism reprograms the homeostasis and differentiation of granulocyte progenitor cells. *J Immunol*. 2023;211(1):91-102.

82. Dinarello A, Betto RM, Diamante L, et al. STAT3 and HIF1α cooperatively mediate the transcriptional and physiological responses to hypoxia. *Cell Death Discov*. 2023;9(1):226.

83. Grillo M, Palmer C, Holmes N, et al. Stat3 oxidation-dependent regulation of gene expression impacts on developmental processes and involves cooperation with Hif-1alpha. *PLoS One*. 2020;15(12):e0244255.

84. Doll L, Aghaallaei N, Dick AM, Welte K, Skokowa J, Bajoghli B. A zebrafish model for HAX1-associated congenital neutropenia. *Haematologica*. 2021;106(5):1311-1320.

85. GTEx Portal. Accessed 16 December 2024. https://gtexportal.org/home/gene/COPZ2

A New Severe Congenital Neutropenia Syndrome Associated with Autosomal Recessive *COPZ1* Mutations

Natalia Borbaran-Bravo et al.

Supplemental information

Supplemental Material and Methods

Isolation and expansion of human CD34$^+$ HSPCs

Cord blood (CB) and bone marrow (BM) samples were acquired from healthy donors (HD) and a *COPZ1*-CN patient under informed consent approved by the Ethics Committee of the University Hospital Tübingen. CD34$^+$ HSPCs were isolated from the mononuclear cell fraction using Ficoll gradient centrifugation followed by magnetic bead separation with the EasySep^{TM} human CD34$^+$ cell selection kit II (Stem Cell Technologies, #17856). CD34$^+$ cells were cultured at a density of 5 x 10^5 cells/ml in StemSpan^{TM} SFEM II hematopoietic stem cell media (Stem Cell Technologies, #09655) supplemented with 1 % penicillin/streptomycin (P/S), 20 ng/ml IL-3, 20 ng/ml IL-6, 20 ng/ml TPO, 50 ng/ml SCF, 50 ng/ml FLT-3L (all cytokines were purchased from R&D Systems) under standard cell culture conditions (37°C, 5% CO_2) .

Whole exome analysis and prioritization of candidate variants

Variant filtering and prioritization of genomic variants were performed using GSvar (https://github.com/imgag/ngs-bits/tree/master/doc/GSvar), an in-house developed viewing and filtering tool. Analysis of copy number variation in all three patients was done by ClinCNV tool (https://github.com/imgag/ClinCNV) and default filter setting. Patients were analyzed with their parents using a multi-sample approach in GSvar. Following predefined filter sets were applied: “multi-sample recessive,” “multi-sample com-het,” and “multi-sample dominant.” The applied filtering criteria for each variant filter set are listed in supplemental Table 7. Intronic variants outside splice regions, synonymous variants, and variants in the non-coding part of a transcript were excluded from further analysis. All remaining candidate variants were manually checked in the IGV browser.

For patients P1 and P2, when the filter set “multi-sample recessive” was applied, we detected only nonsense variant p.Gln141Ter in *COPZ1*. Filter set “multi-sample com-het” prioritized variants in *SLC44A3*. The “multi-sample dominant” filter set provided no variants for further in-depth analysis.

Variant *COPZ1* NM_016057:c.421C>T, p.Gln141Ter has allele frequency of 6.841e-7 (1/1461724 alleles) in gnomAD v4.1.0. No homozygote carriers are reported in gnomAD for LOF variants in *COPZ1*. A detailed description of resulting variants in patients P1 and P2 is provided in supplemental Table 8.

In patient P3, the homozygous *COPZ1* p.Gly132Arg variant was identified among the prioritized variants when the "multi-sample recessive" filter set was applied. Missense variant in *COPZ1* NM_016057:c.394G>C, p.Gly132Arg is known as rs1229660782 and has allele frequency of $5.58e^{-6}$ (9/1612796 alleles) in gnomAD v4.1.0. No homozygote carriers are reported in gnomAD v.4.1.0 for the variant p.Gly132Arg in *COPZ1*. The list of candidate variants included homozygous missense variants in *GAL3ST2*, *ZNF658, PAN2, AVIL, PSG4, KRT81, KRT75*, and PSG4, as well as splice region variant in *GANC*. By applying a “multi-sample dominant” variant filter, *de novo* missense variant rs771654850 was found in *AGAP1*. We also detected novel *de novo* variants ENST00000430863.5:c.914C>G, p.Thr305Arg and ENST00000417856.5:c.1139G>T, p.Gly380Val in *MROH5* and *KLC2*, respectively. Missense and splice region variants in *RAPGEF5* were only left when filtering based on “multi-sample com-het” criteria was applied. A detailed description of the resulting variants in patient P3 is provided in supplemental Table 8. In all patients, we identified no CNVs that affected the *COPZ1* gene region.

Human induced pluripotent stem cell (iPSC) culture

Healthy donor (HD) iPSC line, kindly provided by Prof. T. Moritz and Dr. N. Lachmann, MHH, Hannover, Germany, was cultured on Geltrex LDEV-free, hESC-Qualified, Reduced Growth Factor Basement Membrane Matrix (Thermo Fisher Scientific, #A1413302) coated plates in a density of 2 x 10^5 cells/ml in StemFlex medium (Thermo Fisher Scientific, #A3349401) supplemented with 1 % P/S.

Cell lines

NB4 and HL-60 human acute myeloid leukemia cell lines were obtained from the Leibniz Institute DSMZ-German Collection of Microorganisms and Cell Cultures (Braunschweig, Germany). Cells were maintained in RPMI-1640 medium (Gibco™ A1049101) supplemented with 10% FBS and 1% P/S under standard cell culture conditions. Adult human dermal fibroblasts (HDFa), were obtained from Innoprot (reference nr. P10858). Cells were cultured in Dulbecco's Modified Eagle's Medium/Nutrient

Mixture F-12 Ham (Sigma-Aldrich D6421), supplemented with 10% FBS and 1% P/S, in poly-L-lysine coated flasks (2 µg/cm², T-75 flask) under standard cell culture conditions.

Introduction of *COPZ1* mutations utilizing CRISPR/Cas9-gRNA gene editing

All synthetic sgRNAs, ssODN, and Cas9 proteins were purchased from Integrated DNA Technologies. The sgRNAs and ssODNs used are described in supplemental Tables 3 and 4. Cas9 ribonucleoprotein (RNP) complexes were prepared by incubating Cas9 protein (15 µg) with specific sgRNAs (8 µg) at 25°C for 10 min, shortly before cell nucleofection. Nucleofection was performed using the 4D-Nucleofector X Kit L (Lonza) and the 4D Nucleofector (Lonza) with program CA-123 [1].

To introduce the *COPZ1*-TR mutation, 0.8 - 2 x 10^6 CB $CD34^+$ HSPCs were nucleofected within two days after thawing with the assembled *COPZ1*_p.E136 sgRNA and Cas9 protein. The sgRNA *COPZ1*_p.E136 was also used for nucleofection of 1 x 10^6 HL-60, NB4, and HDFa cells. For iPSCs, 1 x 10^6 cells were nucleofected with sgRNA *COPZ1*_p.Q141X and Cas9 protein combined with 5 µM ssODN *COPZ1*_p.Q141X. Single-cell derived iPSC clones were isolated as previously described [1, 2]. An *AAVS1* RNP nucleofected control was included in all experiments. Editing efficiency and introduced edits were analyzed 72 hours post-nucleofection by Sanger sequencing and subsequent analysis of the targeted genomic region with the Inference of CRISPR Edits (ICE) tool from Synthego (https://ice.synthego.com/).

To introduce the *COPZ1*-MS mutation into CB $CD34^+$ HSPCs, the above protocol was used with 8 µg sgRNA *COPZ1*_p.G132R, 5 µM ssODN *COPZ1*_p.G132R CB and 1 µM AZD7648 [3]. As a control, ssODN *COPZ1* WT CTRL CB instead of ssODN *COPZ1*_p.G132R CB was used.

Embryoid body (EB)-based granulocytic differentiation of iPSCs

iPSCs were dissociated from Geltrex-coated plates using PBS /0.02 % EDTA for 7 min. EB generation was initiated via centrifugation of 20,000 cells per EB in 96-well plates using APEL serum-free differentiation medium (Stemcell Technologies) supplemented with 10 ng/ml bFGF and 10 µM ROCK Inhibitor Y-27632 dihydrochloride (Tocris). The next day, BMP4 (40 ng/ml, R&D Systems) was added to EBs to induce mesodermal differentiation. On day 4, EBs were plated on Geltrex-coated 6-well plates (10 EBs/well) in APEL medium supplemented with VEGF (40 ng/ml) (R&D Systems), SCF (50 ng/ml)

(Peprotech) and IL-3 (50 ng/ml) (Peprotech). For neutrophilic differentiation, the iPSC medium was exchanged to fresh APEL medium supplemented with IL-3 (50 ng/ml) and G-CSF (10 ng/ml) (Granocyte, Chugai) on day 8 and refreshed every 3 days. Hematopoietic suspension cells appeared on days 8 - 10. Suspension cells were harvested and analyzed by flow cytometry on day 14 and day 28 [1, 2].

Liquid culture granulocytic differentiation of CB CD34$^+$ HSPCs

In vitro granulocytic differentiation of CB HSPCs after nucleofection was performed as previously described [4]. Briefly, 24 hours after nucleofection, cells were seeded at a 2× 10^5/ml density. During the first 7 days of differentiation, the cells were kept in expansion medium consisting of RPMI 1640 supplemented with 10% FCS, 1% P/S, 5 ng/ml SCF, 5 ng/ml IL-3, 5 ng/ml GM-CSF, and 1 ng/ml G-CSF. The medium was exchanged every second day. On day 7, the medium was replaced with a differentiation medium consisting of RPMI 1640 supplemented with 10% FCS, 1% P/S, and 1 ng/ml G-CSF. The medium was exchanged every second day until day 14.

Colony Forming Unit (CFU) assay

1,000 fresh CB CD34$^+$ cells or 20,000 suspension cells harvested at day 14 of EB-based hematopoietic differentiation of iPSCs were resuspended in IMDM medium supplemented with 2 % FBS (Stemcell Technologies, #07700) and MethoCult^{TM} Enriched (Stemcell Technologies, #H4435). The cell suspension was plated on 3.5 cm dishes (500 CB CD34$^+$ cells/dish or 10,000 iPSC-derived cells/dish) and evaluated on day 14.

Immunophenotyping of iPSC-derived HSPCs and mature myeloid cells by flow cytometry

30,000 suspension cells derived from EB-based hematopoietic iPSC differentiation were collected on day 14 or 28. The cell suspension was centrifuged at 300 g for 5 min and resuspended in 100 µL staining buffer (PBS/1 % BSA/0.05 % sodium azide) and antibody master mix. For the characterization of HSPCs on day 14 of culture, CD33-BV421 (BioLegend, BL), CD34-PeCy7 (BD Biosciences, BD), KDR-AF647 (BL), CD43-PE (BD), CD41a-FITC (BD), CD235a-FITC (BD), CD45-BV510 (BL), and 7-AAD (BD) were used. For the analysis of mature myeloid cells on day 28 of culture, the following antibodies were combined: CD15-PE (BD), CD16-FITC (BD), CD14-APC-H7 (BD), CD45-BV510 (BL), CD33-BV421 (BL), and 7-AAD (BD). Cells were incubated at 4°C for 30 min in the dark, washed

with FACS buffer, resuspended in 100 µL FACS buffer, and analyzed on a FACS Canto II (BD Biosciences) and FlowJo V10 (BD Biosciences).

Immunophenotyping of CD34$^+$ HSPCs after liquid culture differentiation (LCD) by flow cytometry

50,000 cells were harvested on day 14 of LCD, were spun down at 400 × g for 5 min, and resuspended in 100 µL FACS buffer (PBS/1 % BSA/0.05 % sodium azide) containing the following antibodies: CD45-BV510 (clone HI30; BL); CD34-PE-Cy7 (clone 8G12, BD); CD33-BV421 (clone WM53, BL); CD15-PE (clone W6D3, BL); CD16-APC (clone 3G8, BD); 2 µL CD66b-FITC (clone G10F5, BL); 2 µL CD11b-APC-Cy7 (clone ICRF44, BL); and 2 µL 7AAD (BD). Cells were incubated at 4°C for 30 min in the dark, washed with FACS buffer, resuspended in 100 µL FACS buffer, and analyzed on a FACS LSR Fortessa (BD Biosciences) and FlowJo V10 (BD Biosciences). For the analysis of transduced RFP$^+$ HSPCs, CD15 BV785 (clone SSEA-1, BL), CD16 BV605 (clone 3G8, BL) and CD66b AF700 (clone G10F5, BL) antibody were used.

Morphological analysis

20,000 cells per cytospin slide were centrifuged for 4 min at 250 rpm on cytospin centrifuge, air dried, and stained with May-Grunwald solution for 5 min and Giemsa solution for 20 min.

Western blot analysis

1x10^6 cells were lysed in 200 µl Laemmli buffer, heated for 5 min at 95°C, and centrifugated for 5 min at 3,000 rpm. 20 µl of each sample was loaded on a 10 % SDS gel. The gel was run at 100 V for 2 hours in a running buffer (25 mM Tris, 0.1 % SDS, 192 mM Glycine). After protein separation, membranes (Amersham^{TM} Hybond^{TM}, 0.45 um PVDF) and gels were equilibrated for 15 min in transfer buffer (25 mM Tris, 192 mM Glycine, 20 % Methanol, 0.1 % SDS). The gel and membrane sandwich was assembled in a Mini Trans-Blot Cell (BioRad), and blotting was carried out in a transfer buffer at 100 V for one hour at 4°C. After protein transfer, the membrane was blocked in 5 % milk in TBS-T (Tris-buffered saline, 1% Tween 20) for one hour at room temperature. After incubation, the membrane was washed with TBS-T thrice for 5 min. Primary antibody was added and incubated overnight (ON) at 4°C. After ON incubation, the membrane was washed five times for 5 min in TBS-T at RT. The secondary antibody was diluted 1:2,000 in 5 % TBS-T milk, and the membrane was incubated for one hour at RT.

After that, the membrane was washed with TBS-T five times for 5 min. The membrane strips were incubated with the ECL Western Blotting solution for 5 minutes (Pierce™) and subsequently developed and fixed in an X-ray film cassette in a darkroom for varying exposure times (from 30 seconds to 10 minutes) using the CP1000 AGFA developer. The following antibodies were used: primary rabbit polyclonal anti-COPZ1 antibody (Proteintech, #20440-1-AP), primary rabbit polyclonal anti-α-tubulin antibody (Cell Signaling, #7076), and secondary horseradish peroxidase-conjugated anti-rabbit antibody (Cell Signaling, #7074).

Cloning of human *COPZ1* and *COPZ2* cDNAs and transduction of CB CD34$^+$ HSPCs

Human *COPZ1* and *COPZ2* cDNA sequences were amplified by PCR from Origene plasmids (#RC201023, #RC204853, respectively) with the following primers: COPZ1 LV cloning F, COPZ1 LV cloning R, COPZ2 LV cloning F, COPZ2 LV cloning R (supplemental Table 10). Amplified coding sequences of *COPZ1* and *COPZ2* were cloned into the linearized (with BamHI restriction enzyme) pRRL.PPT.SF.i2DsRedpre vector backbone [5] (kindly provided by Prof. Axel Schambach, MHH, Hannover, Germany) by Gibson assembly using the NEBuilder HiFi DNA Assembly Reaction Kit (NEB, #E2621X), according to the manufacturer's protocol. Virus production and concentration were performed with the Lenti-X™ Concentrator (Takara, #631232) following the manufacturer's instructions. 5 x 10^5 HSPCs per ml of CD34$^+$ expansion media were virus inoculated (MOI 50) 15 min after RNP nucleofection, based on the protocol established by Ngom, M., *et al.*, as detailed in [6] and used for experiments 24 hours after transduction. Depending on the construct, transduction efficiencies varied from 70 to 85%.

Cloning and co-immunoprecipitation of JAGN1 in HEK293 Cells

Human *JAGN1* cDNA was amplified by PCR from the Sino Biological plasmid "Human JAGN1 Gene ORF cDNA clone expression plasmid, C-FLAG tag" (#HG27294-CF) using primers JAGN1 LV F and JAGN1 LV R (supplemental Table 10). The amplified sequence was cloned into the BamHI-linearized pRRL.PPT.SF.i2DsRedpre vector backbone via Gibson assembly using the NEBuilder HiFi DNA Assembly Kit (NEB, #E2621X), following the manufacturer's protocol.

HEK293 cells were transiently transfected with vectors pRRL.PPT.SF.JAGN1.2DsRedpre and pRRL.PPT.SF.COPZ1.i2DsRedpre encoding FLAG-tagged JAGN1 and COPZ1 fused to a Myc-DDK

tag using Lipofectamine 2000 (Thermo Fisher Scientific). After 30 h, cells were lysed by sonication in lysis buffer (20 mM Tris, pH 7.3, 120 mM NaCl, 30 mM KCl, 2 mM MgCl2, 1 % NP-40) containing protease inhibitors (cOmplete, Mini, EDTA-free Protease Inhibitor Cocktail, Roche), 1 mM PMSF, and 0.1 mg/ml DNase I (Sigma-Aldrich). Cell debris was removed by centrifugation at 13,000 *g*. The soluble cell fraction was diluted with an equal volume of binding buffer (PBS, 0.1 % Triton-X100) and incubated with mouse Anti-C-Myc Magnetic Beads (Thermo Fisher Scientific) at 4 °C for 90 min. Samples were extensively washed with binding buffer, and bound proteins were eluted from the Anti-C-Myc Magnetic Beads with C-Myc peptide (10 µg/ml, Sigma-Aldrich) dissolved in water. Eluted samples were separated on a 4-12 % NuPAGE gel (Thermo Fisher Scientific) and analyzed by Western blotting using polyclonal rabbit anti-FLAG (Sigma-Aldrich) as primary antibody to detect FLAG-JAGN1 and Myc-DDK-COPZ1.

RNA Sequencing

For RNA-seq, we collected and isolated RNA from *COPZ1*-TR (n = 2) and *AAVS1* CTRL (n = 2), and from *COPZ1*-MS (n = 3) and WT CTRL (n = 3) samples on day 4 of liquid culture granulocytic differentiation. The quality of RNA samples was verified on Agilent 2100 Bioanalyzer. RNA integrity number > 8 was set as an RNA quality cutoff. RNA-seq samples were prepared using a directional strand-specific mRNA library method and underwent sequencing on the NovoSeq 6000 (Illumina) sequencer at the Novogene (www.novogene.com). We generated, on average, 9 Gb raw data per sample in pair-end 150 bp sequencing mode. Quality analysis and raw data (fastq files) conversion into read counts per gene were performed following the nf-core/rnaseq pipeline (https://github.com/nf-core/rnaseq). The Spliced Transcripts Alignment to a Reference (STAR) software [7] was utilized to map sequencing reads to the human genome, generating at least 60 million mapped reads per sample. Quantification of transcript expression was done by the Salmon tool [8]. Resulting read counts per gene were used to calculate differential gene expression and perform principal component analysis (PCA) in Rstudio using the DESeq2 package [9] and in a web application for RNA-Seq data iDEP (integrated Differential Expression and Pathway analysis) [10] (http://ge-lab.org/idep/). Heat maps were generated by the R package "ComplexHeatmap" [11]. The volcano plots were created by the R package

"EnhancedVolcano" (https://github.com/kevinblighe/EnhancedVolcano). Gene set enrichment analysis (GSEA) was done using iDEP.95 and iDEP.96 versions.

Detection of mitochondrial ROS in NB4 and HL-60 cells by flow cytometry under hypoxic conditions

1 x 10^6 of *AAVS1* edited or *COPZ1*-TR NB4 and HL-60 cells were incubated for 48 hours in a low oxygen incubator (Hypoxilab^{TM}, Oxford Optronix Ltd.), with 1 % O_2, 5 % CO_2, and 94 % N_2 conditions. Mitochondrial ROS was measured by flow cytometry following the protocol from Yun Yang *et al.* [12].

***In vitro* toxicity test of IOX2 in HSPCs**

1.6 x 10^4 $CD34^+$ HSPCs were seeded per well in a 96-well plate in RPMI 1640, supplemented with 10 % FBS, 1 % P/S, 5 ng/ml SCF, IL-3 and GM-CSF and 1 ng/ml G-CSF. Cells were incubated seven days with 1 μM, 5 μM, 10 μM or 50 μM of IOX2 or 1% DMSO. Cells were monitored for seven days in the IncuCyte S3 live cell imaging system (Essen Bio) for time-kinetics analysis with a 20x objective. Cell proliferation was analyzed using IncuCyte S3 Software.

Cholera toxin B subunit (CtxB) intracellular trafficking assay

To measure the effect of *COPZ1*-TR and *COPZ1*-MS mutations on retrograde protein transport from the Golgi to the ER, we performed a CtxB assay [13, 14]. For the *COPZ1*-TR protein, we plated 40,000 *COPZ1*-TR HDFa cells on Lab-Tek Chamber Slides (Thermo Fisher Scientific, 154534). We cultured them at 37°C, 5% CO2 in a humid environment, in DMEM supplemented with 10 % FCS, 1 % P/S, and 1 mM sodium pyruvate. Cells were incubated with 0.15 μg/mL Alexa Fluor 555-labeled CtxB (Molecular Probes, C34776) on ice for 30 min. After washing twice with PBS, the cells were incubated with prewarmed DMEM for the indicated times (time 0 corresponds to 2 hours after exposure to the CtxB; time 8 hours corresponds to 10 hours of incubation with CtxB). Cells were fixed with 4 % paraformaldehyde (Electron Microscopy Sciences) for 10 min and then washed once in saturation buffer (PBS with 1 % BSA, MilliporeSigma), permeabilized with 0.1% Triton buffer for 10 min, and washed twice in permeabilization buffer (PBS containing 0.1 % saponin, Fluka Biochemika, and 0.2 % BSA). Cells were incubated for 45 min with the following primary antibodies: mouse anti-GM130 and goat anti-SERCA2 ATPase antibody (supplemental Table 9), washed twice with 1.5 mL of saponin buffer to remove non-specifically bound antibodies and incubated with secondary antibodies (Donkey anti-mouse

Alexa 647 and Donkey anti-goat Alexa 488) for 30 min (supplemental Table 9). After incubation, cells were washed twice in a saponin buffer and twice with 500 µL of PBS. Nuclear labeling was performed with 1 µg/mL Hoechst for 5 min in the dark. Finally, cells were washed twice with 1.5 mL PBS and mounted with FluorSave (Merck, Cat# 345789).

Zebrafish maintenance and breeding

Wild-type and the previously described transgenic myeloid cell reporter zebrafish line tg(mpo:*gfp*) were used [15]. All zebrafish were kept according to standard protocols and handled under the European Union animal protection directive 2010/63/EU. The local government approved the maintenance (Tierschutzgesetz §11, Abs. 1, Nr. 1, husbandry permit 35/9185.46/Uni TÜ). Furthermore, the generation of *copz1* mutants on tg(mpo:*gfp*) background using CRISPR-Cas9-based knock-out strategy was approved by the local government (Tierschutzgesetz §8, Abs. 1, Tierversuchsvorhaben permit M08/20G).

COPZ1 evolutionary conservation across species

COPZ1 genomic synteny was studied by analyzing the neighboring genes of human and zebrafish *COPZ1* using *ENSEMBL* (http://ensembl.org). Multiple protein alignment was performed using the Clustal Omega [16] web tool on the EMBL-EBI web page (www.ebi.ac.uk/Tools/msa/clustalo/). The neighbor-joining phylogenetic tree of COPZ1 proteins was performed with 1.000 bootstrap replications.

***In vivo* modeling of neutropenia induced by truncated *COPZ1* mutation in zebrafish embryos**

To mimic the truncated *COPZ1* variant found in CN patients, the zebrafish embryos were gene-edited using a CRISPR/Cas9 approach, targeting the position p.Q161 of zebrafish Copz1 protein. To generate Copz1 truncated zebrafish, 5 µM CRISPR/Cas9 RNPs (sgRNA_p.Q161, supplemental Table 3) were injected into a one-cell stage of tg(mpo:*gfp*) embryos and raised until adulthood. The mutants were genotyped by sequencing the affected region using the primers COPZ1_Dr_F and COPZ1_Dr_R (supplemental Table 10). The adult *copz1* gene-edited zebrafish with more than 70 % indels, leading to a truncated Copz1, were selected for further experiments. The offsprings of these *copz1* gene-edited zebrafish were genotyped and used to characterize hematopoiesis and to conduct drug screening.

Characterization of *copz1* expression and hematopoietic cell-specific marker genes in zebrafish embryos using whole mount *in situ* hybridization (WISH)

WISH was performed on – one or two days-old zebrafish embryos as described previously [17]. Briefly, digoxigenin (DIG)- labeled RNA antisense probes for corresponding genes were synthesized using the DIG RNA Labeling kit (SP6/T7) (ROCHE, Cat. No. 11175025910). These probes were generated by linearization of pCR Blunt^{TM} II-TOPO^{TM} vectors (Zero Blunt TOPO PCR Cloning kit, Thermo Fisher, Cat. No. 450031) containing the PCR-amplified complementary sequence of the target genes (supplemental Table 11). Stained cells were manually quantified in the tail region caudal to the yolk extension. Pictures were taken with the microscope-fitted Nikon DS-Fi3 camera and NIS Elements software using a Nikon stereo-fluorescent SMZ18 microscope. Brightness and contrast were adapted for better visualization.

Sudan black staining

To stain the neutrophils with Sudan black, zebrafish embryos were fixated with 4 % PFA/PBS for two hours at room temperature. After washing away the fixation solution, the embryos were incubated with the Sudan black staining solution (ThermoFisher) for 20 min. After the staining process, the embryos were extensively washed with 70 % ethanol, and the positive cells in the hematopoietic tissue were manually quantified.

***In vivo* toxicity test in zebrafish embryos**

One-day-old dechorionized wild-type embryos were incubated in DMSO (control) and different concentrations of IOX2 from 0.1 to 100 µM. The working concentrations of the drugs were based on the toxicity test. The embryonic survival was quantified after two days of treatment, and the concentration without toxic effect on the embryos was selected.

***In vivo* drug testing in zebrafish embryos**

One-day-old dechorionized copz1 gene-edited zebrafish embryos and *hax1* antisense morpholino microinjected embryos on tg(mpo:*gfp*) background were incubated in DMSO (control) or 10µM IOX2 diluted in E3-medium for two days. On day three post-fertilization, the mpo:*gfp*$^{+}$ cells in the hematopoietic tissue of treated embryos were quantified manually using a Nikon stereo-fluorescent SMZ18 microscope [18].

***In silico* modeling of the effects of COPZ1 mutations on protein structure**

We obtained the initial structural models of the free COPZ1 and COPZ1:COPG1 starting from the crystal structure of the bovine COPZ1:COPG1 complex (PDB:3TJZ) [19]. The AlphaFold2 model [20] of the human COPG1 was used to substitute the bovine COPG1 in the complex, as the latter entrained missing coordinates across segments of the HEAT repeat. The structural alignment of the human COPG1 AlphaFold2 model and the bovine COPG1 structure had an RMSD of 0.7 Å. The resulting bovine COPZ1:human COPG1 complex was used as a template to model the full-length human COPZ1:human COPG1, where Modeller v9.22 [21] was used for deriving the final complex. The final complex consisted of the entire COPZ1 domain (positions 1-153) bound to the HEAT (positions 16-318). The free (unbound) COPZ1 structure was extracted from the latter complex. The same procedure was followed to derive models of the free COPZ2, free COPZ1-TR (positions 1-140), COPZ2:COPG1 complex, and COPZ1-TR: COPG1 complex. Similarly, four previously described interaction mutants of *COPZ1* [22] were modeled using the same complex template to compare their impact on the binding stability. These mutants are Mut1: E58K/I59A, Mut2: E87K/L88A, Mut3: E119K/F122A/L123A/D126K, and Mut4: D130K/V133A/I134A/L135A.

Using VMD (v1.9.4) [23], we built cubic simulation cells with solvent padding of 14 Å to the closest periodic boundary in each direction and ionized the systems using 150 mM sodium or chloride ions. We used the CHARMM36 force field and TIP3P water model for all simulations [24]. Each system underwent 10,000 conjugate gradient minimization steps followed by 100 or 600 ns of NPT ensemble at 310 Kelvin. The time step was set to two fs, and a Langevin Piston was set to one Atm at an oscillation period of 200 fs and damping period of 50 fs. A Langevin thermostat was accordingly set with a damping coefficient of one ps^{-1}. A non-bonded interactions distance cutoff was set to 12.0 Å at a switching distance of 10.0 Å with all non-bonded force and pair list evaluations were performed every timestep, and long-range electrostatics were computed using the Smooth Particle Mesh Ewald method as implemented in the NAMD (v2.13) engine [25]. Frames were collected for each 10 ps of the trajectories. Each system was run in three independent replicas, where velocities were randomly initialized in each replica: free COPZ1 full length, bound COPZ1 full length:COPG1, free COPZ1 truncated, bound COPZ1 truncated:COPG1, bound COPZ2 full length:COPG1, COPZ1 mut1:COPG1, COPZ1 mut2:COPG1, COPZ1 mut3:COPG1, COPZ1 mut4:COPG1. These systems were run for 100 ns per

replica (3 replicas each). Furthermore, to obtain more simulation data on the Gly132Arg mutant, we followed the same procedure to spawn four additional systems that were run for longer simulation time. We run free COPZ1, free COPZ1 Gly132Arg, COPZ1:COPG1 and COPZ1 Gly132Arg:COPG1. They, however, were simulated for a total of 600 ns per replica, with 3 replicas run per system.

All analyses were performed using either the MDTraj library (v1.9.7) [26] or VMD (v1.9.4) [23]. All RMSD, RMSF, and order parameter analyses were carried out in the same frame-of-reference aligned along the backbone atoms of the COPZ1 subunit (positions 10 to 140). The interaction energies were calculated across the COPZ1:COPG1 interface for the last 10 ns or 60 ns of the 100 ns or 600 ns simulations, respectively. These non-bonded interaction energies were calculated using the NAMD Energy plugin in VMD, using a dielectric constant of 8. The backbone entropy (ΔS_{bb}) was evaluated using the relationship $\Delta S_{bb} = k_B(1.11 \times log(1 - S_{NH}^2) + 3.8)$, which relates the backbone entropy change to the N-H order parameter S_{NH}^2 [27]. The N-H order parameter was calculated as previously described [28], where the analysis was restricted to the amino acid position 101-140 of the free or bound COPZ1 protein.

DigiWest multiplex protein analysis

Gene-edited $CD34^+$ cells were starved for 16 hours in StemSpan™ SFEM II medium (Stemcell Technologies, #09650) without growth factors, supplemented only with 1 % penicillin-streptomycin. After starvation, the cells were treated with 1 ng/ml of rhG-CSF for 30 min or left untreated. After treatment, cells were washed in PBS and snap-frozen in liquid nitrogen. For protein preparation, cells were lysed on ice in 20-30 µL of lysis buffer containing LDS lysis buffer (Life Technologies, Carlsbad, CA, USA) supplemented with reducing agent (Thermo Fisher Scientific, Waltham, MA, USA), protease inhibitors (Roche Diagnostics GmbH, Mannheim, Germany) and phosphatase inhibitors (Roche Diagnostics GmbH, Mannheim, Germany). Proteins were then denatured by heating at 95 °C for 10 min, transferred to QiaShredder Eppendorf tubes (Eppendorf, Hamburg, Germany), and centrifuged at 16,000 g for 5 min at room temperature. Eluates were stored at -80°C until use. For protein quantification by in-gel staining, 1 µL of lysate was diluted 1:10 (v/v) in lysis buffer, denatured at 70 °C for 10 min, and 10 µL run on a NuPAGE 4-12 % Bis-Tris precast gel (Thermo Fisher Scientific) according to the manufacturer's instructions. The gel was washed with water, and proteins were stained with BlueBandit

(VWR, Darmstadt, Germany) for 1 h. The gel was destained overnight with ddH2O before detection on a LI-COR instrument (LI-COR, Bad Homburg, Germany). Analysis and protein quantification were performed using ImageStudio (LI-COR, Bad Homburg, Germany).

The DigiWest analysis was performed as previously described [29]. Briefly, 10 µg of protein lysate was loaded onto an SDS-polyacrylamide gel, proteins were size separated using the NuPAGE system (Life Technologies), transferred to a PVDF membrane, and biotinylated on the membrane for 1 h using NHS-PEG12-biotin (50 µM) in PBST. The membrane was air dried; the sample lanes were cut into 96 0.5 mm wide strips using an automated cutting plotter (Silhouette America, West Orem, UT, US), and each strip was added to a well of a 96-well plate with 10 µl of elution buffer (8 M urea, 1 % Triton-X100 in 100 mM Tris-HCl pH 9.5). 90 µl of dilution buffer (5% BSA in PBS, 0.02% sodium azide, 0.05 % Tween-20) was added to the eluates, and each eluate was incubated with one different population of neutravidin-coated magnetic colour-coded beads (Luminex, Austin, US). In this setting, each coloured neutravidin bead with bound biotinylated protein represents proteins of a specific molecular weight fraction. A final mixture of 96 protein-loaded bead populations reconstitutes the original protein line, allowing individual antibody incubations. Aliquots of DigiWest bead mixes (approximately 1/200th per well) were added to 96-well plates containing 50 µl of assay buffer (Blocking Reagent for ELISA (Roche, Rotkreuz, CH) supplemented with 0.2 % milk powder, 0.05 % Tween-20 and 0. 02 % sodium azide) and corresponding diluted antibodies (supplemental Table 13) were added to the wells, incubated overnight at 15°C on a shaker, washed twice with PBST and incubated again with species-specific PE (phycoerythrin) conjugated secondary antibodies (Dianova, Hamburg, GER) for 1 h at 23°C. The beads were washed twice with PBST and scored on a Luminex FlexMAP 3D. The specific signal of each antibody was quantified using DigiWest Analyzer software, which detects peaks of appropriate molecular weight and calculates the peak area. Signal intensity was normalized to the total amount of GAPDH, measured as the average from three antibodies per sample.

Supplemental figure legends

Supplemental Figure 1. Conservation of COPZ1 protein among species and the RMSD analysis of the simulation trajectories. A, COPZ1 multisequence alignment confirms the conservation of the amino acid glycine 132 and glutamine 141 among different species. The corresponding positions are

indicated by pink rectangles. **B-J,** C^{α} RMSD plots show that most trajectories showed minimal structural deviation with respect to the first frame, with the relative exception being truncated COPZ1 trajectories. The RMSD values of the COPZ1 domain (three replicas each) of free, full-length COPZ1 **(B)**, free, truncated COPZ1 **(C)**, bound, full-length COPZ1:COPG1 **(D)**, bound, truncated COPZ1:COPG1 **(E)**, COPZ1-mut1:COPG1 **(F)**, COPZ1-mut2:COPG1 **(G)**, COPZ1-mut3:COPG1 **(H)**, COPZ-mut4:COPG1 **(I)**, and bound, full-length COPZ2:COPG1 **(J)**.

Supplemental Figure 2. COPZ1-TR increases the entropic cost of binding to COPG1. A-D, C^{α} RMSF plots highlight the destabilization of the truncated COPZ1 in both free and bound forms. **E-H,** S^2_{NH} order parameter values of the truncated COPZ1 in free and bound forms. Dots and shades represent averaged values and standard deviations across three simulation replicas. **I-L,** The more extended simulations (>600 ns) of *COPZ1* p.Gly132Arg showed only minor RMSD from the starting model, as well as minimal differences between wild type and the p.G132R mutant. The displayed panes show **(A, E)** free, full-length COPZ1, **(B, F)** bound, full-length COPZ1:COPG1, **(C, G)** free COPZ1-TR, **(D, H)** bound COPZ1-TR:COPG1. Whereas the remaining panes **(I-L)** show RMSD values of the COPZ1 domain (three replicas each; extended simulations) of free, full-length COPZ1 **(I)**, bound, full-length COPZ1 p.Gly132Arg:COPG1 **(J),** bound, full-length COPZ1:COPG1**(K)**; and free, full-length COPZ1 p.Gly132Arg **(L)**, respectively.

Supplemental Figure 3. Analysis of the effects of *COPZ1*-TR on granulopoiesis

A, Schematic representation of the genome editing strategy for generating *COPZ1*-TR iPSCs clones. The PAM sequence is highlighted in light blue; the sgRNA sequence is indicated by a pink arrow, and the position of the DNA cut site is marked with a scissors symbol. The nucleotide position corresponding to mutation *COPZ1* p.Gln141Ter is indicated in red, and a silent variant to avoid re-cutting by CRISPR/Cas9 is indicated in yellow. Created with BioRender.com. **B,** Indels composition in iPSCs clone C2 and G2. Percentages were calculated using Inference of CRISPR Edits (ICE) Synthego tool and results of Sanger sequencing. **C,** Scheme for granulocytic differentiation of iPSCs. Created with BioRender.com. **D,** Flow cytometry analysis of iPSC-derived immature hematopoietic cell populations ($CD34^+KDR^+$ endothelial precursor, $CD34^+CD43^+$ hematopoietic progenitor, $CD41a^+CD235a^+CD45^-$ erythro-megakaryocytic progenitor; $CD34^+CD45^+$ hematopoietic/myeloid progenitor $CD33^+CD45^+$

myeloid progenitor) for *COPZ1*-TR and healthy control iPSC-derived cells at day 14 of iPSC differentiation. Data are represented as means (large symbols) from three independent experiments (color-coded: pink, grey, green) performed in technical duplicates (small symbols). ns: not significant. **E,** CRISPR/Cas9 gene editing strategy for generating *COPZ1*-TR mutations in $CD34^+$ cells. The PAM sequence is highlighted in light blue; the sgRNA sequence is indicated by a pink arrow, and the position of the DNA cut site is marked with a scissors symbol. The figure illustrates the observed outcomes following gene editing and repair by non-homologous end joining (NHEJ). The resulting bulk population consists of three distinct alleles, each contributing a different proportion to the total edited population. Created with BioRender.com. **F,** *COPZ1* KO scores calculated by Inference of CRISPR Edits (ICE) Synthego tool on day one of liquid differentiation of $CD34^+$ cells for four healthy donors**,** each indicated in different colour, for *COPZ1* and the *AAVS1* sites. Data are shown as average ± SD.

Supplemental Figure 4. Introduction of *COPZ1*-MS in HSPCs and *copz1* nonsense mutation transmission in zebrafish.

A, Schema of the granulocytic differentiation of gene-edited $CD34^+$ CB-HSPCs**.** Created with BioRender.com. **B,** Total counts of $CD45^+CD15^+CD66b^+CD11b^+CD16^+$ neutrophils on day 14 of LCD in *COPZ1*-TR and *AVVS1* control edited samples of four healthy donors, each indicated in a different colour. Data are represented as means (large symbols) from four donors, performed in technical replicates (small symbols). Statistical significance: $^{**}P < 0.01$. **C,** Schematic representation of the genome editing strategy for generating *COPZ1*-MS CB $CD34^+$ cells. The PAM sequence is highlighted in light blue; the sgRNA sequence is indicated by a pink arrow; the position of mutation *COPZ1* p.Gly132Arg is indicated in red; and the silent variants to avoid re-cutting by CRISPR/Cas9 are indicated in yellow. The same ssODN was used without COPZ1 p.Gly132Arg mutation for WT control. Created with BioRender.com. **D,** Editing efficiency for *COPZ1*-MS and WT CTRL was calculated using the Inference of CRISPR Edits (ICE) tool from Synthego on day one of liquid differentiation of $CD34^+$ cells. HDR represents the knock-in (KI) efficiency percentage, and WT indicates the percentage of unedited cells per sample. Results are shown for four healthy donors, each indicated in a different colour. Data are presented as mean ± SD. **E,** Total counts of $CD45^+CD15^+CD66b^+CD11b^+CD16^+$ neutrophils on day 14 of LCD in *COPZ1*-MS and WT control edited samples of four healthy donors, each indicated in a different colour. Data are represented as mean (large symbols) from four donors, performed in

technical triplicates (small symbols). Statistical significance: ***P < 0.001. **F,** ClustalOmega multisequence alignment of sequences from *copz1* mutant zebrafish. **G,** Genotyping of generation F0 (injected embryos raised until adulthood) adult zebrafish. Representation of indels (%) for each adult zebrafish. **H**, Representative images of mpo:*gfp*$^{+}$ neutrophils at the tail region of 2-day old transgenic Tg(mpo:*gfp*) embryo and *copz1*-gene-edited embryo (F1, offspring of F0). **I,** Genotyping of generation F1 (offspring of F0). Representation of indels (%) for each zebrafish embryo ± SD.

Supplemental Figure 5. Quantification of Sudan Black-positive neutrophils and analysis of bone development in Copz1 TR zebrafish.

A, Quantification of Sudan Black-positive neutrophils in 33 hpf wild-type and Copz1 TR embryos. Data are presented as mean (large symbols) of two experiments. Every small symbol represents one embryo. Statistical significance: ns: not significant. **B-C,** Analysis of bone development in Copz1 TR zebrafish. B, representative images of craniofacial cartilage structures of 4 dpf wilt-type and Copz1 TR embryos stained with Alcian blue. **C,** Analysis of cartilage structures. Statistical significance: ns: not significant. **D,** Representative images of one-month-old larvae with magnification of the affected vertebral column.

Supplemental Figure 6. RNA-seq analysis results of *COPZ1* mutated CD34^{+} HSPCs

A, KO scores were calculated using the Inference of CRISPR Edits (ICE) Synthego tool for the HSPCS samples from CB27 and CB29 on day one of LCD. Data are presented as mean ± SD. **B,** Principal component analysis (PCA) on log-transformed counts per million (CPM) demonstrates the clustering of samples by the groups. The plot of principal component 1 (PC1) vs. principal component 2 (PC2) is shown. **C-E,** Top significant pathways in GSEA with gene sets from the Gene Ontology: "Cell compartments" (**C**), "Jensen compartments" (**D**), and "Kyoto Encyclopedia of Genes and Genomes" (KEGG) (**E**) databases are plotted on the graph. The size of a dot in front of the adj. p-value reflects its significance. **F,** KO scores were calculated using the Inference of CRISPR Edits (ICE) Synthego tool and Sanger sequencing after *AAVS1* and *COPZ1* CRISPR/Cas9 gene editing of the HSPCs samples from CB33 and CB29 donors on day 1 of LCD. **G,** mRNA expression of interferon signature genes (ISGs) in two *COPZ1*-TR HSPC samples (CB33 and CB29) at day 4 of LCD, measured by RT-PCR. The data are normalized to *ACTB* and compared to gene expression of the corresponding gene in *AAVS1* control edited cells using the $2^{-\Delta\Delta Ct}$ method. **H,** Mean fluorescence intensity (MFI) of surface G-CSFR expression in *COPZ1*-MS and WT control-edited cells, measured by flow cytometry at day 4 of liquid

culture differentiation (LCD). Data are presented as mean ± SD from four independent experiments, with each experiment color-coded accordingly. Statistical significance: ns: not significant. **I-J,** KO scores calculated using the Inference of CRISPR Edits (ICE) Synthego tool and Sanger sequencing after *AAVS1* and *COPZ1* TR CRISPR/Cas9 gene editing of the HSPCs samples from donors CB63, CB67, and CB69 **(I)**, from CB33 and CB50 donors **(J).** Data are shown as mean ± SD.

Supplemental Figure 7. CRISPR/Cas9 gene editing efficiency, functional analysis of *COPZ1* TR in leukemia cell lines and skin fibroblasts, co-IP of COPZ1 and JAGN1

A, KO scores calculated using the Inference of CRISPR Edits (ICE) Synthego tool and Sanger sequencing after *AAVS1* and *COPZ1* CRISPR/Cas9 gene editing of NB4 and HL-60 leukemia cell lines. Data are represented as mean ± SD. **B,** Mitochondrial ROS levels were analyzed by flow cytometry in *COPZ1*-TR and *AAVS1* control edited NB4 (left graph) and HL-60 (right graph) leukemia cell lines; graphs show the mean fluorescence intensity (MFI) from oxidized MitoSOX™ Red reagent. Data are represented as mean ± SD derived from three (NB4 cells) and four (HL-60 cells) independent experiments. Statistical significance: *P < 0.05; ns: not significant. **C,** Principal component analysis (PCA) of log-transformed counts per million (CPM) of RNA-seq data sets of three *COPZ1*-MS and three *COPZ1*-WT samples demonstrates the clustering of samples by groups. The plot of principal component 1 (PC1) vs. principal component 3 (PC3) is shown. **D,** Volcano plot of negative log10 transformed adj. p-values against log2 fold change (log2FC) values, showing differentially expressed genes (DEGs) between *COPZ1*-MS vs. WT *COPZ1* HSPCs. Red dots represent the DEGs with log2FC > 1 or < -1 and adj. p-value < 0.05. Genes with -1 < log2FC < 1 and adj. p-value < 0.05 are shown in blue, genes with log2FC > 1 or < -1 and adj. p-value > 0.05 are shown as green dots, grey dots are genes with -1 < log2FC < 1 and adj. p-value > 0.05. Horizontal dashed line marks gene expression with adj. p-value of 0.05; vertical dashed lines represent log2FC = 1 (right line), and log2FC = -1 (left line). The names of the top 14 DEGs are displayed. **E,** KO scores of HDFa 72 hours after *AAVS1* and *COPZ1* CRISPR/Cas9 gene editing. Editing efficiency was calculated using the ICE Synthego tool and Sanger sequencing. **F,G,** Cholera Toxin B Subunit (CtxB) intracellular transport evaluation graphs depict the quantification of the degree of CtxB colocalization with the ER (left) and the Golgi (right) at time zero **(F)** and after 8 hours of incubation with cholera toxin. Data are presented as means from three independent experiments (colour coded for each independent experiment); large symbols represent the

mean of every experiment, and small symbols for every cell measured per experiment. Statistical significance **P < 0.01. ns: not significant. Results of Co-immunoprecipitation (Co-IP) experiments. Lanes 2-4 contain samples of total cell lysates 30 hours post-transfection, showing the expression of FLAG-JAGN1 and Myc-COPZ1. Lines 7-9 depict precipitates of Myc-COPZ1 (line 7), FLAG-JAGN1 (line 8), and a mixture of Myc-COPZ1 and FLAG-JAGN1 (line 9). No co-precipitation of JAGN1 with COPZ1 has been detected.

Supplemental Figure 8. COPZ1 and COPZ2 proteins alignment, and *in vitro* effects of *COPZ2* overexpression on granulocytic differentiation of *COPZ1*-TR HSPCs

A, Human COPZ1, and COPZ2 protein sequence alignment with Clustal Omega. Mutated amino acids are indicated in red. **B,** *COPZ1* (bottom), and *COPZ2* (top) gene expression patterns in various human tissues from https://gtexportal.org/. Hematological and neurological tissues are marked by pink boxes. **C,** Schema of the *in vitro COPZ2* rescue experiment in *COPZ1* mutant $CD34^+$ CB-HSPCs. Cells were thawed and expanded for three days. On day three, mutations in *COPZ1* or *AAVS1* were introduced via CRISPR/Cas9, followed by transduction with *COPZ1*-lv, *COPZ2*-lv or empty RFP-lv. After 24 h, gene-edited and transduced cells were subjected to *in vitro* liquid culture granulocytic differentiation for 14 days. Created with BioRender.com. **D**, KO scores were calculated using the Inference of CRISPR Edits (ICE) Synthego tool and Sanger sequencing after *AAVS1* and *COPZ1* CRISPR/Cas9 gene editing of the HSPCs samples from three healthy donors, indicated by different colours, on day one of LCD. Data are presented as mean ± SD. **E,** Transduction efficiency of HSPCs from five healthy donors, marked by different colours, with the indicated lentiviral constructs, as assessed on day 14 of LCD. Data are represented as mean ± SD. **F,** The percentage of $CD45^+CD15^+CD66b^+CD11b^+CD16^+$ neutrophils on day 14 of LCD. After gene editing (*COPZ1*-TR or *AAVS1* CTRL), cells were transduced with lentiviral particles containing either $Empty^{RFP}$ or $COPZ1\text{-}WT^{RFP}$, or $COPZ2\text{-}WT^{RFP}$ and differentiated to neutrophils for 14 days *in vitro*. The mean of five different experiments (color-coded) is plotted. Large symbols represent the means of technical duplicates (shown as small symbols), for each experiment. **G,** The percentage of myeloblast (MB), promyelocyte (PM), myelocyte (MY), metamyelocyte (MM), band cells (BC), and polymorphonuclear cells (PMN) of counted 100 cells on May-Grünwald-Giemsa stained cytospin preparations of *COPZ1*-TR and *AAVS1* control samples on day 14 of liquid culture differentiation. Cells were transduced with **i**ndicated viruses prior liquid culture differentiation. The

mean of every experiment (color-coded, first experiment in pink, second in grey, and third in green). The mean for each experiment (represented by large symbols) is plotted from technical duplicates or quadruplicates (shown as small symbols). Statistical significance: *P < 0.05; ***P < 0.001; ns: not significant.

Supplemental Figure 9. Effect of IOX2 treatment on granulocytic differentiation of *COPZ1* mutated HSPCs and *copz1* TR zebrafish embryos

A, List of candidate repurposing drugs ranked by the "common gene expression change" matching algorithm score of over one million gene expression profiles from different cell types treated with chemical or genetic perturbagens (CMap). Drugs are listed according to the strength of the enrichment to reverse the *COPZ1* mutant expression signature profile. Selected drug candidates are highlighted in pink. MOA: mechanism of action**;** nLog10: negative log10 transformed false discovery rate (FDR) q-values estimated relative to the null signatures. **B,** Cell toxicity test of IOX2 in zebrafish embryos. Embryonic survival in percentage (%) after two days of treatment at different concentrations (0.1-100 µM of IOX2) is plotted. **C,** Editing efficiency for *COPZ1*-TR and *AAVS1* CTRL cells treated with 10 µM of IOX2. KO score was calculated using the Inference of CRISPR Edits (ICE) tool from Synthego on day one of liquid culture differentiation of $CD34^+$ cells. Results are shown for three healthy donors, each indicated in a different colour. Data are presented as mean ± SD. **D,** Percentage of $CD45^+CD15^+CD66b^+CD11b^+CD16^+$ neutrophils in *COPZ1*-TR and *AAVS1* CTRL cells treated with DMSO or 10 µM of IOX2 on day 14 of LCD. The mean of three individual experiments (large symbols, colour-coded) from technical duplicates (small symbols) are shown. Statistical significance: *P<0.05; ns: not significant. **E,** The percentage of myeloblast (MB), promyelocyte (PM), myelocyte (MY), metamyelocyte (MM), band cells (BC), and polymorphonuclear cells (PMN) of counted 100 cells on May-Grünwald-Giemsa stained cytospin preparations of *COPZ1*-TR and *AAVS1* control samples on day 14 of liquid culture differentiation. Cells were treated with DMSO vehicle or 10 µM of IOX2. The mean of three individual experiments (large symbols, colour-coded) is plotted. Statistical significance: **P<0.01; *P<0.05; ns: not significant. **F,** Primary bone marrow $CD34^+$ HSPCs of reference CN patients (P3) carrying missense *COPZ1* mutation (n = 1, in technical duplicates) on day 14 of differentiation. CFU types: GEMM (granulocytes, erythrocytes, monocytes, megakaryocytes), GM (granulocytes,

monocytes), Im (immature), G (granulocytes), M (monocytes), and BFU-E (burst-forming unit-erythroid). Data represents (large symbols) from a single experiment. Data are plotted as mean from the technical duplicates.

Supplemental tables

Supplemental Table 1. Meta scores of the *in silico* prediction for the effects of the COPZ1 p.Gly132Arg mutation on protein function

Algorithm	Score	Prediction
BayesDel addAF	addAF score 0.3293	Damaging
BayesDel noAF	noAF score0.4903	Damaging
MetaLR	0.6324	Damaging
MetaRNN	0.9566, 0.9566, 0.9566, 0.9566, 0.9566, 0.9566, 0.9566, 0.9566, 0.9566, 0.9566	Damaging, Damaging, Damaging, Damaging, Damaging, Damaging, Damaging, Damaging, Damaging, Damaging
MetaSVM	0.546	Damaging
REVEL	0.869, 0.869, 0.869, 0.869, 0.869, 0.869, 0.869, 0.869, 0.869, 0.869	Pathogenic

Supplemental Table 2. Individual *in silico* prediction algorithms for the effects of the COPZ1 p.Gly132Arg mutation on protein function

Algorithm	Score	Prediction
PolyPhen-2	HumDiv: sensitivity: 0.00; specificity: 1.00 HumVar: sensitivity: 0.00; specificity: 1.00	HumDiv: probably damaging; HumVar: probably damaging
CADD	33	Deleterious
DEOGEN2	0.6034, 0.5011, 0.5011, 0.5017	Damaging, Damaging, Damaging, Damaging
FATHMM-MKL	coding score 0.993	Damaging
FATHMM-XF	coding score 0.9723	Damaging
LIST-S2	0.9523, 0.9523, 0.9931, 0.9523, 0.9922, 0.9523, 0.9931, 0.9523, 0.9931	Damaging, Damaging, Damaging, Damaging, Damaging, Damaging, Damaging, Damaging, Damaging
LRT	0	Deleterious
M-CAP	0.2636	Damaging
Mutation assessor	3.685, 3.685	High, High
MutationTaster	1, 1, 1, 1, 1, 1, 1, 1, 1, 1	Disease causing, Disease causing, Disease causing, Disease causing, Disease causing, Disease causing, Disease causing, Disease causing, Disease causing, Disease causing

PrimateAI	0.8505	Damaging
PROVEAN	-8 -8 -8 -8 -8 -8 -8 -8 -8	Damaging, Damaging, Damaging, Damaging, Damaging, Damaging, Damaging, Damaging, Damaging
SIFT	0, 0, 0, 0, 0, 0, 0, 0, 0	Damaging, Damaging, Damaging, Damaging, Damaging, Damaging, Damaging, Damaging, Damaging

Supplemental Table 3. sgRNAs used for CRISPR/Cas9 gene editing

sgRNA Name	Organism	Sequence 5'- 3'
COPZ1_p.E136	Homo sapiens	CCTGCTGGGGATCACTCTCT
COPZ1_p.Q141X	Homo sapiens	ACCCGGTGTACTACCTACTG
COPZ1_p.Q161	Danio rerio	GGAGAGCGACCCACAGCAGG
AAVS1	Homo sapiens	CTCCCTCCCAGGATCCTCTC
COPZ1 p.G132R	Homo sapiens	GTGGATGAAATTGTAGATGG

Supplemental Table 4. ssODNs used for gene editing of iPSCs and/or CD34$^+$ cells

Name	Sequence 5'- 3'
COPZ1 p.Q141X	GAGGGTGTTTGTGAATAGATGCGGGGATGCAAAGAAACACATTCTTG CTTACCCTTAAGCCACCCGGTGTACTACCTACTGGGGATCACTCTCTA GGATCACCCTGCAAAAACAAAGAAGAGATCATTGTTCACTCTGTCCC GAAGGCCCA
COPZ1 WT CTRL CB	ACATGGAGGGGCTGTTCTTGGCTGTGGATGAAATAGTCGACGGAGGG TAAGTTCTCTGACCTGCCTTGATCTTGGGTGAGGTGGC
COPZ1 p.G132R CB	ACATGGAGGGGCTGTTCTTGGCTGTGGATGAAATAGTCGACGGACGG TAAGTTCTCTGACCTGCCTTGATCTTGGGTGAGGTGGC

Supplemental Table 5. List of differentially expressed genes in *COPZ1* TR vs *COPZ1* WT comparison

In a separate Excel file.

Supplemental Table 6. List of differentially expressed genes in *COPZ1* MS vs *COPZ1* WT comparison.

In a separate Excel file.

Supplemental Table 7. Filtering criteria in predefined filter sets for WES analysis in GSvar

Filtering criteria	multi-	multi-	multi-

	sample recessive	sample com-het	sample dominant
Allele frequency given by gnomAD and if available 1000g	≤ 1%	≤ 0,1%	≤ 0,1%
Sub-population allele frequency given by gnomAD	≤ 1%	≤ 0,1%	≤ 0,1%
The hom/het occurrences of a variant in the internal database of the Institute of Medical Genetics and Applied Genomics, Tuebingen, Germany	≤ 20	≤ 20	≤ 20
The variant impact given by VEP. https://www.ensembl.org/info/genome/variation/prediction/predicted_data.html	HIGH, MODERATE, LOW	HIGH, MODERATE, LOW	HIGH, MODERATE, LOW
Filter that matches variants annotated to be pathogenic by ClinVar or HGMD	KEEP	KEEP	KEEP
Overall allele frequency given by gnomAD and if available 1000g.	≤ 3%	≤ 3%	≤ 3%
ACMG/AMP classification: REMOVE	classes: 1,2	classes: 1,2	classes: 1,2
ACMG/AMP classification: KEEP	classes: 4,5	classes: 4,5	classes: 4,5
Filter for genotype(s) of the 'affected' sample(s),	homozygous	compound heterozygous	heterozygous, homozygous
Filter for genotype of the 'control' sample(s).	heterozygous, wild type	heterozygous, wild type	wild type
Variant quality score	> 100	> 100	> 100

555 **Supplemental Table 8. List of candidate variants in CN patients P1, P2, and P3 after variant**
556 **filtering and prioritization in GSvar**

557 In a separate Excel file.

558 **Supplemental Table 9. Antibody list for CtxB migration assay**

Antibody	Host species	Source	Catalog reference
Anti-GM130	Mouse monoclonal	BD Biosciences	610822
Anti-SERCA2 ATPase	Goat polyclonal	Abcam	Ab219173
Anti Mouse IgG-Alexa 647	Donkey	Invitrogen	A32787
Anti Goat IgG-Alexa 488	Donkey	Invitrogen	A11055

559 **Supplemental Table 10. Primer sequences.**

Primer Name	Application	Organism	Target gene	Sequence 5'- 3'
COPZ1_ex7_F1	Sequencing	H. sapiens	*COPZ1*	GCGTGGATAATCAACCCCTGA
COPZ1_ex7_R1	Sequencing	H. sapiens	*COPZ1*	ACTCCTCTGCCTCAGATGACTG

COPZ1_Dr_F	Sequencing	D. rerio	*copz1*	ATTGCGAGTTGTGAAGAGACGG
COPZ1_Dr_R	Sequencing	D. rerio	*copz1*	GTTCTGTCAGAGGCACGTCAT
COPZ1 LV F	Cloning	H. sapiens	*COPZ1*	ACAGACT-GAGTCGGCCGGTGCCATG-GAGGCGCTGATTTTG
COPZ1 LV R	Cloning	H. sapiens	*COPZ1*	GGGGGGGAGG-GAGAGGGGCGTTAAACCT-TATCGTCGTCATC
COPZ2 LV F	Cloning	H. sapiens	*COPZ2*	ACAGACT-GAGTCGGCCGGTGCCAT-GCAGCGGCCCGAGGCC
COPZ2 LV R	Cloning	H. sapiens	*COPZ2*	GGGGGGGAGG-GAGAGGGGCGTTAAACCT-TATCGTCGTCATCCTTG-TAATCCAGGATATCATTTGCTG
JAGN1 LV F	Cloning	H. sapiens	*JAGN1*	ACAGACTGAGTCGGCCGGT-GATGGCGTCTCGAGCAGGC
JAGN1 LV R	Cloning	H. sapiens	*JAGN1*	GGGGGGGAGG-GAGAGGGGCGTTACT-TATCGTCGTCATCCTTGTAAT-CAGAG
PDK4 qPCR F	qRT-PCR	H. sapiens	*PDK4*	GGAGCATTTCTCGCGCTACA
PDK4 qPCR R	qRT-PCR	H. sapiens	*PDK4*	ACAGGCAATTCTTGTCGCAAA
ALDOC qPCR F	qRT-PCR	H. sapiens	*ALDOC*	ATGCCTCACTCGTACCCAG
ALDOC qPCR R	qRT-PCR	H. sapiens	*ALDOC*	TTTCCACCCCAATTTGGCTCA
BNIP3 qPCR F	qRT-PCR	H. sapiens	*BNIP3*	CAGGGCTCCTGGGTAGAACT
BNIP3 qPCR R	qRT-PCR	H. sapiens	*BNIP3*	CTACTCCGTCCAGACTCATGC
ISG15 qPCR F	qRT-PCR	H. sapiens	*ISG15*	CGCAGATCACCCAGAAGATCG
ISG15 qPCR R	qRT-PCR	H. sapiens	*ISG15*	TTCGTCGCATTTGTCCACCA
IFIT1 qPCR F	qRT-PCR	H. sapiens	*IFIT1*	GCGCTGGGTATGCGATCTC
IFIT1 qPCR R	qRT-PCR	H. sapiens	*IFIT1*	CAGCCTGCCTTAGGGGAAG
MX1 qPCR F	qRT-PCR	H. sapiens	*MX1 q*	GTTTCCGAAGTGGACATCGCA
MX1 qPCR R	qRT-PCR	H. sapiens	*MX1 q*	CTGCACAGGTTGTTCTCAGC
IFNB1 qPCR F	qRT-PCR	H. sapiens	*IFNB1*	GCTTGGATTCCTACAAAGAAGC
IFNB1 qPCR R	qRT-PCR	H. sapiens	*IFNB1*	ATAGATGGTCAATGCGGCGTC
TNF qPCR F	qRT-PCR	H. sapiens	*TNF q*	CCTCTCTCTAATCAGCCCTCTG
TNF qPCR R	qRT-PCR	H. sapiens	*TNF q*	GAGGACCTGGGAGTAGATGAG
USP18 qPCR F	qRT-PCR	H. sapiens	*USP18*	CCTGAGGCAAATCTGTCAGTC
USP18 qPCR R	qRT-PCR	H. sapiens	*USP18*	CGAACACCTGAATCAAGGAGTT
PIM1_q_573_F	qRT-PCR	H. sapiens	*PIM1*	GCTTCGGCTCGGTCTACTC
PIM1_q_680_R	qRT-PCR	H. sapiens	*PIM1*	TGCCATTAGGCAGCTCTCC
CEBPε_qF1	qRT-PCR	H. sapiens	*CEBPε*	TCCATTGACCTCTCCGCCTA
CEBPε_qR1	qRT-PCR	H. sapiens	*CEBPε*	TGGCTTCACGGCAAAGAGAT
GCSFR_q_1278_F	qRT-PCR	H. sapiens	*GCSFR*	CGGATCCAAGGTTATGTGGTT
GCSFR_q1427_R	qRT-PCR	H. sapiens	*GCSFR*	AGGTCCCGGCTGAGTTATAGG

Supplemental Table 11. Gene-specific antisense RNA probes for *in situ* hybridization

Gene	Accesion Number/Eendembl ID	Nucleotide range, bp
copz1	ENSDARG00000017844	59-485
lyz	ENSDARG00000057789	71-458
mpeg1.1	ENSDARG00000055290	859-1417
pu.1	ENSDARG00000000767	161-706
cmyb	ENSDART00000075730	176-819

Supplemental Table 12. DigiWest analysis, relative protein expression

Protein/Protein modification	Relative protein expression normalized to GADPH and to WT			
	COPZ1-MS		COPZ1-TR	
	CB86	CB90	CB86	CB80
Akt substrates - phospho_Ser/Thr 70 kDa	0,92	1,03	0,76	10,36
Akt1 - phospho_Ser129	1,15	0,95	0,46	1,33
Akt1	0,83	1,62	1,80	0,57
A-Raf	0,64	2,30	1,59	2,38
ATG5	0,98	1,06	0,67	0,67
Bcl-xL	0,90	1,00	0,79	0,65
Beclin-1	1,31	0,35	0,69	0,79
C/EBP alpha	1,17	0,96	0,64	0,54
C/EBP alpha	1,06	0,97	0,86	0,72
C/EBP beta	1,41	1,05	0,69	0,72
CD45 (Intracellular Domain)	1,16	1,77	2,26	0,58
c-Myc	1,01	0,74	0,45	0,51
Erk1 p44	1,06	1,31	1,11	0,80
Erk2 p42 - phospho_Thr202/Tyr204	0,95	1,00	0,40	0,31
Erk2 p42	1,08	0,95	0,87	0,71
FoxO3a	1,16	1,29	1,47	0,61
GLUT-1	1,69	1,04	0,43	0,15
Integrin beta2	1,09	1,23	1,43	0,74
LC3B	0,99	1,05	0,82	0,52
LDHA	1,15	0,97	1,28	1,08
MEK1 - phospho_Ser298	0,87	1,20	0,57	0,38
MEK1 - phospho_Thr292	1,00	1,03	0,63	0,44
MEK1/2 - phospho_Ser217/Ser221	1,06	1,06	0,77	0,49
MEK1/2	0,93	0,96	0,63	0,39
mTOR (FRAP) - phospho_Ser2448	0,89	1,91	0,89	0,33
mTOR (FRAP)	1,03	1,06	0,84	0,54
NF-kB p105	0,78	1,70	1,39	0,33
NF-kB p50	1,09	1,01	0,78	0,63
NF-kB p52	1,41	1,17	0,91	0,34

p21 (Waf1, Cip1, CDKN1A)	0,92	1,20	0,55	0,18
p38 MAPK - phospho_Thr180/Tyr182	1,10	0,70	1,22	0,99
p38 MAPK	1,01	1,00	0,92	0,81
p70 S6 kinase	1,01	1,64	1,48	0,44
PDK1 (PDHK1) - phospho_Ser241	0,79	1,25	1,28	0,49
PI3-kinase p101	1,56	1,09	1,34	0,92
PI3-kinase p85 alpha	0,92	1,96	1,25	0,66
S6 ribosomal protein - phos-pho_Ser235/Ser236	1,34	1,83	1,95	0,70
S6 ribosomal protein - phos-pho_Ser240/Ser244	1,38	2,12	1,84	0,54
S6 ribosomal protein	1,22	2,58	2,89	0,59
SHP-2	1,23	2,34	2,30	0,87
STAT 3 - acetyl_Lys685	1,49	1,57	0,87	1,05
STAT 3 - phospho_Tyr705	1,00	0,85	0,84	0,43
STAT 3	0,98	1,03	0,92	0,57
STAT 5 - phospho_Tyr694	1,05	1,03	0,47	0,20
STAT 5 alpha	1,06	1,10	0,90	0,55
STAT 5	1,00	1,28	1,12	0,59
STAT 5, Peak2	0,69	1,14	2,14	0,81
TBK1 (NAK)	1,06	1,26	0,75	0,71

562 **Supplemental Table 13. Antibody used for DigiWest assay**

Antigen	Supplier	Product No.	Species	Uniprot #	Assay Dilution	RRID Antibody ID
Actin beta	Cell Signaling	4970	rb	P60709	200	AB_2223172
Akt substrates - pSer/Thr	Cell Signaling	9611	rb	na	200	AB_330302
Akt1	Cell Signaling	2938	rb	P31749	200	AB_915788
Akt1 - pSer473	Cell Signaling	9018	rb	P31749	200	AB_2629283
Akt1 - pSer129	Cell Signaling	13461	rb	P31749	200	AB_2798226
A-Raf	Cell Signaling	4432	rb	P10398	200	AB_330813
ATG5	Cell Signaling	12994	rb	Q9H1Y0	50	AB_2630393
Bcl2	Cell Signaling	4223	rb	P10415	200	AB_1903909
Bcl-xL	Cell Signaling	2764	rb	Q07817	200	AB_2228008
Beclin-1	Cell Signaling	3738	rb	Q14457	200	AB_490837
C/EBP alpha	Cell Signaling	8178	rb	P49715	200	AB_11178517
C/EBP beta	Cell Signaling	3087	rb	P17676	200	AB_2078052
C/EBP beta - pThr235	Cell Signaling	3084	rb	P17676	200	AB_2260359
CD45 (Intracellular Domain)	Cell Signaling	13917	rb	P08575	200	AB_2750898
c-Myc	Cell Signaling	9402	rb	P01106	200	AB_2151827
Erk1/2 (MAPK p44/42)	Cell Signaling	4695	rb	P27361, P28482	200	AB_390779

Erk1/2 (MAPK p44/42) - pThr202/Tyr204	Cell Signaling	9101	rb	P27361, P28482	200	AB_331646
FoxO3a	Cell Signaling	2497	rb	O43524	200	AB_836876
FoxO3a - pSer413	Cell Signaling	8174	rb	O43524	200	AB_10889562
FoxO3a - pSer294	Cell Signaling	5538	rb	O43524	150	AB_10696878
GAPDH	Cell Signaling	97166	ms	P04406	200	AB_2756824
GAPDH	Sigma	PLA0125	rb	P04406	1000	AB_2910561
GAPDH	Cell Signaling	5174	rb	P04406	200	AB_10622025
GLUT-1	Millipore	07-1401	rb	P11166	200	AB_1587074
IkappaB alpha	Cell Signaling	9242	rb	P25963	200	AB_331623
IkappaB alpha - pSer32	Cell Signaling	2859	rb	P25963	200	AB_561111
Integrin alpha-M (ITGAM, CD11B, CR3A)	abcam	ab133357	rb	P08151	200	AB_2650514
Integrin beta2	Cell Signaling	73663	rb	P06107	200	AB_2799842
Jak 1	Cell Signaling	3344	rb	P23458	200	AB_2265054
Jak 1 - pTyr1034/Tyr1035	Cell Signaling	3331	rb	P23458	200	AB_2265057
Jak 2	Cell Signaling	3230	rb	O60674	200	AB_2128522
Jak 2 - pTyr1007/Tyr1008	Cell Signaling	3771	rb	O60674	200	AB_330403
LC3B	Cell Signaling	2775	rb	Q9GZQ8	100	AB_915950
LDHA	Cell Signaling	2012	rb	P00338	200	AB_2137173
MEK1	Cell Signaling	9124	rb	Q02750	200	AB_330804
MEK1 - pThr286	Cell Signaling	9127	rb	Q02750	200	AB_331654
MEK1 - pThr292	Cell Signaling	26975	rb	Q02750	200	AB_2798935
MEK1 - pSer298	Cell Signaling	98195	rb	Q02750	200	AB_2800299
MEK1/2	Cell Signaling	9126	rb	Q02750, P36507	200	AB_331778
MEK1/2 - pSer217/Ser221	Cell Signaling	9154	rb	Q02750, P36507	200	AB_2138017
mTOR (FRAP)	Cell Signaling	2983	rb	P42345	200	AB_2105622
mTOR (FRAP) - pSer2448	Cell Signaling	5536	rb	P42345	100	AB_10691552
NF-kappaB p100/p52	Cell Signaling	4882	rb	Q00653	200	AB_10695537
NF-kappaB p105/p50	Cell Signaling	3035	rb	P19838	200	AB_330564
NF-kappaB p65	abcam	ab76311 (2229-1)	rb	Q04206	1000	AB_2179019
NF-kappaB p65 - pSer536	Cell Signaling	3033	rb	Q04206	200	AB_331284
NF-kappaB p65 - pSer468	Cell Signaling	3039	rb	Q04206	200	AB_330579

NIK (NF-kappaB inducing Kinase)	Cell Signaling	4994	rb	Q99558	200	AB_2297422
P21 - pThr145	Invitrogen	PA5-12646	rb	P38936	200	AB_10979470
p21 (Waf1, Cip1, CDKN1A)	Cell Signaling	2947	rb	P38936	200	AB_823586
p38 MAPK	Cell Signaling	9212	rb	Q16539, P53778, Q15759	200	AB_330713
p38 MAPK - pThr180/Tyr182	Cell Signaling	4511	rb	Q16539	200	AB_2139682
p70 S6 kinase	Cell Signaling	2708	rb	P23443	200	AB_390722
p70 S6 kinase - pThr421/Ser424	Cell Signaling	9204	rb	P23443	200	AB_2265913
PDK1	Cell Signaling	3062	rb	Q15118	200	AB_2236832
PDK1 - pSer241	Cell Signaling	3061	rb	Q15118	200	AB_2161919
PI3-kinase p101	Cell Signaling	5569	rb	Q8WYR1	200	AB_10829448
PI3-kinase p85 alpha	abcam	ab40755 (1675-1)	rb	P27986	200	AB_777258
PI3-kinase p85/p55 - pp85 Tyr458/ p55 Tyr199	Cell Signaling	4228	rb	Q92569	200	AB_659940
S6 ribosomal protein	Cell Signaling	2217	rb	P62753	200	AB_331355
S6 ribosomal protein - pSer240/Ser244	Cell Signaling	2215	rb	P62753	200	AB_331682
S6 ribosomal protein - pSer235/Ser236	Cell Signaling	2211	rb	P62753	200	AB_331679
SHP-2	abcam	ab32159	rb	Q06124	200	AB_779072
SOCS-3	Cell Signaling	2932	rb	O14543	200	AB_2286460
STAT 3	Cell Signaling	4904	rb	P40763	200	AB_331269
STAT 3 - acetylLys685	Cell Signaling	2523	rb	P40763	200	AB_561524
STAT 3 - pTyr705	Cell Signaling	9145	rb	P40763	200	AB_2491009
STAT 3 - pSer727	Cell Signaling	9134	rb	P40763	200	AB_331589
STAT 5	Cell Signaling	9363	rb	P43403	200	AB_2218658
STAT 5 - pTyr694	Cell Signaling	9359	rb	P42229	200	AB_823649
STAT 5 alpha	abcam	ab32043	rb	P42229	200	AB_778107
TBK1 (NAK)	Cell Signaling	3504	rb	Q9UHD2	200	AB_2255663
TBK1 (NAK) - pSer172	Cell Signaling	5483	rb	Q9UHD2	200	AB_10693472

563

564

565

Supplemental references

1. Dannenmann, B., M. Nasri, K. Welte, and J. Skokowa, *CRISPR/Cas9 Genome Editing of Human-Induced Pluripotent Stem Cells Followed by Granulocytic Differentiation.* Methods Mol Biol, 2020. **2115**: p. 471-483.
2. Lachmann, N., et al., *Large-scale hematopoietic differentiation of human induced pluripotent stem cells provides granulocytes or macrophages for cell replacement therapies.* Stem Cell Reports, 2015. **4**(2): p. 282-96.
3. Selvaraj, S., et al., *High-efficiency transgene integration by homology-directed repair in human primary cells using DNA-PKcs inhibition.* Nat Biotechnol, 2024. **42**(5): p. 731-744.
4. Mir, P., et al., *Gene Knockout in Hematopoietic Stem and Progenitor Cells Followed by Granulocytic Differentiation.* Methods Mol Biol, 2020. **2115**: p. 455-469.
5. Schott, J.W., et al., *Improved retroviral episome transfer of transcription factors enables sustained cell fate modification.* Gene Ther, 2014. **21**(11): p. 938-49.
6. Ngom, M., et al., *UM171 Enhances Lentiviral Gene Transfer and Recovery of Primitive Human Hematopoietic Cells.* Mol Ther Methods Clin Dev, 2018. **10**: p. 156-164.
7. Dobin, A., et al., *STAR: ultrafast universal RNA-seq aligner.* Bioinformatics, 2013. **29**(1): p. 15-21.
8. Patro, R., et al., *Salmon provides fast and bias-aware quantification of transcript expression.* Nat Methods, 2017. **14**(4): p. 417-419.
9. Love, M.I., W. Huber, and S. Anders, *Moderated estimation of fold change and dispersion for RNA-seq data with DESeq2.* Genome Biol, 2014. **15**(12): p. 550.
10. Ge, S.X., E.W. Son, and R. Yao, *iDEP: an integrated web application for differential expression and pathway analysis of RNA-Seq data.* BMC Bioinformatics, 2018. **19**(1): p. 534.
11. Gu, Z., R. Eils, and M. Schlesner, *Complex heatmaps reveal patterns and correlations in multidimensional genomic data.* Bioinformatics, 2016. **32**(18): p. 2847-9.
12. Yang, Y., et al., *A flow-cytometry-based protocol for detection of mitochondrial ROS production under hypoxia.* STAR Protoc, 2021. **2**(2): p. 100466.
13. Karlsson, P., et al., *Loss of vps54 function leads to vesicle traffic impairment, protein mis-sorting and embryonic lethality.* Int J Mol Sci, 2013. **14**(6): p. 10908-25.
14. Delafontaine, S., et al., *Heterozygous mutations in the C-terminal domain of COPA underlie a complex autoinflammatory syndrome.* J Clin Invest, 2024. **134**(4).
15. Renshaw, S.A., et al., *A transgenic zebrafish model of neutrophilic inflammation.* Blood, 2006. **108**(13): p. 3976-8.
16. Madeira, F., et al., *The EMBL-EBI search and sequence analysis tools APIs in 2019.* Nucleic Acids Res, 2019. **47**(W1): p. W636-W641.
17. Quiring, R., et al., *Large-scale expression screening by automated whole-mount in situ hybridization.* Mech Dev, 2004. **121**(7-8): p. 971-6.
18. Doll, L., et al., *A zebrafish model for HAX1-associated congenital neutropenia.* Haematologica, 2021. **106**(5): p. 1311-1320.
19. Yu, X., M. Breitman, and J. Goldberg, *A structure-based mechanism for Arf1-dependent recruitment of coatomer to membranes.* Cell, 2012. **148**(3): p. 530-42.
20. Varadi, M., et al., *AlphaFold Protein Structure Database: massively expanding the structural coverage of protein-sequence space with high-accuracy models.* Nucleic Acids Res, 2022. **50**(D1): p. D439-D444.
21. Webb, B. and A. Sali, *Comparative Protein Structure Modeling Using MODELLER.* Curr Protoc Bioinformatics, 2016. **54**: p. 5 6 1-5 6 37.

22. Yu, W., J. Lin, C. Jin, and B. Xia, *Solution Structure of Human ζ-COP: Direct Evidences for Structural Similarity between COP I and Clathrin-Adaptor Coats.* Journal of Molecular Biology, 2009. **386**(4): p. 903-912.
23. Humphrey, W., A. Dalke, and K. Schulten, *VMD: visual molecular dynamics.* J Mol Graph, 1996. **14**(1): p. 33-8, 27-8.
24. Huang, J. and A.D. MacKerell, Jr., *CHARMM36 all-atom additive protein force field: validation based on comparison to NMR data.* J Comput Chem, 2013. **34**(25): p. 2135-45.
25. Phillips, J.C., et al., *Scalable molecular dynamics on CPU and GPU architectures with NAMD.* J Chem Phys, 2020. **153**(4): p. 044130.
26. McGibbon, R.T., et al., *MDTraj: A Modern Open Library for the Analysis of Molecular Dynamics Trajectories.* Biophys J, 2015. **109**(8): p. 1528-32.
27. Sharp, K.A., E. O'Brien, V. Kasinath, and A.J. Wand, *On the relationship between NMR-derived amide order parameters and protein backbone entropy changes.* Proteins, 2015. **83**(5): p. 922-30.
28. ElGamacy, M., et al., *Mapping Local Conformational Landscapes of Proteins in Solution.* Structure, 2019. **27**(5): p. 853-865 e5.
29. Treindl, F., et al., *A bead-based western for high-throughput cellular signal transduction analyses.* Nat Commun, 2016. **7**: p. 12852.

A

```
splP61923COPZ1_HUMAN        MEALILEPSLYTVKAILILDNDGDRLFAKYYDDTYPSVKEQKAFEKNIFNKTHRTDSEIA 60
splI0FQ09I0FQ09_MACMU       MEALILEPSLYTVKAILILDNDGDRLFAKYYDDTYPSVKEQKAFEKNIFNKTHRTDSEIA 60
P61924COPZ1_MOUSE           MEALILEPSLYTVKAILILDNDGDRLFAKYYDDTYPSVKEQKAFEKNIFNKTHRTDSEIA 60
splQ9IB48Q9IB48_DANRE       MDTLILEPSLYTVKAVLIMDNDGERLYAKYYDDTYPTVKEQKAFEKNIFNKTHRTDSEIA 60
splA0AUT9A0AUT9_XENLA       MDAVLLDPSLYTVKAVLILDNDGERLFAKYYDETYPTVKEQKAFEKNIFNKTHRTDSEIA 60
                            *:::::*:********:**:****:**:******:***:**********************

splP61923COPZ1_HUMAN        LLEGLTVVYKSSIDLYFYVIGSSYENELMLMAVLNCLFDSLSQMLRKNVEKRALLENMEG 120
splI0FQ09I0FQ09_MACMU       LLEGLTVVYKSSIDLYFYVIGSSYENELMLMAVLNCLFDSLSQMLRKNVEKRALLENMEG 120
P61924COPZ1_MOUSE           LLEGLTVVYKSSIDLYFYVIGSSYENELMLMAVLNCLFDSLSQMLRKNVEKRALLENMEG 120
splQ9IB48Q9IB48_DANRE       LLEGLTVVYKSNIDLYFYVIGSSHENELMLMSVLNCLFDSLSQMLRKNVEKRALLENMEG 120
splA0AUT9A0AUT9_XENLA       LLEGLTVVYKSSIDLYFYVIGSSHENELMLMAVLNCLFDSLSQMLRKNVEKRTLLENMEG 120
                            **********.**********:*******:********************:*******

splP61923COPZ1_HUMAN        LFLAVDEIVDGGVILESDPCQYVHRVALRGEDVPLTEQTVSQVLQSAKEQIKWSLLR    177
splI0FQ09I0FQ09_MACMU       LFLAVDEIVDGGVILESDPCQYVHRVALRGEDVPLTEQTVSQVLQSAKEQIKWSLLR    177
P61924COPZ1_MOUSE           LFLAVDEIVDGGVILESDPCQYVHRVALRGEDVPLTEQTVSQVLQSAKEQIKWSLLR    177
splQ9IB48Q9IB48_DANRE       LFLAVDEIVDGGVILESDPCQYVHRVALRGDDVPLTEQTVTQVLQSAKEQIKWSLLR    177
splA0AUT9A0AUT9_XENLA       LFLAVDEIIDGGVILESDPCQYVHRVALRGDDVPLTEQTVSQVLQSAKEQIKWSLLR    177
                            ********:*********************:*********:****************
```

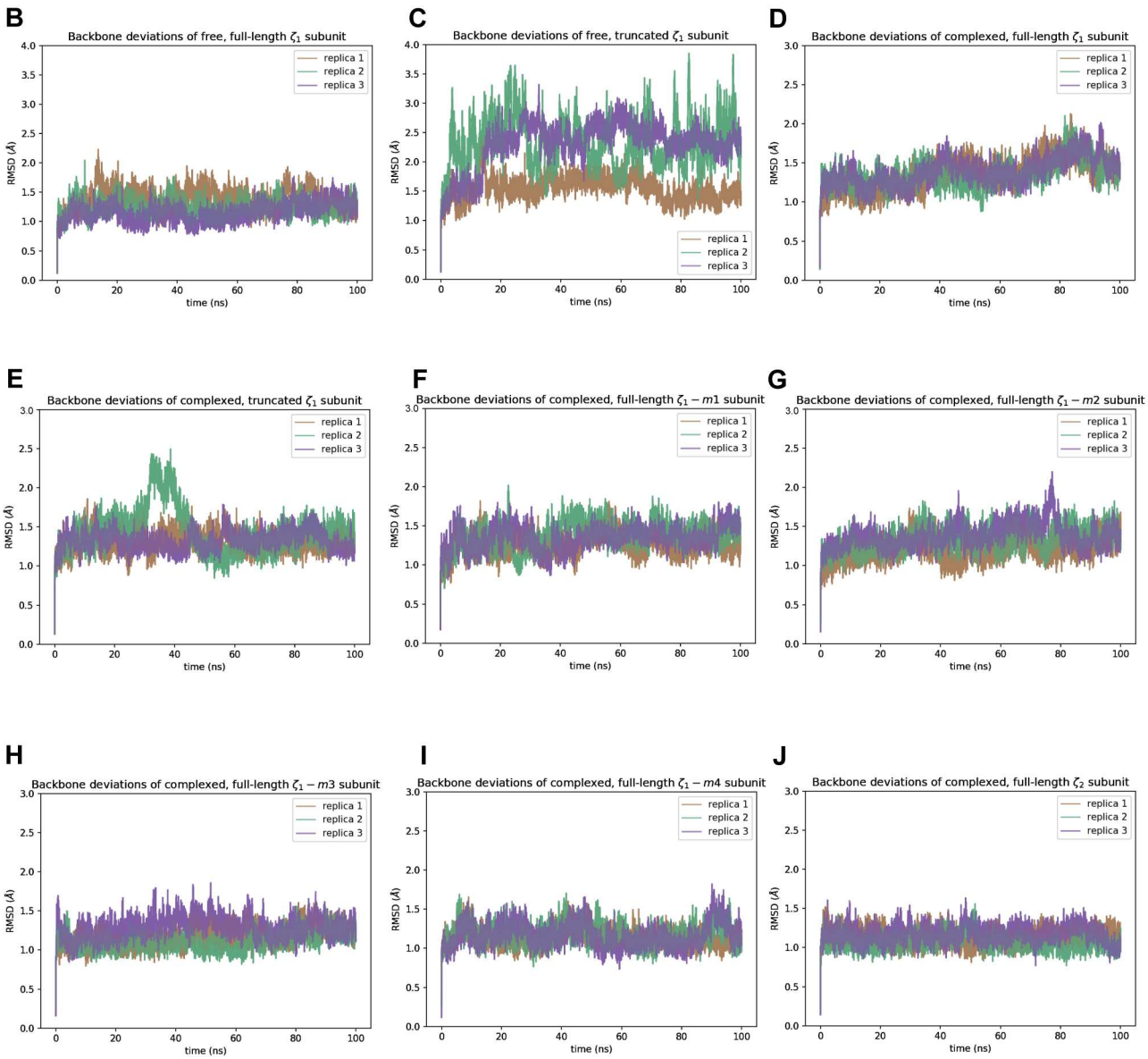

Supplemental figure 1

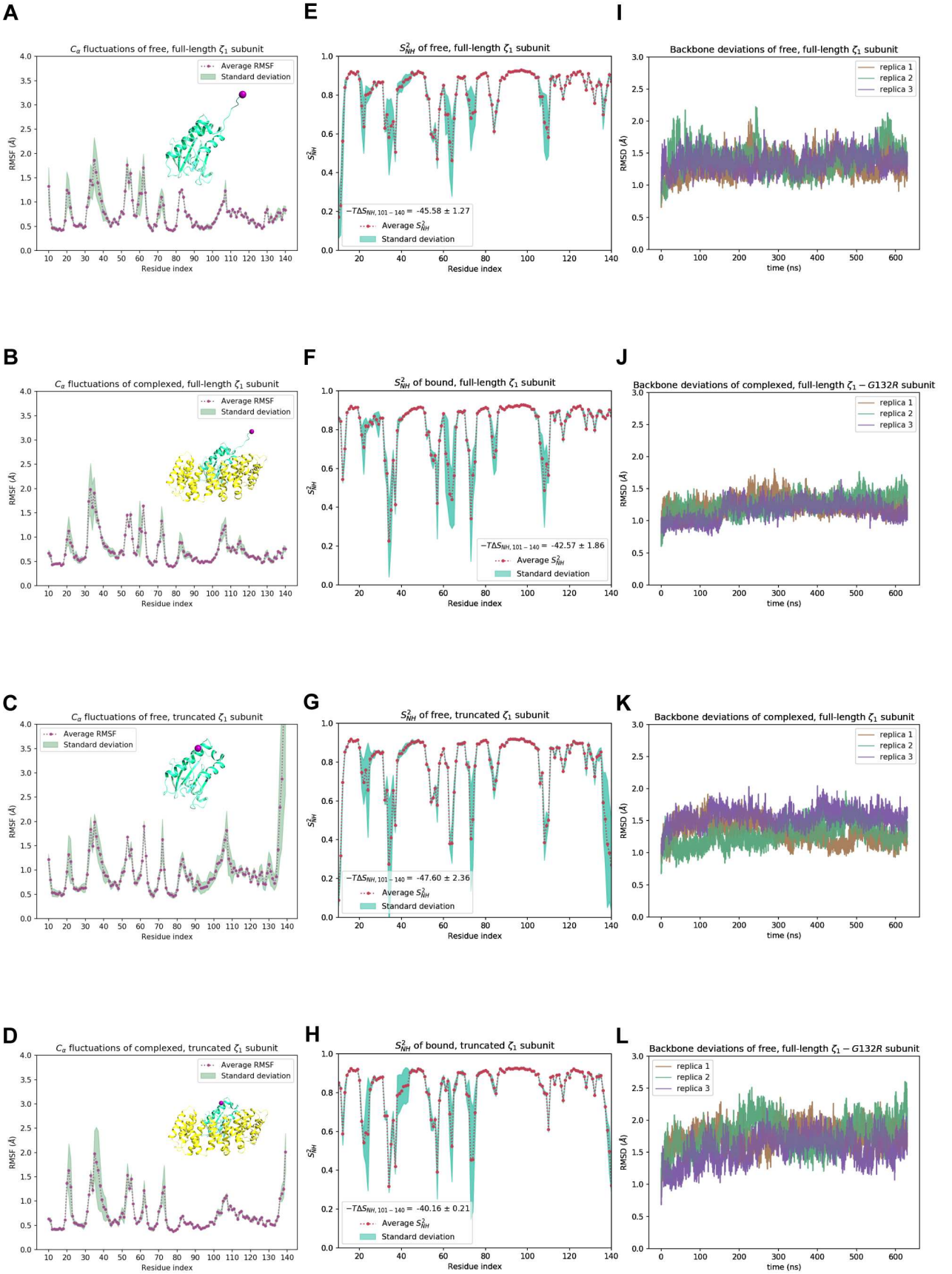

Supplemental figure 2

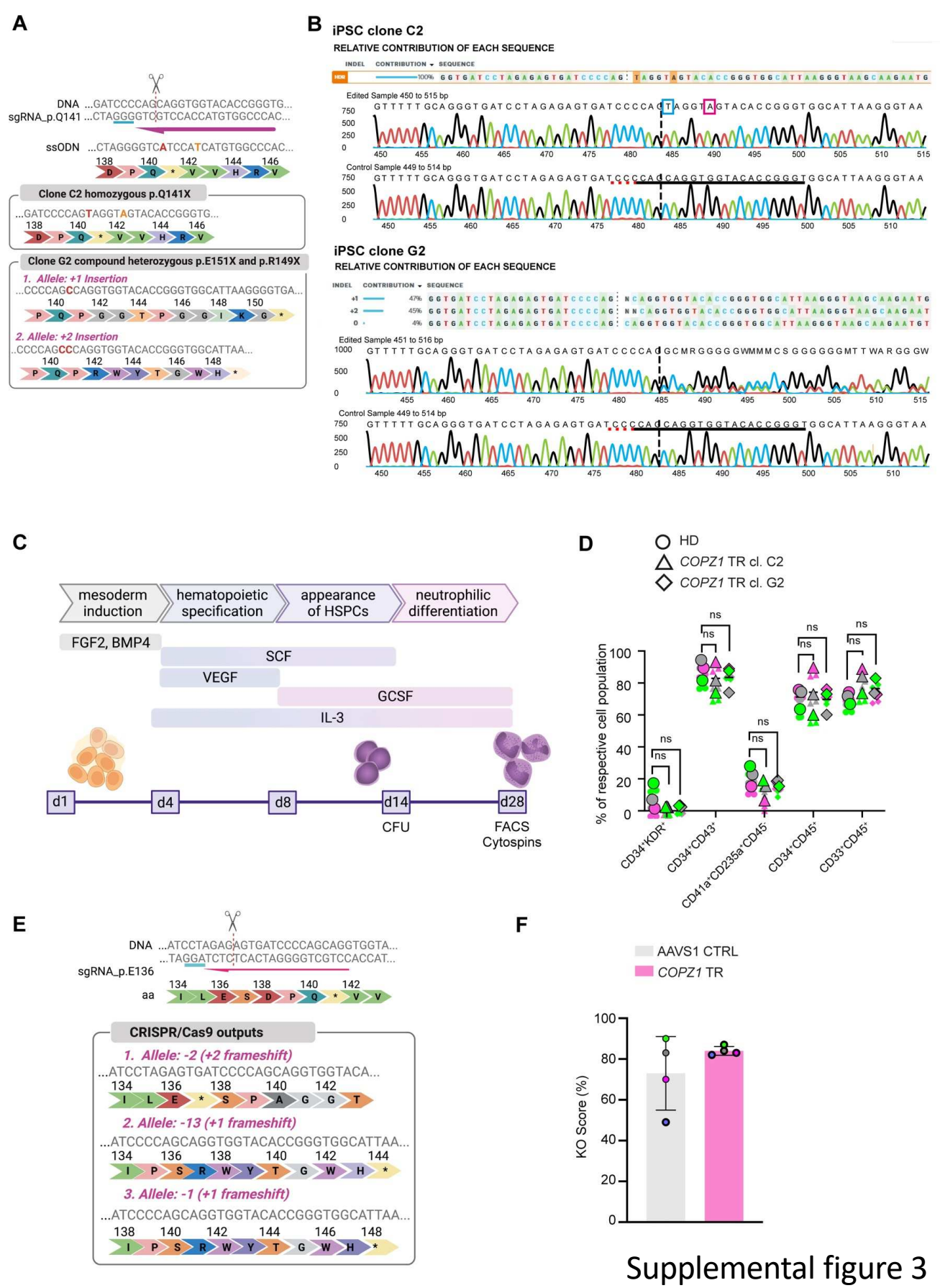

Supplemental figure 3

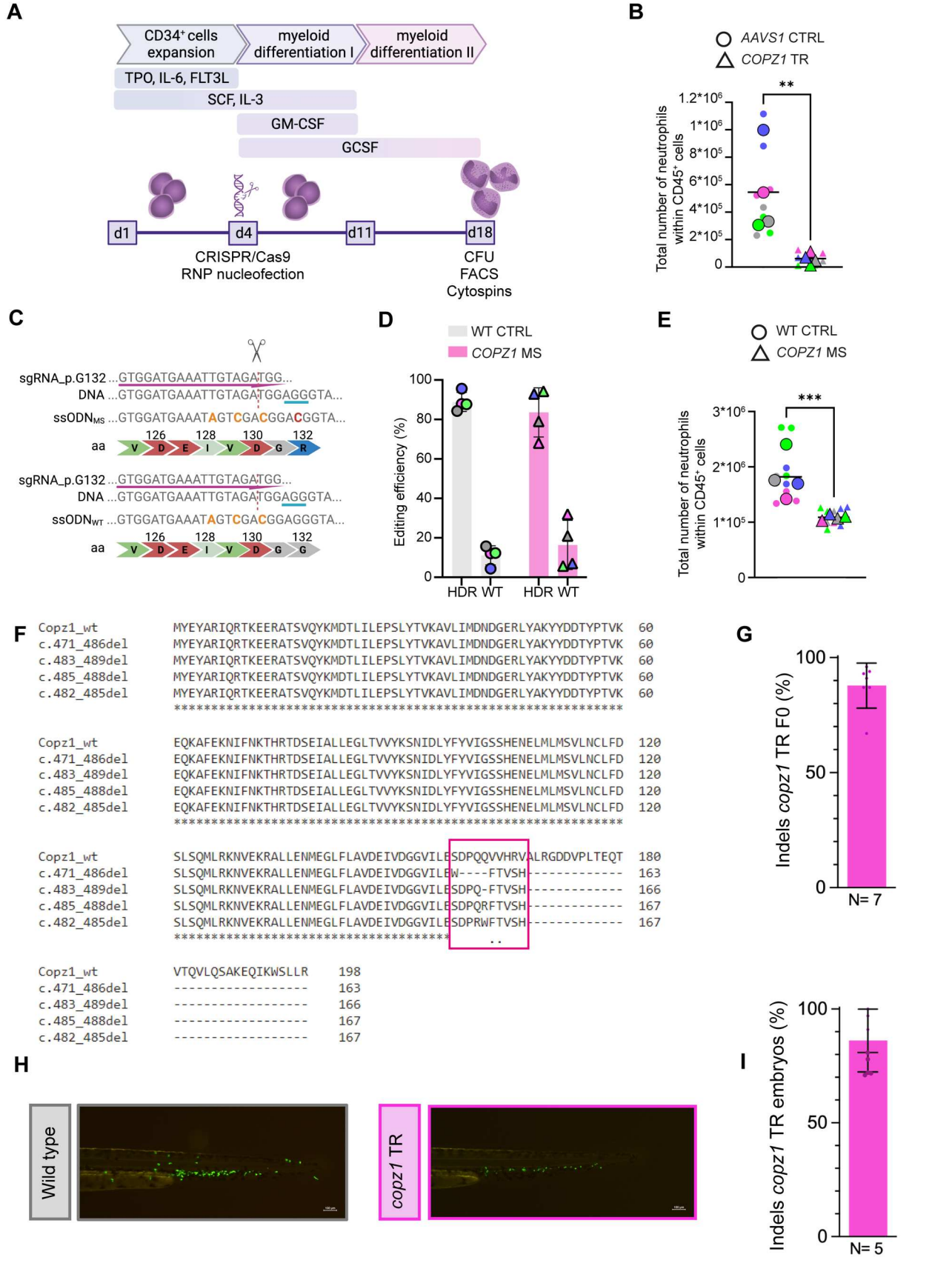

Supplemental figure 4

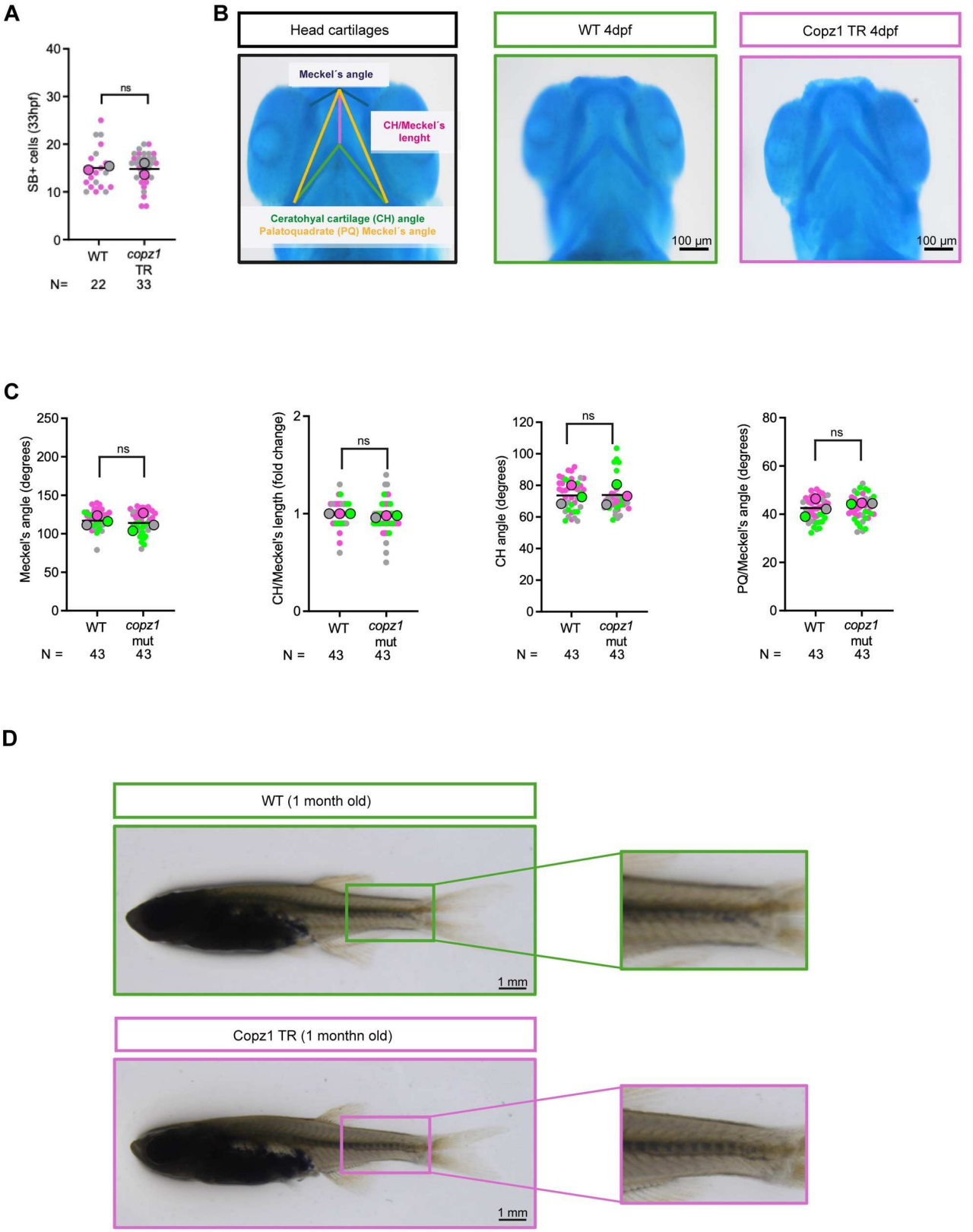

Supplemental figure 5

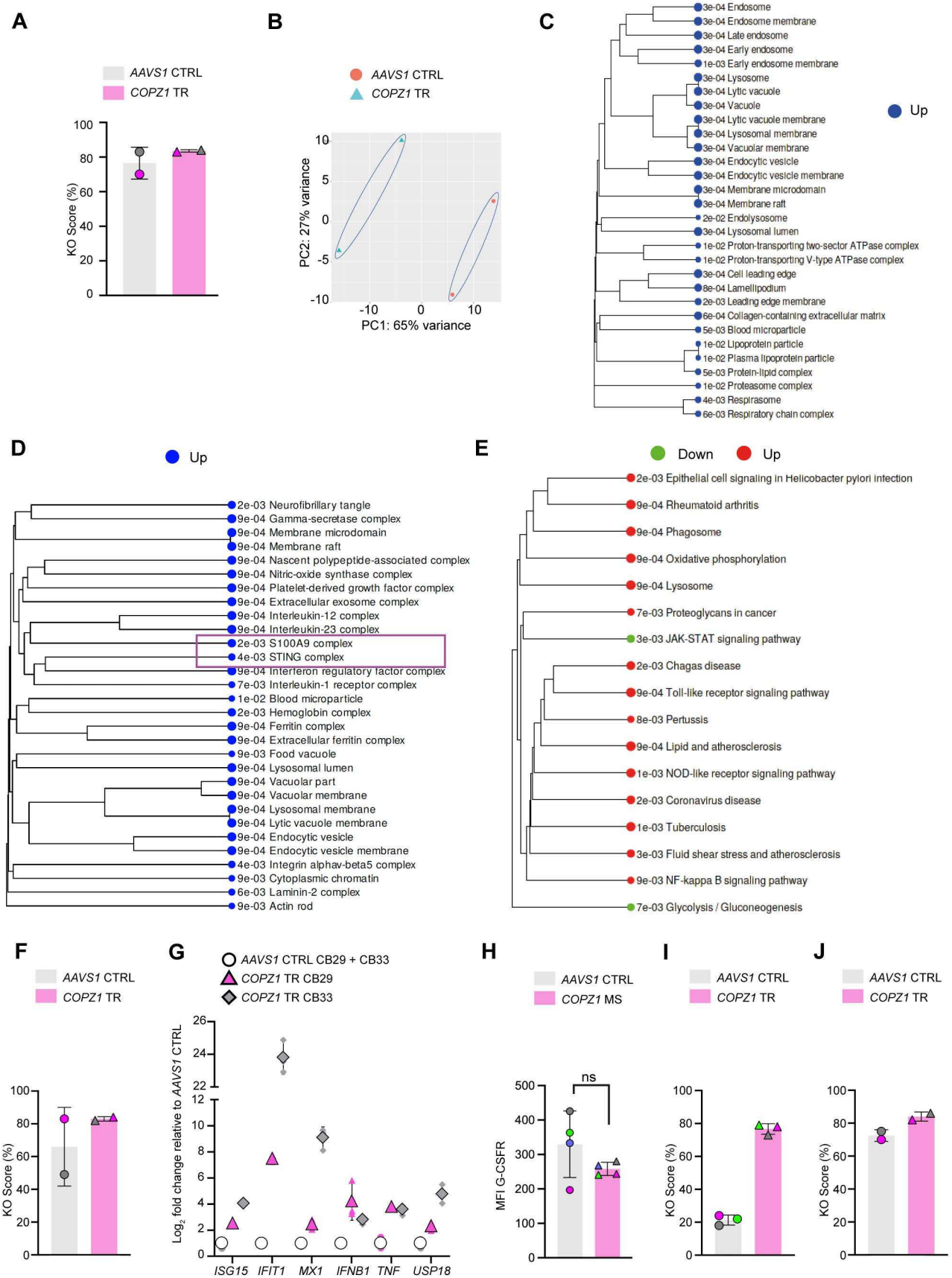

Supplemental figure 6

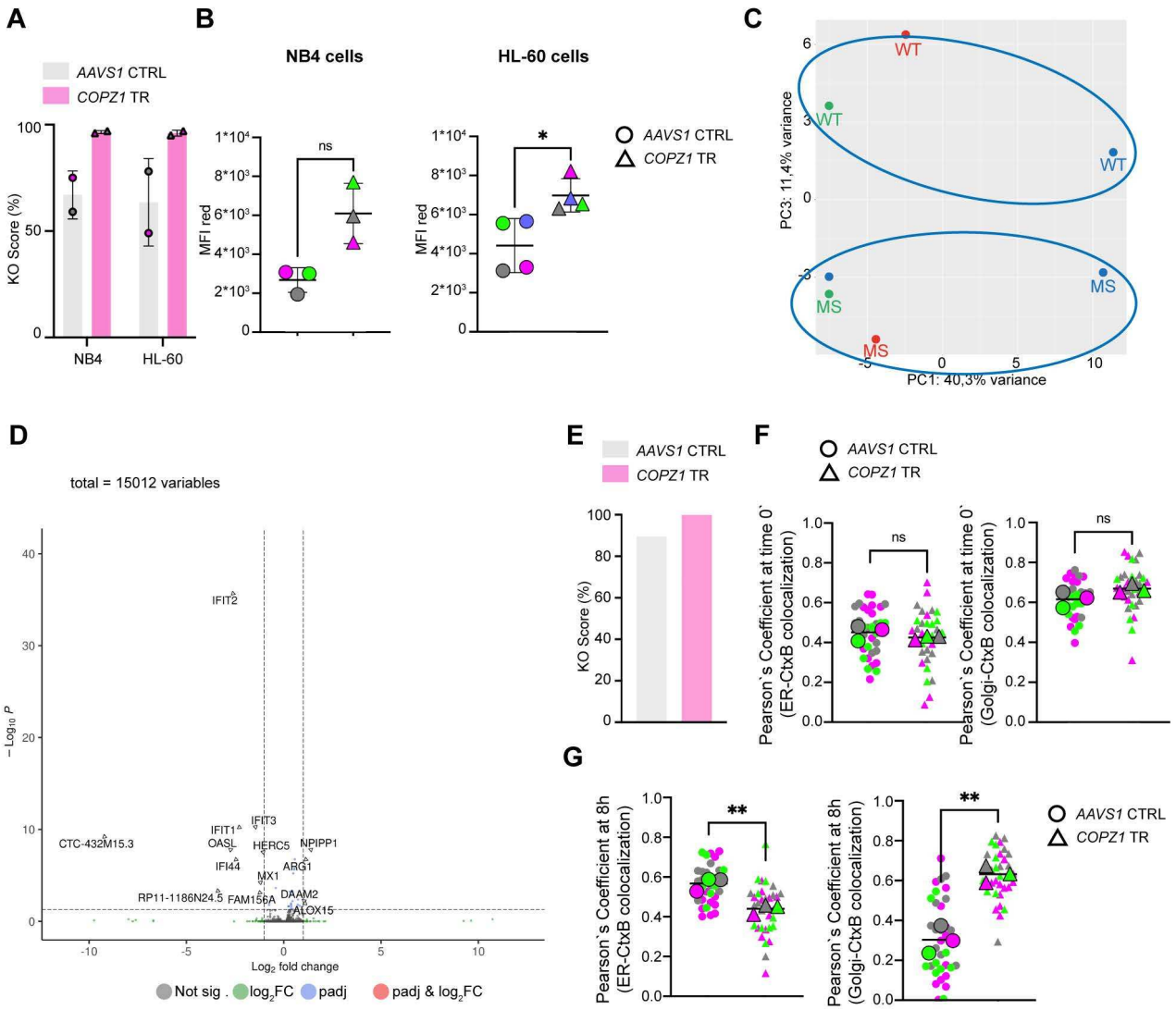

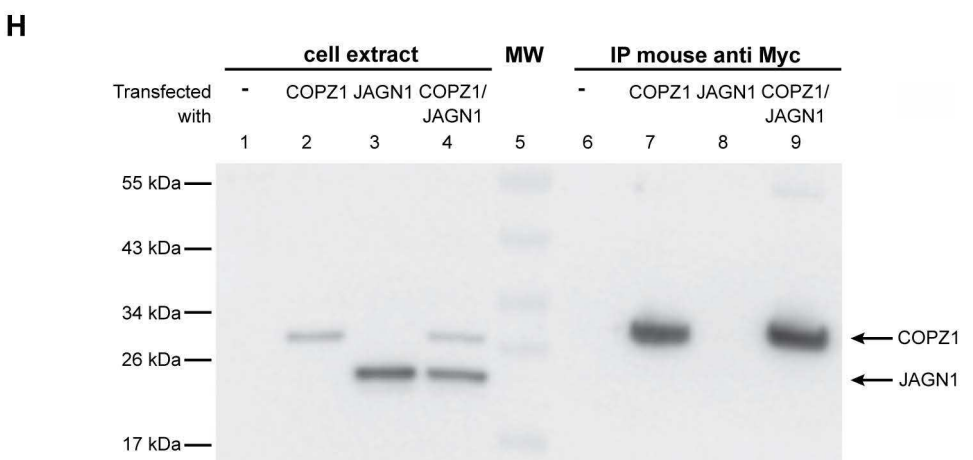

Supplemental figure 7

A

Identical positions	128
Identity	60,952%
Similar positions	35
Program	ClustalO

```
COPZ1_HUMAN   1   - ------ - ------ ---- --- - --- --------- ---MEALILEPSLYTVKAILILDNDGDRLF   27
COPZ2_HUMAN   1   MQRPEAWPRPHPGEGAAAAQAGGPAPPARAGEPSGLRLQEPSLYTIKAVFILDNDGRRLL   60
                                                  : ** *** *. ** : .** * * *  * *.

COPZ1_HUMAN   28  AKYYDDTYPS VKEQ KAFEKNI FNKTHRTDSEIA LLEG L TVVYKS SIDLYFYV IGSSYENE   87
COPZ2_HUMAN   61  AKYYDDTFPSMKEQMVFEKNVFNKTSR TE SEIAFFGGMT I VYKNSIDLFLYVVGSSYENE   120
                  *  ******* *:** : *** .**** *. **** ** : **** :: *  : *: * * : **** : :** : ******* **

COPZ1_HUMAN   88  LMLMAVLNCLFDSLSQMLRKNVEKR ALLEN MEG LFLAVDEIVDGGVILESDPQQVVHRVA   147
COPZ2_HUMAN   121 LMLMSVL TCLF ESLNHMLRKNVEKRWLLLENMDGAFLVLDEIV DGGVILESDPQQV IQKVN   180
                  *  **** .** .*** .** .: * ********** ***** : :*  **. .:**** * ***** **** * ***:: : *

COPZ1_HUMAN   148 LRGE DV PLTEQT VSQVLQSAKEQIKWSLLR                                  177
COPZ2_HUMAN   181 FRADDG GLTEQSVAQVLQSAKEQIKWSLLK                                  210
                  :*. : *    **** : *: * * * * * ** ** * * * :
```

B

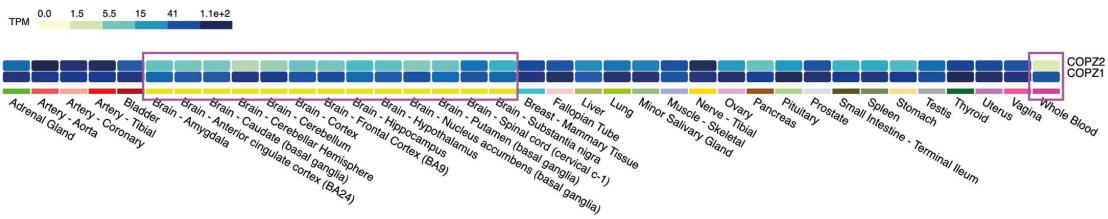

C

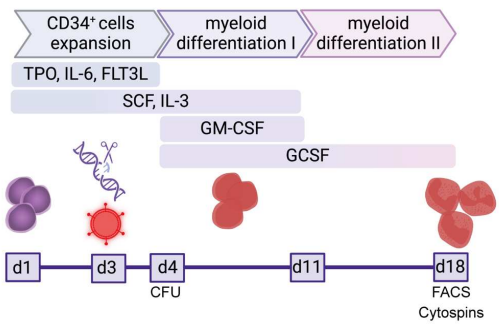

D

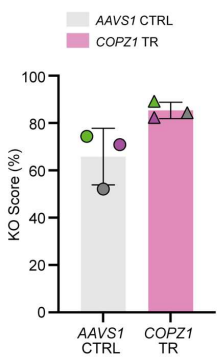

E

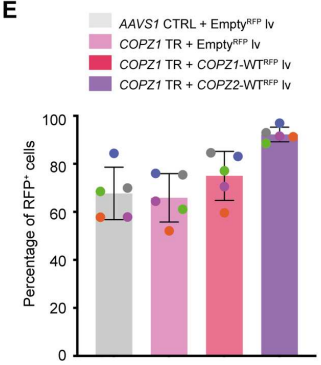

F

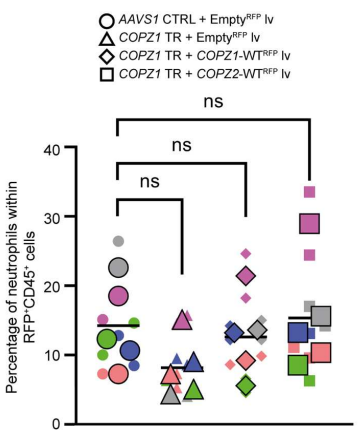

G

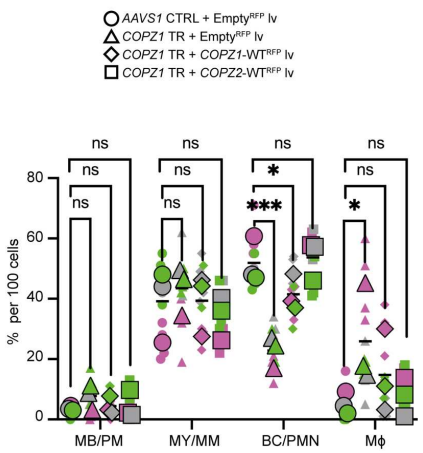

Supplemental figure 8

A

Medicament	Cell type	Dose	MOA	nlog10
BRD-A27640568	A375	10 µM	-666	15.65
VU-0418934-2	A375	10 µM	-666	15.65
BRD-K70161581	HCC515	10 µM	-666	15.65
nitazoxanide	VCAP	10 µM	Antiprotozoal	15.65
BRD-K81795824	A375	10 µM	-666	15.65
BRD-K96072942	A375	10 µM	-666	15.65
VU-0410183-2	HCC515	10 µM	-666	15.65
VU-0418934-2	HCC515	10 µM	-666	15.65
IOX2	**HELA**	**10 µM**	**HIF Inhibitor**	**15.65**
BRD-K63668467	U2OS	10 µM	-666	15.65
BRD-K70161581	A375	10 µM	-666	15.65
IOX2	**HUVEC**	**10 µM**	**HIF Inhibitor**	**15.65**
BRD-K63668467	U2OS	10 µM	-666	15.65
BRD-K61717269	A549	10 µM	-666	15.65
VU-0418939-2	HCC515	10 µM	-666	15.65
ZNF655	HEK293T	200 ng	-666	15.65
MAN2B1	HA1E		-666	15.65
VU-0418947-2	PC3	10 µM	HIF modulator	15.65

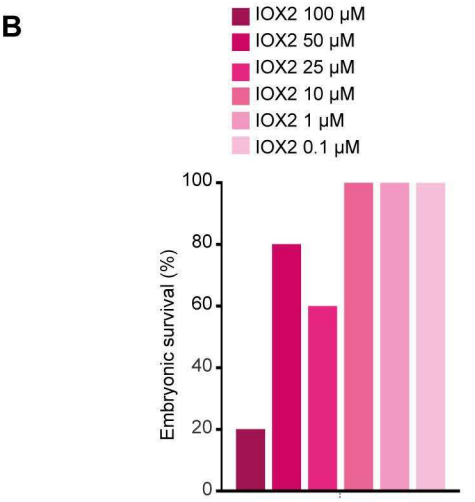

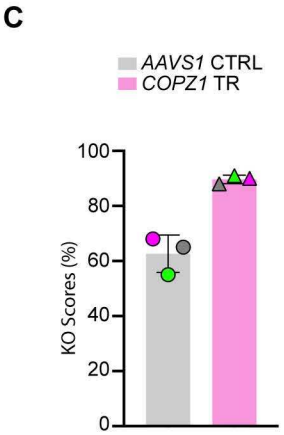

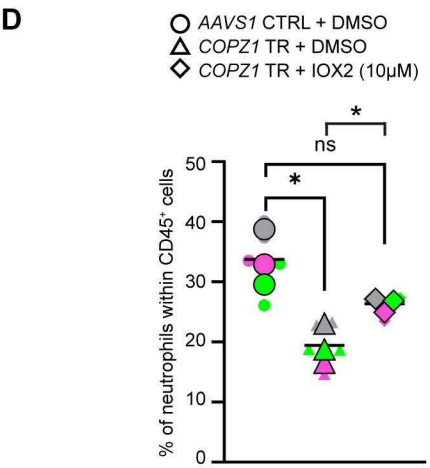

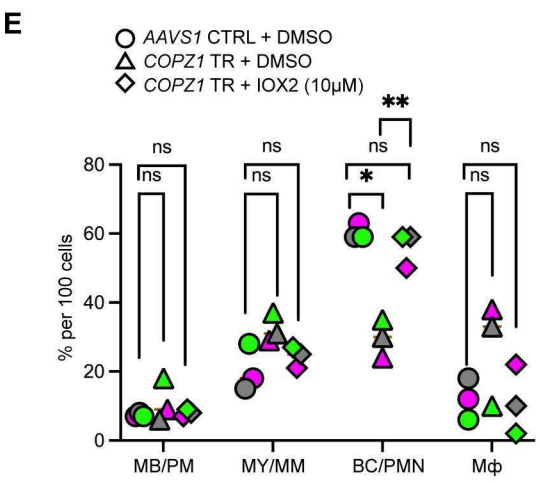

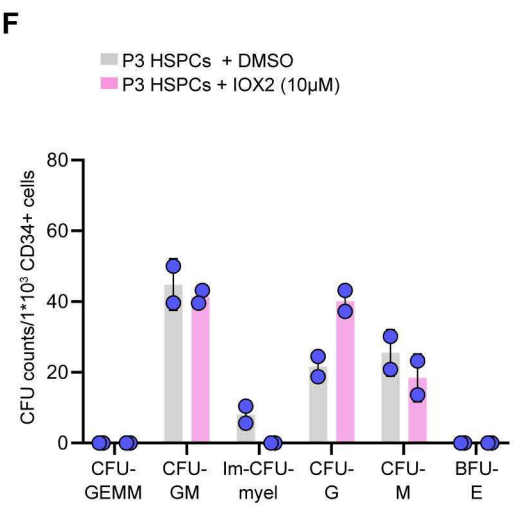

Supplemental figure 9

D. M. Nasri*, B. Dannenmann*, **L. Doll**, B. Findik, F. Bernhard, S. Kandabarau, M. Kliminakou, M. Gawaz, C. Lengerke, C. Zeidler, K. Welte, J. Skokowa, *'Flavopiridol restores granulopoiesis in experimental models of severe congenital neutropenia.' Mol Ther* (2025); 33 (6): 2851-2871.

Molecular Therapy
Original Article

Flavopiridol restores granulopoiesis in experimental models of severe congenital neutropenia

Masoud Nasri,[1,5] Benjamin Dannenmann,[1,5] Larissa Doll,[1] Betül Findik,[1] Franka Bernhard,[1] Sergey Kandabarau,[1] Maksim Klimiankou,[1] Meinrad Gawaz,[2] Claudia Lengerke,[1] Cornelia Zeidler,[1] Karl Welte,[1,3] and Julia Skokowa[1,4]

[1]Department of Oncology, Hematology, Clinical Immunology and Rheumatology, University Hospital Tuebingen, 72076 Tuebingen, Germany; [2]Department of Cardiology and Angiology, University Hospital Tuebingen, 72076 Tuebingen, Germany; [3]Department of Pediatric Hematology, Oncology, and Bone Marrow Transplantation, Children's Hospital, University Hospital Tuebingen, 72076 Tuebingen, Germany; [4]Gene and RNA Therapy Center (GRTC), Tuebingen University, 72076 Tuebingen, Germany

Severe congenital neutropenia (CN) patients require life-long treatment with recombinant human granulocyte colony-stimulating factor (rhG-CSF), but some show no response. We sought to establish a therapy for CN that targets signaling pathways causing maturation arrest of granulocytic progenitors. We developed an isogenic induced pluripotent stem cell (iPSC) *in vitro* model of CN associated with *ELANE* mutations (*ELANE*-CN) and performed an *in silico* drug repurposing analysis of the transcriptomics of iPSC-generated hematopoietic stem and progenitor cells. We identified flavopiridol, a Food and Drug Administration (FDA)-approved pan-cyclin-dependent kinase inhibitor, as a potential therapeutic. Treatment with low-dose flavopiridol rescued defective granulopoiesis in primary CD34$^+$ cells of CN patients with different inherited gene mutations *in vitro* and in two zebrafish CN models *in vivo* without any toxic effects and leading to functional granulocytes. Flavopiridol also restored granulopoiesis caused by diminished *CEBPA* expression, a known defective signaling molecule in CN. Thus, we described for the first time a potential therapy for CN with flavopiridol that could be potentially used to treat patients with different types of neutropenia.

INTRODUCTION

Severe congenital neutropenia (CN) is a heterogeneous pre-leukemia bone marrow failure syndrome characterized by an arrested granulopoiesis and the absence of mature neutrophils in the bone marrow and peripheral blood. CN can be chronically treated with recombinant human granulocyte colony-stimulating factor (rhG-CSF) by daily subcutaneous injections.[1] rhG-CSF can induce severe bone pain, splenomegaly, and vasculitis in some CN patients,[2–4] causing therapy non-compliance and underscoring the need for additional/alternative therapies. The identification of new therapies clearly requires a deep understanding of molecular disease-causing mechanisms. Among the genes mutated in CN patients are *ELANE*, encoding neutrophil elastase protein[5,6]; *HAX1*, which is translated into hematopoietic cell-specific Lyn substrate 1 (HCLS1)-associated protein 1[7]; *SRP54*, signal recognition particle 54[8]; and *JAGN1*, which encodes Jagunal homolog 1 protein.[9] CN patients with *ELANE* mutations represent the largest group.[10] We and others previously proposed key potential mechanisms of the maturation arrest of granulopoiesis in CN hematopoietic stem and progenitor cells (HSPCs).

We found that LEF-1 (lymphoid enhancer binding factor 1) and C/EBPα (CCAAT enhancer binding protein alpha)—key transcription factors with granulopoietic activity—are severely downregulated in myeloid progenitor cells of CN patients.[11,12] We also found hyperactivation of the enzyme nicotinamide phosphoribosyltransferase (NAMPT)[13] in myeloid progenitor cells of CN patients. We further demonstrated the therapeutic potential of these findings, showing that treatment with the NAMPT substrate, nicotinamide (Vitamin B3), acts through sirtuin-dependent activation of NAMPT-triggered protein deacetylation to potentiate the effects of rhG-CSF in CN.[13–15]

A major drawback in the development of new therapeutic modalities for patients with inherited bone marrow failure syndromes is limitations in available experimental models. There is a limited number of available animal models of bone marrow failure syndromes in which relevant mutated genes are expressed or lead to the disease phenotype. Mice with *Hax1*-KO or transgenic expression of CN-associated *ELANE* mutation do not have neutropenia.[16,17] Rao et al. recently described a mouse model of *ELANE*-CN by introducing truncating *ELANE* mutations into the healthy donor cord blood CD34$^+$ cells and transplanting them into the immunocompromised mice.[18] We have reported successful engraftment of *ELANE*-CN bone marrow CD34$^+$ cells in NSG mice after inhibition of *ELANE* expression.[19] Despite some

Received 22 November 2023; accepted 31 October 2024;
https://doi.org/10.1016/j.ymthe.2024.10.031.

[5]These authors contributed equally

Correspondence: Prof. Julia Skokowa, Division of Translational Oncology, Department of Hematology, Oncology, Clinical Immunology and Rheumatology, University Hospital Tuebingen, Otfried-Mueller Strasse 10, 72076 Tübingen, Germany.
E-mail: julia.skokowa@med.uni-tuebingen.de

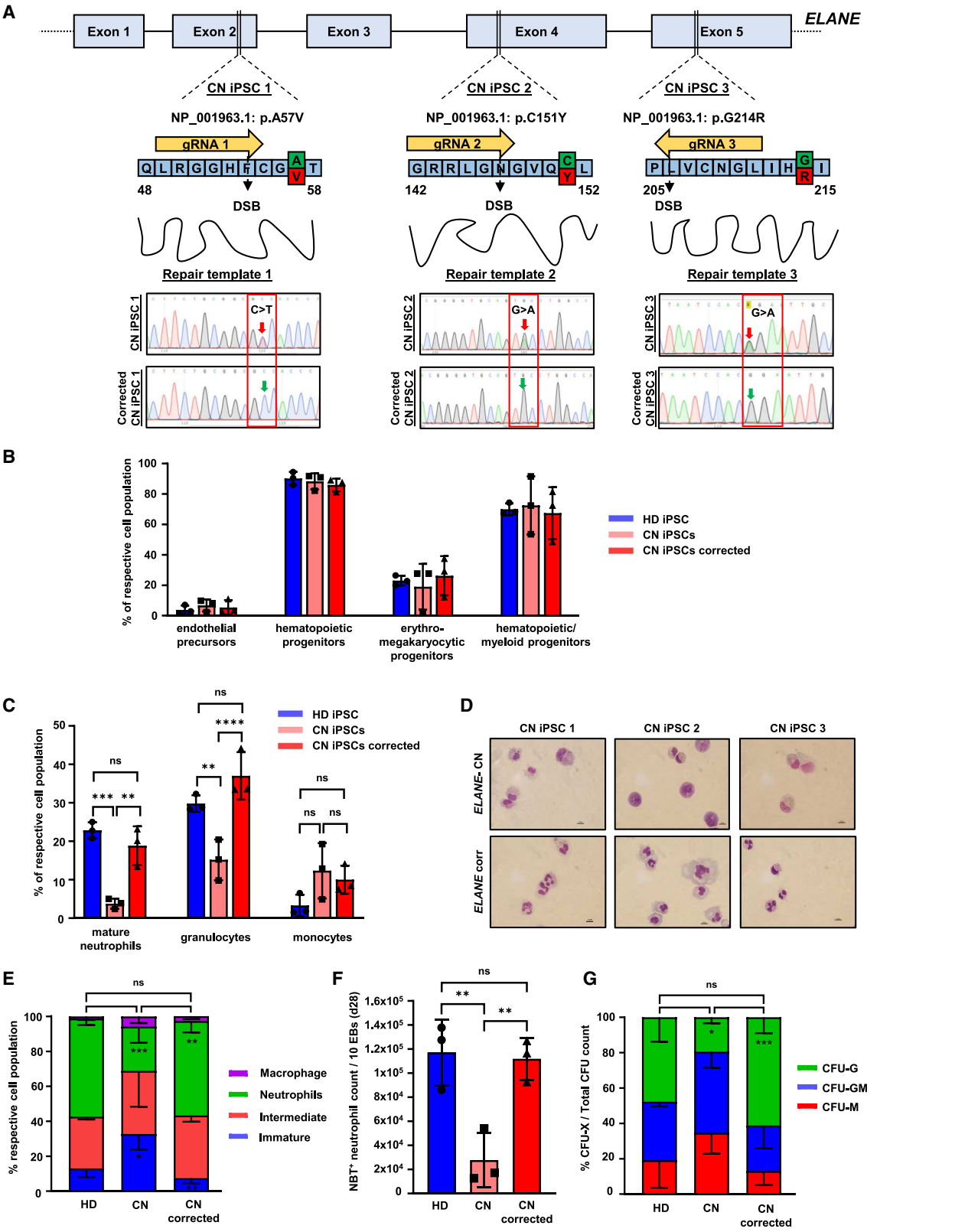

(legend on next page)

limitations, induced pluripotent stem cell (iPSC) technology has become an indispensable experimental tool in laboratories working on pre-leukemia bone marrow failure syndromes.[20] We have developed an iPSC model of CN attributable to *ELANE* mutations.[21] We also modeled stepwise leukemogenesis in *ELANE*-CN iPSCs and identified CMPD1, an inhibitor of MK2a (MAPK-activated protein kinase 2a) phosphorylation, with selective activity against CN/AML blasts.[22] Ruiz-Gutierrez et al. also modeled leukemia development in Shwachman-Diamond syndrome (SDS) in iPSCs and found that inhibition of the TGF-β pathway can rescue hematopoiesis in SDS.[23] Doulatov et al. have recently applied drug screening to the iPSC model of Diamond-Blackfan anemia (DBA) and found that SMER28, a small-molecule-inducer of autophagy, enhanced erythropoiesis in DBA.[24]

In the current study, we generated isogenic *ELANE*-CN iPSC lines, applied *in silico* drug screening analysis, and identified flavopiridol, an FDA-approved drug, to efficiently restore granulopoiesis in iPSC-derived and primary hematopoietic stem and progenitor cells (HSPCs) from *ELANE*-CN patients and primary HSPCs from CN patients carrying *ELANE, HAX1, JAGN1,* or *SRP54* mutations. Zebrafish embryos with genetic defects in *hax1* or *jagn1b* also responded to flavopiridol therapy.

RESULTS

CRISPR-Cas9-based correction of *ELANE* mutations restores granulocytic differentiation of *ELANE*-CN iPSCs

We first established a pipeline for CRISPR-Cas9-based correction of CN-associated inherited *ELANE* mutations in *ELANE*-CN patient-derived iPSCs.[25] Using this pipeline, we generated isogenic counterparts of three *ELANE*-CN iPSC lines: *ELANE*-CN iPSC 1: p.A57V, *ELANE*-CN iPSC 2: p.C151Y, *ELANE*-CN iPSC 3: p.G214R (Figure 1A), one isogenic clone per iPSC line. To investigate whether *ELANE* correction caused any chromosomal copy number alterations or other off-target effects in iPSCs, we performed shallow whole-genome sequencing (sWGS) of all three corrected iPSC lines. Analysis of the sequencing data using the quantitative DNA sequencing for chromosomal aberrations (QDNAseq) pipeline[26] revealed no detectable DNA copy number alterations in the edited *ELANE*-CN iPSC lines (Figure S1A). Furthermore, analysis of the top 50 predicted off-target sites for each guide RNA (gRNA) used, identified computationally using the Benchling platform and the algorithm published by Hsu et al.,[27] revealed no evidence of off-target mutations at the sWGS-covered sites (Table S1). The *ELANE*-CN iPSCs used have been previously characterized.[22,28] We selected hot-spot *ELANE* mutations that are strongly associated with lack of or poor response to G-CSF and leukemogenic transformation.[10]

The isogenic iPSC lines were differentiated toward neutrophils *in vitro* for 28 days. Characterization of hematopoietic progenitor cells at day 14 of iPSC differentiation by flow cytometry showed no significant changes in corrected iPSC lines (*ELANE*-CN corr) relative to the respective CN patient iPSC lines (*ELANE*-CN), including $CD34^+CD45^+$ HSPCs (Figure 1B). We next compared terminal myeloid differentiation in *ELANE*-CN corr and *ELANE*-CN cell lines by flow cytometry-based analysis of surface markers for mature neutrophils ($CD15^+CD16^+CD45^+$) and granulocytes ($CD15^+CD11b^{+-}CD45^+$) as well as morphological analyses of cytospin preparations of May-Grunwald-Giemsa-stained cells harvested at day 28 of differentiation (Figures 1C–1E). These analyses demonstrated successful restoration of neutrophilic differentiation in iPSC lines expressing the corrected *ELANE* gene (Figure 1C). An evaluation of superoxide anion production using nitro-blue tetrazolium test (NBT) assay further demonstrated the functionality of *ELANE*-CN corr iPSC-derived neutrophils (Figure 1F). Colony-forming unit (CFU) assay for iPSC-derived $CD34^+CD45^+$ cells further displayed increased granulocytic differentiation (CFU-G) and reduced macrophage differentiation (CFU-M) after *ELANE* mutation correction, comparable to healthy donor (HD) levels, for all three CN patients (Figure 1G). We previously showed upregulation of the unfolded protein response (UPR) in iPSC-derived $CD34^+CD45^+$ cells from CN patients compared with those from HDs.[21] Here, we demonstrated a significant reduction of mRNA expression of *ATF4*, one of the UPR

Figure 1. Hematopoietic differentiation of *ELANE*-CN and *ELANE*-CN corrected iPSC lines

(A) Scheme of CRISPR-Cas9 RNP-mediated *ELANE* mutation correction in *ELANE*-CN iPSC 1–3 lines. The gRNAs highlight the position of the designed guide RNA for each subsequent correction strategy and arrows indicate double-strand break (DSB) position. Repair templates represent the single-stranded oligodeoxynucleotides (ssODN) carrying the *ELANE* gene reference sequence for each subsequent correction strategy. Sanger sequencing traces of edited regions in *ELANE*-CN and *ELANE*-CN mutation-corrected (*ELANE*-CN corr) iPSC lines are indicated. (B) Flow cytometry analysis of iPSC-derived immature hematopoietic cell populations: endothelial precursors ($CD34^+KDR^+$ cells), hematopoietic progenitors ($CD34^+CD43^+$ cells), erythro-megakaryocytic progenitors ($CD41a^+CD235a^+CD45^-$ cells) and hematopoietic/myeloid progenitors ($CD34^+CD45^+$ cells) for *HD*, *ELANE*-CN 1–3, and *ELANE*-CN 1–3 corr iPSC-derived cells at day 14 of iPSC differentiation. Data are represented as mean ± SD from three independent experiments, each in duplicate. All group comparisons were not significant. (C) Flow cytometry analysis of iPSC-derived cell populations of mature neutrophils ($CD15^+CD16^+CD45^+$ cells), granulocytes ($CD15^+CD11b^+CD45^+$ cells), and monocytes ($CD14^+CD11b^+CD45^+$ cells) for HD, *ELANE*-CN 1–3 and *ELANE*-CN 1–3 corr iPSC-derived cells at day 28 of hematopoietic iPSC differentiation. Data are represented as mean ± SD from three independent experiments, each in duplicate. Group comparisons are indicated, $^{**}p < 0.01$, $^{***}p < 0.001$, $^{****}p < 0.0001$, ns: not significant. (D) Representative cytospin images of iPSC-derived hematopoietic cells on day 28 of differentiation stained with May-Grunwald-Giemsa are shown for indicated iPSC lines. Scale bar represents 10 μm. (E) Analysis of May-Grunwald-Giemsa stained cytospins of cells isolated at day 28 of iPSC differentiation of indicated iPSC lines. The morphology of more than 100 cells was analyzed for each cytospin slide. Percentages of respective cell populations are shown. Data are represented as mean ± SD from three independent experiments, each in duplicate, including group comparisons, $^{*}p < 0.05$, $^{**}p < 0.01$, $^{***}p < 0.001$, ns: not significant (for all CFU types). (F) NBT assay of neutrophils derived from indicated iPSC lines. Counts of NBT^+ neutrophils produced from 10 EBs/sample on day 28 are shown. Data are represented as mean ± SD from three independent experiments, each in duplicate, including group comparisons, $^{**}p < 0.01$, ns: not significant. (G) CFU assay of HD, *ELANE*-CN 1–3, and *ELANE*-CN 1–3 corr iPSC-derived $CD34^+CD45^+$ cells isolated at day 14 of iPSC differentiation. Percentages of CFU types are shown for indicated iPSC lines. Data are represented as mean ± SD from three independent experiments, each in duplicate, including group comparisons, $^{*}p < 0.05$, $^{***}p < 0.001$, ns: not significant (for all CFU types).

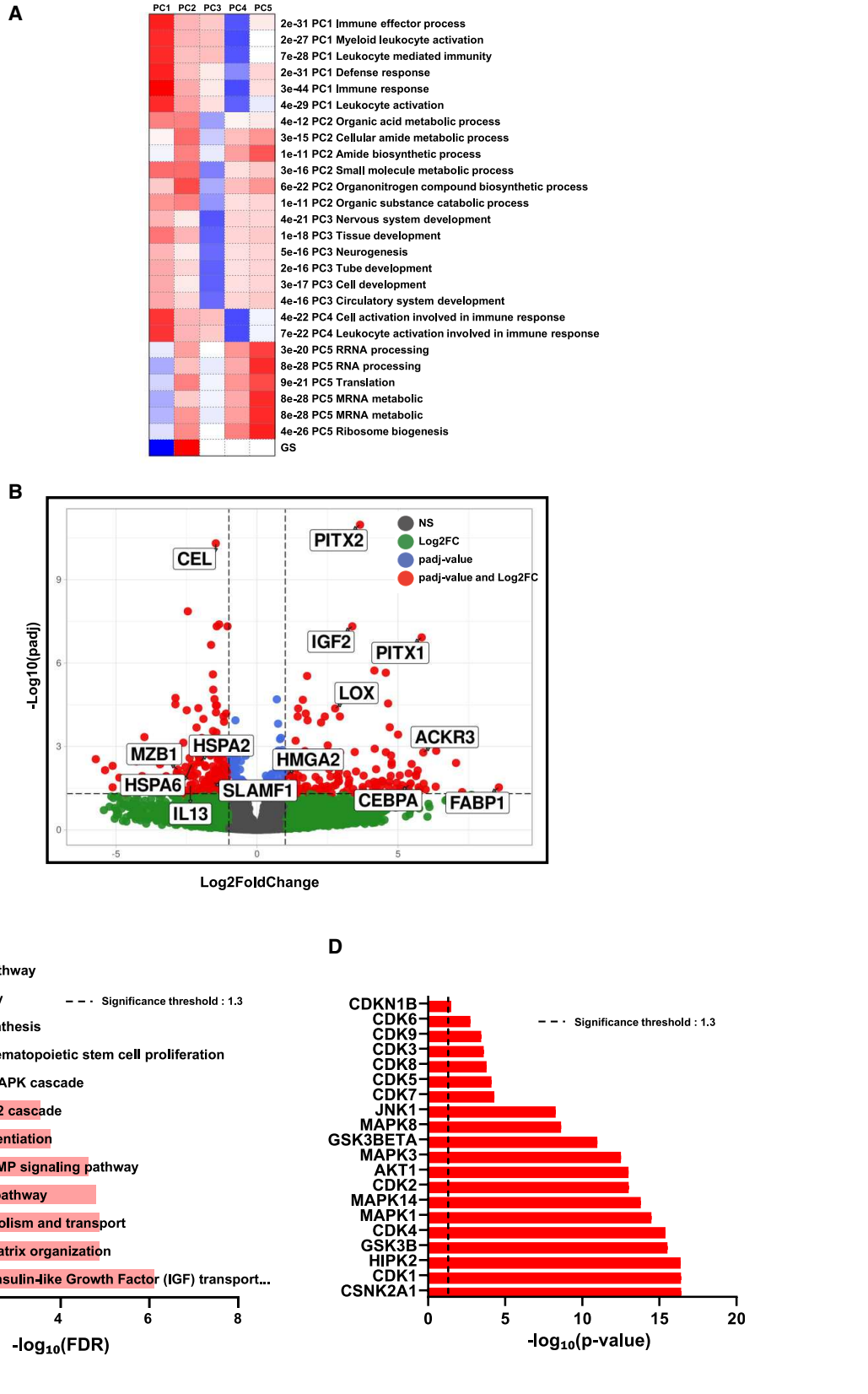

(legend on next page)

effectors, in iPSC-derived $CD34^+CD45^+$ cells derived from all three isogenic iPSC lines. Other UPR-related genes were regulated mutation-specific, in line with our previous observation[29] (Figure S1B). Taken together, these results demonstrate the successful establishment of an isogenic iPSC model of *ELANE*-CN.

Identification of signaling pathways dysregulated by *ELANE* mutations

We next performed transcriptome profiling of isogenic CN iPSC-derived $CD34^+CD45^+$ HSPCs isolated on day 14 of hematopoietic differentiation with the goal of gaining insight into disease pathomechanisms and exploring potentially druggable pathways. Among the highly and significantly enriched biological events revealed by unsupervised pathway analysis of PCA (principal-component analysis) rotation were "myeloid leukocyte activation," "leukocyte-mediated immunity," "defense response," and "leukocyte activation" (Figure 2A). To conduct multiple supervised analyses, we extracted differentially expressed genes (DEGs) between CN and CN-corrected hematopoietic progenitor cells (Figure 2B; Table S2). Among these DEGs, 150 genes, including *CEBPA, PITX2*, *IGF2,* and *LOX*, were significantly upregulated upon correction of *ELANE* mutations, whereas 188 genes, including *CEL, HSPA2, HSPA6, IL13,* and *SLAMF1*, were significantly downregulated. We validated selected DEGs by performing quantitative reverse transcription-polymerase chain reaction (RT-qPCR) on selected genes based on their potential or known role in hematopoiesis or granulopoiesis (Figure S2A). RT-qPCR results confirmed most of the DEGs identified by RNA-seq analysis and further showed that expression levels of selected genes were *ELANE* mutation-specific. Functional enrichment of upregulated genes among the list of DEGs using the gProfiler web server[30] (database version: e109_eg56_p17_1d3191d) identified the signaling pathways, "regulation of insulin-like growth factor (IGF) transport and uptake by insulin-like growth factor binding proteins (IGFBPs)," "retinoid metabolism and transport," "Wnt signaling pathway," and "regulation of MAPK cascade" as being activated upon correction of *ELANE* mutations in CN iPSCs (Figure 2C). A pathway enrichment analysis of downregulated genes returned no significant results (data not shown). Representation of functional interactions between DEGs using the reactome functional interaction (FI) network,[31] a manually curated, pathway-based protein functional interaction network that covers over 60% of human proteins, showed a highly connected interaction network between DEGs, including *CEBPA* interactions with *APOB*, *TF*, *CEL*, and *IGF2* (Figure S2B). To computationally predict the upstream regulatory network of these DEGs, we performed an eXpression2Kinases (X2K) analysis.[32] This X2K analysis showed that cyclin-dependent kinases (CDKs) are major players upstream of the DEGs (Figure 2D).

L1000CDS-based transcriptomics analysis reveals flavopiridol as a potential inducer of granulopoiesis in CN

The DEG signature, which considers the difference between HSPCs derived from isogenic *ELANE*-CN iPSC lines, was submitted to the LINCS L1000 Characteristic Direction Signatures (L1000CDS) search engine[33] and Connectivity Map (CMAP) database.[34] Based on our analyses, we evaluated all proposed small molecules (Table S3) and selected nine candidates for further evaluation. These molecules were chosen based on their potential mechanisms of action connected to hematopoiesis, granulopoiesis, and signaling systems known to be affected in CN HSPCs (Figure 3A). We first screened selected small molecules for their effects on *in vitro* granulopoiesis in the *ELANE*-CN iPSC 1 line using CFU assays. The concentrations of small molecules were chosen according to published half-maximal inhibitory concentration (IC_{50}) values from individual datasheets. Screening results showed that 40 nM flavopiridol, an FDA-approved pan-CDK inhibitor, markedly restored granulocytic differentiation (Figure 3B). To further validate screening results, we tested flavopiridol on $CD34^+CD45^+$ cells derived from *ELANE*-CN iPSC lines 1–3 in CFU assays. Notably, this treatment restored granulopoiesis in all three *ELANE*-CN iPSCs, significantly increasing CFU-granulocytes (CFU-Gs) and significantly decreasing CFU-macrophages (CFU-Ms) (Figure 3C). Flavopiridol treatment was as efficient as *ELANE* mutation correction (Figure S3).

Flavopiridol enhances granulocytic differentiation of healthy donor HSPCs

To assess the potential toxicity of 40 nM flavopiridol on primary healthy $CD34^+$ cells and polymorphonuclear neutrophils (PMNs), we treated them with either 40 nM flavopiridol or vehicle control (DMSO) for 48 h or 3 h, respectively and assessed apoptosis and cell viability. We found no difference between groups (Figures 4A, 4B, and S4A). Real-time monitoring of $CD34^+$ cell proliferation over 4 days using IncuCyte-based live cell imaging also revealed comparable proliferation rates between the flavopiridol and DMSO-treated groups (Figure S4B). To investigate the effects of flavopiridol on *in vitro* granulopoiesis under normal physiological conditions, we treated healthy $CD34^+$ cells with 40 nM flavopiridol or DMSO and performed CFU assay and granulocytic liquid culture differentiation (LCD). We

Figure 2. RNA-seq analysis of *ELANE*-CN and *ELANE*-CN corrected iPSC-derived $CD34^+CD45^+$ cells

(A) Pathway analysis of principal-component analysis (PCA) rotation used to identify biological pathways that are significantly enriched in genes that contribute to the variation captured by the principal components (PCs) in a PCA. PCA loadings, as input for gene expression data, were used to run pathway analysis with the PGSEA package. These loadings represent the contribution of each gene to the variation explained by the corresponding PC. For each pathway, the PAGE algorithm, which performs a one-sample t test on each gene set (GS) in the biological processes branch of Gene Ontology (GO), was applied. The adjusted *p* values are used to rank the pathways for each of the first five PCs. The pathways are labeled with FDR first, followed by the principal components (PC1, PC2, and so on until PC5). The color indicates whether the genes in a pathway are predominantly upregulated (red) or downregulated (blue) in samples associated with the PC. (B) Volcano plot showing differentially expressed genes (DEGs) upon *ELANE* correction in *ELANE*-CN iPSC 1–3. The x- axis shows the log2 fold change (magnitude of change), and the y-axis shows the −log10 adjusted *p* value (statistical significance). Colors represent the significance of the genes in terms of *p* value and log2 fold change. Selected genes are annotated. (C) Functional enrichment analysis using a list of significantly upregulated genes in CN iPSCs after *ELANE* correction. Data are displayed as −log10 adjusted *p* value (FDR). (D) Expression to Kinases (X2K) prediction analysis of the upstream regulatory network of DEGs. Data are displayed as −log10 adjusted *p* value.

A

Nr.	Perturbation	Reported mechanism of action	Gene expression signature database	Score	FDA approval status
1	**VX745 (S1458/Neflamapimod)**	p38α inhibitor	LINCS	0.0336	-
2	**SL-327**	MEK1/2 inhibitor	LINCS	0.0308	-
3	**Importazole**	Importin-β inhibitor	LINCS	0.0476	-
4	**SAHA (Vorinostat)**	HDAC inhibitor	LINCS	0.0420	FDA-approved
5	**Lapatinib**	EGFR and ErbB2 inhibitor	LINCS	0.0364	FDA-approved
6	**Flavopiridol (Alvocidib)**	pan-CDK inhibitor (CDKs 1,2,4,5,6,9)	LINCS	0.0336	FDA-approved
7	**MPEP**	mGlu5 receptor inhibitor	CMap	0.3	-
8	**Zelavespib (PU-H71)**	HSP90 inhibitor	CMap	0.56	-
9	**Quiflapon (MK-0591)**	FLAP inhibitor, leukotriene biosynthesis inhibitor	LINCS	0.0392	-

B

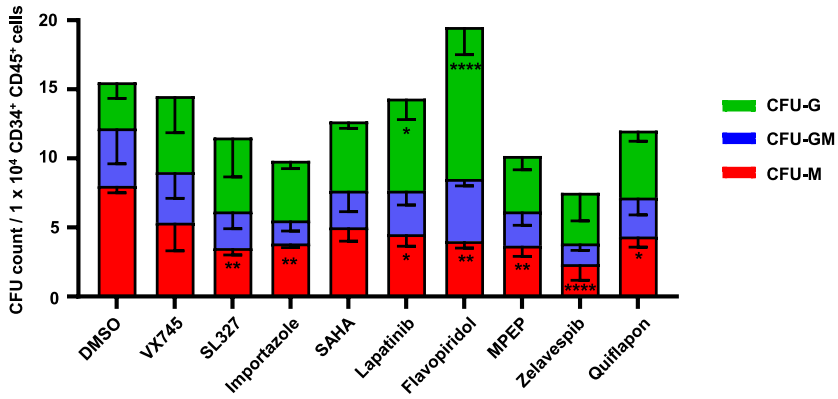

C

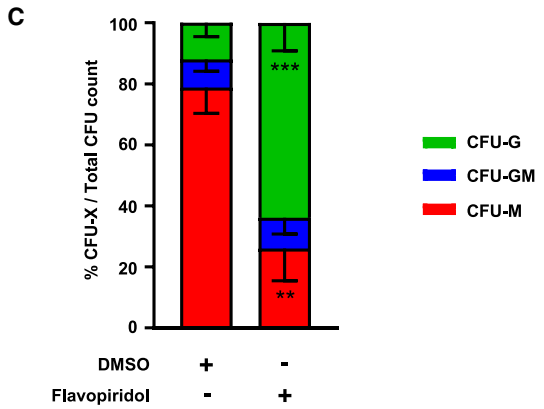

(legend on next page)

observed a significant increase in granulocyte colony-forming unit (CFU-G) numbers in the flavopiridol-treated group compared with DMSO (Figure 4C). Consistent with this, LCD assays also revealed a significant enhancement of granulocytic differentiation upon flavopiridol treatment (Figures 4D and S4C). Apoptosis and viability of *in vitro*-generated neutrophils were comparable between flavopiridol and DMSO groups (Figures S4D and S4E). In addition, the ability of *in vitro*-generated neutrophils to phagocytize pHrodo green *S. aureus* bioparticles (Figure 4E) and to generate reactive oxygen species (ROS) in response to formylmethionyl-leucyl-phenylalanine (fMLP) stimulation was similar between flavopiridol and DMSO-treated samples (Figure 4F).

We further performed RNA-seq of neutrophils derived from $CD34^+$ cells from four healthy donors (HDs 1–4) differentiated with either 40 nM flavopiridol or DMSO. DEGs were identified using the DESeq2 algorithm between the DMSO and flavopiridol groups (Figure 5A; Table S4). A total of 438 genes, including neutrophil-related genes *DEFA4, DEFA1, PRTN3, AZU1, CTSG, ELANE,* and *CEBPE* were significantly upregulated upon 40 nM flavopiridol treatment. In contrast, 732 genes, including inflammation-related genes *CPA3, IL1RL1, HPGDS, PTGDR2, PTGER3;* immature stem cell-related genes *TAL1, PROM1, FLT3;* and the negative regulator of granulopoiesis *SOCS3*, were significantly downregulated. The gProfiler Functional enrichment[30] (database version: e111_eg58_p18_f463989d) analysis of upregulated DEGs revealed enrichment in pathways related to "extracellular matrix organization," "neutrophil-mediated immunity," "regulation of interleukin-1 production," "myeloid leukocyte differentiation," and "positive regulation of p38 MAPK cascade" (Figure 5B). Conversely, downregulated DEGs were enriched in pathways associated with "inflammatory response," "leukocyte apoptotic process," and "regulation of response to stress" (Figure 5C). Subsequently, using gene set enrichment analysis (GSEA) on transcriptomic data, as described by Subramanian et al. and Mootha et al.,[35,36] we identified significant enrichment of gene sets related to neutrophil degranulation and downregulation of pathways associated with inflammatory response, interferon gamma response, tumor necrosis factor (TNF)α signaling via nuclear factor (NF)-κB, Myc target genes, and apoptosis (Figure 5D).

Flavopiridol restores granulopoiesis in HSPCs from CN patients with different inherited gene mutations

To further evaluate the universality of flavopiridol as a treatment option for CN patients regardless of the underlying genetic cause, we treated primary bone marrow $CD34^+$ HSPCs from two *ELANE*-CN patients (CN 1: NP_001963.1, p.Val101Glu; CN 2: NP_001963.1, p.Pro139Leu), one *HAX1*-CN patient (CN 3: NP_006109.2, p.W44X), one *JAGN1*-CN patient (CN 4: NP_115881.3, p.His44Tyr), and one *SRP54*-CN patient (CN 5: NP_003127.1, pT117del) with 40 nM of flavopiridol and performed CFU and LCD assays. CFU assays showed significantly elevated levels of CFU-G in all CN groups treated with flavopiridol (Figures 6A and S5A). In line with this, flavopiridol restored granulopoiesis in $CD34^+$ HSPCs of all studied CN patients compared with the DMSO-treated group, as evidenced by the elevated numbers of mature neutrophils ($CD45^+CD15^+CD16^+$) (Figure 6B). Moreover, a morphological examination of cytospin preparations of mature granulocytes generated on day 14 of differentiation also showed restoration of granulopoiesis in all studied CN patients (Figures 6C and 6D). Interestingly, mRNA expression of the UPR-related genes *DDIT3, HSPA5, ATF4,* and *ATF6*, known to be activated in CN, remained unchanged in the flavopiridol and DMSO-treated cells (Figure S5B).

Flavopiridol induces granulocytic differentiation of *CEBPA*-deficient HSPCs

We next investigated the mechanism underlying flavopiridol's restorative effects on granulopoiesis in CN. We previously demonstrated severely reduced expression levels of the myeloid-specific transcription factor C/EBPα in myeloid progenitor cells of CN patients.[11] C/EBPα plays a key role in activating granulocytic differentiation of HSPCs,[37–41] and severely reduced C/EBPα expression in CN may be an essential reason for the maturation arrest of granulopoiesis in these patients. C/EBPα is known to arrest hematopoietic cell proliferation through direct inhibition of CDK2 and CDK4, thereby inducing myeloid differentiation.[42] Notably, flavopiridol also inhibits CDK2 and CDK4, among other CDKs.[43] We found that flavopiridol treatment significantly suppressed mRNA expression of the CDK2/4 target genes, *CCND2* (Cyclin D2) and *RBL1* (Retinoblastoma-like protein 1),[44] in myeloid cells generated on day 14 of LCD for five CN patients presented in Figure 6 compared with DMSO-treated samples (Figure S5C). We hypothesized that, in CN HSPCs, expressing diminished levels of C/EBPα, CDKs cannot be inhibited, and granulocytic differentiation cannot be initiated. Accordingly, treatment of CN HSPCs with flavopiridol would promote granulopoiesis by mimicking the inhibitory activity of C/EBPα on CDKs. To test this hypothesis, we re-capitulated CN-specific reduction of C/EBPα in HSPCs by interrupting its expression using CRISPR-Cas9 gene editing targeting the p42 isoform of C/EBPα in primary healthy donor $CD34^+$ cells by using a ribonucleoprotein complex of gRNA and HiFi spCas9, referred as *CEBPA* knockout (KO) (Figure 7A). Gene-edited HSPCs exhibited an INDEL efficiency of 58%–79%, as assessed by DECODR (Deconvolution of Complex DNA Repair)[45] analysis of Sanger sequencing of edited cells on day 0 (48 h post electroporation and at the time when LCD was started) and day 14 (the endpoint of the LCD) (Figures 7B and S6). As

Figure 3. Flavopiridol induces granulopoiesis of CN HSPCs *in vitro*

(A) Selected small molecules from L1000CDS and CMAP databases that mimic the gene expression pattern of *ELANE*-CN iPSC-derived $CD34^+CD45^+$ cells after mutation correction. (B) CFU assay of *ELANE*-CN p.A57V iPSC-derived $CD34^+CD45^+$ cells isolated at day 14 of iPSC differentiation. Small molecules were added at plating of CFU assay. CFU counts are shown. Data are represented as mean ± SD of three independent experiments, each in duplicate. The significant difference between all small molecules and DMSO control is indicated, $^*p < 0.05$, $^{**}p < 0.01$, $^{****}p < 0.0001$. (C) Analysis of CFU assay of *ELANE*-CN 1–3 iPSC-derived $CD34^+CD45^+$ cells isolated at day 14 of iPSC differentiation in the presence of flavopiridol (40 nM) or DMSO (0.1%). Percentages of CFU types are shown for indicated iPSC lines. Data are represented as mean ± SD from three independent experiments, each in duplicate. The significant difference between groups is indicated, $^{**}p < 0.01$, $^{***}p < 0.001$.

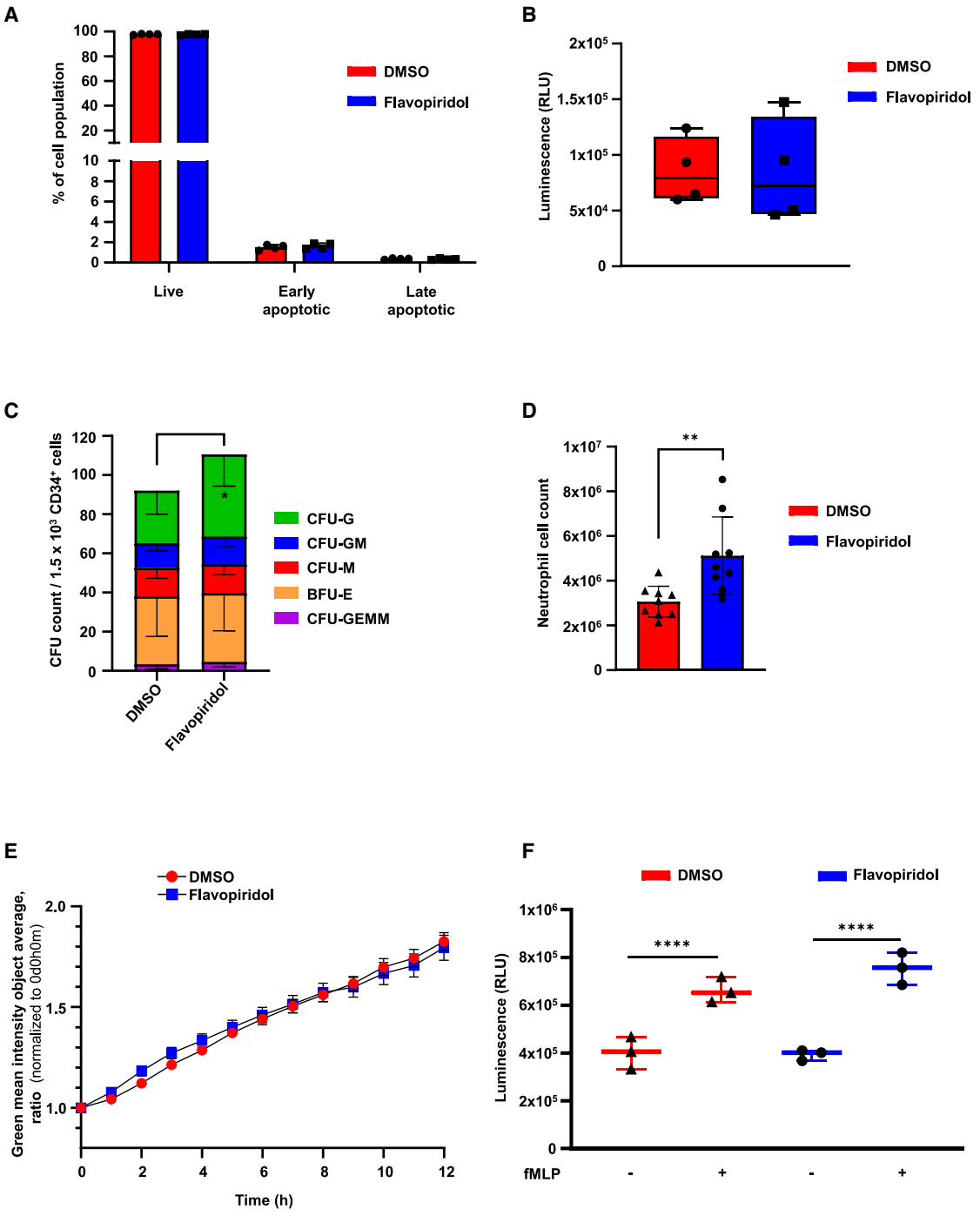

Figure 4. Flavopiridol treatment enhanced granulocytic differentiation of primary CD34⁺ HSPCs of healthy controls

(A) Annexin V apoptosis assay to assess live (Annexin V^-/$DAPI^-$), early apoptotic (Annexin V^+/$DAPI^-$), and late apoptotic (Annexin V^+/$DAPI^+$) populations after 48 h of culture of primary $CD34^+$ HSPCs from four healthy controls (HD 1–4) treated with flavopiridol (40 nM) or DMSO (0.1%). Data are represented as mean ± SD from four healthy donors, each in duplicate. (B) Viability of primary $CD34^+$ HSPCs from four healthy controls (HD 1–4) treated with flavopiridol (40 nM) or DMSO (0.1%) for 48 h measured using RealTime-Glo MT Cell Viability Assay. Data are represented as mean ± SD from four healthy donors, each in triplicate. (C) CFU assay of $CD34^+$ HSPCs isolated from nine healthy donors (HD 1–9) and treated with flavopiridol (40 nM) or DMSO (0.1%). Counts of CFU types are shown. Data are represented as mean ± SD of nine healthy donors, each in duplicate. The significant difference between groups is indicated, *$p < 0.05$. (D) Absolute counts of mature neutrophils ($CD15^+CD16^+CD45^+$ cells) derived from nine HD $CD34^+$ HSPCs (HD 1–9) at day 14 of liquid culture differentiation (LCD) treated with flavopiridol (40 nM) or DMSO (0.1%). Data are represented as mean ± SD from nine

(legend continued on next page)

expected, *CEBPA* KO led to a reduction of CFU-G levels and LCD-generated mature neutrophils (flow cytometry analysis of $CD45^+CD15^+CD16^+$ cells and morphological assessment) compared with mock-electroporated cells (Figures 7C–7F). Interestingly, flavopiridol treatment of *CEBPA* KO cells led to a significant increase of CFU-G formation capacity and LCD-generated mature neutrophil numbers, as compared with DMSO-treated samples (Figures 7C–7F). Absolute CFU-G numbers did not reach that of control cells, which can be explained by the fact that we induced *CEBPA* knockout but not *CEBPA* downregulation as observed in CN HSPCs.[11] An elevated number of BFU-E colonies in all studied groups in this experiment can be explained by the usage of cord blood $CD34^+$ cells, which generally have stronger erythroid differentiation potential, as compared with bone marrow or iPSC-derived $CD34^+$ cells.[46]

To identify if the pan-CDK inhibition activity of flavopiridol is needed to rescue granulopoiesis or if the inhibition of specific CDKs will have a similar effect, we selected specific small molecule inhibitors for CDK1 (CDK1i: Ro-3306, from MedChemExpress [MCE]), CDK2 (CDK2i: AUZ 454, from MCE), and CDK4/6 (CDK4/6i: Ribociclib, from MCE) and tested their IC50 values indicated on respective datasheets on the proliferation of cord blood-derived $CD34^+$ cells using IncuCyte. All inhibitors did not show any significant change of $CD34^+$ cell proliferation rate compared with DMSO control for three healthy donors (Figure S7A). Next, we tested these small molecules in CFU assay of CN1-iPSC-derived $CD34^+$ cells. Only the CDK2 inhibitor AUZ 454 led to a significant increase of CFU-G colonies compared with DMSO control; however, to a significantly lower extent than flavopiridol, and the total CFU count was lower than for flavopiridol as well (Figure S7B).

Flavopiridol rescues defective granulopoiesis in *jagn1b*-KO as well as *hax1*-KD and *cebpa*-KD zebrafish embryos *in vivo*

Finally, we studied the effect of flavopiridol on granulopoiesis *in vivo* in zebrafish models. First, we tested the toxicity of flavopiridol on zebrafish embryos and found that treatment with flavopiridol at concentrations up to 10 μM diluted in zebrafish media was not toxic (data not shown). To study the effect of flavopiridol on neutrophils, we treated zebrafish embryos from the transgenic myeloid cell reporter line Tg (mpo:*gfp*) with flavopiridol or DMSO for 2 days and quantified the mpo:gfp^+-neutrophils at 72 h postfertilization (hpf). (Figure 8A) We saw no negative effect on neutrophil counts after flavopiridol treatment when compared with DMSO-treated embryos (Figure 8B). We next evaluated the effects of flavopiridol on HSPCs by analyzing the expression pattern of the HSPC-specific marker gene *cmyb*, using whole mount *in situ* hybridization (WISH) at 72 hpf, after 2 days of flavopiridol treatment (Figure 8A). Moreover, we quantified the cells, after 1 day of flavopiridol treatment, in the transgenic reporter line Tg (cd41:*gfp*), where at early stages of development HSPCs are cd41:gfp^+, (Figure S8A). Both approaches showed that flavopiridol at a dose of 10 μM, the highest non-toxic dose, did not affect the total number of HSPCs compared with DMSO-treated control embryos (Figures 8C and S8B).

We then tested whether flavopiridol restored granulopoiesis in a CN setting *in vivo* using two zebrafish models of CN: *hax1*-knockdown (KD) zebrafish embryos—an *in vivo HAX1*-CN model[47] and *jagn1b*-knockout zebrafish embryos (*jagn1b*-KO)—an *in vivo JAGN1*-CN model[48] (Figures 8D and S8C). We could not recapitulate the *ELANE*-CN phenotype in zebrafish because this species lacks the *elane* gene. We found that treatment of *hax1*-KD and *jagn1b*-KO zebrafish embryos with flavopiridol for 2 days significantly rescued the number of neutrophils (mpo:gfp^+ cells), restoring them to a level similar to that in wild-type controls (Figures 8E and 8F). In previous investigations, we have already shown that neither the *hax1* knockdown nor the *jagn1b* knockout affect HSPCs.[47,48] In this study we showed that flavopiridol treatment of *hax1*-KD or *jagn1b*-KO zebrafish embryos also had no effect on HSPCs by analyzing the *cmyb* expression pattern using WISH (Figures S8D–S8F). Importantly, flavopiridol was also able to completely restore granulopoiesis in *cebpa*-KD zebrafish embryos compared with that in the DMSO-treated wild-type group (Figure 8G). These data further underscore the potential of flavopiridol to rescue defective granulopoiesis in CN independent of genetic background.

DISCUSSION

We applied an isogenic model of *ELANE*-CN to identify the pathological mechanisms of defective granulopoiesis downstream of *ELANE* mutations. We assume that, by identifying druggable mechanisms of neutropenia downstream of *ELANE* mutations, we can potentially generalize this finding to patients with other CN-causing genetic defects. Our previous investigations consistently identified severely reduced expression of *LEF1*[11,49] and *CEBPA*[11] and elevated levels of *NAMPT*[13] or phosphorylated *STAT5A*[50] in myeloid progenitor cells of CN patients with e.g. *ELANE*, or *HAX1* mutations. This is in line with the shared morphological defects—maturation arrest of granulopoiesis at the stage of promyelocytes/myelocytes—and clinical picture—response to G-CSF, types of frequent bacterial infections and frequency of leukemogenic transformation—in these groups of patients.[51] Our current expression analyses confirmed the inhibition of *CEBPA* levels by mutated *ELANE*. Correction of *ELANE* mutations also caused a diverse array of changes in gene expression, exemplified by upregulation of mRNA for, e.g., *PITX1*, *PITX2*, *IGF2*, *FABP1,* and *LOX* and inhibition of mRNA expression for, e.g., *HSPA2*, *HSPA6*,

healthy donors, each in duplicate. The significant difference between groups is indicated, $^{**}p < 0.01$. (E) Phagocytosis kinetic of pHrodo green *S. aureus* bioparticles by *in vitro* differentiated neutrophils derived from $CD34^+$ HSPCs of four healthy donors (HD 1–4) at day 14 of differentiation treated with flavopiridol (40 nM) or DMSO (0.1%), using IncuCyte ZOOM System. Data represent means ± SD from four healthy donors, each in duplicates. (F) Hydrogen peroxide (H_2O_2) reactive oxygen species (ROS) levels measured in three *in vitro* differentiated healthy donors' (HD 1–3) neutrophils treated with flavopiridol (40 nM) or DMSO (0.1%) after stimulation with formylmethionine-leucyl-phenylalanine (fMLP) for 30 min. Data represent means ± SD from three healthy donors, each in duplicate. The significant difference between groups is indicated, $^{****}p \leq 0.0001$.

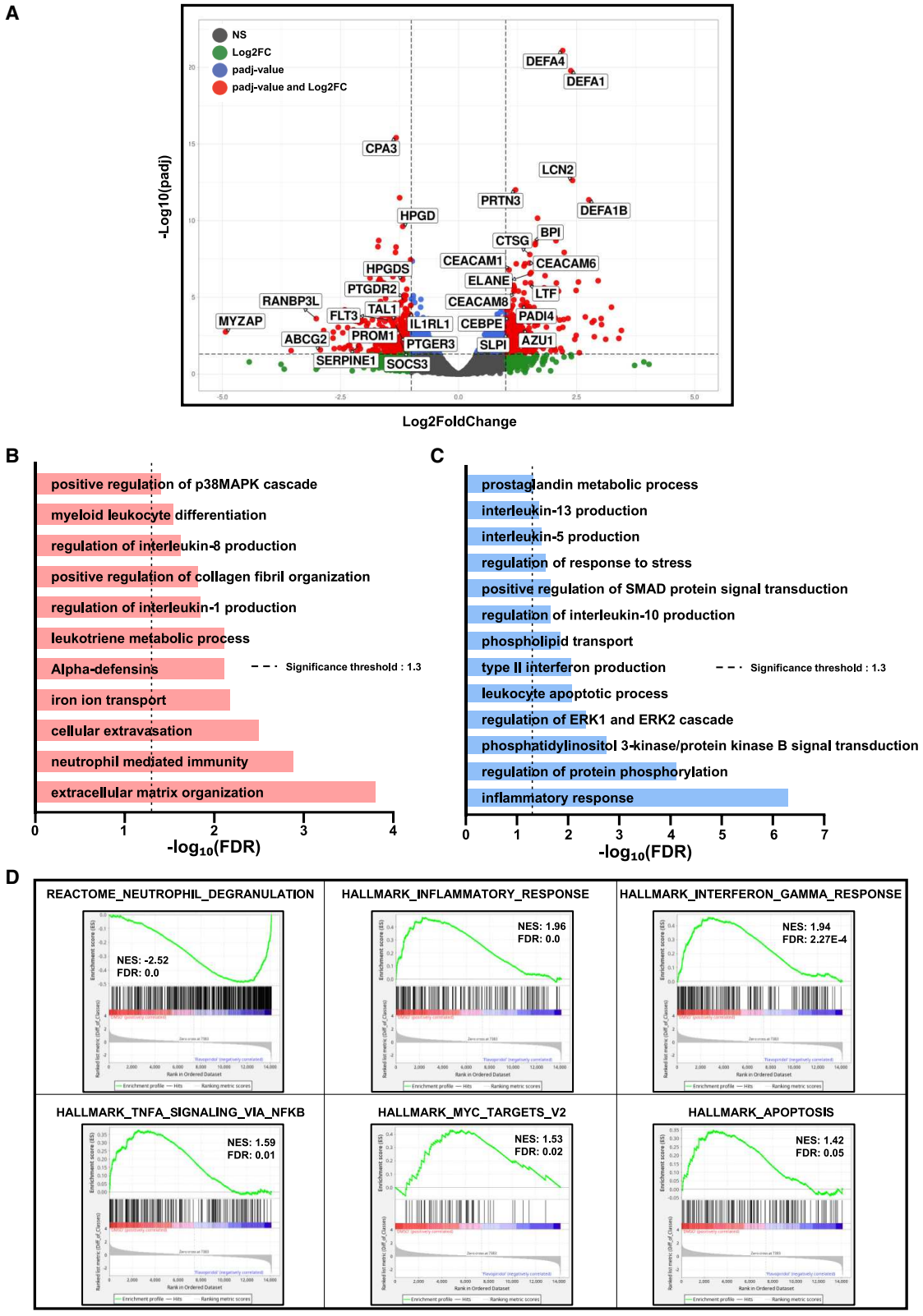

(legend on next page)

CEL, *SLAMF1*, and *MZB1*. These data argue for the potential, albeit less extensively investigated, role of homeobox genes, IGF signaling, retinoid metabolism and transport, fatty acid and lipid metabolism, and lysyl oxidase-triggered cross-linking of matrix proteins during granulopoiesis. Another potential mechanism that may contribute to defective granulopoiesis is the hyperactivation of heat-shock proteins, a pathway most likely triggered by the activated UPR by mutated *ELANE*.[17,21,29,52] Using the isogenic iPSC model, we confirmed activation of the expression of some UPR genes by mutated *ELANE* with different effects depending on the position of *ELANE* mutation.[29] We also found that the expression of lymphoid-cell-specific genes such as *CEL*, *SLAMF1*, and *MZB1* were activated in *ELANE*-mutated cells. These findings suggest the deregulation of transcriptional programs, leading to a bias toward lymphopoiesis over granulopoiesis during the process of lineage specification and cellular "decision-making." A potential limitation of our study is the possible different composition of cell populations used for transcriptomics analysis. We reduced this bias as much as possible by using immature HSPCs with comparable flow cytometry profiles.

To clinically translate our findings, we performed drug repurposing analysis to identify small molecules that mimic the gene expression in HSPCs after correction of *ELANE* mutations. We found that flavopiridol at a dose of 40 nM—a concentration up to 10-fold lower than that usually used to treat cancer patients[53,54]—successfully restored neutrophilic differentiation of *ELANE*-CN iPSCs and did not affect the survival and proliferation of healthy donor HSPCs or mature neutrophils. Intriguingly, primary HSPCs obtained from CN patients with various gene mutations associated with CN, including *ELANE, HAX1*, *JAGN1,* and *SRP54*, as well as two zebrafish models of CN (deficient for *Hax1* or *Jagn1b*) responded to flavopiridol treatment. Flavopiridol-exposed *in vitro*-generated neutrophils also showed normal functions. These data not only reinforce the potential of flavopiridol as a universal therapy for CN patients, but they also validate our hypothesis regarding the shared pathomechanisms of neutropenia downstream of different CN-associated mutations. Additional studies on the *in vivo* efficacy of flavopiridol in a mouse model of CN should be performed. Flavopiridol is used for the treatment of patients with several malignancies, including AML.[53,55] In these settings, flavopiridol is applied at high concentrations of up to 50 mg/m^2/d, which corresponds to plasma levels of unbound flavopiridol of up to 400 nM.[54–56] At this dose, flavopiridol is toxic and can even induce neutropenia.[57] Low-dose flavopiridol treatment has also been investigated in several non-cancer diseases. Chao et al. showed that flavopiridol blocked HIV-1 replication in both single-round and viral spread assays with an IC50 of less than 10 nM.[58] Schmerwitz et al. stated that 100 nM of flavopiridol is effective against severe inflammation-associated pathologies, such as atherosclerosis, arthritis, or asthma.[59] We have also observed anti-inflammatory properties of flavopiridol-treated healthy donor neutrophils through the downregulation of pathways accounted to "inflammatory response," "IFN-g response," and "TNF-a response." The dose-dependent efficacy of flavopiridol might be explained by the dose-dependent selectivity of flavopiridol for different CDKs. It has been reported that flavopiridol inhibits CDK 1, 2, 4, and 9 with an IC50 of 20–40 nM.[60] We found that specific inhibition of CDK1 or CDK4/6 did not restore granulopoiesis in CN, while CDK2 inhibition could partially induce granulopoiesis in CN, indicating that inhibition of several CDKs by flavopiridol is required. Interestingly, *CEBPA* is known to inhibit proliferation and induce myeloid differentiation of HSPCs by inhibiting the activity of CDK2 and CDK4.[42] This study together with our previous investigations confirmed *CEBPA* downregulation as one of the most promising mechanisms underlying the maturation arrest of granulopoiesis in *ELANE*-CN patients.[11] Our recent publication further supports the important role of *CEBPA* downregulation in the pathogenesis of CN—rescue of CN HSPCs with *CEBPA* restores granulocytic differentiation *in vitro*.[61] *CEBPA* downregulation is a key event downstream of several other deregulated pathways and flavopiridol treatment was able to rescue this. We therefore hypothesized that the granulopoietic defect observed in CN HSPCs was attributable to the diminished expression of *CEBPA* and consequent inadequate inhibition of CDK2 and CDK4 activity. X2K enrichment analysis, which enables inference of upstream regulatory networks from DEG signatures, confirmed this hypothesis, showing that deregulated pathways in CN are mainly related to CDKs. Inhibition of *CEBPA* in healthy donors' HSPCs *in vitro* and in wild-type zebrafish embryos *in vivo* abolished granulopoiesis, recapitulating the CN phenotype. Flavopiridol treatment rescued defective granulopoiesis *in vitro* and *in vivo* in *CEBPA*-deficient HSPCs. The observed downregulation of *CEBPA* in hematopoietic cells of CN patients with different causative gene mutations provides an explanation for flavopiridol's effects on granulocytic differentiation of CN patients' HSPCs. The role of UPR activation in *CEBPA* downregulation is still unclear. Flavopiridol treatment did not modulate the expression of UPR-related genes in CN HSPCs. There are two explanations for these observations: first, flavopiridol rescues the pathological pathways downstream but not upstream of the UPR; second, the UPR is not solely responsible for the maturation arrest of granulopoiesis, and additional pathways are involved. CN is a pre-leukemia

Figure 5. RNA-seq analysis of neutrophils derived from CD34$^+$ HSPCs of healthy donors treated with flavopiridol or DMSO

(A) Volcano plot showing differentially expressed genes (DEGs) between DMSO (0.1%) and flavopiridol (40 nM) treated *in vitro*-generated neutrophils from four healthy controls (HD 1–4). The x-axis shows the log2 fold-change (magnitude of change), and the y-axis shows the −log10 adjusted *p* value (statistical significance). Colors represent the significance of the genes in terms of *p* value and log2 fold-change. Selected genes are annotated. (B and C) Functional enrichment analysis using a list of significantly upregulated (B) and downregulated (C) genes in *in vitro*-generated neutrophils treated with flavopridol (40 nM) or DMSO (0.1%). Data are displayed as −log10 adjusted *p* value (FDR). (D). Gene set enrichment analysis (GSEA) of neutrophil degranulation, inflammatory response, interferon gamma response, TNFα signaling via NF-κB, MYC targets V2, and apoptosis signaling pathways between DMSO (0.1%) and favopiridol (40 nM) treated *in vitro*-generated neutrophils from four healthy controls (HD 1–4). NES, normalized enrichment score; FDR, false discovery rate.

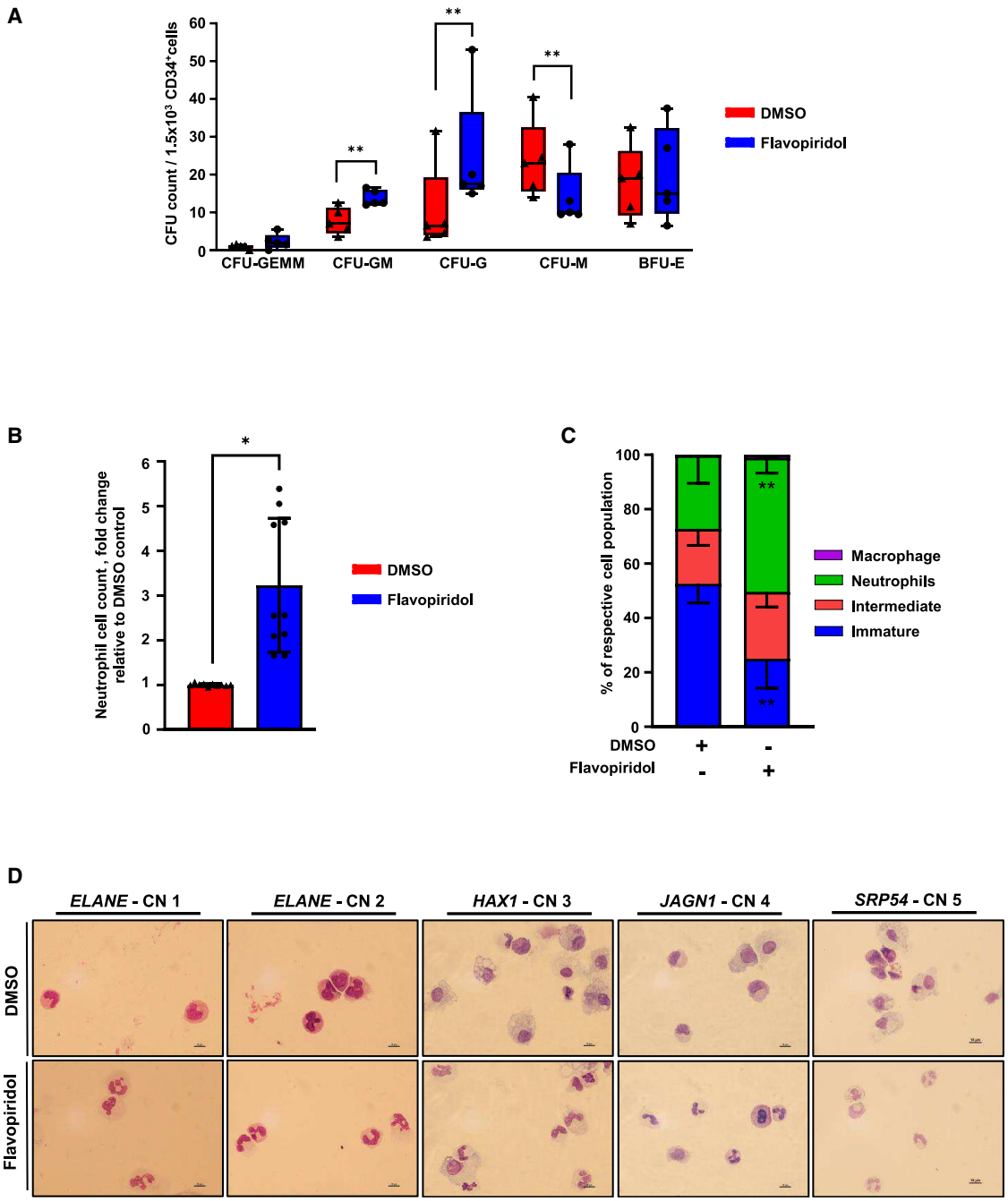

Figure 6. Flavopiridol rescued defective granulopoiesis in CD34⁺ HSPCs of CN patients with different genetic backgrounds *in vitro*

(A) CFU assay of HSPCs from five CN patients with *ELANE* (two patients), *HAX1*, *JAGN1,* and *SRP54* (one patient each) mutations treated with flavopiridol (40 nM) or DMSO (0.1%). CFU counts are shown. Data are represented as mean ± SD from five patients, each in duplicate. The significant difference between groups is indicated, $^{**}p < 0.01$. (B) Absolute counts of mature neutrophils ($CD15^+CD16^+CD45^+$) derived from CN $CD34^+$ HSPCs at day 14 of liquid culture differentiation (LCD) treated with flavopiridol (40 nM) or DMSO (0.1%). Fold-change relative to DMSO control is shown. Data are represented as mean ± SD from five patients, each in duplicate, including group comparison, $^{*}p < 0.05$. (C) Analysis of May-Grunwald-Giemsa stained cytospin slides from terminally differentiated cells on day 14 of liquid culture differentiation (LCD) treated with flavopiridol (40 nM) or DMSO (0.1%). The morphology of more than 100 cells was analyzed for each cytospin slide. Percentages of cell populations are shown. Data are represented as mean ± SD from five patients, each in duplicate, including group comparison, $^{**}p < 0.01$. (D) Representative images of May-Grunwald-Giemsa-stained cytospin preparations of CN $CD34^+$ HSPCs on day 14 of LCD treated with flavopiridol (40 nM) or DMSO (0.1%). Scale bar represents 10 μm.

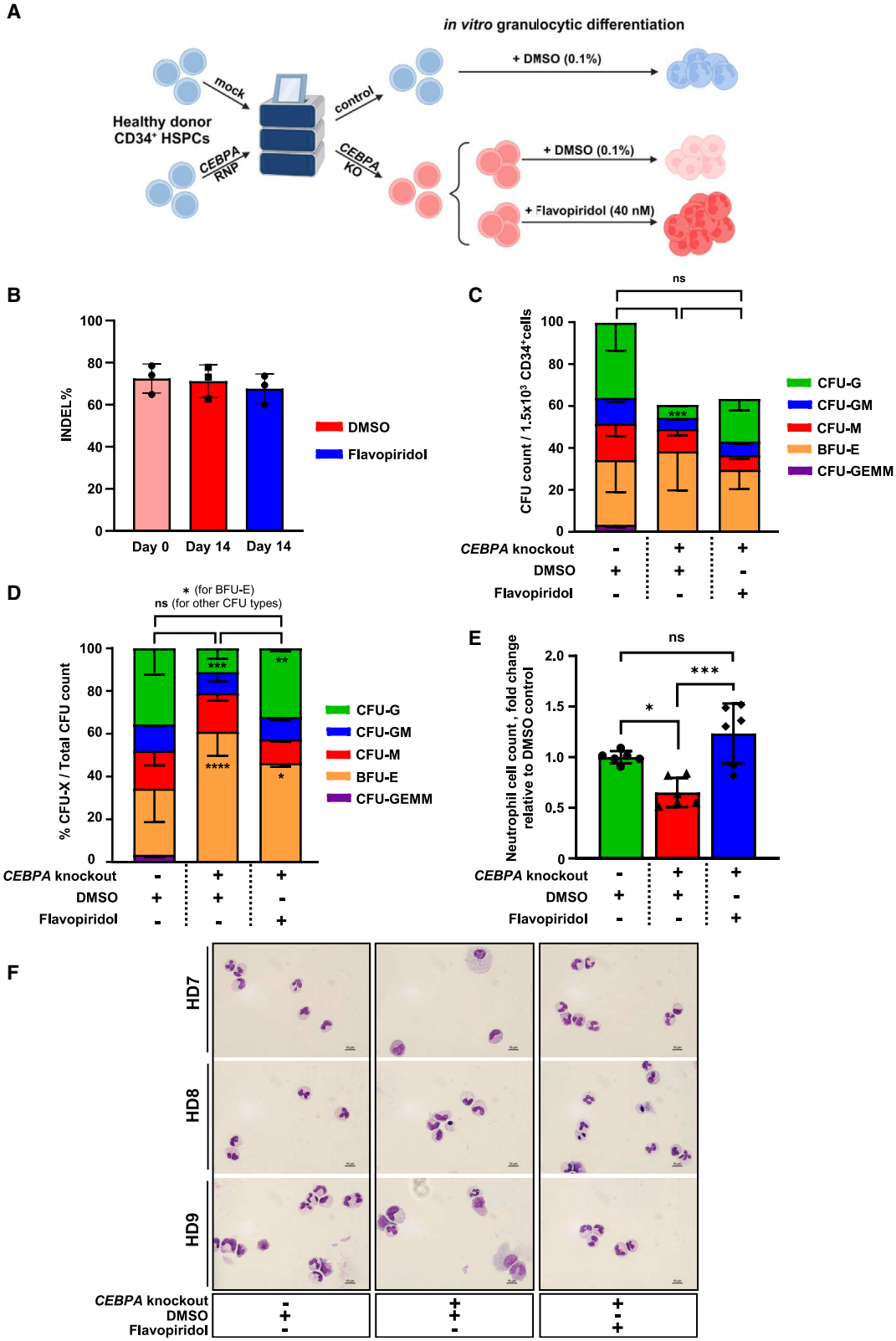

(legend on next page)

syndrome, and given the anti-cancer effects of flavopiridol, further studies will clarify the potential protective effect of flavopiridol treatment on the leukemogenic transformation of hematopoiesis in CN.

Previous studies in zebrafish embryos showed that prolonged flavopiridol treatment, high doses, or multiple dosing can cause side effects such as reduced length, curved tail, and heart edema.[62] In contrast, we did not observe any of these side effects by administrating a single dose of 10 μM flavopiridol and 2 days of incubation. It is likely that flavopiridol may affect embryonic development but not the adult organism. However, it should be evaluated whether long-term treatment with low-dose flavopiridol could have potential side effects common to high-dose flavopiridol or other CDK inhibitors, such as nausea, diarrhea, fatigue, neutropenia, anemia, or low platelet counts, e.g., in adult mice *in vivo*. To this end, we observed no toxic effects of flavopiridol during 14 days of differentiation in the CFU assay or LCD. In the latter, it was added to the culture medium every other day. Several neutrophil-related genes like *DEFA4, DEFA1, PRTN3, AZU1, CTSG, ELANE* and *CEBPE* were upregulated in flavopiridol-treated neutrophils. Low-dose flavopiridol treatment is also boosting granulopoiesis in healthy individuals *in vitro* but not in wild-type zebrafish embryos *in vivo*, which is in line with previously published studies, where total *mpo*$^+$ neutrophils[63,64] and *cmyb*$^+$ HSPCs[64] were not affected by flavopiridol treatment. This could be explained by the fact that zebrafish embryos have additional compensatory mechanisms that mitigate the effect of CDK inhibition during early embryonic development to adapt to the perturbations in cell cycle regulation, which is very active and important during the developmental stage of the organism. This can involve compensatory changes in transcriptional regulators or functional compensation through other CDKs. Alternatively, the lack of granulopoietic induction could also be explained by a dose-dependent effect of flavopiridol since it is administered by water. The neutropenic zebrafish embryos might be more susceptible to the induction of granulopoiesis by flavopiridol than wild-type embryos. Additional *in vivo* dose escalation studies in zebrafish embryos and mice receiving flavopiridol intravenously or intraperitoneally will address this issue. Interestingly, it was shown recently that the number of cells expressing the neutrophil marker *lysozyme C* (*lyz*) were negatively affected by flavopiridol treatment.[64] Additional studies analyzing *lyz*-expressing cells and the expression levels of *lysozyme C* using our model should further clarify this discrepancy.

Taken together, we describe the successful application of an isogenic iPSC model of CN to delineate the defective signaling pathways and, more importantly, to identify an FDA-approved drug capable of rescuing defective neutrophilic differentiation in CN. Our findings may encourage similar studies in patients with other monogenic bone marrow failure syndromes or genetic diseases affecting other organs and tissues. The challenge in applying flavopiridol may stem from its intravenous delivery route. For CN patients who do not respond to rhG-CSF, intravenous injections of flavopiridol may be an option. New oral formulations of CDK inhibitors, such as orally bioavailable flavopiridol-like copper-containing liposomes[65] or the oral phosphate prodrug of flavopiridol, TP-1287,[66] are currently in clinical trials and need to be evaluated in CN.

MATERIALS AND METHODS

iPSC culture

Human induced pluripotent stem cells (iPSC) were cultured on Geltrex LDEV-free reduced growth factor basement membrane matrix (Thermo Fisher Scientific, #A1413201) coated plates in a density of 2×10^5 cells/mL in StemFlex medium (Thermo Fisher Scientific, #A3349401) supplemented with 1% penicillin/streptomycin. The Healthy Donor (HD) iPSC line was kindly provided by Prof. T. Moritz and Dr. N. Lachmann, MHH Hannover. The HD iPSC line and *ELANE*-CN iPSC lines were characterized elsewhere.[22,28,67]

The study was conducted according to Helsinki's declaration. Informed written consent was obtained from study participants and the ethics committee of the University Hospital Tuebingen approved the study.

CRISPR-Cas9-based *ELANE* mutation correction in CN iPSCs

Specific single-guide RNAs (sgRNA) for targeting different regions of the *ELANE* gene: cut site 1: chr19 [CTGCGCGGAGGCCACT TCTG, +852,970: −852,970], NM_001972.3, Exon 2; NP_001963.1 p. F54, cut site 2: chr19 [GGGACGCCGCCTGGGCAACG, +855,637: −855,637], NM_001972.3, Exon 4; NP_001963.1 p. N147, and cut site 3: chr19 [TTAGCCCGTTGCAGACCAAG, +855,980: −855,980], NM_001972.3, Exon 5; NP_001963.1 p. V207 and single-stranded

Figure 7. Flavopiridol treatment rescued defective granulopoiesis in HD *CEBPA* knockout HSPCs

(A) Scheme of CRISPR-Cas9-based *CEBPA* knockout (KO) in HD CD34$^+$ HSPCs (HD 7–9) and subsequent flavopiridol treatment. Created with BioRender.com. (B) Editing efficiency of *CEBPA* knockout in CD34$^+$ HSPCs of HD7–9 at the day of starting granulocytic differentiation (day 0) and the experimental endpoint (day 14). Data are represented as mean ± SD from duplicates for HD7-9. (C) CFU assay of three healthy donors (HD 7–9) control or *CEBPA* KO CD34$^+$ HSPCs treated with flavopiridol (40 nM) or DMSO (0.1%). CFU counts are shown. Data are represented as mean ± SD from three healthy donors, each in duplicate. The significant difference between groups is indicated, ***$p < 0.001$, ns: not significant (for all CFU types). (D) CFU assay of three healthy donors (HD 7–9) control or *CEBPA* KO HSPCs cells treated with flavopiridol (40 nM) or DMSO (0.1%). CFU percentages of each CFU type are shown. Data are represented as mean ± SD from three healthy donors, each in duplicate, including group comparison, *$p < 0.05$, **$p < 0.01$, ***$p < 0.001$, ****$p < 0.0001$. (E) Absolute counts of mature neutrophils (CD15$^+$CD16$^+$CD45$^+$ cells) derived from HD controls or *CEBPA* KO HSPCs at day 14 of liquid culture differentiation (LCD) treated with flavopiridol (40 nM) or DMSO (0.1%). Fold-change relative to DMSO control is shown. Data are represented as mean ± SD from three healthy donors, each in duplicate, including group comparisons, *$p < 0.05$, ***$p < 0.001$, ns: not significant. (F) Representative cytospin images of May-Grunwald-Giemsa-stained cytospin preparations of HD controls or *CEBPA* KO HSPCs at day 14 of LCD treated with flavopiridol (40 nM) or DMSO (0.1%). Scale bar represents 10 μm.

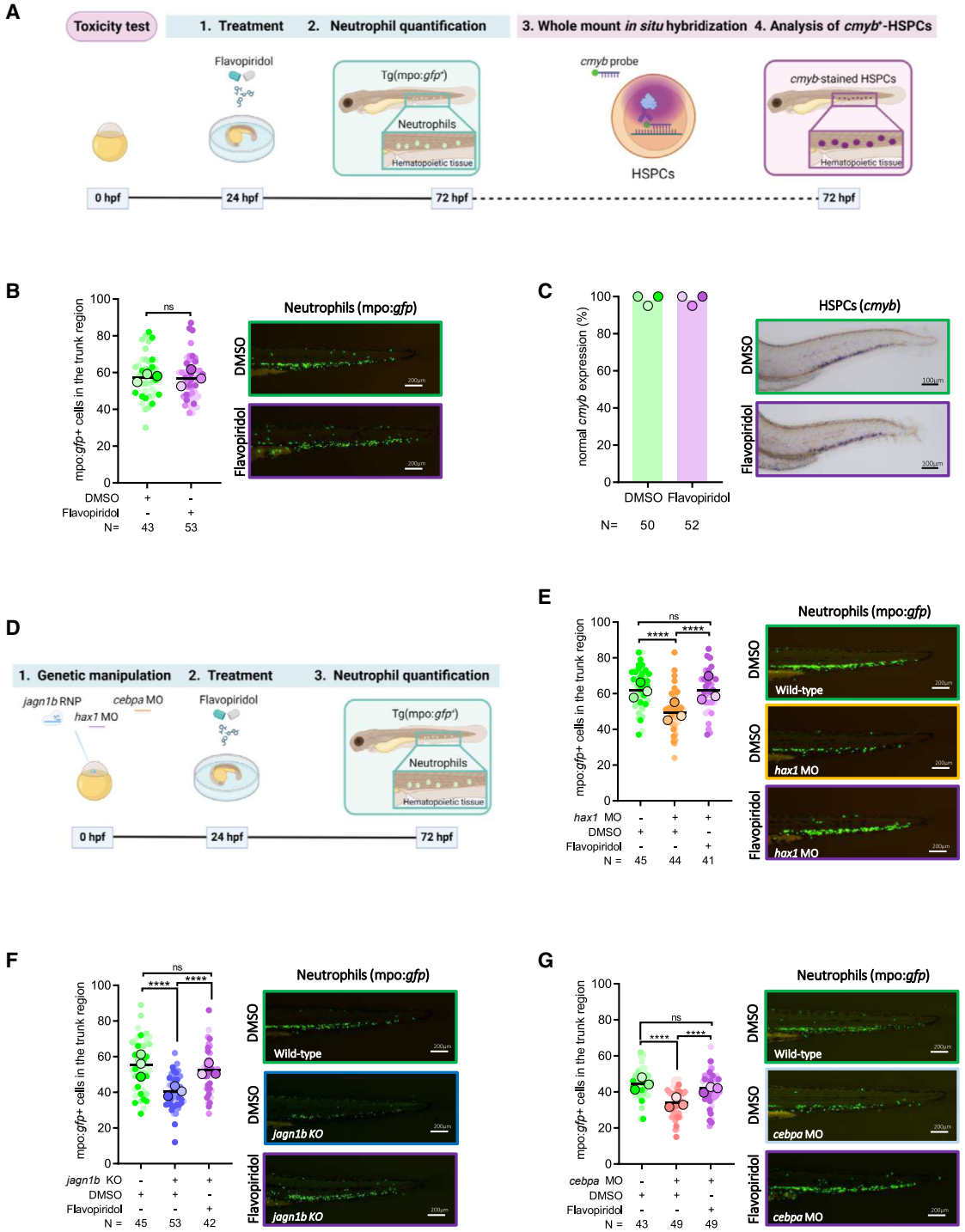

Figure 8. Flavopiridol treatment of *hax1* knockdown, *jagn1b* knockout, or *cebpa* knockdown zebrafish embryos restored defective granulopoiesis

(A) Experimental procedure for flavopiridol toxicity test on neutrophils and HSPCs using the myeloid transgenic reporter line Tg(mpo:*gfp*) and whole mount *in situ* hybridization (WISH) with the HSPC-specific *cmyb* probe. At 24 h postfertilization (hpf), embryos were treated with flavopiridol (10 μM) or DMSO (0.1%) and at 72 hpf, the mpo:*gfp*$^{+}$-neutrophils were quantified, and the WISH was performed. Created with BioRender.com. (B) Effect of flavopiridol treatment on neutrophils in wild-type embryos. Left panel shows the absolute counts of neutrophils (mpo:*gfp*$^{+}$ cells), at 72 hpf in wild-type (wt) zebrafish embryos treated with flavopiridol (10 μM) or DMSO (0.1%) for 2 days. Each small dot represents an individual embryo. Each big dot represents the mean of an independent experiment. The statistical analysis was performed using an unpaired, t-test, ns:

(legend continued on next page)

oligodeoxynucleotides (ssODN) as repair template for each subsequent sgRNA (Table S5) were designed using Benchling [Biology Software] retrieved from https://benchling.com and ordered via Integrated DNA Technologies (IDT). Electroporation of iPSCs was carried out using the Amaxa nucleofection system (P3 primary cell kit, #V4XP-3024) according to the manufacturer's instructions. Briefly, 1×10^6 CN iPSCs were electroporated with assembled gRNA (8 μg) and HiFiCas9 (15 μg) protein (Integrated DNA Technologies) and 1 μM repair template. Clonal isolation of gene-edited iPSCs was done as described previously.[25]

Assessing genome editing efficiency

Genomic DNA was isolated using the QuickExtract DNA extraction kit (Lucigen, #QE09050). PCR was carried out using the GoTaq G2 Hot Start Taq Polymerase (Promega, #M7405) and gene-specific primers (Table S6). The PCR products were purified by ExoSAP, which is a master mix of one part of Exonuclease I 20 U/μL (Thermo Fisher Scientific, #EN0581) and two parts of FastAP thermosensitive alkaline phosphatase 1 U/μL (Thermo Fisher Scientific, #EF0651). Sanger sequencing of purified PCR products was performed by Microsynth. Analysis of CRISPR-Cas9-based genome editing was performed by Deconvolution of Complex DNA Repair (DECODR) web tool.[45]

EB-based hematopoietic differentiation of iPSCs

iPSCs were dissociated from geltrex-coated plates using PBS/EDTA (0.02%) for 7 min. EB generation was performed via centrifugation of 20,000 cells per EB in 96-well plates using STEMdiff APEL2 serum-free differentiation medium (StemCell Technologies) supplemented with bFGF (10 ng/mL) and ROCK Inhibitor Y-27632 dihydrochloride (10 μM) (Tocris). The next day, BMP4 (40 ng/mL) (BioLegend) was added to the culture to induce mesodermal differentiation. On day 4, EBs were plated on geltrex-coated six-well plates (10 EBs/well) in APEL2 medium supplemented with VEGF (40 ng/mL) (R&D Systems), SCF (50 ng/mL) (Peprotech), and interleukin (IL)-3 (50 ng/mL) (Peprotech). For neutrophilic differentiation, the medium was changed 3 days later to fresh APEL medium supplemented with IL-3 (50 ng/mL) and G-CSF (10 ng/mL) (Granocyte, Chugai). The first hematopoietic suspension cells appeared on days 8–10. Suspension cells were harvested and analyzed by flow cytometry on day 14 and day 28 as described before.[25]

Surface marker analysis of the granulopoietic differentiation by flow cytometry

A total of 3×10^4 suspension cells collected from the EB-based hematopoietic differentiation system were used for flow cytometry. For cell surface marker staining, cells were prepared in PBS/1% BSA containing 0.05% sodium azide and stained with specific mouse monoclonal anti-human antibodies. For detection of hematopoietic progenitor cells at day 14, a multicolor flow cytometry antibody panel for "early-stage" hematopoietic differentiation using the following antibodies was applied: CD33-BV421 (BioLegend, BL), CD34-PE-Cy7 (BD Biosciences, BD), KDR-AF647 (BL), CD43-PE (BD), CD41a-FITC (BD), CD235a-FITC (BD), CD45-BV510 (BL), and 7-AAD (BD). For the detection of mature myeloid cells, a multicolor flow cytometry antibody panel for "late-stage" hematopoietic differentiation at day 28 using the following antibodies was applied: CD15-PE (BD), CD16-FITC (BD), CD14-APC-H7 (BD), CD45-BV510 (BL), CD33-BV421 (BL), and 7-AAD (BD). Anti-mouse IgGk beads (BD) were used for compensation. Samples were analyzed using FACSCanto II (BD) and FlowJo software V10 (BD).

NBT assay

A total of 20,000 floating cells were harvested from EB-based myeloid differentiation culture on day 28 and incubated with nitro-blue tetrazolium (NBT) solution (Sigma) for 10 min at 37°C and 10 min at room temperature in the dark. Cytospin slides of NBT-stained cells were prepared and additionally stained with May Grunwald-Giemsa. NBT^+ neutrophils were counted and the total amount of NBT^+ neutrophils produced by 10 EBs was calculated.

CFU assay

A total of 10,000 $CD34^+$ $CD45^+$ suspension cells from EB-based iPSC hematopoietic differentiation at day 14 or 1,500 primary $CD34^+$ HSPCs were used for CFU assay. Cells were resuspended in Iscove's modified Dulbecco's medium supplemented with 2% fetal bovine serum (FBS) (StemCell Technologies) and added to Methocult H4435 enriched medium (StemCell Technologies). The cell suspension was plated on 3.5-cm dishes. Colonies were counted after 10–14 days. Small molecules for screening and validation were added in the following concentrations, which correspond to published IC50 concentrations from individual datasheets: VX745 (9 nM, Biomol), SL-327 (220 nM, Biomol), Importazole (150 nM, Biomol), SAHA (10 nM, Biomol), Lapatinib (19 nM, Biomol), Flavopiridol (40 nM, Biomol/Cayman

not significant. N represents the total number of analyzed embryos. The right panel shows representative images. Scale bar represents 200 μm. (C) Effect of flavopiridol treatment on HSPCs in wild-type embryos. Left panel shows the percentage of 72 hpf embryos with a normal *cmyb* expression pattern, representing a normal number of HSPCs of embryos treated with flavopiridol (10 μM) or DMSO (0.1%), each dot represents the value (in %) of an independent experiment. N represents the total number of analyzed embryos. The right panel shows representative images. Scale bar represents 200 μm. (D) Experimental procedure for flavopiridol treatment of *jagn1b*-, *hax1*-, and *cebpa*-deficient embryos. At the one-cell stage, either 5 μM *jagn1b* CRISPR-Cas9 RNPs, 1 mM *hax1* morpholino, or 0.5mM *cebpa* morpholino was injected in tg(mpo:*gfp*) blastomere to interfere with the respective gene function. At 24 hpf, the embryos were treated with flavopiridol (10 μM) or DMSO (0.1%) and at 72 hpf, mpo:gfp^+ neutrophils were quantified. Created with BioRender.com. (E–G) Neutrophil quantification after flavopiridol treatment in *hax1*-knockdown (E), *jagn1b*-knockout (F), or *cebpa*-knockdown (G) embryos. Left panels show absolute counts of neutrophils (mpo:gfp^+ cells) after 2 days of flavopiridol (10 μM) or DMSO (0.1%) treatment compared with the wild-type counterparts. Each small dot represents the value of an independent embryo. Each big dot represents the mean of an independent experiment. N represents the total number of analyzed embryos. The statistical analysis was performed using Kruskall-Wallis test for multiple comparisons. ns: not significant, $^{****}p < 0.0001$. The right panels show representative pictures. Scale bar represents 200 μm.

Chemicals), MPEP (36 nM, Selleckchem), Zelavespib (51 nM, Selleckchem), Quiflapon (6 nM, TargetMol), Ro-3306 (20 nM, MCE), AUZ 454 (50 nM, MCE), and Ribociclib (10 nM, MCE).

Morphological analysis

iPSC-derived hematopoietic cells from day 28 of iPSC differentiation or day 14 of primary $CD34^+$ HSPCs differentiation were centrifuged for 5 min, 250 rpm onto glass slides and stained with May-Grunwald-Solution for 5 min and Giemsa-Solution for 20 min.

Expansion and liquid culture granulocytic differentiation of primary human $CD34^+$ HSPCs

Bone marrow samples from CN patients were collected during the routine annual follow-up recommendation by the Severe Chronic Neutropenia International Registry and cord blood samples from healthy donors were obtained from University Women's Hospital Tuebingen. The study was conducted according to Helsinki's declaration. Informed written consent was obtained from the study participants and the ethics committee of the University Hospital Tuebingen approved the study. $CD34^+$ HSPCs were isolated from the bone marrow mononuclear cell fraction from five CN patients and cord blood of nine healthy donors (HDs) by Ficoll gradient centrifugation and magnetic bead separation using the human CD34 MicroBead Kit (Miltenyi Biotech, #130-046-703). $CD34^+$ cells were expanded for up to 7 days in $CD34^+$ cell expansion medium (StempSpan, StemCell Technologies) supplemented with 1% penicillin/streptomycin, 1% Glutamine and cytokines: IL-3 (20 ng/mL), IL-6 (20 ng/mL), thrombopoietin (TPO) (20 ng/mL), stem cell factor (SCF) (50 ng/mL), and FMS-like tyrosine kinase 3 ligand (FLT3L) (50 ng/mL). All cytokines were purchased from Peprotech. During the last 2 days of expansion, $CD34^+$ cells were treated with small molecules (Flavopiridol or others) or DMSO. A total of 1,500 cells were then used for CFU assay for each condition. The rest of the cells were cultured for 7 days in differentiation medium 1 (RPMI supplemented with 10% fetal calf serum [FCS], 1% penicillin/streptomycin, and human recombinant cytokines: 5 ng/mL SCF [Peprotech], 5 ng/mL IL-3 [Peprotech], 5 ng/mL GM-CSF [Peprotech], 1 ng/mL G-CSF [Granocyte, Chugai] and flavopiridol [40 nM] or DMSO [0.1%]) at a density of $>2 \times 10^5$ cells/mL, followed by 7 days in differentiation medium 2 (RPMI supplemented with 10% FCS, 1% penicillin/streptomycin, 1 ng/mL G-CSF [Granocyte, Chugai] and flavopiridol [40 nM] or DMSO [0.1%]). Half of the differentiation medium was refreshed every second day for the entire LCD. After 14 days, 50,000 cells were used for morphological analysis and 1.5×10^5 cells were used for flow cytometry analysis stained with the following antibodies: CD45-BV510 (BL), CD34-PE-Cy7 (BD), CD33-BV421 (BL), CD15-PE (BL), CD16-APC (BD), CD66b-FITC (BL), CD11b-APC-Cy7 (BD), 7AAD (BD). Anti-mouse IgGk beads (BD) were used for compensation. Samples were analyzed using FACSCanto II (BD) and FlowJo software V10 (BD).

CEBPA knockout in primary healthy $CD34^+$ HSPCs

Specific single-guide RNA (sgRNA) for targeting the *CEBPA* gene (cut site: chr19 [5′- ggcggcgactttgactaccc - 3′, +2,601: −2,601], NP_004355.2 p. Y108) was designed using Benchling (Biology Software) retrieved from https://benchling.com and ordered via Integrated DNA Technologies (IDT). Electroporation was carried out using the Amaxa nucleofection system (P3 primary cell kit, #V4XP-3024) according to the manufacturer's instructions. 1×10^6 human primary $CD34^+$ HSPCs were electroporated with assembled gRNA (8 μg) and HiFiCas9 (15 μg) protein (Integrated DNA Technologies).

Quantitative RT-PCR

RNA was isolated using RNeasy Micro Kit (Qiagen) and cDNA was prepared from 1 μg of total RNA with the Omniscript RT Kit (Qiagen). qPCR was performed with SYBR Green qPCR master mix (Roche) on a Light Cycler 480 (Roche). Target gene expression was normalized to GAPDH and/or ACTB as housekeeper genes. Primer sequences are presented in Table S7.

RNA-seq

mRNA was isolated using RNeasy Mini- or Micro Kit (Qiagen). RNA quality was assessed using an Agilent 2100 Bioanalyzer. Samples with high RNA integrity numbers (RIN >8) were selected. A total of 400 ng of RNA was sent for RNA sequencing (Novogene). The nf-core RNA-seq pipeline[68]—a framework for community-curated bioinformatics pipelines—was used to process and extract the gene-level count matrix for each sample. Principal-component analysis (PCA), pathway analysis of PCA rotation, and the DESeq2-based differential analysis of count data were performed using iDEP web tool.[69] The volcano plot of DEGs was generated using EnhancedVolcano R-package accessible via https://github.com/kevinblighe/EnhancedVolcano. Functional enrichment of DEGs was performed using the gProfiler web server[30] (Statistical method: Benjamini-Hochberg FDR, database version: e109_e.g., 56_p17_1d3191d or e111_e.g.,58_p18_f463989d). Cytoscape ReactomeFI plugin was used to generate functional interactions network between DEGs.[31] eXpression2Kinases (X2K) webtool[32] (accessed via https://maayanlab.cloud/X2K/) was used to predict the upstream regulatory network of DEGs.

DNA copy number and off-target analysis using sWGS

DNA was extracted using QIAamp DNA Mini Kit (Qiagen) and sent to Novogene for sWGS. Raw reads were preprocessed with fastp[70] v0.23.4 and mapped to hg38 human reference with bwa v0.7.17 (https://doi.org/10.48550/arXiv.1303.3997). Alignments were checked for predicted off-target events using samtools (v1.15.1), mpileup command[71] on off-target candidate regions ±3 bases. Copy number analysis was performed with Bioconductor QDNASeq[26] (v1.40.0) package with genome bins annotations from the package QDNASeq.hg38 accessible via (https://github.com/asntech/QDNAseq.hg38). All settings default except for segmentation step: smoothBy = 5, undo.SD = 10, alpha = 1e−20, transformFun = "sqrt."

Zebrafish maintenance and breeding

For the zebrafish analyses, the previously described transgenic reporter lines Tg(mpo:*gfp*)[72] and Tg(cd41:*gfp*)[73] were used. Zebrafish maintenance was approved by the local government (Tierschutzgesetz §11, Abs. 1, Nr. 1, husbandry permit 35/9185.46/Uni TÜ). All

zebrafish were maintained according to standard protocols and handled in accordance with the European Union animal protection directive 2010/63/EU.

Flavopiridol toxicity test on mpo:*gfp*$^+$ neutrophils and cd41:*gfp*$^+$ HSPCs in zebrafish embryos *in vivo*

One-day-old dechorionized Tg(mpo:*gfp*) and Tg(cd41:*gfp*) zebrafish embryos were incubated in 0.1% DMSO (control) or 10 μM flavopiridol in E3 zebrafish medium for 1 day for the analysis of HSPCs and 2 days for the analysis of neutrophils. The mpo:*gfp*$^+$ neutrophils and cd41:*gfp*$^+$ HSPCs in the hematopoietic tissue were quantified manually using a Nikon stereo fluorescent SMZ18 microscope.

WISH assay

RNA *in situ* hybridization of 72 hpf zebrafish DMSO- or flavopiridol-treated embryos was performed using *cmyb* digoxigenin-labeled RNA antisense probes as previously described.[74]

Analysis of the effect of flavopiridol treatment on neutrophil counts in genetically modified zebrafish embryos *in vivo*

To interfere with *hax1* and *cebpa* function, 1 mM and 0.5 mM morpholino (GeneTools, *hax1*: 5′-CGCAGGTGAGTTTGTCAAATTGTTA-3′, *cebpa*: 5′- TCGTAGAGGTTTGCTTGCTCCATG-3′) were injected into one-cell stage Tg(mpo:*gfp*) embryos. To interfere with *jagn1b* function, 5 μM *jagn1b* RNPs (IDT, Alt-R CRISPR-Cas9 sgRNA 5′-ATGGCATCACGAGCAGGACCA-3′, Alt-R S.p. Cas9 Nuclease V3) were injected into one-cell stage Tg(mpo:*gfp*) embryos. Dechorionized 1-day-old injected and un-injected embryos were incubated in DMSO (control) or 10 μM flavopiridol diluted in zebrafish medium for 2 days. At 72 hpf postfertilization, the mpo:*gfp* $^+$ cells in the hematopoietic tissue were quantified manually using a Nikon stereo fluorescent SMZ18 microscope and images were taken with a Nikon DS-Fi3 camera.

Assessment of proliferation kinetics using the IncuCyte ZOOM system

Primary CD34$^+$ HSPCs (10,000 cells per well) in a 96-well plate were cultured in CD34$^+$ cell expansion medium (StempSpan, StemCell Technologies) supplemented with 1% penicillin-streptomycin, 1% Glutamine, and cytokines: IL-3 (20 ng/mL), IL-6 (20 ng/mL), TPO (20 ng/mL), SCF (50 ng/mL), and FLT3L (50 ng/mL) along with 40 nM flavopiridol or 0.1% DMSO in IncuCyte ZOOM system (Essen Bio) at 37°C, 5% CO2. The cells were monitored over 5 days. The analysis was conducted using IncuCyte S3 Software.

RealTime-Glo MT Cell Viability Assay

Cell viability was measured using RealTime-Glo MT Cell Viability kit (Promega, #G9711). Briefly, 10,000 primary CD34$^+$ HSPCs or PMNs were seeded per well of white, clear-bottomed 96-well plates in RPMI 1640 medium supplemented with 10% FCS and 1% penicillin-streptomycin along with 40 nM flavopiridol or 0.1% DMSO. The luminescence signal was recorded at multiple time points using a Glomax plate reader (Promega) according to the manufacturer's protocol.

Isolation, treatment, and viability test of primary human polymorphonuclear neutrophils

Primary neutrophils of healthy donors were isolated using EasySep Direct Human Neutrophil Isolation Kit (StemCell Technologies, #19666) according to the manufacturer's protocol. A total of 10,000 neutrophils were treated with flavopiridol (40 nM) or DMSO (0.1%) for 3 h and viability was measured using RealTime-Glo MT Cell Viability kit (Promega, #G9711) as described above.

Annexin V apoptosis assay

A total of 50,000 cells treated with DMSO or flavopiridol for 2 days during CD34$^+$ cell expansion or treated for 14 days during LCD were resuspended in 1× Annexin V Binding Buffer (BD) and stained with Annexin V-APC antibody (BD) for 15 min at room temperature in the dark. Cells were washed and resuspended in 1× Binding buffer with 1:1,000 DAPI (Sigma). Samples were analyzed using FACSCanto II (BD) and FlowJo software V10 (BD).

Statistical analysis

For cell experiments, differences in mean values between two groups were analyzed using two-sided, unpaired Student's t tests using GraphPad Prism 9 software or Microsoft Excel 2019. In Figures 6A and S5A two-sided, paired Student's t test was used. One-way ANOVA with Dunnett's test was applied for multiple group comparison with one variable. Two-way ANOVA with Tukey's test was used for multiple group comparisons with two variables comparing all means with each other. Two-way ANOVA with Dunnett's test was used for multiple group comparisons with two variables comparing all means to control mean. For zebrafish experiments, the normal data distribution was assessed with the Kolmogorov-Smirnov test. For normally distributed data, an unpaired Student's t test was used for single comparisons between two groups, and ANOVA for multiple comparisons. For non-normally distributed data, unpaired two-tailed Wilcoxon-Mann-Whitney test or Kruskal-Wallis test was used.

DATA AND CODE AVAILABILITY

For original data, please get in touch with Julia.skokowa@med.uni-tuebingen.de.

ACKNOWLEDGMENTS

This work was supported by the DFG (project no 455056283 and 491561957), the BMBF consortium MyPred (grant no 1GM2207G), the Madeleine Schickedanz-Kinderkrebsstiftung, the COST (European Cooperation in Science and Technology) Action CA18233 "European Network for Innovative Diagnosis and Treatment of Chronic Neutropenias" EuNet-INNOCHRON, and NIH (Federal Award No: 5R24AI162637-02 Subaward No: GENFD0002539063). We thank the Flow Cytometry Core Facility of the University Hospital Tuebingen for technical support.

AUTHOR CONTRIBUTIONS

M.N., B.D., and J.S. made initial observations and designed the experiments. J.S. acquired funding, provided resources, and supervised the project. M.N. and B.D. designed and performed CRISPR-Cas9 experiments, analysis of RNA-seq data, *in silico* drug analysis, designed and conducted iPSC and primary HSPC differentiation experiments, and analyzed the data; L.D. designed and performed all zebrafish experiments and analyzed the data; B.F. assisted with HD iPSC differentiation and the granulocytic differentiation of primary HSPCs, PCR, and Sanger sequencing of *CEBPA* knockout HSPCs; F.B. assisted with May-Grunwald-Giemsa staining of cytospin preparations; S.K. and M.K. performed sWGS and assisted with the analysis of RNA-seq ; J.S., M.N., B.D., and L.D. wrote the manuscript;

K.W., C.Z., C.L., and M.G. provided patients' and healthy donors' material and gave insightful comments.

DECLARATION OF INTERESTS

M.N., B.D., L.D., and J.S. have filed a patent on the invention described in this study.

SUPPLEMENTAL INFORMATION

Supplemental information can be found online at https://doi.org/10.1016/j.ymthe.2024.10.031.

REFERENCES

1. Welte, K., Gabrilove, J., Bronchud, M.H., Platzer, E., and Morstyn, G. (1996). Filgrastim (r-metHuG-CSF): the first 10 years. Blood *88*, 1907–1929.
2. Welte, K., Zeidler, C., and Dale, D.C. (2006). Severe congenital neutropenia. Semin. Hematol. *43*, 189–195. https://doi.org/10.1053/j.seminhematol.2006.04.004.
3. Skokowa, J., Germeshausen, M., Zeidler, C., and Welte, K. (2007). Severe congenital neutropenia: inheritance and pathophysiology. Curr. Opin. Hematol. *14*, 22–28. https://doi.org/10.1097/00062752-200701000-00006.
4. Dale, D.C., Bonilla, M.A., Davis, M.W., Nakanishi, A.M., Hammond, W.P., Kurtzberg, J., Wang, W., Jakubowski, A., Winton, E., and Lalezari, P. (1993). A randomized controlled phase III trial of recombinant human granulocyte colony-stimulating factor (filgrastim) for treatment of severe chronic neutropenia. Blood *81*, 2496–2502.
5. Horwitz, M., Benson, K.F., Person, R.E., Aprikyan, A.G., and Dale, D.C. (1999). Mutations in ELA2, encoding neutrophil elastase, define a 21-day biological clock in cyclic haematopoiesis. Nat. Genet. *23*, 433–436. https://doi.org/10.1038/70544.
6. Dale, D.C., Person, R.E., Bolyard, A.A., Aprikyan, A.G., Bos, C., Bonilla, M.A., Boxer, L.A., Kannourakis, G., Zeidler, C., Welte, K., et al. (2000). Mutations in the gene encoding neutrophil elastase in congenital and cyclic neutropenia. Blood *96*, 2317–2322.
7. Klein, C., Grudzien, M., Appaswamy, G., Germeshausen, M., Sandrock, I., Schäffer, A.A., Rathinam, C., Boztug, K., Schwinzer, B., Rezaei, N., et al. (2007). HAX1 deficiency causes autosomal recessive severe congenital neutropenia (Kostmann disease). Nat. Genet. *39*, 86–92. https://doi.org/10.1038/ng1940.
8. Bellanné-Chantelot, C., Schmaltz-Panneau, B., Marty, C., Fenneteau, O., Callebaut, I., Clauin, S., Docet, A., Damaj, G.L., Leblanc, T., Pellier, I., et al. (2018). Mutations in the SRP54 gene cause severe congenital neutropenia as well as Shwachman-Diamond-like syndrome. Blood *132*, 1318–1331. https://doi.org/10.1182/blood-2017-12-820308.
9. Boztug, K., Järvinen, P.M., Salzer, E., Racek, T., Mönch, S., Garncarz, W., Gertz, E.M., Schäffer, A.A., Antonopoulos, A., Haslam, S.M., et al. (2014). JAGN1 deficiency causes aberrant myeloid cell homeostasis and congenital neutropenia. Nat. Genet. *46*, 1021–1027. https://doi.org/10.1038/ng.3069.
10. Makaryan, V., Zeidler, C., Bolyard, A.A., Skokowa, J., Rodger, E., Kelley, M.L., Boxer, L.A., Bonilla, M.A., Newburger, P.E., Shimamura, A., et al. (2015). The diversity of mutations and clinical outcomes for ELANE-associated neutropenia. Curr. Opin. Hematol. *22*, 3–11. https://doi.org/10.1097/moh.0000000000000105.
11. Skokowa, J., Cario, G., Uenalan, M., Schambach, A., Germeshausen, M., Battmer, K., Zeidler, C., Lehmann, U., Eder, M., Baum, C., et al. (2006). LEF-1 is crucial for neutrophil granulocytopoiesis and its expression is severely reduced in congenital neutropenia. Nat. Med. *12*, 1191–1197. https://doi.org/10.1038/nm1474.
12. Skokowa, J., Klimiankou, M., Klimenkova, O., Lan, D., Gupta, K., Hussein, K., Carrizosa, E., Kusnetsova, I., Li, Z., Sustmann, C., et al. (2012). Interactions among HCLS1, HAX1 and LEF-1 proteins are essential for G-CSF–triggered granulopoiesis. Nat. Med. *18*, 1550–1559. https://doi.org/10.1038/nm.2958.
13. Skokowa, J., Lan, D., Thakur, B.K., Wang, F., Gupta, K., Cario, G., Brechlin, A.M., Schambach, A., Hinrichsen, L., Meyer, G., et al. (2009). NAMPT is essential for the G-CSF-induced myeloid differentiation via a NAD+-sirtuin-1-dependent pathway. Nat. Med. *15*, 151–158. https://doi.org/10.1038/nm.1913.
14. Deordieva, E., Shvets, O., Voronin, K., Maschan, A., Welte, K., Skokowa, J., Novichkova, G., and Shcherbina, A. (2021). Nicotinamide (vitamin B3) treatment improves response to G-CSF in severe congenital neutropenia patients. Br. J. Haematol. *192*, 788–792. https://doi.org/10.1111/bjh.17313.
15. Hoffmann, D., Kuehle, J., Lenz, D., Philipp, F., Zychlinski, D., Lachmann, N., Moritz, T., Steinemann, D., Morgan, M., Skokowa, J., et al. (2020). Lentiviral gene therapy and vitamin B3 treatment enable granulocytic differentiation of G6PC3-deficient induced pluripotent stem cells. Gene Ther. *27*, 297–306. https://doi.org/10.1038/s41434-020-0127-y.
16. Chao, J.R., Parganas, E., Boyd, K., Hong, C.Y., Opferman, J.T., and Ihle, J.N. (2008). Hax1-mediated processing of HtrA2 by Parl allows survival of lymphocytes and neurons. Nature *452*, 98–102. https://doi.org/10.1038/nature06604.
17. Nanua, S., Murakami, M., Xia, J., Grenda, D.S., Woloszynek, J., Strand, M., and Link, D.C. (2011). Activation of the unfolded protein response is associated with impaired granulopoiesis in transgenic mice expressing mutant Elane. Blood *117*, 3539–3547. https://doi.org/10.1182/blood-2010-10-311704.
18. Rao, S., Yao, Y., Soares de Brito, J., Yao, Q., Shen, A.H., Watkinson, R.E., Kennedy, A.L., Coyne, S., Ren, C., Zeng, J., et al. (2021). Dissecting ELANE neutropenia pathogenicity by human HSC gene editing. Cell Stem Cell *28*, 833–845.e5. https://doi.org/10.1016/j.stem.2020.12.015.
19. Nasri, M., Ritter, M.U., Mir, P., Dannenmann, B., Kaufmann, M.M., Arreba-Tutusaus, P., Xu, Y., Borbaran-Bravo, N., Klimiankou, M., Lengerke, C., et al. (2024). CRISPR-Cas9n-mediated ELANE promoter editing for gene therapy of severe congenital neutropenia. Mol. Ther. *32*, 1628–1642. https://doi.org/10.1016/j.ymthe.2024.03.037.
20. Doulatov, S., Vo, L.T., Chou, S.S., Kim, P.G., Arora, N., Li, H., Hadland, B.K., Bernstein, I.D., Collins, J.J., Zon, L.I., and Daley, G.Q. (2013). Induction of multipotential hematopoietic progenitors from human pluripotent stem cells via respecification of lineage-restricted precursors. Cell stem cell *13*, 459–470.
21. Dannenmann, B., Zahabi, A., Mir, P., Oswald, B., Bernhard, R., Klimiankou, M., Morishima, T., Schulze-Osthoff, K., Zeidler, C., Kanz, L., et al. (2019). Human iPSC-based model of severe congenital neutropenia reveals elevated UPR and DNA damage in CD34+ cells preceding leukemic transformation. Exp. Hematol. *71*, 51–60.
22. Dannenmann, B., Klimiankou, M., Oswald, B., Solovyeva, A., Mardan, J., Nasri, M., Ritter, M., Zahabi, A., Arreba-Tutusaus, P., Mir, P., et al. (2021). iPSC modeling of stage-specific leukemogenesis reveals BAALC as a key oncogene in severe congenital neutropenia. Cell Stem Cell *28*, 906–922.e6.
23. Ruiz-Gutierrez, M., Bölükbaşı, Ö.V., Alexe, G., Kotini, A.G., Ballotti, K., Joyce, C.E., Russell, D.W., Stegmaier, K., Myers, K., Novina, C.D., et al. (2019). Therapeutic discovery for marrow failure with MDS predisposition using pluripotent stem cells. JCI Insight *4*, e125157.
24. Doulatov, S., Vo, L.T., Macari, E.R., Wahlster, L., Kinney, M.A., Taylor, A.M., Barragan, J., Gupta, M., McGrath, K., Lee, H.Y., et al. (2017). Drug discovery for Diamond-Blackfan anemia using reprogrammed hematopoietic progenitors. Sci. Transl. Med. *9*, eaah5645.
25. Dannenmann, B., Nasri, M., Welte, K., and Skokowa, J. (2020). CRISPR/Cas9 genome editing of human-induced pluripotent stem cells followed by granulocytic differentiation. Methods Mol. Biol. *2115*, 471–483.
26. Scheinin, I., Sie, D., Bengtsson, H., van de Wiel, M.A., Olshen, A.B., van Thuijl, H.F., van Essen, H.F., Eijk, P.P., Rustenburg, F., Meijer, G.A., et al. (2014). DNA copy number analysis of fresh and formalin-fixed specimens by shallow whole-genome sequencing with identification and exclusion of problematic regions in the genome assembly. Genome Res. *24*, 2022–2032. https://doi.org/10.1101/gr.175141.114.
27. Hsu, P.D., Scott, D.A., Weinstein, J.A., Ran, F.A., Konermann, S., Agarwala, V., Li, Y., Fine, E.J., Wu, X., Shalem, O., et al. (2013). DNA targeting specificity of RNA-guided Cas9 nucleases. Nat. Biotechnol. *31*, 827–832. https://doi.org/10.1038/nbt.2647.
28. Nasri, M., Ritter, M., Mir, P., Dannenmann, B., Aghaallaei, N., Amend, D., Makaryan, V., Xu, Y., Fletcher, B., Bernhard, R., et al. (2020). CRISPR/Cas9-mediated ELANE knockout enables neutrophilic maturation of primary hematopoietic stem and progenitor cells and induced pluripotent stem cells of severe congenital neutropenia patients. Haematologica *105*, 598–609. https://doi.org/10.3324/haematol.2019.221804.
29. Nustede, R., Klimiankou, M., Klimenkova, O., Kuznetsova, I., Zeidler, C., Welte, K., and Skokowa, J. (2016). ELANE mutant–specific activation of different UPR pathways in congenital neutropenia. Br. J. Haematol. *172*, 219–227.

30. Raudvere, U., Kolberg, L., Kuzmin, I., Arak, T., Adler, P., Peterson, H., and Vilo, J. (2019). g: Profiler: a web server for functional enrichment analysis and conversions of gene lists (2019 update). Nucleic Acids Res. *47*, W191–W198.

31. Fabregat, A., Jupe, S., Matthews, L., Sidiropoulos, K., Gillespie, M., Garapati, P., Haw, R., Jassal, B., Korninger, F., May, B., et al. (2018). The reactome pathway knowledgebase. Nucleic Acids Res. *46*, D649–D655.

32. Clarke, D.J.B., Kuleshov, M.V., Schilder, B.M., Torre, D., Duffy, M.E., Keenan, A.B., Lachmann, A., Feldmann, A.S., Gundersen, G.W., Silverstein, M.C., et al. (2018). eXpression2Kinases (X2K) Web: linking expression signatures to upstream cell signaling networks. Nucleic Acids Res. *46*, W171–W179.

33. Duan, Q., Reid, S.P., Clark, N.R., Wang, Z., Fernandez, N.F., Rouillard, A.D., Readhead, B., Tritsch, S.R., Hodos, R., Hafner, M., et al. (2016). L1000CDS2: LINCS L1000 characteristic direction signatures search engine. NPJ Syst. Biol. Appl. *2*, 16015–16112.

34. Lamb, J. (2007). The Connectivity Map: a new tool for biomedical research. Nat. Rev. Cancer *7*, 54–60.

35. Mootha, V.K., Lindgren, C.M., Eriksson, K.F., Subramanian, A., Sihag, S., Lehar, J., Puigserver, P., Carlsson, E., Ridderstråle, M., Laurila, E., et al. (2003). PGC-1alpha-responsive genes involved in oxidative phosphorylation are coordinately downregulated in human diabetes. Nat. Genet. *34*, 267–273. https://doi.org/10.1038/ng1180.

36. Subramanian, A., Tamayo, P., Mootha, V.K., Mukherjee, S., Ebert, B.L., Gillette, M.A., Paulovich, A., Pomeroy, S.L., Golub, T.R., Lander, E.S., and Mesirov, J.P. (2005). Gene set enrichment analysis: a knowledge-based approach for interpreting genome-wide expression profiles. Proc. Natl. Acad. Sci. USA *102*, 15545–15550. https://doi.org/10.1073/pnas.0506580102.

37. Radomska, H.S., Huettner, C.S., Zhang, P., Cheng, T., Scadden, D.T., and Tenen, D.G. (1998). CCAAT/enhancer binding protein alpha is a regulatory switch sufficient for induction of granulocytic development from bipotential myeloid progenitors. Mol. Cell. Biol. *18*, 4301–4314.

38. Zhang, P., Nelson, E., Radomska, H.S., Iwasaki-Arai, J., Akashi, K., Friedman, A.D., and Tenen, D.G. (2002). Induction of granulocytic differentiation by 2 pathways. Blood *99*, 4406–4412. https://doi.org/10.1182/blood.v99.12.4406.

39. Cammenga, J., Mulloy, J.C., Berguido, F.J., MacGrogan, D., Viale, A., and Nimer, S.D. (2003). Induction of C/EBPalpha activity alters gene expression and differentiation of human CD34+ cells. Blood *101*, 2206–2214. https://doi.org/10.1182/blood-2002-05-1546.

40. Ross, S.E., Radomska, H.S., Wu, B., Zhang, P., Winnay, J.N., Bajnok, L., Wright, W.S., Schaufele, F., Tenen, D.G., and MacDougald, O.A. (2004). Phosphorylation of C/EBPalpha inhibits granulopoiesis. Mol. Cell. Biol. *24*, 675–686. https://doi.org/10.1128/MCB.24.2.675-686.2004.

41. Suh, H.C., Gooya, J., Renn, K., Friedman, A.D., Johnson, P.F., and Keller, J.R. (2006). C/EBPalpha determines hematopoietic cell fate in multipotential progenitor cells by inhibiting erythroid differentiation and inducing myeloid differentiation. Blood *107*, 4308–4316. https://doi.org/10.1182/blood-2005-06-2216.

42. Wang, H., Iakova, P., Wilde, M., Welm, A., Goode, T., Roesler, W.J., and Timchenko, N.A. (2001). C/EBPα arrests cell proliferation through direct inhibition of Cdk2 and Cdk4. Mol. Cel *8*, 817–828.

43. Sedlacek, H.H. (2001). Mechanisms of action of flavopiridol. Crit. Rev. Oncol. Hematol. *38*, 139–170. https://doi.org/10.1016/S1040-8428(00)00124-4.

44. May, B. (2023). Transcriptional regulation of granulopoiesis. Release#V85. https://doi.org/10.3180/R-HSA-9616222.1.

45. Bloh, K., Kanchana, R., Bialk, P., Banas, K., Zhang, Z., Yoo, B.C., and Kmiec, E.B. (2021). Deconvolution of complex DNA repair (DECODR): establishing a novel deconvolution algorithm for comprehensive analysis of CRISPR-edited sanger sequencing data. CRISPR J. *4*, 120–131.

46. Hordyjewska, A., Popiołek, Ł., and Horecka, A. (2015). Characteristics of hematopoietic stem cells of umbilical cord blood. Cytotechnology *67*, 387–396.

47. Doll, L., Aghaallaei, N., Dick, A.M., Welte, K., Skokowa, J., and Bajoghli, B. (2021). A zebrafish model for HAX1-associated congenital neutropenia. Haematologica *106*, 1311–1320. https://doi.org/10.3324/haematol.2019.240200.

48. Doll, L., Welte, K., Skokowa, J., and Bajoghli, B. (2024). A JAGN1-associated severe congenital neutropenia zebrafish model revealed an altered G-CSFR signaling and UPR activation. Blood Adv. *8*, 4050–4065. https://doi.org/10.1182/bloodadvances.2023011656.

49. Skokowa, J., and Welte, K. (2007). LEF-1 is a decisive transcription factor in neutrophil granulopoiesis. Ann. N. Y. Acad. Sci. *1106*, 143–151. https://doi.org/10.1196/annals.1392.012.

50. Gupta, K., Kuznetsova, I., Klimenkova, O., Klimiankou, M., Meyer, J., Moore, M.A.S., Zeidler, C., Welte, K., and Skokowa, J. (2014). Bortezomib inhibits STAT5-dependent degradation of LEF-1, inducing granulocytic differentiation in congenital neutropenia CD34(+) cells. Blood *123*, 2550–2561. https://doi.org/10.1182/blood-2012-09-456889.

51. Skokowa, J., Dale, D.C., Touw, I.P., Zeidler, C., and Welte, K. (2017). Severe congenital neutropenias. Nat. Rev. Dis. Primers *3*, 17032. https://doi.org/10.1038/nrdp.2017.32.

52. Grenda, D.S., Johnson, S.E., Mayer, J.R., McLemore, M.L., Benson, K.F., Horwitz, M., and Link, D.C. (2002). Mice expressing a neutrophil elastase mutation derived from patients with severe congenital neutropenia have normal granulopoiesis. Blood *100*, 3221–3228. https://doi.org/10.1182/blood-2002-05-1372.

53. Zeidner, J.F., and Karp, J.E. (2015). Clinical activity of alvocidib (flavopiridol) in acute myeloid leukemia. Leuk. Res. *39*, 1312–1318.

54. Senderowicz, A.M., Headlee, D., Stinson, S.F., Lush, R.M., Kalil, N., Villalba, L., Hill, K., Steinberg, S.M., Figg, W.D., Tompkins, A., et al. (1998). Phase I trial of continuous infusion flavopiridol, a novel cyclin-dependent kinase inhibitor, in patients with refractory neoplasms. J. Clin. Oncol. *16*, 2986–2999. https://doi.org/10.1200/JCO.1998.16.9.2986.

55. Wiernik, P.H. (2016). Alvocidib (flavopiridol) for the treatment of chronic lymphocytic leukemia. Expert Opin. Investig. Drugs *25*, 729–734.

56. LaCerte, C., Ivaturi, V., Gobburu, J., Greer, J.M., Doyle, L.A., Wright, J.J., Karp, J.E., and Rudek, M.A. (2017). Exposure-Response Analysis of Alvocidib (Flavopiridol) Treatment by Bolus or Hybrid Administration in Newly Diagnosed or Relapsed/Refractory Acute Leukemia Patients. Clin. Cancer Res. *23*, 3592–3600. https://doi.org/10.1158/1078-0432.CCR-16-2629.

57. Tan, A.R., Headlee, D., Messmann, R., Sausville, E.A., Arbuck, S.G., Murgo, A.J., Melillo, G., Zhai, S., Figg, W.D., Swain, S.M., and Senderowicz, A.M. (2002). Phase I clinical and pharmacokinetic study of flavopiridol administered as a daily 1-hour infusion in patients with advanced neoplasms. J. Clin. Oncol. *20*, 4074–4082. https://doi.org/10.1200/JCO.2002.01.043.

58. Chao, S.-H., Fujinaga, K., Marion, J.E., Taube, R., Sausville, E.A., Senderowicz, A.M., Peterlin, B.M., and Price, D.H. (2000). Flavopiridol inhibits P-TEFb and blocks HIV-1 replication. J. Biol. Chem. *275*, 28345–28348.

59. Schmerwitz, U.K., Sass, G., Khandoga, A.G., Joore, J., Mayer, B.A., Berberich, N., Totzke, F., Krombach, F., Tiegs, G., Zahler, S., et al. (2011). Flavopiridol protects against inflammation by attenuating leukocyte-endothelial interaction via inhibition of cyclin-dependent kinase 9. Arterioscler. Thromb. Vasc. Biol. *31*, 280–288.

60. Montagnoli, A., Valsasina, B., Croci, V., Menichincheri, M., Rainoldi, S., Marchesi, V., Tibolla, M., Tenca, P., Brotherton, D., Albanese, C., et al. (2008). A Cdc7 kinase inhibitor restricts initiation of DNA replication and has antitumor activity. Nat. Chem. Biol. *4*, 357–365. https://doi.org/10.1038/nchembio.90.

61. Zeidler, A., Borbaran-Bravo, N., Dannenmann, B., Ritter, M., Nasri, M., Klimiankou, M., Kandabarau, S., Zahabi, A., König, J., Zeidler, C., et al. (2024). Differential transcriptional control of hematopoiesis in congenital and cyclic neutropenia patients harboring ELANE mutations. Haematologica *109*, 1393–1402.

62. Matrone, G., Mullins, J.J., Tucker, C.S., and Denvir, M.A. (2016). Effects of cyclin dependent kinase 9 inhibition on zebrafish larvae. Cell Cycle *15*, 3060–3069.

63. Hoodless, L.J., Lucas, C.D., Duffin, R., Denvir, M.A., Haslett, C., Tucker, C.S., and Rossi, A.G. (2016). Genetic and pharmacological inhibition of CDK9 drives neutrophil apoptosis to resolve inflammation in zebrafish in vivo. Sci. Rep. *5*, 36980.

64. Belt, A.J., Grant, S., Tombes, R.M., and Rothschild, S.C. (2024). Myeloid Targeted Human MLL-ENL and MLL-AF9 Induces cdk9 and bcl2 Expression in Zebrafish Embryos. Plos Genet. *20*, e1011308.

65. Chen, K.T.J., Militao, G.G.C., Anantha, M., Witzigmann, D., Leung, A.W.Y., and Bally, M.B. (2021). Development and characterization of a novel flavopiridol formulation for treatment of acute myeloid leukemia. J. Control Release *333*, 246–257.

66. Kim, W., Haws, H., Peterson, P., Whatcott, C.J., Weitman, S., Warner, S.L., Bearss, D.J., and Siddiqui-Jain, A. (2017). TP-1287, an oral prodrug of the cyclin-dependent kinase-9 inhibitor alvocidib. Cancer Res. *77*, 5133.

67. Ackermann, M., Lachmann, N., Hartung, S., Eggenschwiler, R., Pfaff, N., Happle, C., Mucci, A., Göhring, G., Niemann, H., Hansen, G., et al. (2014/02/01/2014). Promoter and lineage independent anti-silencing activity of the A2 ubiquitous chromatin opening element for optimized human pluripotent stem cell-based gene therapy. Biomaterials *35*, 1531–1542. https://doi.org/10.1016/j.biomaterials.2013.11.024.

68. Ewels, P.A., Peltzer, A., Fillinger, S., Patel, H., Alneberg, J., Wilm, A., Garcia, M.U., Di Tommaso, P., and Nahnsen, S. (2020). The nf-core framework for community-curated bioinformatics pipelines. Nat. Biotechnol. *38*, 276–278.

69. Ge, S.X., Son, E.W., and Yao, R. (2018). iDEP: an integrated web application for differential expression and pathway analysis of RNA-Seq data. BMC bioinformatics *19*, 534–624.

70. Chen, S. (2023). Ultrafast one-pass FASTQ data preprocessing, quality control, and deduplication using fastp. Imeta *2*, e107. https://doi.org/10.1002/imt2.107.

71. Danecek, P., Bonfield, J.K., Liddle, J., Marshall, J., Ohan, V., Pollard, M.O., Whitwham, A., Keane, T., McCarthy, S.A., Davies, R.M., and Li, H. (2021). Twelve years of SAMtools and BCFtools. Gigascience *10*, giab008. https://doi.org/10.1093/gigascience/giab008.

72. Basheer, F., Rasighaemi, P., Liongue, C., and Ward, A.C. (2019). Zebrafish Granulocyte Colony-Stimulating Factor Receptor Maintains Neutrophil Number and Function throughout the Life Span. Infect. Immun. *87*, e00793-18. https://doi.org/10.1128/iai.00793-18.

73. Lin, H.F., Traver, D., Zhu, H., Dooley, K., Paw, B.H., Zon, L.I., and Handin, R.I. (2005). Analysis of thrombocyte development in CD41-GFP transgenic zebrafish. Blood *106*, 3803–3810. https://doi.org/10.1182/blood-2005-01-0179.

74. Quiring, R., Wittbrodt, B., Henrich, T., Ramialison, M., Burgtorf, C., Lehrach, H., and Wittbrodt, J. (2004). Large-scale expression screening by automated whole-mount in situ hybridization. Mech. Dev. *121*, 971–976. https://doi.org/10.1016/j.mod.2004.03.031.

YMTHE, Volume *33*

Supplemental Information

Flavopiridol restores granulopoiesis in experimental models of severe congenital neutropenia

Masoud Nasri, Benjamin Dannenmann, Larissa Doll, Betül Findik, Franka Bernhard, Sergey Kandabarau, Maksim Klimiankou, Meinrad Gawaz, Claudia Lengerke, Cornelia Zeidler, Karl Welte, and Julia Skokowa

Supplemental Information

Supplemental Tables

Table S1. Prediction and Validation of Off-Target Sites for gRNAs by Shallow Whole-Genome Sequencing

Provided as separate excel file.

Table S2. Differentially expressed genes (DEGs) between *ELANE*-CN 1-3 corr and CN 1-3 iPSC-derived $CD34^{+}CD45^{+}$ cells.

Provided as separate excel file.

Table S3. List of 50 small molecules of L1000 CDS analysis and top 10 candidates of CMAP analysis, based on scores.

Provided as separate excel file.

Table S4. Differentially expressed genes (DEGs) between DMSO and flavopiridol (40 nM) treated *in vitro* generated neutrophils from four healthy controls.

Provided as separate excel file.

Table S5. Repair template sequences for *ELANE* mutation correction in CN iPSCs

Repair template 1	5'CGGCCCCACGCGTGGCCCTTCATGGTGTCCCTGCAGCTGCGCGGA GGCCACTTCTGCGGCGCCACCCTGATTGCGCCCAACTTCGTCATGTC GGCCGCGCACTGCGTGGCGAATGTGTGAGTA-3'
Repair template 2	5'GCCAACGTGCAGGTGGCCCAGCTGCCGGCTCAGGGACGCCGCCT GGGCAACGGGGTGCAGTGCCTGGCCATGGGCTGGGGCCTTCTGGGC AGGAACCGTGGGATCGCCAGCGTCCTGCAGGAG-3'
Repair template 3	5'CGGGGCAAAGGCATCGGGGTAGAGCCCTGAGGCGCAGCCTCCCC GGACGAAGGAGGCAATTCCGTGGATTAGCCCGTTGCAGACCAAGG GGCTGCCGGAGTCCCCCTGTGGAGGCAGACAAGG-3'

Table S6. PCR primer sequences for assessing genome editing efficiency

Primer name	Sequence (5' to 3')
*ELANE*_Ex2_F	GGCTCCTTGGCAGGCACTCA
*ELANE*_Ex2_R	CACCTCACAGACCGGGACGC
*ELANE*_Ex4_F	CGCCCTGAGCCTTGGTGACG
*ELANE*_Ex4_R	AGCCACGGTGCCTGTTGCTG
*ELANE*_Ex5_F	CAGCCCGGACTGCAGCAACA
*ELANE*_Ex5_R	GACCCGGGCAGCCCTTCTCA
*CEBPA*_F	CCCATGGAGTCGGCCGACTTCT
*CEBPA*_R	CAGTGCGCGATCTGGAACTGCA

Table S7. qRT-PCR primer sequences

Target gene	Forward primer (5'→ 3')	Reverse primer (5'→ 3')
GAPDH	CTGGGCTACACTGAGCACC	AAGTGGTCGTTGAGGGCAATG
ACTB	TTCCTGGGCATGGAGTC	CAGGTCTTTGCGGATGATGTC
DDIT3	CTGACTGAGGAGGAGCCAGAAC	GGTTCTCCCTTGGTCTTCCTCC
HSPA5	AGGACAAGAAGGAGGACGTGG	GGTTGGAGGTGAGCTGGTTC
ATF4	TCCCATCTCCAGGTGTTCTC	CAGCTCTTTGCACTCACCAG
ATF6	TGCTCTCTTTGCTGAACTCGG	GCTGGAGAAAGTGGCTGAGGT
CCND2	GCCACCTGGATGCTGGAGGTCT	AGTCGGGACCCCAGCCAAGAAA
RBL1	CCCCGCACAAGAATGGGTCAGG	ACGCGTTTGGCAGGGGATTCTG
LOX	ACCACAGGCGATTTGCATGTA	GGCAGTCTATGTCTGCACCA
PITX1	GAGTCGTCTGACACGGAGCTGC	CTTCTTGGCTGGGTCGTCTGCG
PITX2	ACTTTCCAGAGGAACCGCTACC	TAAGGTTGGTCCACACAGCGAT
CEBPA	CCGGACTTGGTGCGTCTAAG	AGGCATTGGAGCGGTGAGT
HMGA2	GGAAGACCCAAAGGCAGCAAAA	CTTGGCCGTTTTTCTCCAGTGG
ACKR3	ATCCAGGCCAAGACCACAGGCT	GTGCTGCACGAGACTGACCACC
SLAMF1	TCTCCTTGACCTTCGTGCTGTT	TCCCAACTGCCGGAGAATCTTT
HSPA2	GCAGACGCAGACCTTCACCACC	GGTCAGGTCGAACTTGCCCAGC
HSPA6	ACTCGCTGGAGGCCCATGTCTT	CTCTGCCAGCTGGTTGTGCTCC

Supplemental Figures

A

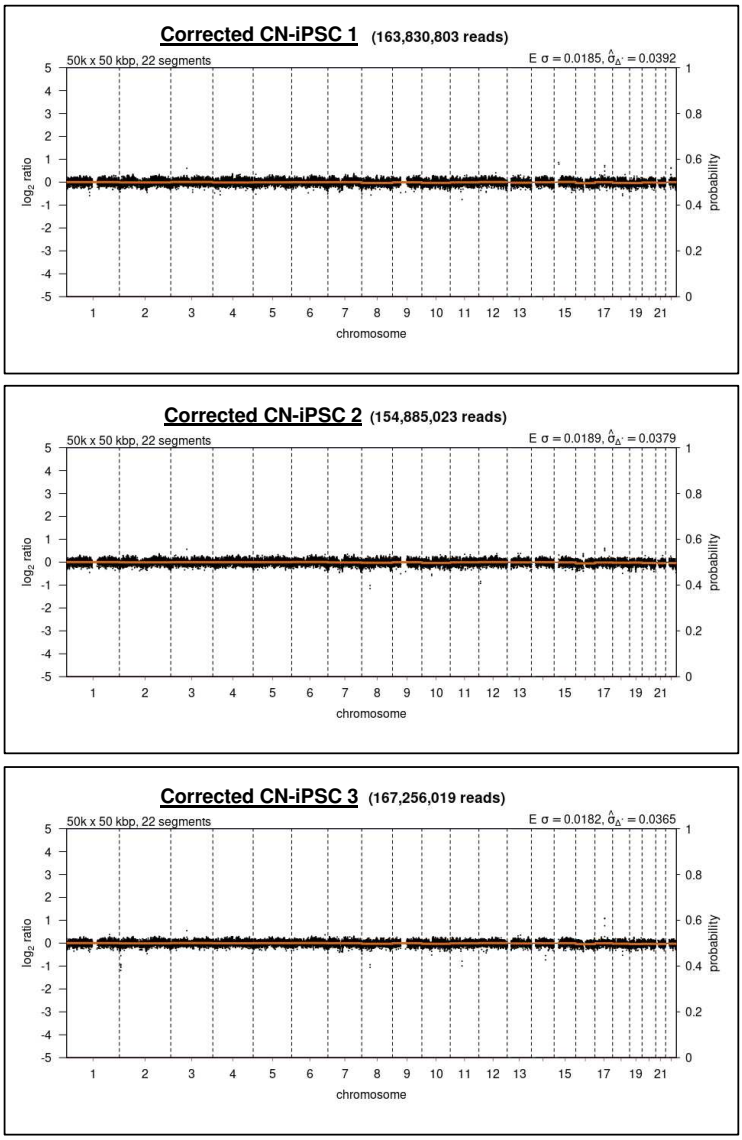

B

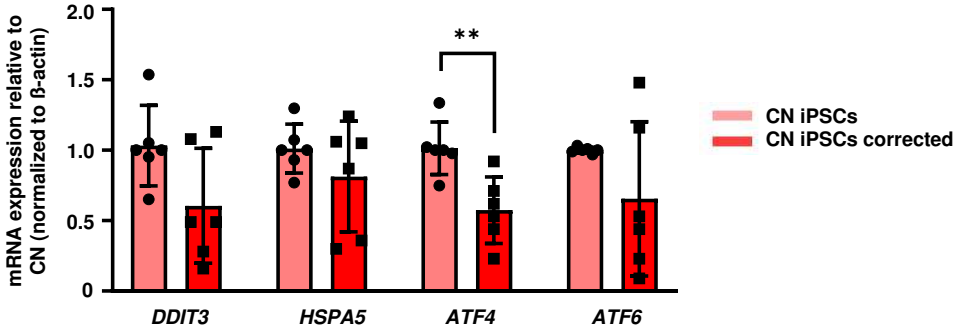

Figure S1. Analysis of differentiation potential and unfolded protein response (UPR) of *ELANE*-CN and *ELANE*-CN corrected iPSC-derived $CD34^+CD45^+$ cells (related to Figure 1).

A. Copy number profile for corrected *ELANE*-CN iPSC lines. Black scattered dots display normalized and smoothed copy number signal, solid orange line displays normalized segmented copy number state. Details are explained in methods. **B.** qRT-PCR analysis of mRNA expression of unfolded protein response (UPR) genes in iPSC-derived $CD34^+CD45^+$ cells isolated on day 14 of iPSC differentiation of indicated iPSC lines. Gene expression levels were normalized to β-actin and are shown relative to *ELANE*-CN. Data are represented as mean ± SD from duplicates of three independent experiments. The significant difference between groups is indicated, $^{**}P < 0.01$

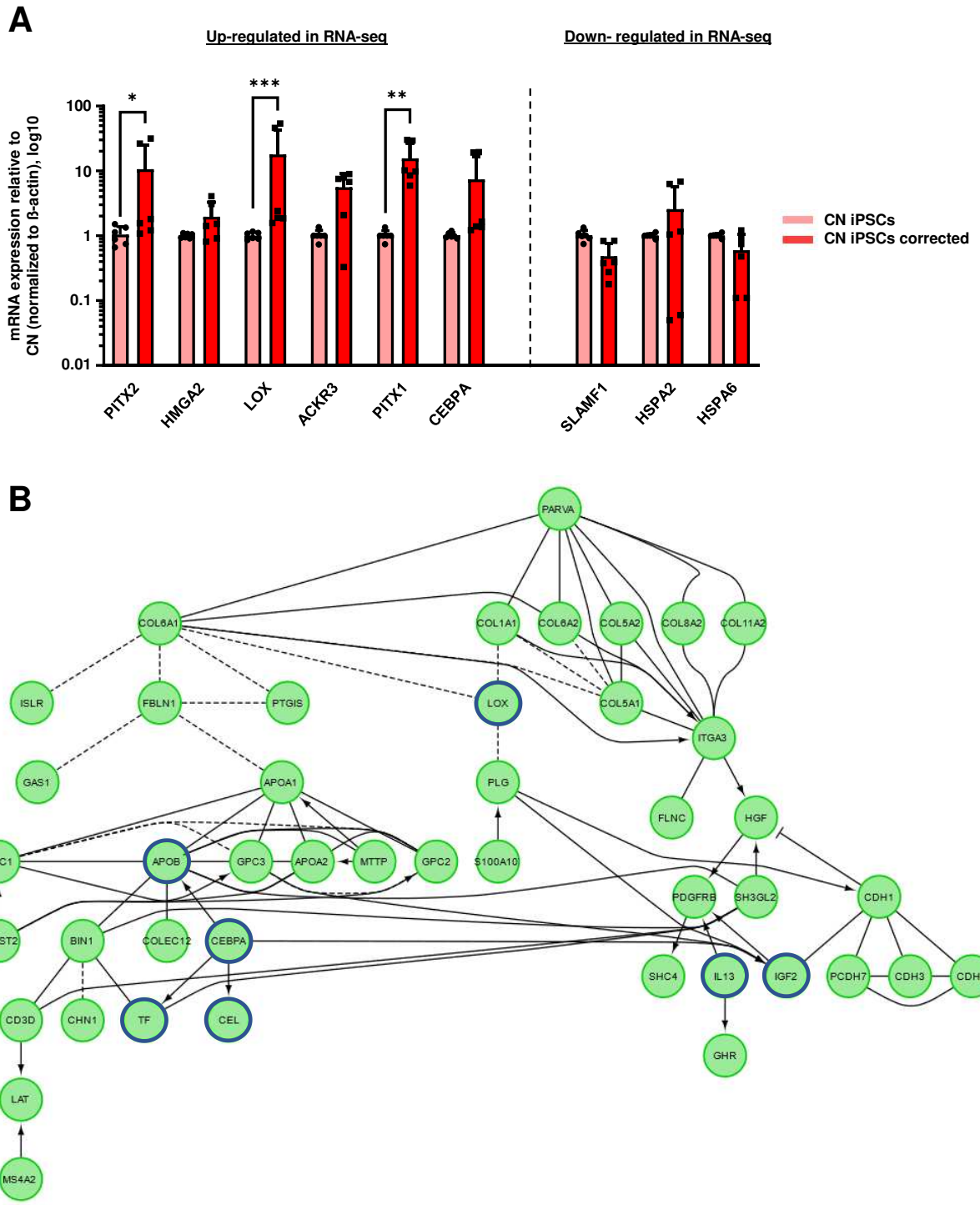
A
Up-regulated in RNA-seq
Down- regulated in RNA-seq
mRNA expression relative to CN (normalized to ß-actin), log10
100
10
1
0.1
0.01
*
***
**
PITX2
HMGA2
LOX
ACKR3
PITX1
CEBPA
SLAMF1
HSPA2
HSPA6
CN iPSCs
CN iPSCs corrected
B
PARVA
COL6A1
COL1A1
COL6A2
COL5A2
COL8A2
COL11A2
ISLR
FBLN1
PTGIS
LOX
COL5A1
ITGA3
GAS1
APOA1
PLG
FLNC
HGF
GPC1
APOB
GPC3
APOA2
MTTP
GPC2
S100A10
PDGFRB
SH3GL2
CDH1
HS6ST2
BIN1
COLEC12
CEBPA
SHC4
IL13
IGF2
PCDH7
CDH3
CDH5
CD3D
CHN1
TF
CEL
GHR
LAT
MS4A2

Figure S2. DEGs validated by qRT-PCR and visualization of functional interactions among DEGs using a reactome curated dataset (related to Figure 2).

A. qRT-PCR analysis of mRNA expression of selected genes in CN-iPSC 1-3 derived $CD34^{+}CD45^{+}$ cells isolated on day 14 of iPSC differentiation of indicated iPSC lines. Gene expression levels were normalized to β-actin and relative to *ELANE*-CN. Up- and down-regulated genes in the RNA-seq dataset are visually separated by a dashed line. Data represent means ± SD from duplicates of three independent experiments. The significant difference between groups is indicated, *P < 0.05, **P < 0.01, ***P < 0.001. **B.** Reactome functional interaction (FI) network representation of DEGs. The genes that are mentioned in the main manuscript are encircled blue.

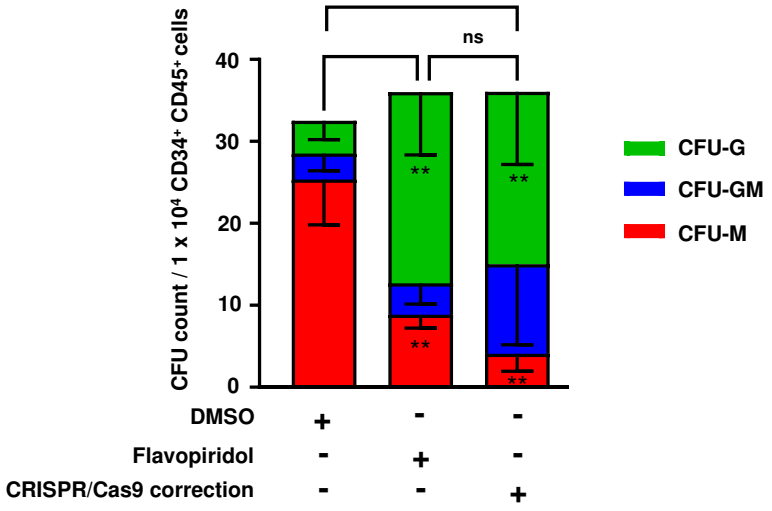

Figure S3. CRISPR/Cas9 correction or flavopiridol treatment are capable of inducing granulopoiesis in CN (related to Figure 3).

CFU assay of CN iPSC-derived $CD34^+CD45^+$ cells of all three CN-iPSC CRISPR/Cas9 corrected lines or CN-iPSC lines isolated at day 14 of iPSC differentiation treated with flavopiridol (40 nM) vs DMSO (0.1%) added at day 1 of CFU assay. CFU counts of CFU types are shown. Data are represented as mean ± SD of duplicates from three independent experiments. The significant difference between groups is indicated, **P < 0.01, ns: not significant (for all CFU types).

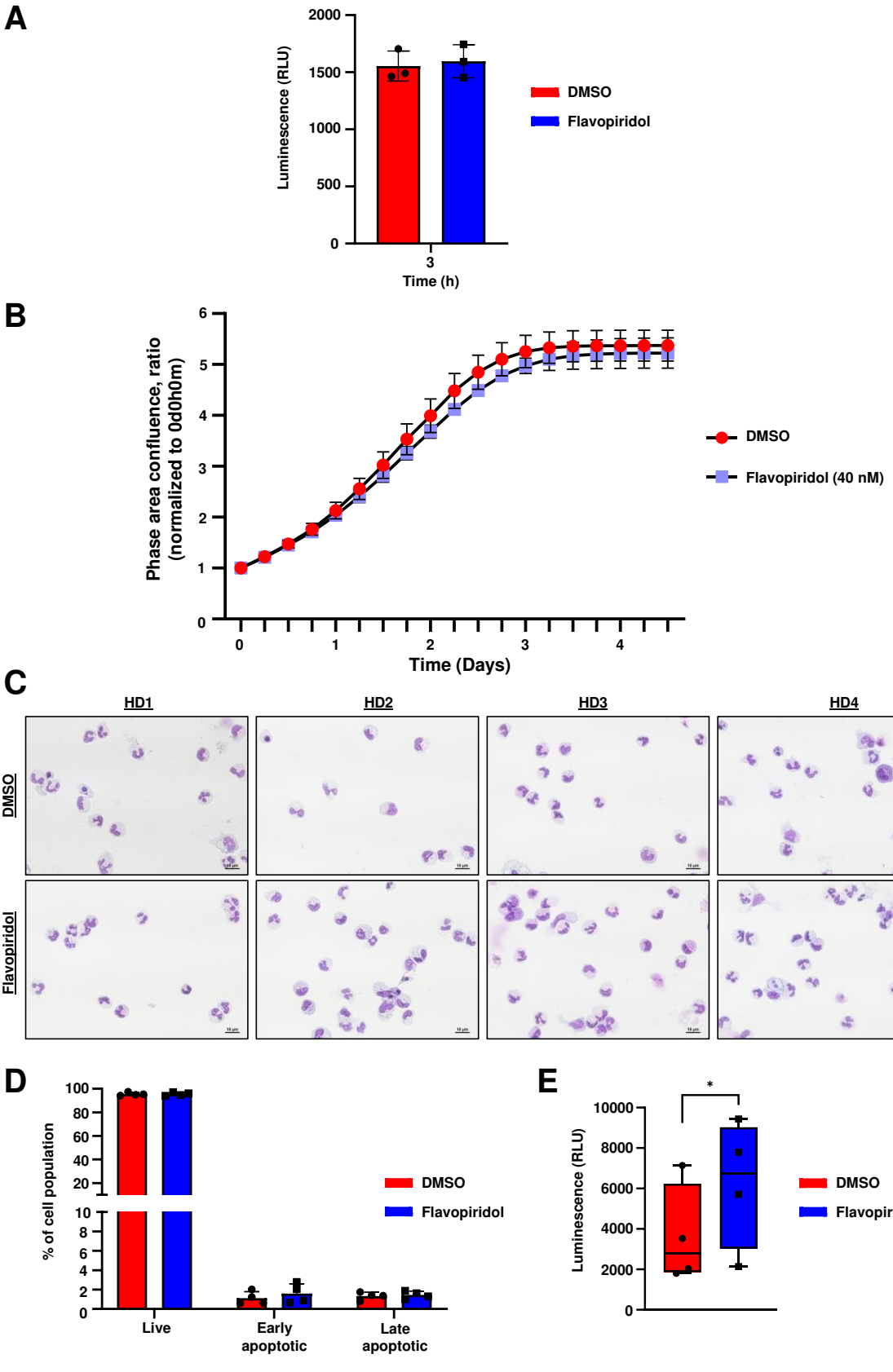
A
Luminescence (RLU)
2000
1500
1000
500
0
3
Time (h)
DMSO
Flavopiridol
B
Phase area confluence, ratio
(normalized to 0d0h0m)
6
5
4
3
2
1
0
0
1
2
3
4
Time (Days)
DMSO
Flavopiridol (40 nM)
C
HD1
HD2
HD3
HD4
DMSO
Flavopiridol
D
% of cell population
100
80
60
40
20
10
8
6
4
2
0
Live
Early apoptotic
Late apoptotic
DMSO
Flavopiridol
E
*
Luminescence (RLU)
10000
8000
6000
4000
2000
0
DMSO
Flavopiridol

Figure S4. Flavopiridol was not toxic for human primary neutrophils, human primary CD34$^+$ HSPCs and *in vitro* differentiated neutrophils (related to Figure 4).

A. Viability assay of PMNs from three healthy donors treated for 3 hours with flavopiridol (40 nM) using luminescence-based real-time MT-GLO assay. Data are represented as mean ± SD from three healthy donors. **B.** Proliferation kinetics of HD5-7 CD34$^+$ HSPCs treated with flavopiridol (40 nM) or DMSO (0.1%), assessed by IncuCyte ZOOM System. Data are represented as mean ± SD from three healthy donors. **C.** Representative cytospin images of May-Grunwald-Giemsa-stained cytospin preparations of four HD CD34$^+$ HSPCs (HD 1-4) at day 14 of LCD treated with flavopiridol (40 nM) or DMSO (0.1%). Scale bar represents 10 µm. **D.** Annexin V apoptosis assay to assess the live (Annexin V$^-$/DAPI$^-$), early apoptotic (Annexin V$^+$/DAPI$^-$), and late apoptotic (Annexin V$^+$/DAPI$^+$) populations of *in vitro* differentiated neutrophils derived from human primary CD34$^+$ hematopoietic stem cells of four healthy donors (HD 1-4) treated with 40 nM flavopiridol or DMSO (0.1%). Data are represented as mean ± SD from four healthy donors. **E.** Viability of *in vitro* differentiated neutrophils derived from human primary CD34$^+$ hematopoietic stem cells of four healthy donors (HD 1-4) treated with 40 nM flavopiridol or DMSO (0.1%) measured using RealTime-Glo MT Cell Viability Assay. Data are represented as mean ± SD from four healthy donors. The significant difference between groups is indicated, *P < 0.05.

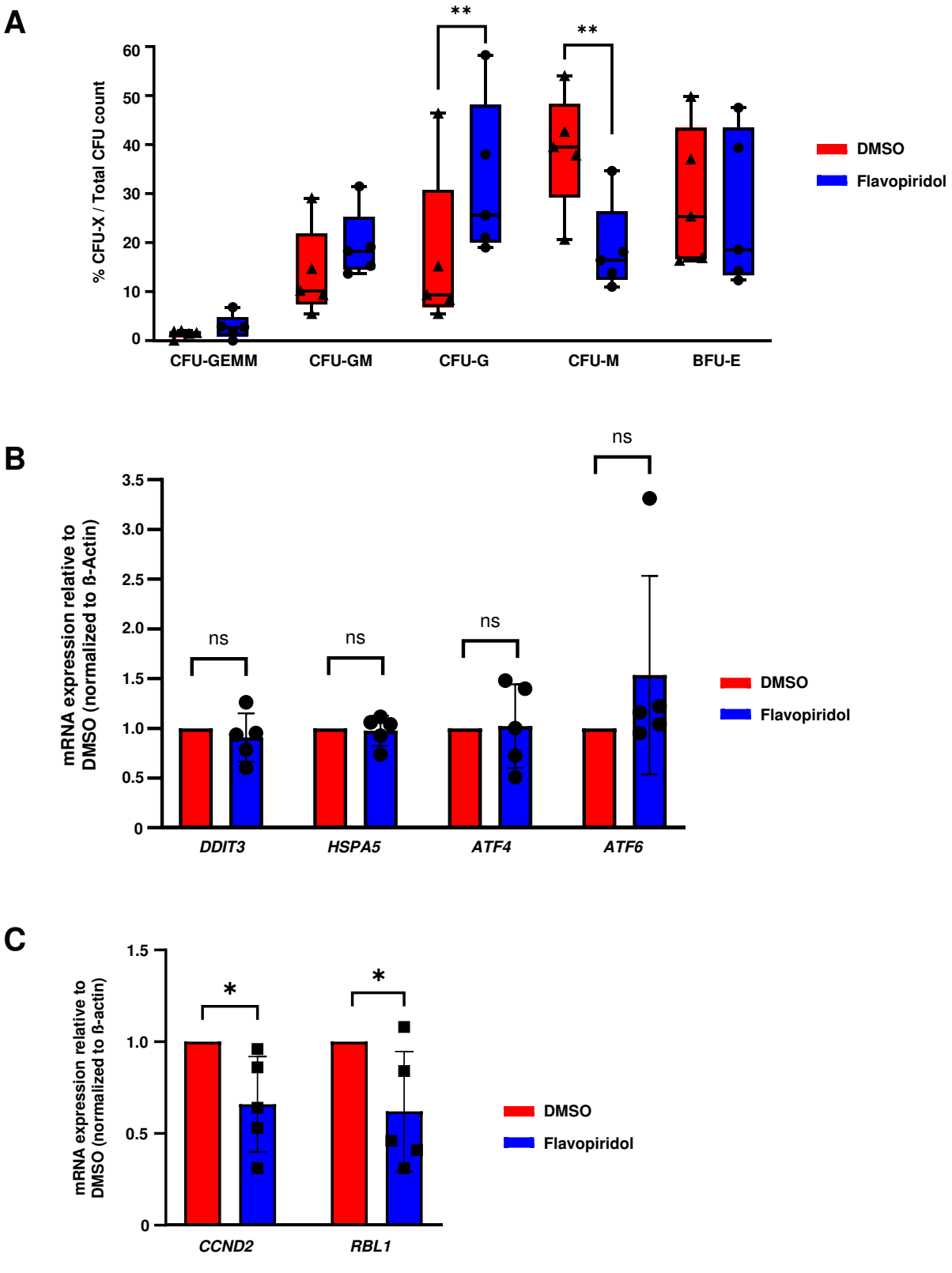
A
% CFU-X / Total CFU count
60
50
40
30
20
10
0
**
**
CFU-GEMM
CFU-GM
CFU-G
CFU-M
BFU-E
DMSO
Flavopiridol
B
mRNA expression relative to DMSO (normalized to ß-Actin)
3.5
3.0
2.5
2.0
1.5
1.0
0.5
0
ns
ns
ns
ns
DDIT3
HSPA5
ATF4
ATF6
DMSO
Flavopiridol
C
mRNA expression relative to DMSO (normalized to ß-actin)
1.5
1.0
0.5
0
*
*
CCND2
RBL1
DMSO
Flavopiridol

Figure S5. Flavopiridol restored granulopoiesis in CD34$^+$ HSPCs of CN patients with different genetic backgrounds and regulates CDK2/4 target genes, but not UPR genes (related to Figure 6).

A. CFU assay of CN CD34$^+$ HSPC cells treated with flavopiridol (40 nM) or DMSO (0.1%). CFU percentages of CFU types are shown. Data are represented as mean ± SD from five patients, each in duplicates, including group comparisons, **P < 0.01. **B.** qRT-PCR analysis of UPR genes *DDIT3, HSPA5, ATF4* and *ATF6* mRNA expression in HSPCs of five CN patients (CN1-5) treated with flavopiridol (40 nM) or DMSO (0.1%) for 48 hours. Gene expression levels were normalized to β-actin and are shown relative to DMSO (0.1%). Data are represented as mean ± SD from five patients, including group comparisons, ns: not significant. **C.** qRT-PCR analysis of *CCND2* and *RBL1* mRNA expression in myeloid cells of five CN patients (CN 1-5) at day 14 of LCD treated with flavopiridol (40 nM) or DMSO (0.1%). Gene expression levels were normalized to β-actin and are shown relative to CN. Data are represented as mean ± SD from five patients, including group comparisons, *P < 0.05.

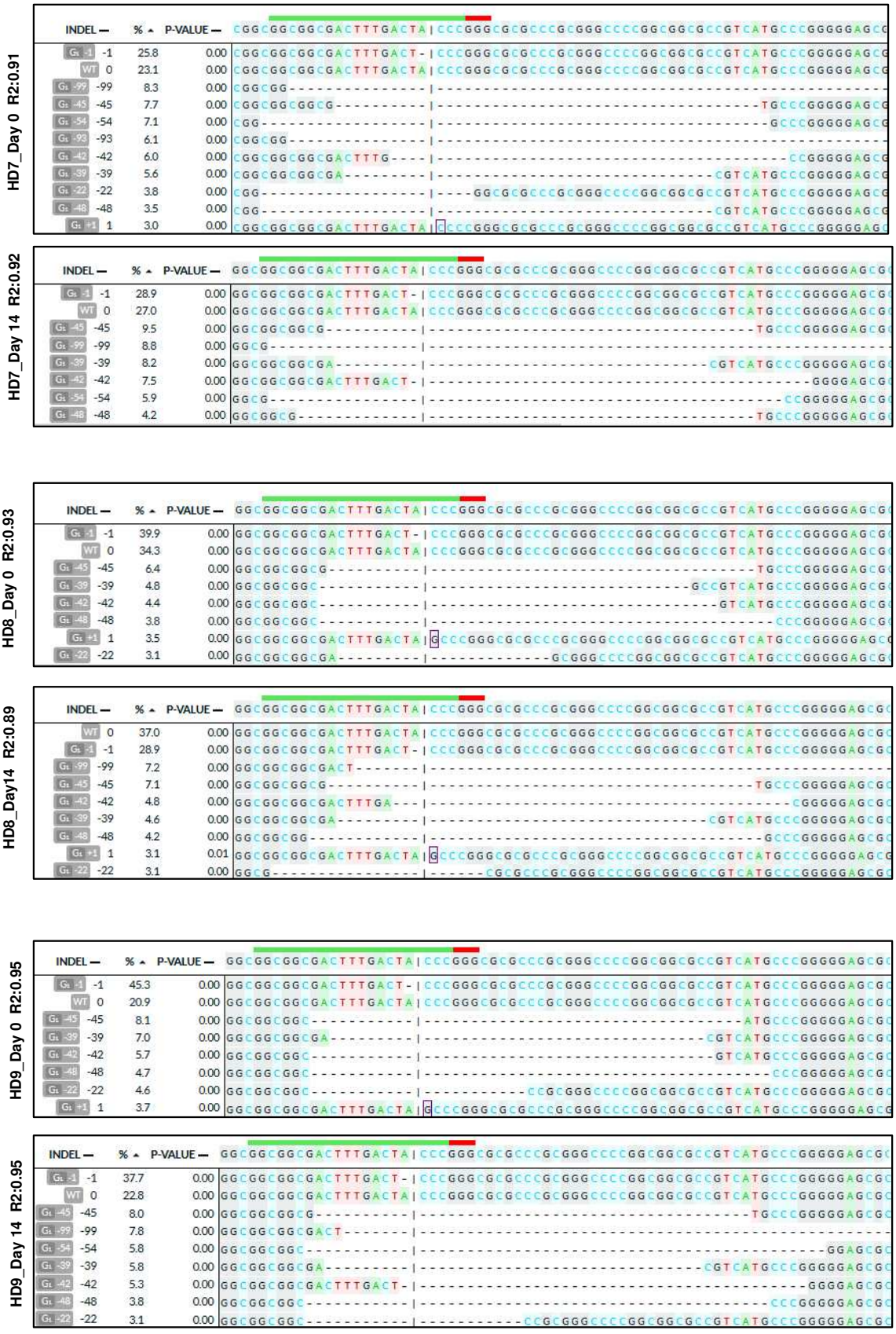
HD7_Day 0 R2:0.91
HD7_Day 14 R2:0.92
HD8_Day 0 R2:0.93
HD8_Day14 R2:0.89
HD9_Day 0 R2:0.95
HD9_Day 14 R2:0.95

Figure S6. DECODR analysis of sanger sequencing results of *CEBPA* knockout in healthy donors HSPCs (related to Figure 7).

Editing efficiency of *CEBPA* knockout at the day of starting granulocytic differentiation (day 0) and the experimental endpoint (day 14) treated with DMSO (0.1%) of three representative HDs (HD 7-9) analyzed by Deconvolution of Complex DNA Repair (DECODR) tool. The program's output includes a report containing results for a subset of predicted sequences (with their contributions and p-values), as well as an R^2 value to measure the goodness of fit for each sample.

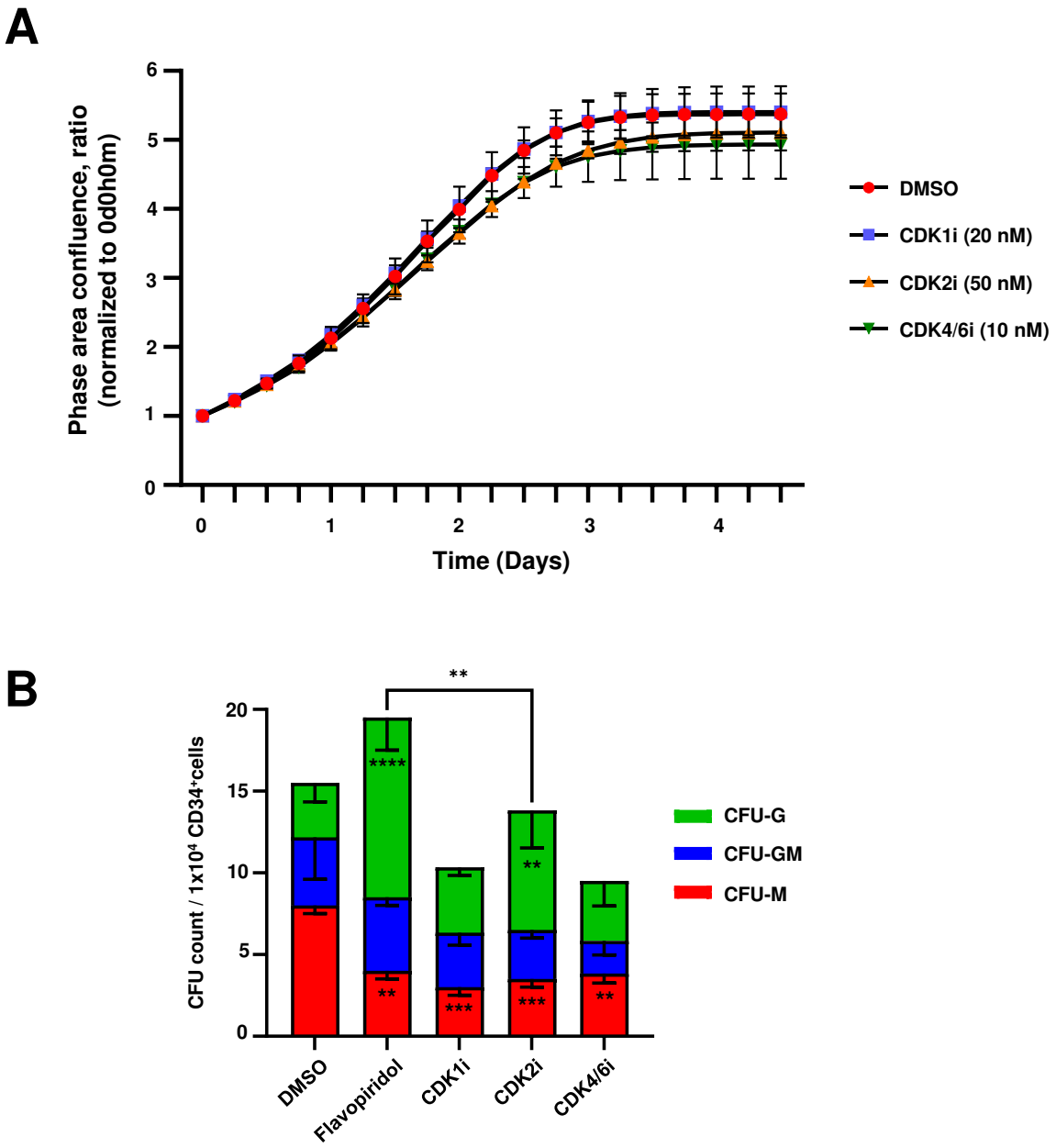

Figure S7. Toxicity and efficacy evaluation of CDK 1, 2 and 4/6 inhibitors (related to Figure 7).

A. Proliferation kinetics of HD 5-7 CD34⁺ HSPCs treated with CDK1i (Ro-3306, 20 nM), CDK2i (AUZ 454, 50 nM), CDK4/6i (Ribociclib, 10 nM) or DMSO (0.1%), assessed by IncuCyte ZOOM System. Data are represented as mean ± SD from three healthy donors. **B.** CFU assay of CN1 (*ELANE* MUT p.A57V) iPSC-derived CD34⁺CD45⁺ cells isolated at day 14 of iPSC differentiation in the presence of the respective

small molecules or DMSO. CFU counts are shown. Data are represented as mean ± SD of duplicates from three independent experiments. The significant difference between each small molecule and DMSO control is shown and the comparison between flavopiridol and CDK2i, **P < 0.01, ***P < 0.001, ****P < 0.0001.

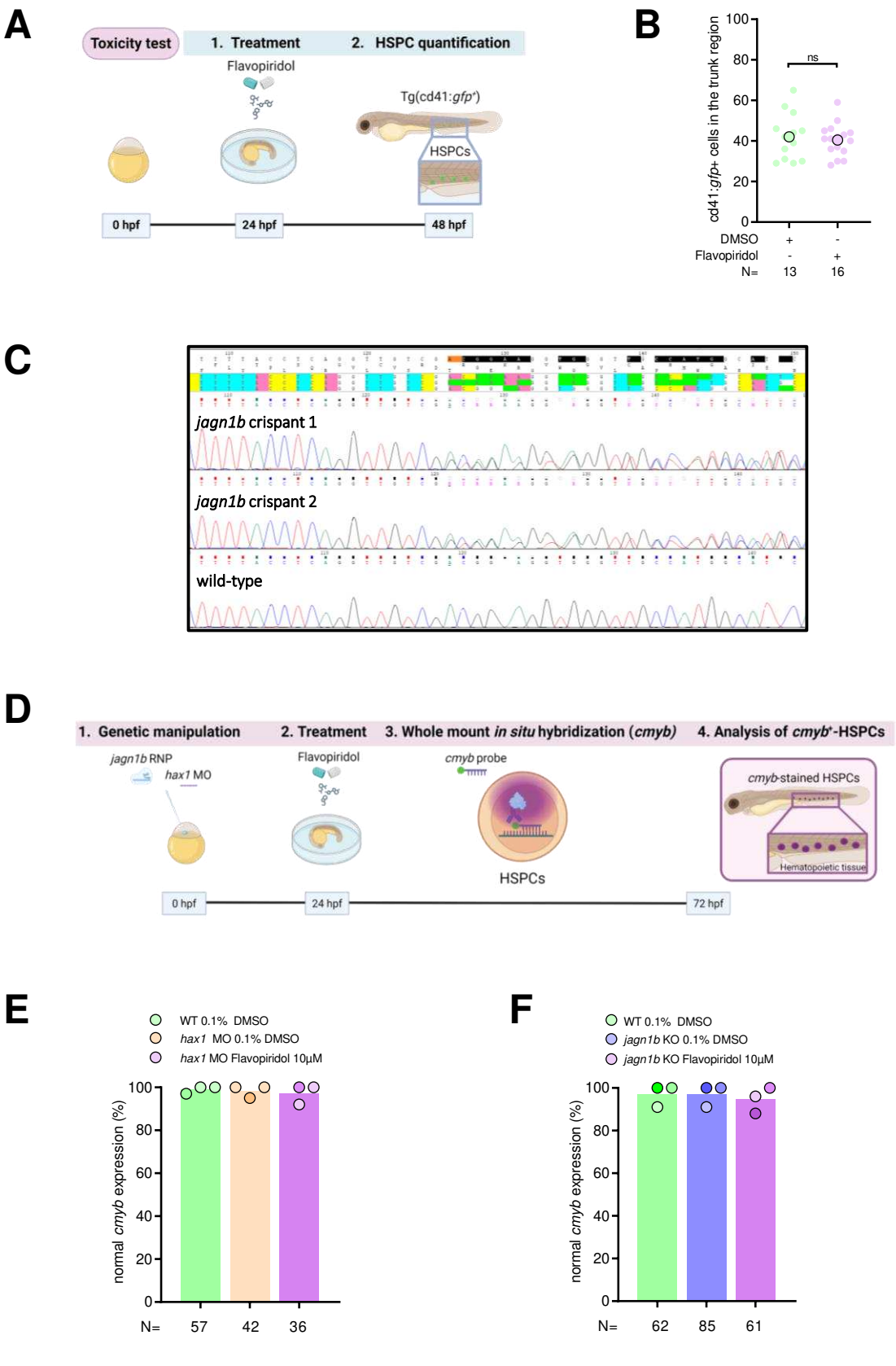
A
Toxicity test
1. Treatment
2. HSPC quantification
Flavopiridol
Tg(cd41:gfp+)
HSPCs
0 hpf
24 hpf
48 hpf
B
cd41:gfp+ cells in the trunk region
ns
DMSO
Flavopiridol
N=
13
16
C
jagn1b crispant 1
jagn1b crispant 2
wild-type
D
1. Genetic manipulation
2. Treatment
3. Whole mount in situ hybridization (cmyb)
4. Analysis of cmyb+-HSPCs
jagn1b RNP
hax1 MO
Flavopiridol
cmyb probe
HSPCs
cmyb-stained HSPCs
Hematopoietic tissue
0 hpf
24 hpf
72 hpf
E
WT 0.1% DMSO
hax1 MO 0.1% DMSO
hax1 MO Flavopiridol 10µM
normal cmyb expression (%)
N=
57
42
36
F
WT 0.1% DMSO
jagn1b KO 0.1% DMSO
jagn1b KO Flavopiridol 10µM
normal cmyb expression (%)
N=
62
85
61

Figure S8. *In vivo* flavopiridol treatment procedure of zebrafish embryos (related to Figure 8).

A. Experimental toxicity test procedure on HSPCs using transgenic tg(cd41:*gfp*) reporter zebrafish embryos. At 24 hours post fertilization (hpf), embryos were treated with flavopiridol (10 µM) or DMSO (0.1 %) and at 48 hpf the cd41:*gfp*$^{+}$ HSPCs were quantified in the hematopoietic tissue (marked in square). Created with BioRender.com. **B.** Absolute counts of HSPCs (cd41:*gfp*$^{+}$ cells) in wild-type zebrafish embryos treated with flavopiridol (10 µM) or DMSO (0.1 %). Each dot represents the value of an individual embryo. The statistical analysis was performed using an unpaired, two-tailed Wilcoxon-Mann-Whitney test, ns: not significant. **C.** *Jagn1b* crispant genotyping. After genetic manipulation using the CRISPR/Cas9-approach, the targeted region of the *jagn1b* gene was amplified from two crispant embryos and compared to the wild-type sequence to determine the efficiency of gene editing. Two representative sequences of *jagn1b* are shown compared to the wild-type sequence. **D.** Experimental procedure of flavopiridol treatment of genetically modified, *hax1*-knockdown (KD) and *jagn1b*-knockout (KO), zebrafish embryos and the analysis of the effect on HSPCs. At one-cell stage, the zebrafish embryos were genetically modified by microinjection of either a *hax1*-specific morpholino or a *jagn1b*-specific CRISPR/Cas9 RNP. At 24 hpf the embryos were treated with flavopiridol (10 µM) and at 72 hpf whole mount *in situ* hybridization (WISH) against the HSPC-marker *cmyb* was performed and analyzed. Created with BioRender.com. **E-F.** Analysis of *cmyb* expression pattern using WISH after DMSO- or flavopiridol-treatment in *hax1*-KD (**E**) or *jagn1b*-KO (**F**) embryos. Each dot represents the percentage of zebrafish embryos with a normal *cmyb* expression pattern of an independent experiment.